Intermolecular Anionic Mixed-Valence and π-Dimer Complexes of Ortho-Pentannulated BisAzaCoroneneDiimides

Arthur H G David, Maxime Roger, Olivier Alévêque, Heorhii Melnychenko, Laura Le Bras, Magali Allain, Adèle Gapin, David Canevet, Olivier Ségut, Eric Levillain, et al.

▶ **To cite this version:**

Arthur H G David, Maxime Roger, Olivier Alévêque, Heorhii Melnychenko, Laura Le Bras, et al.. Intermolecular Anionic Mixed-Valence and π-Dimer Complexes of Ortho-Pentannulated BisAza-CoroneneDiimides. Angewandte Chemie International Edition, 2024, 10.1002/anie.202413616 . hal-04731867

HAL Id: hal-04731867

https://univ-angers.hal.science/hal-04731867v1

Submitted on 11 Oct 2024

HAL is a multi-disciplinary open access archive for the deposit and dissemination of scientific research documents, whether they are published or not. The documents may come from teaching and research institutions in France or abroad, or from public or private research centers.

L'archive ouverte pluridisciplinaire **HAL**, est destinée au dépôt et à la diffusion de documents scientifiques de niveau recherche, publiés ou non, émanant des établissements d'enseignement et de recherche français ou étrangers, des laboratoires publics ou privés.

Distributed under a Creative Commons Attribution - NonCommercial - NoDerivatives 4.0 International License

Intermolecular Anionic Mixed-Valence and π-Dimer Complexes of Ortho-Pentannulated BisAzaCoroneneDiimides

Arthur H. G. David,[a] Maxime Roger,[a] Olivier Alévêque,[a] Heorhii Melnychenko,[a] Laura Le Bras,*[b] Magali Allain,[a] Adèle Gapin,[a] David Canevet,[a] Olivier Ségut,[a] Eric Levillain,*[a] and Antoine Goujon*[a]

[a] MOLTECH-Anjou, SFR MATRIX, Univ Angers, CNRS, 2 Bd Lavoisier, 49000 Angers, France

eric.levillain@univ-angers.fr

antoine.goujon@univ-angers.fr

[b] Laboratoire Chrono-environnement (UMR 6249), Université de Franche-Comté, 16 route de Gray, 25030 Besançon, France

laura.le_bras@univ-fcomte.fr

Table of Contents

1. Materials and Methods

Materials and General Methods. Thin Layer Chromatography (TLC) was conducted on pre-coated aluminium sheets with 0.20 mm MerckAlugram SIL G/UV254 with fluorescent indicator UV254. Column chromatography was carried out using Sigma-Aldrich silica gel 60 (particle size 63-200 μm). UV-Vis absorption spectra were recorded on a Shimadzu UV-1800 UV-Vis spectrophotometer using quartz cells. Fluorescence was measured on a Shimadzu RF-6000 Spectrophotometer using quartz cells. Quantum Yields were measured on a Jasco FP-8500 Spectrophotometer equipped with an ILF-835 integration sphere. Cyclic voltammetry experiments were carried out at room temperature under Argon in a glovebox with a Bio-Logic SAS SP-150 potentiostat. Photoreactions were performed on an easy-Photochem flow photoreactor from Vapourtec equipped with a photochemical reactor UV-150 equipped with white LEDs (for BACDs **1,6-BACD-Ph**, **1,7-BACD-Ph**, **1,6-BACD-CF_3**, **1,7-BACD-CF_3**, **1,6-BACD-OMe**, **1,7-BACD-OMe**, **C-1,6**, **C-1,7**, and AzaBPDI **S2**) or on an EvoluChem PhotoRedOx Box™ photoreactor equipped with a HCK1012-01-005 EvoluChem LED Spotlight (18 W) from HepatoChem (for AzaBPDIs **Br-aPDI-Ph**, **Br-aPDI-CF_3**, and **Br-aPDI-OMe**). Reactions requiring microwave irradiation were achieved using a Biotage® Initiator+ microwave system with a Robot Eight system. Nuclear magnetic resonance (NMR) ^{1}H and ^{13}C spectra were obtained on a Bruker 300 MHz Avance III spectrometer (300 MHz for ^{1}H), or 500 MHz Advance III HD spectrometer (500 MHz for ^{1}H, 470 MHz for ^{19}F and 125 MHz for ^{13}C), or 600 MHz Avance Neo spectrometer (600 MHz for ^{1}H and 150 MHz for ^{13}C). Chemical shifts were reported in ppm according to tetramethylsilane using the solvent residual signal as an internal reference ($CDCl_3$: δ_H = 7.26 ppm, δ_C = 77.16 ppm; $C_2D_2Cl_4$: δ_H = 6.00 ppm, δ_C = 73.78 ppm; toluene-d_8: δ_H = 2.09 ppm). Coupling constants (J) were given in Hz. Unless otherwise stated, NMR spectra were measured at 298 K. Resonance multiplicity was described as s (singlet), d (doublet), t (triplet), q (quartet), m (multiplet), dd (doublet of doublets), td (triplet of doublets), and br (broad signal). Carbon spectra were acquired with a complete decoupling for the proton. High resolution mass spectrometry (HRMS) was performed with a JEOL JMS-700 B/E. Chemicals were purchased from Sigma Aldrich, Acros Organics, Fisher Scientific, Alfa Aesar, Combi-Block, Fluorochem, and were used as received. Solvents were purchased from Sigma Aldrich, Fluorochem, or Fischer Scientific while deuterated solvents were purchased from Sigma Aldrich. Compounds **NH_2PDI**,[S1] **1,6-(NH_2)$_2$PDI**[S2], **1,7-(NH_2)$_2$PDI** [S2] and **S1**[S1] were synthesized following reported procedures in the literature.

Abbreviations. AFM: atomic force microscopy; AzaBPDI: azabenzannulatedperylene diimide; BACD: bisazacoronene diimide; DDQ: 2,3-dichloro-5,6-dicyanobenzoquinone; Fc: ferrocene; HOMO: highest occupied molecular orbital; HRMS: high resolution mass spectrometry; LUMO: lowest unoccupied molecular orbital; NMR: nuclear magnetic resonance; NMP: N-methyl-2-pyrrolidone; MS: mass spectrometry; MW: microwave; rt: room temperature; PC: principal component; TFA: trifluoroacetic acid; TLCV: cyclic voltammetry experiments under thin-layer; VT: variable temperature.

2. Synthesis

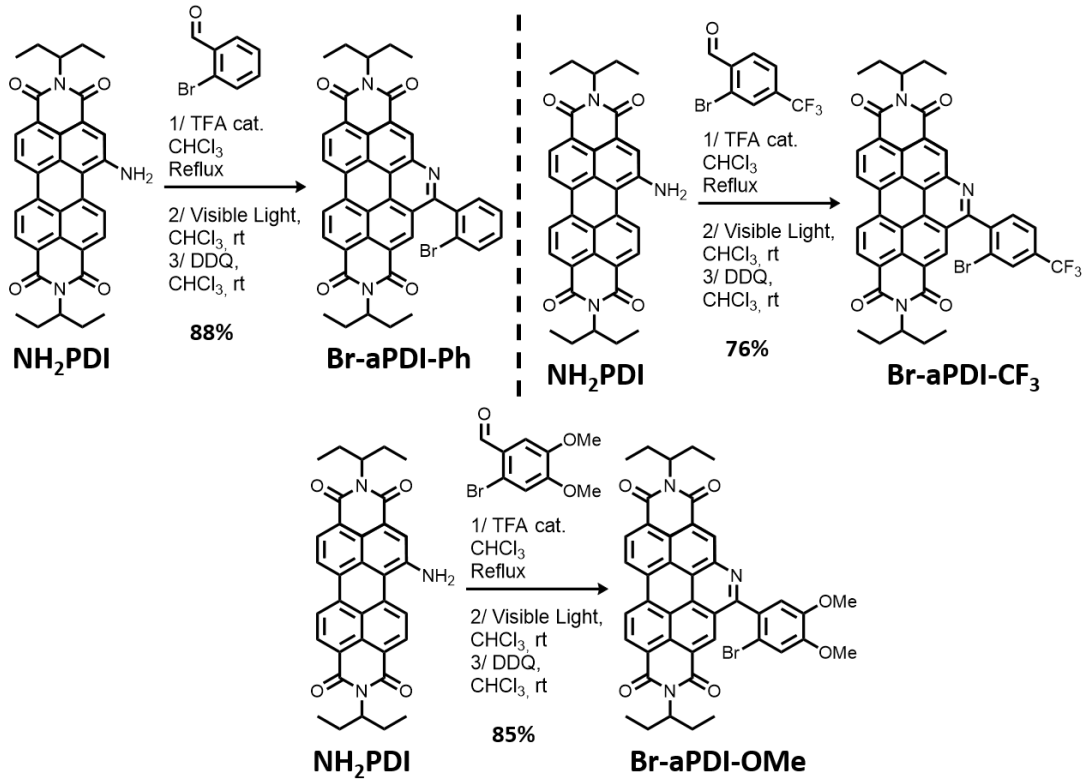

Scheme S1. Synthesis of AzaBPDIs **Br-aPDI-Ph**, **Br-aPDI-CF$_3$**, and **Br-aPDI-OMe**.

Compound Br-aPDI-Ph. 2-Bromobenzaldehyde (630 µL, 5.40 mmol) and TFA (50 µL) were added to a solution of **NH$_2$PDI** (1.00 g, 1.83 mmol) in $CHCl_3$ (30 mL). The solution was refluxed until the complete disappearance of the amine according to TLC. The resulting purple solution was concentrated to dryness and the solid was redissolved in $CHCl_3$ (35 mL). The solution was irradiated in a white light photoreactor (white LED, 18W) and stirred at rt until complete disappearance of the imine according to TLC. DDQ (415 mg, 1.83 mmol) was added to the resulting green solution and the mixture was stirred for 2 min at rt. The solution was washed with aqueous $NaHCO_{3(sat.)}$ (20 mL) and water (20 mL). The organic layer was dried over anhydrous $MgSO_4$ and the solvent was evaporated under reduced pressure. The crude material was purified by column chromatography (SiO_2, CH_2Cl_2) and further precipitated from

CH_2Cl_2/pentane to yield **Br-aPDI-Ph** (1.15 g, 88%) as an orange solid. ^{1}H NMR (500 MHz, $CDCl_3$): δ 9.66 (s, 1H), 9.37 (m, 2H), 9.20 – 9.10 (m, 3H), 7.89 (dd, *J* = 8.2, 1.1 Hz, 1H), 7.72 (dd, *J* = 7.5, 1.8 Hz, 1H), 7.66 (td, *J* = 7.5, 1.2 Hz, 1H), 7.55 (td, *J* = 7.8, 1.8 Hz, 1H), 5.22 – 5.09 (m, 2H), 2.33 (m, 4H), 2.00 (m, 4H), 0.97 (m, 12H). ^{13}C NMR (125 MHz, $CDCl_3$): δ 160.8, 144.5, 139.2, 134.6, 133.6, 133.1, 131.7, 131.3, 129.1, 128.6, 128.2, 127.0, 124.2, 123.9, 123.4, 123.3, 123.2, 122.9, 119.5, 58.2, 25.2, 11.6. HRMS calcd. for $C_{41}H_{33}N_3O_4Br$ ($[M+H]^+$): 710.1649, found: 710.1665.

Compound Br-aPDI-CF$_3$. 2-Bromo-4-(trifluoromethyl)benzaldehyde (350 mg, 1.38 mmol) and TFA (50 µL) were added to a solution of **NH$_2$PDI** (250 mg, 0.458 mmol) in $CHCl_3$ (10 mL). The solution was refluxed until the complete disappearance of the amine according to TLC. The resulting purple solution was concentrated to dryness and the solid was redissolved in $CHCl_3$ (35 mL). The solution was irradiated in a white light photoreactor (white LED, 18W) and stirred at rt until complete disappearance of the imine according to TLC. DDQ (136 mg, 0.599 mmol) was added to the resulting green solution and the mixture was stirred for 2 min at rt. The solution was washed with aqueous $NaHCO_{3(sat.)}$ (20 mL) and water (20 mL). The organic layer was dried over anhydrous $MgSO_4$ and the solvent was evaporated under reduced pressure. The crude material was purified by column chromatography (SiO_2, CH_2Cl_2) and further precipitated from CH_2Cl_2/pentane to yield **Br-aPDI-CF$_3$** (270 g, 76%) as an orange solid. ^{1}H NMR (500 MHz, $CDCl_3$): δ 9.64 (s, 1H), 9.41 (m, 2H), 9.19 (m, 2H), 9.05 (s, 1H), 8.17 (d, *J* = 1.6 Hz, 1H), 7.93 (dd, *J* = 8.0, 1.7 Hz, 1H), 7.86 (d, *J* = 7.8 Hz, 1H), 5.22 – 5.10 (m, 2H), 2.34 (m, 4H), 2.00 (m, 4H), 0.97 (m, 12H). ^{13}C NMR (125 MHz, $CDCl_3$): δ 159.3, 144.5, 142.8, 134.6, 133.5 (q, *J* = 33.4 Hz), 133.2, 132.2, 130.7 (q, *J* = 3.6 Hz), 129.2, 128.7, 127.1, 125.1 (q, *J* = 3.6 Hz), 124.4, 124.1, 123.8, 123.4, 123.2, 123.2 (q, *J* = 273.1 Hz), 122.5, 119.7, 58.3, 25.2, 11.6, 11.5. ^{19}F NMR (470 MHz, $CDCl_3$): δ −62.78 (s). HRMS calcd. for $C_{42}H_{31}N_3O_4F_3Br$ ($[M]^-$): 777.1456, found: 777.1448.

Compound Br-aPDI-OMe. 6-Bromoveratraldehyde (295 mg, 1.20 mmol) and TFA (50 µL) were added to a solution of **NH$_2$PDI** (200 mg, 0.367 mmol) in $CHCl_3$ (10 mL). The solution was refluxed until the complete disappearance of the amine according to TLC. The resulting purple solution was concentrated to dryness and the solid was redissolved in $CHCl_3$ (35 mL). The solution was irradiated in a white light photoreactor (white LED, 18W) and stirred at rt until complete disappearance of the imine according to TLC. DDQ (100 mg, 0.440 mmol) was added to the resulting green solution and the mixture was stirred for 2 min at rt. The solution was washed with aqueous $NaHCO_{3(sat.)}$ (20 mL) and water (20 mL). The organic layer was dried over anhydrous $MgSO_4$ and the solvent was evaporated under reduced pressure. The crude

material was purified by column chromatography (SiO_2, CH_2Cl_2 to CH_2Cl_2/MeOH 96:4) and further precipitated from CH_2Cl_2/pentane to yield **Br-aPDI-OMe** (240 g, 85%) as a dark orange solid. ^{1}H NMR (500 MHz, $CDCl_3$): δ 9.64 (s, 1H), 9.33 (m, 2H), 9.19 – 9.09 (m, 3H), 7.31 (s, 1H), 7.25 (s, 1H), 5.17 (m, 2H), 4.06 (s, 3H), 3.97 (s, 3H), 2.32 (m, 4H), 2.01 (m, 4H), 0.98 (m, 12H). ^{13}C NMR (125 MHz, $CDCl_3$): δ 160.8, 150.9, 149.2, 144.4, 134.5, 133.1, 131.1, 129.0, 128.6, 127.0, 124.1, 123.7, 123.3, 123.1, 123.0, 119.4, 116.0, 114.2, 113.8, 58.3, 56.6, 56.5, 25.3, 25.2, 11.6, 11.6. HRMS calcd. for $C_{43}H_{37}N_3O_6Br$ ([M+H]$^+$): 770.1860, found: 770.1858.

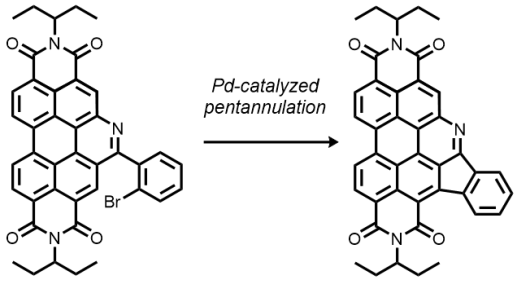

Scheme S2. Optimization of the synthesis of *ortho*-pentannuled AzaBPDI **aPDI-Ph**. Optimized conditions can be found in Table S1.

Table S1. Optimization of the intramolecular C−H *ortho*-pentannulation of AzaBPDI **Br-PDI-Ph**. All reactions have been carried out in NMP (6 mL, 12 mM) at 160 °C under MW irradiation for 2 h.

Entry	Catalyst	Ligand	Base	Yield, %
1	$Pd(OAc)_2$, 10%	$P(tBu)_3{\cdot}HBF_4$, 20%, PivOH, 30%	Cs_2CO_3, 2 equiv.	54
2	$Pd(dba)_2$, 10%	$P(Cy)_3{\cdot}HBF_4$, 20%	DBU, 3 equiv.	Inseparable mixture
3	$PdCl_2(PPh_3)_2$, 10%	/	DBU, 2 equiv.	61
4	$PdCl_2(MeCN)_2$, 10%	$P(Cy)_3{\cdot}HBF_4$, 20%	DBU, 2 equiv.	45
5	$Pd(dba)_2$, 10%	SPhos, 20%	DBU, 2 equiv.	83
6	$Pd(dba)_2$, 10%	SPhos, 20%	Cs_2CO_3, 2 equiv.	0

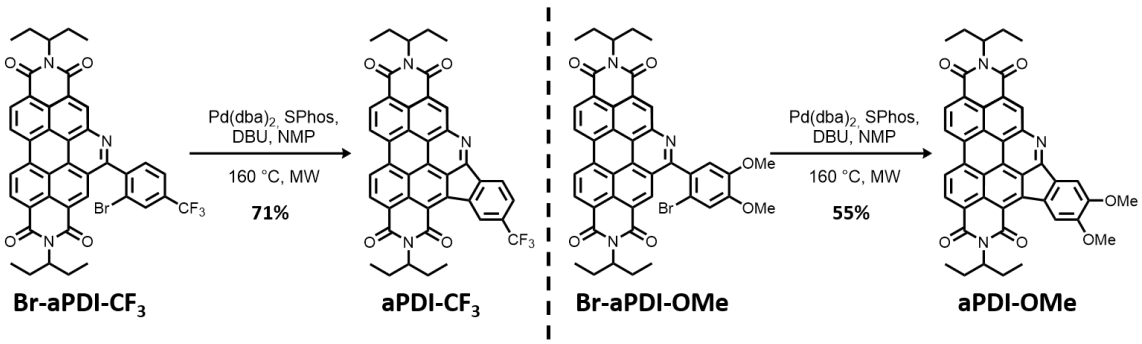

Scheme S3. Synthesis of *ortho*-pentannulated AzaBPDIs **aPDI-CF$_3$**, and **aPDI-OMe**.

General procedure for preparation of compounds aPDI-Ph, aPDI-CF_3, and aPDI-OMe.

Degassed anhydrous NMP (6 mL) and DBU (0.14 mmol, 2 equiv.) were added into a microwave tube containing either **Br-aPDI-Ph**, **Br-aPDI-CF_3**, or **Br-aPDI-OMe** (70 µmol, 1 equiv.), $Pd(dba)_2$ (7 µmol, 0.1 equiv.) and SPhos (14 µmol, 0.2 equiv.) under an argon atmosphere. The resulting mixture was stirred for 2 h at 160 °C under MW irradiation. The resulting suspension was diluted with CH_2Cl_2 (50 mL) and washed with H_2O (4 × 100 mL). The organic layer was dried over anhydrous $MgSO_4$ and the solvent was removed under vacuum. The crude was purified by column chromatography (SiO_2) using gradient of CH_2Cl_2/Et_2O as eluent.

Compound aPDI-Ph. Yield = 36 mg, 83%. ^{1}H NMR (500 MHz, $CDCl_3$): δ 9.22 (m, 1H), 9.11 (s, 1H), 8.83 – 8.67 (m, 4H), 8.00 (m, 1H), 7.54 (m, 2H), 5.17 (m, 2H), 2.37 (m, 4H), 2.22 – 2.00 (m, 4H), 1.09 (m, 12H). ^{13}C NMR (125 MHz, $CDCl_3$): δ 160.0, 146.2, 141.8, 141.8, 139.8, 133.4, 132.8, 132.5, 132.1, 131.4, 130.6, 126.4, 124.7, 124.1, 123.7, 123.5, 123.3, 123.3, 121.5, 118.3, 58.5, 58.3, 25.3, 11.8, 11.7. HRMS calcd. for $C_{41}H_{32}N_3O_4$ ($[M+H]^+$): 630.2387, found: 630.2384.

Compound aPDI-CF_3. Yield = 30 mg, 69%. ^{1}H NMR (500 MHz, $CDCl_3$): δ 9.65 (s, 1H), 9.20 (s, 1H), 8.92 – 8.77 (m, 4H), 8.19 (d, *J* = 7.7 Hz, 1H), 7.86 (d, *J* = 7.7 Hz, 1H), 5.22 (m, 2H), 2.40 (m, 4H), 2.13 (m, 4H), 1.09 (m, 12H). ^{13}C NMR (150 MHz, 328 K, $CDCl_3$): δ 164.1, 163.3, 158.0, 146.0, 144.5, 140.0, 139.7, 134.1, 134.0 (q, *J* = 32.0 Hz), 133.0, 132.3, 131.4, 130.1, 129.6, 129.3 (q, *J* = 3.4 Hz), 128.8 (q, *J* = 3.3 Hz), 126.3, 125.9, 124.8, 124.2, 124.1 (q, *J* = 272.6 Hz), 123.9, 123.7, 123.4, 123.0, 122.9, 122.8, 121.2, 121.0, 117.8, 103.8, 58.9, 58.6, 25.4, 25.4, 11.8, 11.8.^{19}F NMR (470 MHz, $CDCl_3$): δ −62.47 (s). HRMS calcd. for $C_{42}H_{30}N_3O_4F_3$ ($[M]^-$): 697.2194, found: 697.2199.

Compound aPDI-OMe. Yield = 21 mg, 47%. ^{1}H NMR (600 MHz, 328 K, $CDCl_3$): δ 9.05 (br s, 1H), 8.90 – 8.56 (br m, 5H), 7.47 (br s, 1H), 5.19 (m, 2H), 4.14 (two s, 6H), 2.38 (m, 4H), 2.12 (m, 4H), 1.09 (t, *J* = 7.4 Hz, 12H). ^{13}C NMR (150 MHz, 328 K, $CDCl_3$): δ 164.7, 160.5, 152.8, 151.9, 146.2, 142.3, 136.3, 134.1, 133.7, 133.2, 132.8, 131.0, 130.9, 129.3, 126.4, 125.7, 125.4, 124.5, 123.7, 123.5, 123.1, 122.8, 121.3, 118.8, 118.2, 115.5, 106.2, 58.4, 58.4, 56.6, 56.5, 25.4, 25.4, 11.8, 11.7. HRMS calcd. for $C_{43}H_{36}N_3O_6$ ($[M+H]^+$): 690.2599, found: 690.2596.

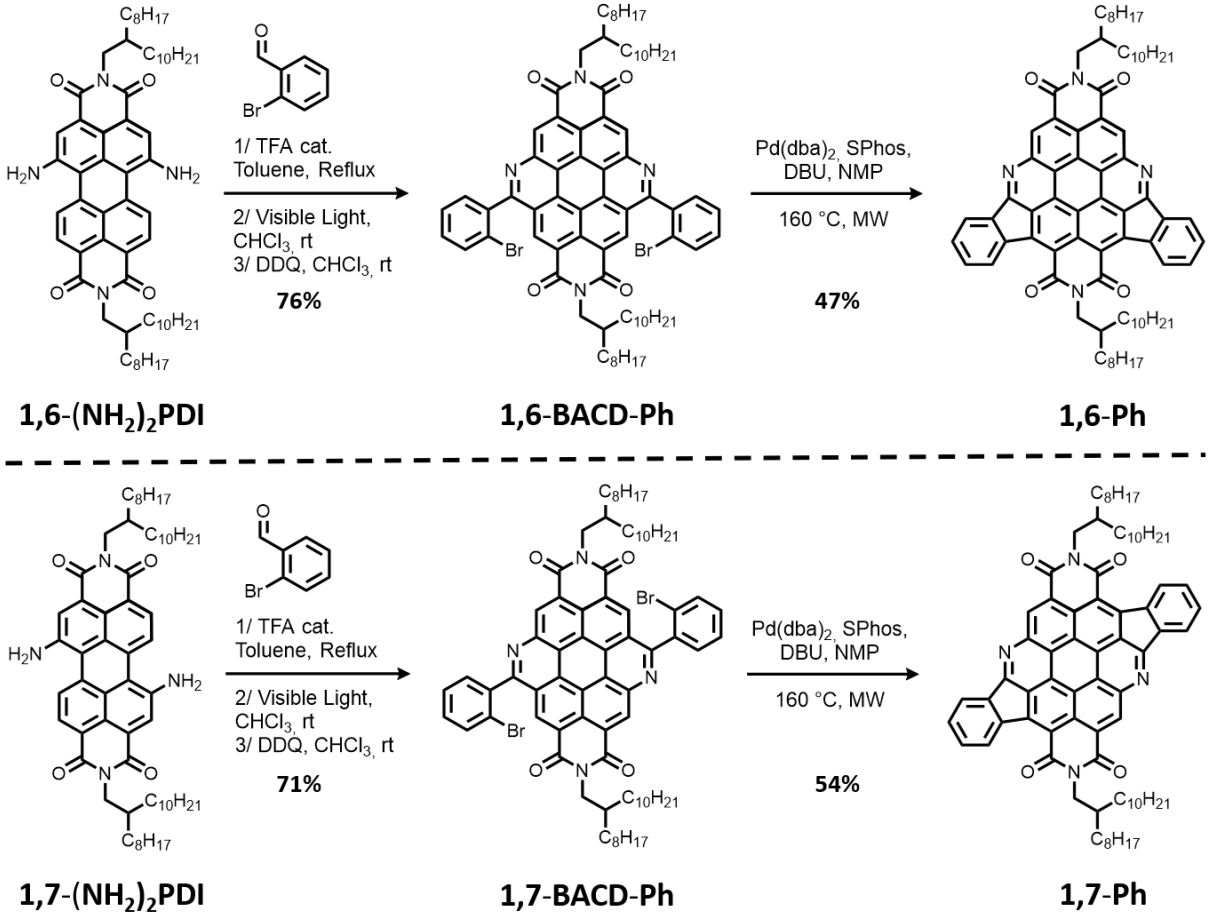

Scheme S4. Synthesis of regiopure *ortho*-pentannulated BACDs **1,6-Ph** and **1,7-Ph**.

Compound 1,6-BACD-Ph. 2-Bromobenzaldehyde (192 mg, 1.04 mmol) and 2 drops of TFA were added to a solution of **1,6-(NH$_2$)$_2$PDI** (102 mg, 0.104 mmol) in toluene (10 mL). The solution was refluxed for 1 h. The solvent was evaporated under reduced pressure and the resulting solution was redissolved in $CHCl_3$ (50 mL). The solution was irradiated in a continuous flow photoreactor (750 µL/min, 30 °C). Subsequently, DDQ (47 mg, 0.21 mmol) was added to the solution and the mixture was stirred for 1 h at room temperature. The crude material was purified by column chromatography (SiO_2, CH_2Cl_2/hexane 1:1, then CH_2Cl_2) to afford **1,6-BACD-Ph** (104 mg, 76%) as a yellow solid. ^{1}H NMR (500 MHz, 328 K, $CDCl_3$): δ 10.26 – 9.96 (m, 2H), 9.83 – 9.73 (m, 2H), 8.14 – 7.57 (m, 8H), 4.46 – 4.27 (m, 4H), 2.29 – 2.07 (m, 2H), 1.50 – 0.99 (m, 64H), 0.81 (m, 12H). ^{13}C NMR (125 MHz, $CDCl_3$): δ 164.4, 164.3, 164.1, 163.9, 162.4, 143.7, 143.2, 139.3, 139.1, 133.8, 133.7, 132.5, 132.4, 132.4, 132.2, 132.0, 131.9, 131.6, 129.9, 128.4, 128.3, 127.6, 127.3, 126.9, 125.7, 125.0, 123.3, 123.2, 123.2, 123.1, 123.1, 123.0, 122.8, 120.3, 119.7, 119.4, 118.2, 117.6, 45.7, 45.6, 45.4, 37.3, 37.2, 36.9, 36.9, 32.1, 32.0, 31.9, 31.8, 30.2, 29.9, 29.8, 29.8, 29.7, 29.4, 26.8, 26.7, 22.8, 14.2. The ^{1}H and ^{13}C spectra display two diastereoisomers because of the formation of atropisomers on account

of the presence of bromine atoms on the *ortho* position of the peripheral phenyl ring. HRMS calcd. for $C_{78}H_{95}N_4O_4Br_2$ ($[M+H]^+$): 1309.5715, found: 1309.5723.

Compound 1,6-Ph. Degassed anhydrous NMP (3 mL) and DBU (26 µL, 0.17 mmol) were added into a microwave tube containing **1,6-BACD-Ph** (56 mg, 43 µmol), $Pd(dba)_2$ (5 mg, 9 µmol) and SPhos (8 mg, 0.02 mmol) under argon. The mixture was stirred for 2 h at 160 °C under MW irradiation. The resulting suspension was poured into H_2O (400 mL), filtered and washed with H_2O (50 mL). The solid was purified by column chromatography (SiO_2, CH_2Cl_2/Et_2O 100:0 to 98:2, then CH_2Cl_2/MeOH 95:5) to afford **1,6-Ph** (23 mg, 47%) as an orange solid. ^{1}H NMR (600 MHz, 328 K, $CDCl_3$): δ 8.75 – 8.40 (m, 4H), 7.65 (br, 2H), 7.32 – 7.17 (m, 4H), 4.09 (br, 2H), 3.75 (br, 2H), 2.11 (br, 1H), 1.91 (br, 1H), 1.61 – 1.13 (m, 64H), 0.87 (m, 12H). ^{1}H NMR (500 MHz, 393 K, $C_2D_2Cl_4$): δ 9.14 (s, 2H), 9.00 (m, 2H), 8.027 (m, 2H), 7.51 (m, 4H), 4.33 (d, *J* = 7.2 Hz, 2H), 4.18 (d, *J* = 7.2 Hz, 2H), 2.25 (m, 1H), 2.14 (m, 1H), 1.67 – 1.23 (m, 64H), 0.90 (m, 12H). ^{13}C NMR (150 MHz, 328 K, $CDCl_3$): δ 163.1, 161.8, 160.7, 144.6, 140.8, 140.5, 139.9, 132.8, 131.9, 131.8, 128.7, 124.8, 123.8, 122.9, 122.7, 118.4, 117.6, 114.1, 45.7, 45.5, 37.4, 36.9, 32.2, 32.2, 32.2, 32.1, 32.0, 31.7, 30.5, 30.5, 30.0, 30.0, 29.9, 29.6, 29.6, 29.6, 26.8, 26.5, 22.9, 22.9, 22.8, 22.8, 14.2, 14.2, 14.2, 14.2. HRMS calcd. for $C_{78}H_{93}N_4O_4$ ($[M+H]^+$): 1149.7191, found: 1149.7178.

Compound 1,7-BACD-Ph. 2-Bromobenzaldehyde (200 mg, 1.08 mmol) and 2 drops of TFA were added to a solution of **1,7-$(NH_2)_2$PDI** (106 mg, 0.108 mmol) in toluene (10 mL). The solution was refluxed for 1 h. The solvent was evaporated under reduced pressure and the resulting solution was redissolved in $CHCl_3$ (50 mL). The solution was irradiated in a continuous flow photoreactor (750 µL/min, 30 °C). Subsequently, DDQ (49 mg, 0.22 mmol) was added to the solution and the mixture was stirred for 1 h at room temperature. The crude material was purified by column chromatography (SiO_2, CH_2Cl_2/petroleum ether 1:1, then CH_2Cl_2) to give **1,7-BACD-Ph** (101 mg, 71%) as a yellow solid. ^{1}H NMR (500 MHz, $CDCl_3$): δ 10.29 (s, 1H), 9.96 (br, 1H), 9.74 (s, 1H), 9.55 (br, 1H), 8.18 – 7.87 (m, 4H), 7.78 – 7.62 (m, 4H), 4.39 – 4.20 (m, 4H), 2.11 (m, 2H), 1.51 – 1.09 (m, 73H), 0.80 (m, 12H). ^{13}C NMR (125 MHz, $CDCl_3$): δ 164.4, 164.1, 164.0, 163.9, 163.6, 162.5, 162.4, 143.2, 142.7, 139.3, 139.0, 134.2, 133.8, 133.7, 132.1, 131.9, 131.6, 131.5, 130.6, 130.2, 129.9, 128.4, 128.3, 127.0, 126.3, 125.3, 125.0, 124.8, 124.6, 123.7, 123.3, 123.2, 123.2, 123.0, 119.9, 119.2, 118.7, 118.0, 45.6, 45.5, 37.1, 37.0, 32.0, 31.9, 30.3, 30.2, 29.8, 29.8, 29.8, 29.7, 29.4, 26.8, 26.7, 22.8, 14.2. The ^{1}H and ^{13}C spectra display two diastereoisomers because of the formation of atropisomers on

account of the presence of bromine atoms on the *ortho* position of the peripheral phenyl ring. HRMS calcd. for $C_{78}H_{95}N_4O_4Br_2$ ($[M+H]^+$): 1309.5715, found: 1309.5731.

Compound 1,7-Ph. Degassed anhydrous NMP (3 mL) and DBU (34 µL, 0.23 mmol) were added into a microwave tube containing **1,7-BACD-Ph** (74 mg, 56 µmol), $Pd(dba)_2$ (6 mg, 0.01 mmol) and SPhos (10 mg, 0.025 mmol) under argon. The mixture was stirred for 2 h at 160 °C under MW irradiation. The resulting suspension was poured into H_2O (600 mL), filtered and washed with H_2O (50 mL). The solid was purified by column chromatography (SiO_2, CH_2Cl_2/Et_2O 100:0 to 96:4, then CH_2Cl_2/MeOH 97:3) to afford **1,7-Ph** (35 mg, 54%) as an orange solid. ^{1}H NMR (500 MHz, $CDCl_3$): δ 8.62 – 8.02 (m, 4H), 7.46 (br, 2H), 7.14 (br, 4H), 3.70 (br, 4H), 1.85 (br, 2H), 1.44 – 1.16 (m, 64H), 0.86 (m, 12H). ^{1}H NMR (500 MHz, 393 K, $C_2D_2Cl_4$): δ 9.25 (s, 2H), 9.18 (d, *J* = 7.1 Hz, 2H), 8.10 (d, *J* = 6.5 Hz, 2H), 7.56 (m, 4H), 4.34 (d, *J* = 7.3 Hz, 5H), 2.22 (m, 3H), 1.67 – 1.22 (m, 85H), 0.89 (m, 16H).^{13}C NMR (125 MHz, $CDCl_3$): δ 162.2, 161.9, 161.6, 143.8, 140.5, 138.8, 132.7, 132.2, 132.0, 131.4, 125.4, 124.8, 123.6, 123.5, 118.9, 117.4, 116.4, 114.3, 45.0, 36.9, 32.2, 32.1, 31.5, 30.5, 30.0, 30.0, 30.0, 29.9, 29.9, 29.6, 29.6, 26.5, 22.9, 22.9, 14.3, 14.3. HRMS calcd. for $C_{78}H_{93}N_4O_4$ ($[M+H]^+$): 1149.7191, found: 1149.7180.

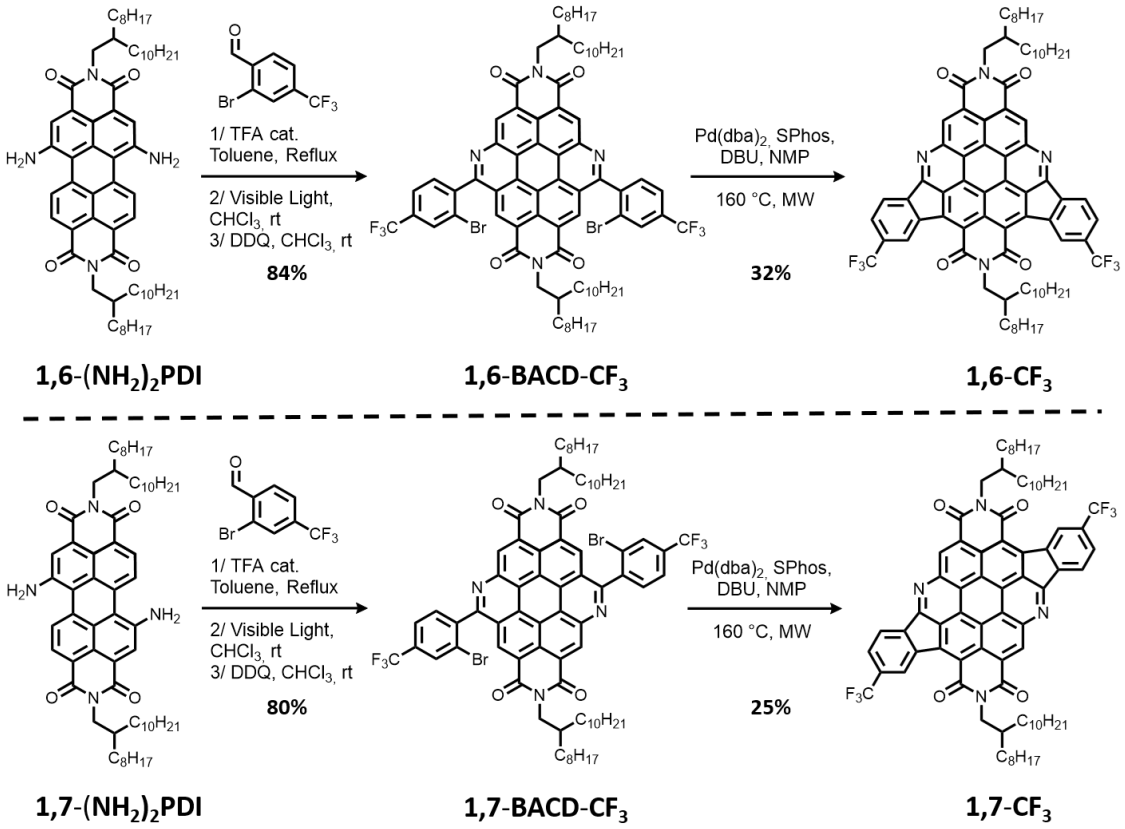

Scheme S5. Synthesis of regiopure *ortho*-pentannulated BACDs **1,6-CF$_3$** and **1,7-CF$_3$**.

Compound 1,6-BACD-CF$_3$. 2-Bromo-4-(trifluoromethyl)benzaldehyde (288 mg, 1.14 mmol) and 2 drops of TFA were added to a solution of **1,6-(NH$_2$)$_2$PDI** (112 mg, 0.114 mmol) in toluene (10 mL). The solution was refluxed for 1 h. The solvent was evaporated under reduced pressure and the resulting solution was redissolved in $CHCl_3$ (50 mL). The solution was irradiated in a continuous flow photoreactor (750 µL/min, 30 °C). Subsequently, DDQ (52 mg, 0.23 mmol) was added to the solution and the mixture was stirred for 1 h at room temperature. The crude material was purified by column chromatography (SiO_2, CH_2Cl_2/petroleum ether 1:1, then CH_2Cl_2) to give **1,6-BACD-CF$_3$** (138 mg, 84%) as a yellow solid. ^{1}H NMR (500 MHz, 328 K, $CDCl_3$): δ 10.03 – 9.27 (m, 4H), 8.73 – 7.90 (m, 6H), 4.44 – 3.90 (m, 4H), 2.24 – 1.81 (m, 2H), 1.58 – 1.09 (m, 64H), 0.81 (m, 12H). ^{13}C NMR (125 MHz, $CDCl_3$): δ 164.0, 163.7, 162.6, 161.2, 161.0, 143.4, 142.7, 142.2, 134.0 (q, *J* = 33.4 Hz), 133.1, 132.6, 132.1, 132.0, 131.5, 130.9, 130.7 (q, *J* = 3.5 Hz), 129.9, 127.6, 127.3, 127.3, 126.1, 125.4, 125.2 (q, *J* = 3.3 Hz), 123.8, 123.7, 123.7, 123.4, 123.2 (q, *J* = 273.0 Hz), 123.0, 122.5, 122.3, 121.3, 119.7, 119.4, 118.5, 118.4, 117.9, 116.4, 45.9, 45.8, 45.3, 45.0, 37.5, 37.3, 36.8, 36.7, 33.8, 32.0, 32.0, 32.0, 32.0, 31.8, 31.7, 30.3, 30.3, 30.2, 30.2, 30.2, 30.1, 29.9, 29.9, 29.8, 29.8, 29.8, 29.8, 29.7, 29.7, 29.5, 29.5, 29.4, 29.4, 26.9, 26.8, 26.6, 22.8, 22.8, 14.2, 14.2. The ^{1}H and ^{13}C spectra display two diastereoisomers because of the formation of atropisomers on account of the presence of bromine atoms on the *ortho* position of the peripheral phenyl ring. ^{19}F NMR (470 MHz, 328 K, $CDCl_3$): δ −62.88. HRMS calcd. for $C_{80}H_{93}N_4O_4F_6Br_2$ ($[M+H]^+$): 1445.5462, found: 1445.5477.

Compound 1,6-CF$_3$. Degassed anhydrous NMP (3 mL) and DBU (38 µL, 0.25 mmol) were added into a microwave tube containing **1,6-BACD-CF$_3$** (91 mg, 63 µmol), $Pd(dba)_2$ (7 mg, 0.01 mmol) and SPhos (10 mg, 0.025 mmol) under argon. The mixture was stirred for 2 h at 160 °C under MW irradiation. The resulting suspension was poured into H_2O (500 mL), filtered and washed with H_2O (50 mL). The solid was purified by column chromatography (SiO_2, CH_2Cl_2/petroleum ether 50:50 to 90:10, then CH_2Cl_2/Et_2O 95:5) to afford **1,6-CF$_3$** (26 mg, 32%) as an orange solid. ^{1}H NMR (500 MHz, 328 K, $CDCl_3$): δ 9.38 (s, 2H), 8.84 (s, 2H), 8.09 (d, *J* = 7.4 Hz, 2H), 7.89 (d, *J* = 7.5 Hz, 2H), 4.20 (m, 4H), 2.11 (m, 2H), 1.55 – 0.98 (m, 64H), 0.84 (m, 12H). ^{1}H NMR (500 MHz, 393 K, $C_2D_2Cl_4$): δ 9.80 (s, 2H), 9.55 (s, 2H), 8.46 (d, *J* = 7.5 Hz, 2H), 8.02 (d, *J* = 7.9 Hz, 2H), 4.56 – 4.39 (m, 4H), 2.26 (m, 2H), 1.56 – 1.19 (m,

64H), 0.90 – 0.81 (m, 12H). ^{13}C NMR (125 MHz, $CDCl_3$): δ 162.5, 162.2, 159.6, 144.6, 143.4, 141.4, 139.1, 135.0, 131.9, 129.7, 128.8, 124.9, 124.0, 123.1, 122.7, 120.0, 117.8, 114.2, 45.5, 45.4, 40.3, 40.2, 38.3, 37.5, 37.1, 36.8, 33.9, 33.6, 32.9, 32.6, 32.1, 32.1, 31.7, 31.6, 30.4, 30.4, 30.3, 30.0, 29.9, 29.6, 29.6, 29.5, 29.5, 29.1, 27.3, 26.9, 26.6, 26.4, 23.3, 22.9, 22.8, 22.8, 14.3, 14.3, 14.3, 14.2. ^{19}F NMR (470 MHz, $CDCl_3$): δ −62.65. HRMS calcd. for $C_{80}H_{91}N_4O_4F_6$ ($[M+H]^+$): 1285.6939, found: 1285.6970.

Compound 1,7-BACD-CF$_3$. 2-Bromo-4-(trifluoromethyl)benzaldehyde (268 mg, 1.06 mmol) and 2 drops of TFA were added to a solution of **1,7-(NH$_2$)$_2$PDI** (104 mg, 0.106 mmol) in toluene (10 mL). The solution was refluxed for 1 h. The solvent was evaporated under reduced pressure and the resulting solution was redissolved in $CHCl_3$ (50 mL). The solution was irradiated in a continuous flow photoreactor (750 µL/min, 30 °C). Subsequently, DDQ (48 mg, 0.21 mmol) was added to the solution and the mixture was stirred for 1 h at room temperature. The crude material was purified by column chromatography (SiO_2, CH_2Cl_2/petroleum ether 1:1, then CH_2Cl_2) to yield **1,7-BACD-CF$_3$** (122 mg, 80%) as a yellow solid. ^{1}H NMR (300 MHz, $CDCl_3$): δ 10.32 – 10.06 (m, 2H), 9.72 – 9.56 (m, 2H), 8.30 – 7.95 (m, 6H), 4.33 (m, 4H), 2.12 (br, 2H), 1.53 – 1.07 (m, 64H), 0.80 (m, 12H). ^{13}C NMR (125 MHz, $CDCl_3$): δ 164.2, 164.0, 163.9, 163.6, 161.2, 161.1, 143.2, 142.9, 142.8, 142.6, 134.4, 134.0, 133.9 (q, *J* = 33.5 Hz), 132.4, 130.9 (q, *J* = 3.4 Hz), 130.0, 129.9, 129.8, 127.0, 126.7, 125.5, 125.3, 125.2, 125.0, 124.0, 123.8, 123.7, 123.7, 123.2 (q, *J* = 273.0 Hz), 122.9, 122.8, 119.9, 119.5, 118.8, 118.4, 45.7, 45.6, 37.1, 37.1, 32.0, 32.0, 31.9, 30.2, 29.9, 29.8, 29.8, 29.7, 29.7, 29.4, 26.7, 26.7, 26.7, 22.8, 14.2. The ^{1}H and ^{13}C spectra display two diastereoisomers because of the formation of atropisomers on account of the presence of bromine atoms on the *ortho* position of the peripheral phenyl ring. ^{19}F NMR (470 MHz, 328 K, $CDCl_3$): δ −62.88. HRMS calcd. for $C_{80}H_{93}N_4O_4F_6Br_2$ ($[M+H]^+$): 1445.5462, found: 1445.5491.

Compound 1,7-CF$_3$. Degassed anhydrous NMP (3 mL) and DBU (22 µL, 0.15 mmol) were added into a microwave tube containing **1,7-BACD-CF$_3$** (54 mg, 37 µmol), $Pd(dba)_2$ (4 mg, 7 µmol) and SPhos (6 mg, 0.01 mmol) under argon. The mixture was stirred for 2 h at 160 °C under MW irradiation. The resulting suspension was poured into H_2O (400 mL), filtered and washed with H_2O (50 mL). The solid was purified by column chromatography (SiO_2, CH_2Cl_2/petroleum ether 50:50 to 100:0) to afford **1,7-CF$_3$** (12 mg, 25%) as an orange solid. ^{1}H

NMR (500 MHz, 328 K, $CDCl_3$): δ 9.39 (s, 2H), 8.86 (s, 2H), 7.99 (d, *J* = 7.4 Hz, 2H), 7.78 (d, *J* = 7.5 Hz, 2H), 4.27 (d, *J* = 7.4 Hz, 4H), 2.13 (br, 2H), 1.55 – 1.06 (m, 64H), 0.84 (m, 12H). ^{1}H NMR (500 MHz, 393 K, $C_2D_2Cl_4$): δ 9.71 (s, 2H), 9.50 (s, 2H), 8.35 (d, *J* = 7.6 Hz, 2H), 7.94 (d, *J* = 7.6 Hz, 2H), 4.48 (d, *J* = 7.2 Hz, 4H), 2.27 (m, 2H), 1.55 – 1.22 (m, 64H), 0.88 (m, 12H). ^{13}C NMR (125 MHz, 328 K, $CDCl_3$): δ 162.8, 162.4, 161.3, 144.8, 144.0, 141.7, 138.5, 133.0, 129.6, 128.9, 126.5, 126.2, 125.0, 124.5, 124.1, 122.8, 119.4, 117.3, 115.1, 45.7, 37.8, 37.4, 37.2, 34.1, 33.8, 32.1, 32.1, 32.0, 30.4, 29.9, 29.6, 29.5, 27.0, 26.7, 23.3, 22.8, 22.8, 14.1, 14.1. ^{19}F NMR (470 MHz, 328 K, $CDCl_3$): δ −62.99. HRMS calcd. for $C_{80}H_{91}N_4O_4F_6$ ($[M+H]^+$): 1285.6939, found: 1285.6970.

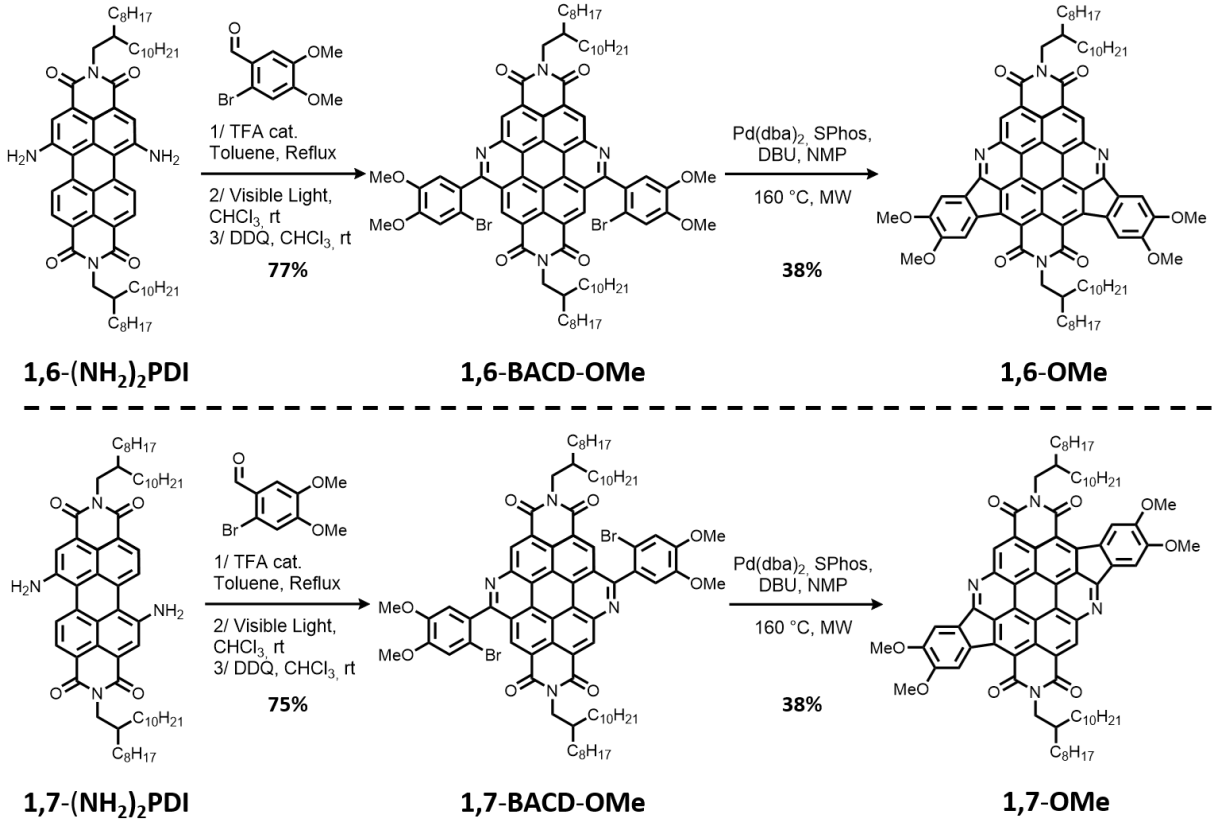

Scheme S6. Synthesis of regiopure *ortho*-pentannulated BACDs **1,6-OMe** and **1,7-OMe**.

Compound 1,6-BACD-OMe. 6-Bromoveratraldehyde (250 mg, 1.02 mmol) and 2 drops of TFA were added to a solution of **1,6-(NH2)2PDI** (100 mg, 0.102 mmol) in toluene (10 mL). The solution was refluxed for 1 h. The solvent was evaporated and the resulting solution was redissolved in $CHCl_3$ (50 mL). The solution was irradiated in a continuous flow photoreactor (750 µL/min, 30 °C). Subsequently, DDQ (46 mg, 0.20 mmol) was added to the

solution and the mixture was stirred for 1 h at room temperature. The crude material was purified by column chromatography (SiO_2, CH_2Cl_2/petroleum ether 1:1, then CH_2Cl_2/Et_2O 100:0 to 98:2) to give **1,6-BACD-OMe** (112 mg, 77%) as an orange solid. ^{1}H NMR (500 MHz, 328 K, $CDCl_3$): δ 10.18 – 7.88 (m, 6H), 7.55 – 7.08 (m, 2H), 4.52 – 3.93 (m, 16H), 2.25 – 1.01 (m, 66H), 0.79 (m, 12H). ^{13}C NMR (125 MHz, $CDCl_3$): δ 163.7, 162.5, 151.1, 149.3, 148.8, 143.4, 141.7, 133.9, 132.9, 132.4, 132.0, 131.1, 130.6, 130.3, 129.9, 128.6, 126.8, 125.5, 124.6, 123.1, 123.0, 122.8, 117.8, 116.2, 115.9, 115.8, 115.6, 115.4, 114.6, 113.7, 113.1, 112.9, 56.8, 56.7, 45.7, 44.9, 37.4, 36.9, 32.0, 32.0, 32.0, 32.0, 31.7, 30.4, 30.2, 30.20, 29.9, 29.8, 29.8, 29.7, 29.7, 29.7, 29.5, 29.5, 29.4, 26.8, 26.6, 26.6, 22.8, 22.8, 22.7, 14.2, 14.2, 14.2. The ^{1}H and ^{13}C spectra display two diastereoisomers because of the formation of atropisomers on account of the presence of bromine atoms on the *ortho* position of the peripheral phenyl ring. HRMS calcd. for $C_{82}H_{103}N_4O_8Br_2$ ($[M+H]^+$): 1429.6137, found: 1429.6151.

Compound 1,6-OMe. Degassed anhydrous NMP (3 mL) and DBU (15 µL, 0.10 mmol) were added into a microwave tube containing **1,6-BACD-OMe** (36 mg, 25 µmol), $Pd(dba)_2$ (3 mg, 5 µmol) and SPhos (4 mg, 0.01 mmol) under argon. The mixture was stirred for 2 h at 160 °C under MW irradiation. The resulting suspension was poured into H_2O (300 mL), filtered and washed with H_2O (50 mL). The solid was purified by column chromatography (SiO_2, CH_2Cl_2/MeOH 100:0 to 97:3) to afford **1,6-OMe** (12 mg, 38%) as a brown solid. ^{1}H NMR (500 MHz, 393 K, $C_2D_2Cl_4$): δ 9.15 (s, 2H), 8.68 (s, 2H), 7.52 (s, 2H), 4.33 – 4.14 (m, 16H), 2.16 (m, 2H), 1.53 – 1.07 (m, 64H), 0.89 (m, 12H). ^{13}C NMR (125 MHz, 393 K, $C_2D_2Cl_4$): δ 163.4, 162.8, 161.3, 152.3, 152.1, 145.1, 135.5, 134.8, 131.8, 124.6, 117.9, 115.8, 56.3, 55.9, 37.0, 32.2, 32.1, 31.6, 31.6, 31.6, 29.9, 29.5, 29.5, 29.4, 29.4, 29.3, 29.0, 29.0, 29.0, 28.9, 26.5, 22.3, 22.2, 13.6. MS: calcd. for $C_{82}H_{100}N_4O_8$ ($[M]^-$): 1268.8 found: 1268.6. HRMS calcd. for $C_{82}H_{101}N_4O_8$ ($[M+H]^+$): 1269.7614, found: 1269.7638.

Compound 1,7-BACD-OMe. 6-Bromoveratraldehyde (107 mg, 1.09 mmol) and 2 drops of TFA were added to a solution of **1,7-$(NH_2)_2$PDI** (107 mg, 0.109 mmol) in toluene (10 mL). The solution was refluxed for 1 h. The solvent was removed and the resulting solution was redissolved in $CHCl_3$ (50 mL). The solution was irradiated in a continuous flow photoreactor (750 µL/min, 30 °C). Subsequently, DDQ (50 mg, 0.22 mmol) was added to the solution and the mixture was stirred for 1 h at room temperature. The crude material was

purified by column chromatography (SiO_2, CH_2Cl_2/Et_2O 100:0 to 98:2) to yield **1,7-BACD-OMe** (117 mg, 75%) as an orange solid. ^{1}H NMR (500 MHz, 328 K, $CDCl_3$): δ 10.33 – 9.26 (m, 4H), 8.06 – 7.29 (m, 4H), 4.44 – 3.93 (m, 16H), 2.13 (m, 2H), 1.55 – 0.95 (m, 64H), 0.80 (m, 12H). ^{13}C NMR (125 MHz, $CDCl_3$): δ 164.4, 164.2, 162.5, 162.0, 151.2, 149.3, 143.2, 134.1, 131.2, 131.0, 130.6, 129.9, 127.0, 125.3, 125.0, 123.7, 123.5, 119.9, 118.7, 116.2, 115.8, 115.5, 114.4, 113.8, 113.1, 56.8, 56.7, 56.6, 56.5, 45.6, 45.3, 37.1, 32.1, 32.0, 32.0, 31.9, 31.8, 30.3, 30.2, 29.9, 29.9, 29.8, 29.8, 29.8, 29.8, 29.7, 29.7, 29.5, 29.5, 29.5, 29.4, 26.7, 26.6, 22.8, 22.8, 22.8, 14.2, 14.2, 14.2. The ^{1}H and ^{13}C spectra display two diastereoisomers because of the formation of atropisomers on account of the presence of bromine atoms on the *ortho* position of the peripheral phenyl ring. HRMS calcd. for $C_{82}H_{103}N_4O_8Br_2$ ($[M+H]^+$): 1429.6137, found: 1429.6140.

Compound 1,7-OMe. Degassed anhydrous NMP (3 mL) and DBU (28 µL, 0.19 mmol) were added into a microwave tube containing **1,7-BACD-OMe** (68 mg, 48 µmol), $Pd(dba)_2$ (5 mg, 0.01 mmol) and SPhos (8 mg, 0.02 mmol) under argon. The mixture was stirred for 2 h at 160 °C under MW irradiation. The resulting suspension was poured into H_2O (400 mL), filtered and washed with H_2O (50 mL). The solid was purified by column chromatography (SiO_2, CH_2Cl_2/MeOH 100:0 to 97:3) to afford **1,7-OMe** (23 mg, 38%) as a brown solid. ^{1}H NMR (500 MHz, 393 K, $C_2D_2Cl_4$): δ 10.32 – 7.05 (br, 6H), 4.86 – 3.55 (br, 16H), 2.78 – 2.02 (br, 2H), 1.60 – 0.73 (br, 76H). Despite trying to record NMR spectra in different NMR solvents, i.e., $CDCl_3$, $C_2D_2Cl_4$, toluene-d_8, at very high temperature, 55 °C, 120 °C, and 100 °C, respectively, ^{1}H NMR spectra of compound **1,7-OMe** exhibit extremely broad resonances in the aliphatic region while in the aromatic region protons appear to be almost silent in all solvents. This phenomenon is attributed to the fact that compound **1,7-OMe** is strongly self-associating, creating self-assembled supramolecular nanostructures rendering the aromatic protons silent in NMR spectroscopy on account of the π-π interactions between the BACD cores. For the exact same reason, its 13C NMR spectrum at high temperature is silent in the aromatic region of the spectrum. ^{13}C NMR (500 MHz, 393 K, $C_2D_2Cl_4$): δ 32.1, 31.3, 29.8, 29.4, 28.9, 26.5, 22.2, 13.5. MS: calcd. for $C_{82}H_{100}N_4O_8$ ($[M]^-$): 1268.8 found: 1268.7. HRMS calcd. for $C_{82}H_{101}N_4O_8$ ($[M+H]^+$): 1269.7614, found: 1269.7603.

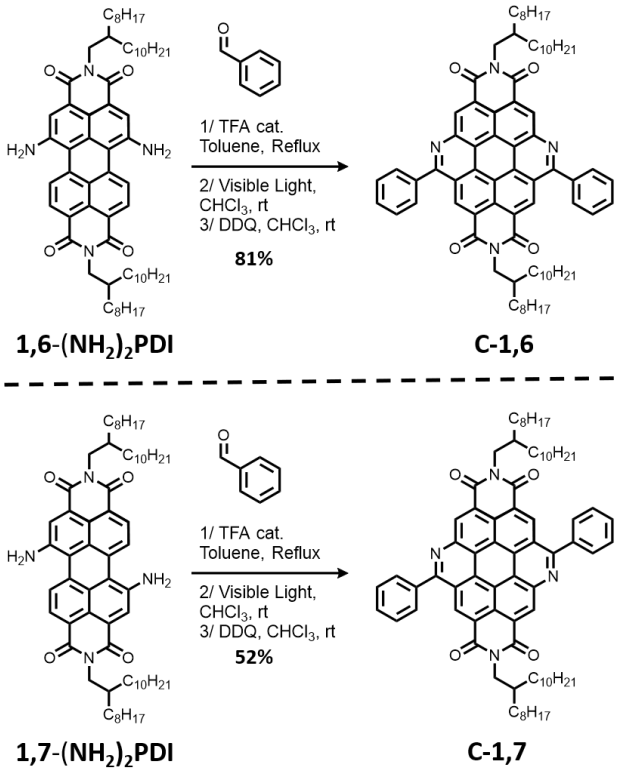

Scheme S7. Synthesis of regiopure BACDs **C-1,6** and **C-1,7**.

Compound C-1,6. Benzaldehyde (190 µL, 1.83 mmol) and 2 drops of TFA were added to a solution of **1,6-$(NH_2)_2$PDI** (180 mg, 0.183 mmol) in toluene (6 mL). The solution was refluxed for 1 h. The solvent was removed and the resulting solution was redissolved in $CHCl_3$ (35 mL). The solution was irradiated in a continuous flow photoreactor (600 µL/min, 30 °C). Subsequently, DDQ (125 mg, 0.551 mmol) was added to the solution and the mixture was stirred for 2 h at room temperature. The crude material was purified by column chromatography (SiO_2, $CHCl_3$/Et_2O 100:0 to 98:2) to yield **C-1,6** (172 mg, 81%) as an orange solid. ^{1}H NMR (600 MHz, $CDCl_3$): δ 9.98 (s, 2H), 9.85 (s, 2H), 8.21 (m, 4H), 7.86 – 7.77 (m, 6H), 4.35 (m, 4H), 2.15 (m, 2H), 1.52 – 1.11 (m, 64H), 0.79 (m, 12H). ^{13}C NMR (150 MHz, $CDCl_3$): δ 163.9, 162.8, 143.3, 138.3, 132.3, 131.5, 131.3, 130.3, 129.5, 127.1, 126.5, 125.1, 122.2, 121.8, 121.7, 119.2, 118.8, 116.6, 45.7, 45.4, 37.1, 36.9, 32.0, 32.0, 31.9, 31.9, 30.3, 30.3, 30.3, 29.8, 29.8, 29.8, 29.8, 29.5, 29.5, 26.8, 26.8, 26.7, 22.8, 14.2. HRMS calcd. for $C_{78}H_{97}N_4O_4$ ($[M+H]^+$): 1153.7504, found: 1153.7532.

Compound C-1,7. Benzaldehyde (190 µL, 1.83 mmol) and 2 drops of TFA were added to a solution of **1,7-$(NH_2)_2$PDI** (180 mg, 0.183 mmol) in toluene (6 mL). The solution was refluxed for 1 h. The solvent was removed and the resulting solution was redissolved in $CHCl_3$

(35 mL). The solution was irradiated in a continuous flow photoreactor (600 µL/min, 30 °C). Subsequently, DDQ (166 mg, 0.731 mmol) was added to the solution and the mixture was stirred for 2 h at room temperature. The crude material was purified by column chromatography (SiO_2, $CHCl_3$/Et_2O 100:0 to 98:2) to yield **C-1,7** (111 mg, 52%) as an orange solid. ^{1}H NMR (600 MHz, $CDCl_3$): δ 9.74 (s, 2H), 9.44 (s, 2H), 8.04 (d, *J* = 7.0 Hz, 4H), 7.69 – 7.61 (m, 6H), 4.31 (d, *J* = 7.5 Hz, 4H), 2.10 (m, 2H), 1.52 – 1.11 (m, 64H), 0.79 (m, 12H). ^{13}C NMR (150 MHz, $CDCl_3$): δ 163.7, 163.3, 162.6, 142.2, 137.9, 132.5, 131.0, 130.1, 129.8, 129.2, 125.4, 123.8, 123.5, 122.6, 121.7, 118.2, 116.5, 45.5, 37.0, 32.0, 32.0, 31.9, 30.3, 29.9, 29.8, 29.8, 29.5, 29.5, 26.8, 22.8, 22.8, 14.2. HRMS calcd. for $C_{78}H_{97}N_4O_4$ ($[M+H]^+$): 1153.7504, found: 1153.7534.

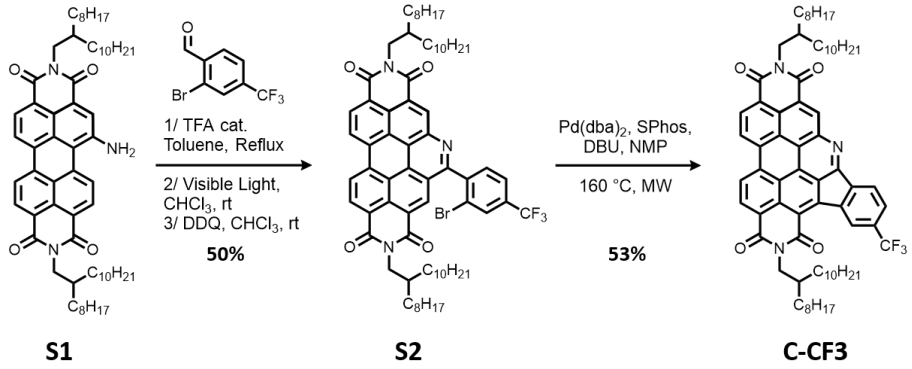

Scheme S8. Synthesis of *ortho*-pentannulated AzaBPDI **C-CF$_3$**.

Compound S2. 2-Bromo-4-(trifluoromethyl)benzaldehyde (112 mg, 0.442 mmol) and 2 drops of TFA were added to a solution of **S1** (85 mg, 0.088 mmol) in toluene (4 mL). The solution was refluxed for 3 h. The solvent was removed and the resulting solution was redissolved in $CHCl_3$ (35 mL). The solution was irradiated in a continuous flow photoreactor (300 µL/min, 30 °C). Subsequently, DDQ (44 mg, 0.21 mmol) was added to the solution and the mixture was stirred for 2 h at room temperature. The crude material was purified by column chromatography (SiO_2, $CHCl_3$/petroleum ether 70:30 to 100:0) and further precipitated from $CHCl_3$/MeOH to yield **S2** (53 mg, 50%) as a greenish solid. ^{1}H NMR (500 MHz, $CDCl_3$): δ 9.42 (s, 1H), 9.22 – 8.93 (m, 5H), 8.18 (s, 1H), 7.97 (m, 2H), 4.18 (m, 4H), 2.03 (m, 2H), 1.49 – 1.11 (m, 64H), 0.82 (td, J = 6.9, 3.0 Hz, 12H). ^{13}C NMR (125 MHz, $CDCl_3$): δ 163.7, 163.7, 163.4, 159.4, 144.1, 142.6, 134.7, 134.2, 133.6 (q, *J* = 33.1 Hz), 132.8, 132.4, 131.6, 131.3, 130.7 (q, *J* = 3.1 Hz), 129.7, 128.8, 128.2, 126.5, 126.0, 125.2 (q, *J* = 3.4 Hz), 124.2, 124.1,

123.9, 123.7, 123.2 (q, J = 273.0 Hz), 123.1, 122.9, 122.8, 122.6, 122.3, 119.3, 45.3, 45.1, 37.0, 36.8, 32.0, 32.0, 32.0, 31.9, 30.2, 29.9, 29.8, 29.8, 29.7, 29.5, 26.7, 26.7, 26.6, 22.8, 14.2. ^{19}F NMR (470 MHz, $CDCl_3$): δ −62.78. HRMS calcd. for $C_{72}H_{92}N_3O_4BrF_3$ ($[M+H]^+$): 1198.6218, found: 1198.6254.

Compound C-CF$_3$. Degassed anhydrous NMP (2 mL) and DBU (23 µL, 0.15 mmol) were added into a microwave tube containing **S2** (45 mg, 38 µmol), $Pd(dba)_2$ (4 mg, 5 µmol) and SPhos (3 mg, 0.01 mmol) under argon. The mixture was stirred for 2 h at 160 °C under MW irradiation. The resulting suspension was poured into H_2O (70 mL), filtered and washed with H_2O (50 mL). The solid was purified by column chromatography (SiO_2, $CHCl_3$/cyclohexane 80:20 to 100:0) and further precipitated from $CHCl_3$/MeOH to afford **C-CF$_3$** (24 mg, 53%) as an orange solid. ^{1}H NMR (500 MHz, $CDCl_3$): δ 9.34 (s, 1H), 8.79 – 8.42 (m, 5H), 7.93 – 7.72 (m, 2H), 4.27 – 4.02 (m, 4H), 2.11 – 1.95 (m, 2H), 1.52 – 1.08 (m, 64H), 0.82 (m, 12H). ^{13}C NMR (125 MHz, $CDCl_3$): δ 163.2, 163.2, 162.8, 162.5, 157.5, 145.5, 143.9, 139.3, 138.9, 133.9 (q, J = 32.2 Hz), 133.7, 132.6, 131.9, 131.1, 129.3, 129.2, 128.6, 125.6, 125.3, 124.0, 123.9, 123.6 (q, J = 273.2 Hz), 123.3, 122.8, 122.7, 122.3, 122.2, 120.9, 120.4, 119.7, 117.1, 45.2, 45.0, 37.1, 36.8, 32.1, 32.1, 32.1, 31.9, 31.9, 31.8, 31.7, 30.4, 30.3, 29.9, 29.9, 29.8, 29.8, 29.6, 29.5, 29.5, 26.7, 26.5, 22.8, 22.8, 22.8, 22.8, 14.3, 14.2, 14.2. ^{19}F NMR (470 MHz, $CDCl_3$): δ −62.46. HRMS calcd. for $C_{72}H_{91}N_3O_4F_3$ ($[M+H]^+$): 1118.6956, found: 1118.6677.

3. Absorption and Emission Spectroscopies

Absorption spectra were recorded at 20 °C at various concentration between *ca.* 3×10^{-7} M and *ca.* 4×10^{-4} M in $CHCl_3$. Absorption spectra of thin films were prepared on glass slides, previously cleaned with soapy water, deionized water, acetone and ethanol, using a spin coater by depositing 80 µL of a solution of the compound (10 mg/mL in $CHCl_3$, 1500 rpm for 60 s). After recording a first spectrum, the thin films were annealed for 10 min at 100 °C. The fluorescence spectra were recorded at 20 °C at a concentration of *ca.* 1.0×10^{-6} M. For fluorescence measurements, a fixed slit-width of 5.0 nm and an integration time of 200 nm/s were selected.

Table S2. Fluorescence quantum yields of compounds **aPDI-Ph**, **aPDI-CF$_3$**, **aPDI-OMe**, **1,6-Ph**, **1,7-Ph**, **1,6-CF$_3$**, **1,7-CF$_3$**, **1,6-OMe**, and **1,7-OMe**.

Compound	Φ_f / %
aPDI-Ph	14
aPDI-CF$_3$	20
aPDI-OMe	Not fluorescent
1,6-Ph	6
1,7-Ph	5
1,6-CF$_3$	4
1,7-CF$_3$	8
1,6-OMe	Not fluorescent
1,7-OMe	Not fluorescent

For the self-association investigation, solutions of extended BACDs **1,6-Ph**, **1,7-Ph**, **1,6-CF$_3$**, **1,7-CF$_3$**, **1,6-OMe**, and **1,7-OMe** at different concentrations were prepared in $CDCl_3$. The UV-Vis spectra at each concentration was recorded and the equilibrium constant was determined by non-linear least-squares fitting, performed employing a custom MATLAB software developed in-house, using the isodesmic model given in Eq. 1:[S3,S4]

$$\alpha_{agg} = 1 - \frac{2K_aC+1-\sqrt{4K_aC+1}}{2{K_a}^2C^2} \quad \text{(Eq. 1)}$$

α_{agg} stands for the fraction of aggregated molecules; C denotes the concentration; and K_a represents the self-association constant for the isodesmic model. α_{agg} was determined by hypothesizing that at the lowest concentration (*ca.* 3×10^{-7} M) the solution was only containing monomeric species, therefore $\alpha_{agg} = 0$. Hence, this point ($\alpha_{agg} = 0$) was deleted for the determination of the self-association constant.

It must be noted that a monomer–dimer model[S3] was tested to determine the equilibrium constant for the self-association of extended BACDs **1,6-Ph**, **1,7-Ph**, **1,6-CF$_3$**, **1,7-CF$_3$**, **1,6-OMe**, and **1,7-OMe**, however, this model only provided good fittings for two compounds: **1,6-Ph** and **1,6-OMe**. Thus, since the isodesmic model provides good fittings for all extended BACDs **1,6-Ph**, **1,7-Ph**, **1,6-CF$_3$**, **1,7-CF$_3$**, **1,6-OMe**, and **1,7-OMe**, we can strongly consider

the self-association of these extended BACDs to be isodesmic. In addition, both models were tested for the extended AzaBPDIs **aPDI-Ph**, **aPDI-CF$_3$**, and **aPDI-OMe**, but did not fit.

Table S3. Self-association constants (K_a) of extended BACDs **1,6-Ph**, **1,7-Ph**, **1,6-CF$_3$**, **1,7-CF$_3$**, **1,6-OMe**, and **1,7-OMe** using an isodesmic model.

Compound	K_a / M^{-1}
1,6-Ph	$(2.0 \pm 0.2) \times 10^5$
1,7-Ph	$(1.5 \pm 0.1) \times 10^5$
1,6-CF$_3$	$(1.1 \pm 0.1) \times 10^5$
1,7-CF$_3$	$(5.7 \pm 0.1) \times 10^4$
1,6-OMe	$(5.1 \pm 0.1) \times 10^5$
1,7-OMe	$(1.3 \pm 0.1) \times 10^5$

To know the sizes of the aggregates formed by the extended BACDs **1,6-Ph**, **1,7-Ph**, **1,6-CF$_3$**, **1,7-CF$_3$**, **1,6-OMe**, and **1,7-OMe** at given concentrations, the number average aggregate size (N) for the isodesmic model can be calculated using Eq. 2:[S3]

$$N = \frac{1+\sqrt{4K_aC+1}}{2} \quad \text{(Eq. 2)}$$

N stands for the number average aggregate size; C denotes the concentration; and K_a represents the self-association constant for the isodesmic model.

Table S4. Number average aggregate size (N) of extended BACDs **1,6-Ph**, **1,7-Ph**, **1,6-CF$_3$**, **1,7-CF$_3$**, **1,6-OMe**, and **1,7-OMe** using an isodesmic model depending on the concentration.

C / M	N					
	Compound					
	1,6-Ph	**1,7-Ph**	**1,6-CF$_3$**	**1,7-CF$_3$**	**1,6-OMe**	**1,7-OMe**
1.0×10^{-7}	1.02	1.01	1.01	1.01	1.05	1.01
1.0×10^{-6}	1.17	1.13	1.10	1.05	1.37	1.12
1.0×10^{-5}	2.01	1.82	1.68	1.41	2.82	1.75
1.0×10^{-4}	5.05	4.41	3.91	2.94	7.68	4.17
1.0×10^{-3}	14.8	12.8	11.2	8.07	23.2	12.0

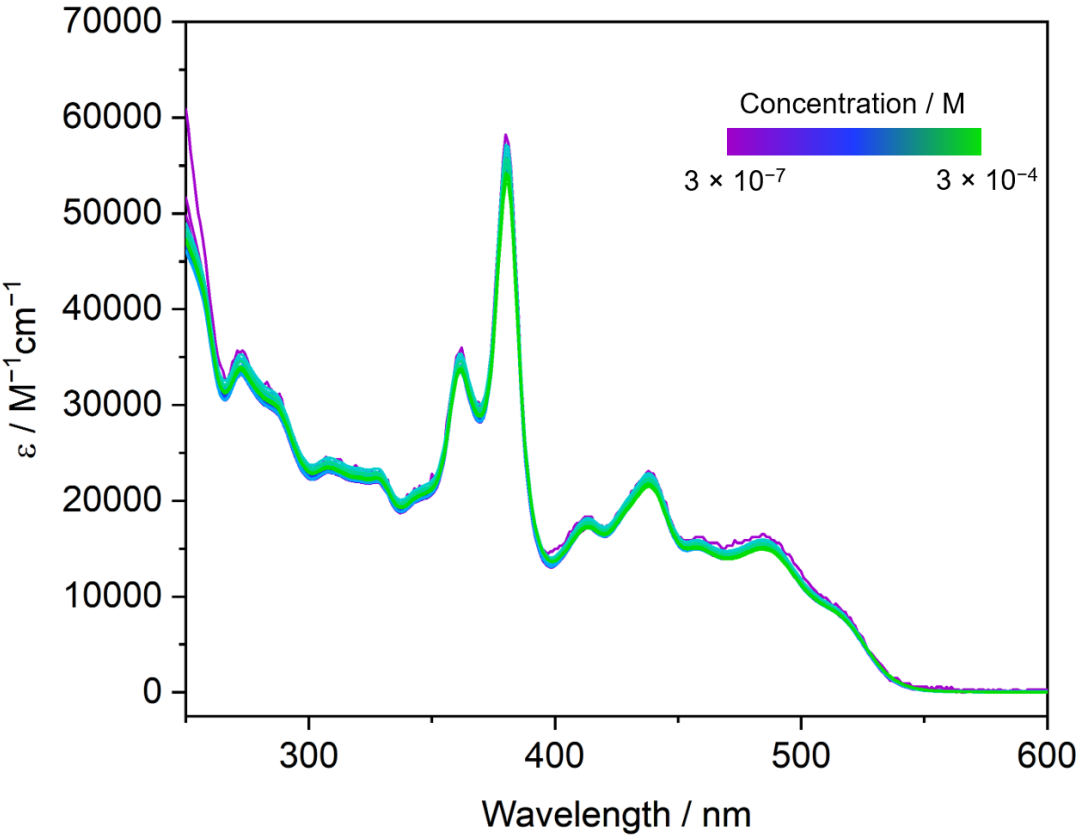

Figure S1. Absorption spectra of **aPDI-Ph** recorded at various concentrations, between *ca.* 3×10^{-7} M and *ca.* 3×10^{-4} M, in $CHCl_3$ exhibiting a minor concentration dependence of the apparent molar absorption coefficient values (ε)

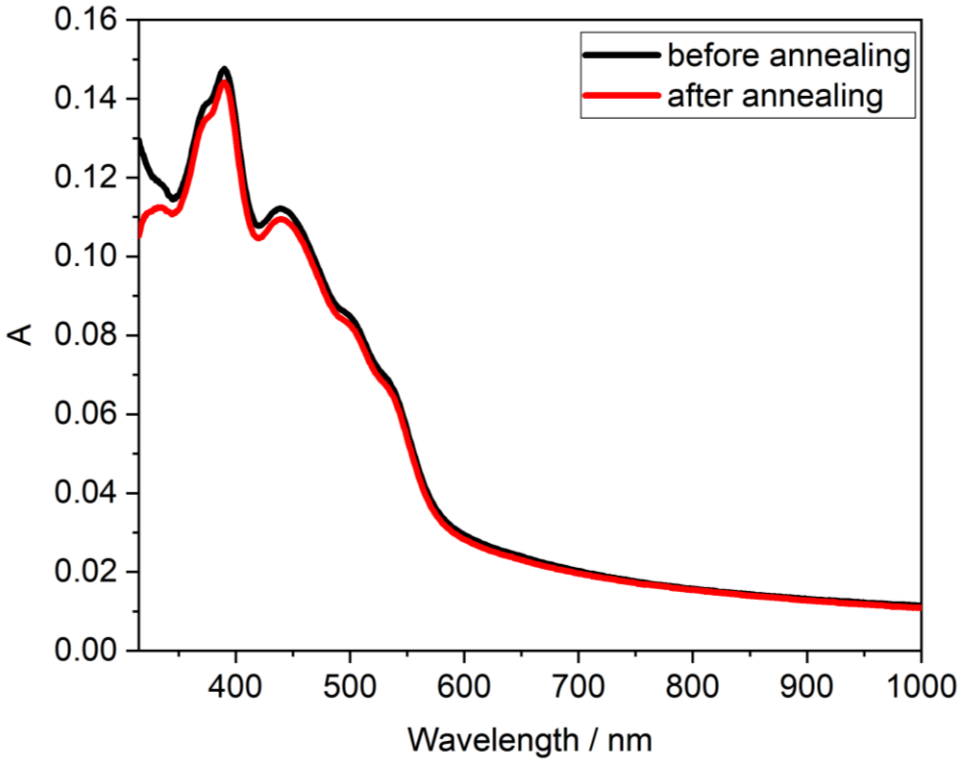

Figure S2. Absorption spectra of the thin film of **aPDI-Ph** before (black line) and after (red line) annealing

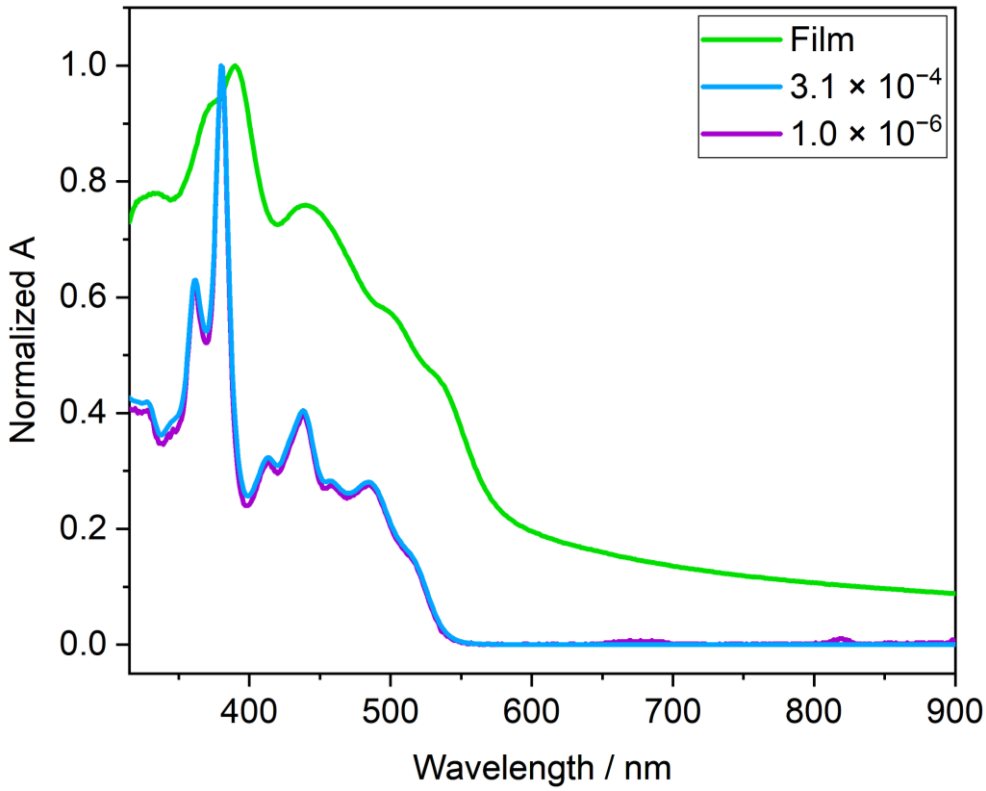

Figure S3. Comparison between the normalized absorption spectra of **aPDI-Ph** in $CHCl_3$ solution at concentrations of 1.0×10^{-6} M (purple line) and 3.1×10^{-4} M (blue line) and as a thin film after annealing (green line)

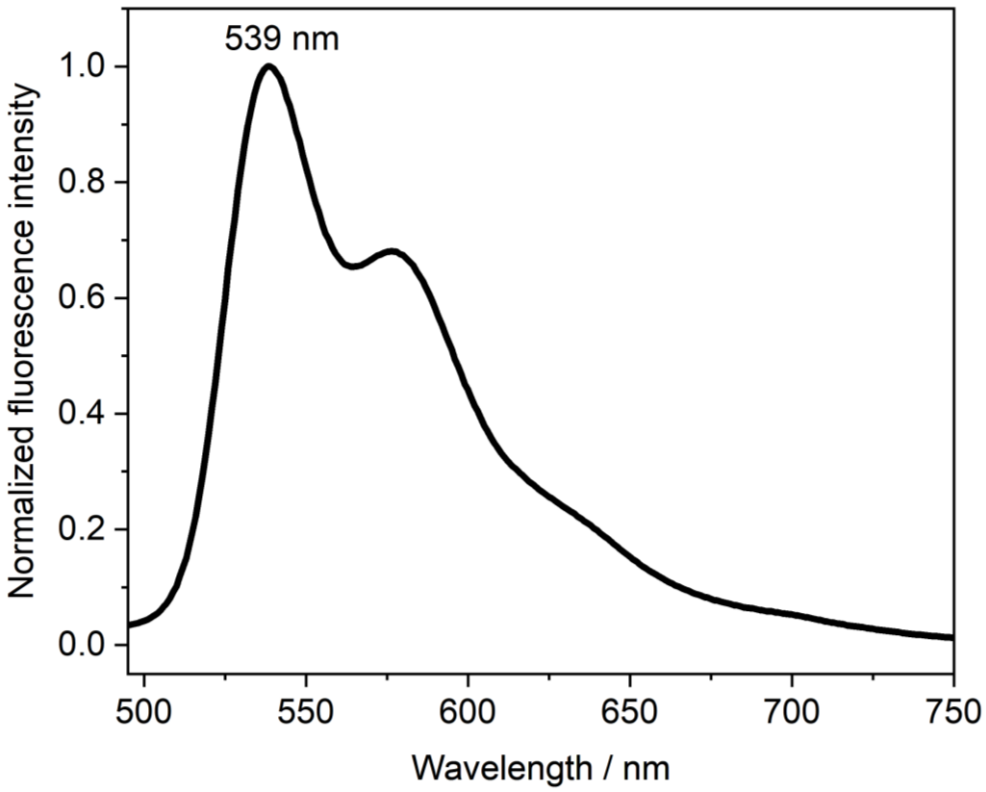

Figure S4. Normalized emission spectra (λ_{exc} = 484 nm) of **aPDI-Ph** recorded in $CHCl_3$

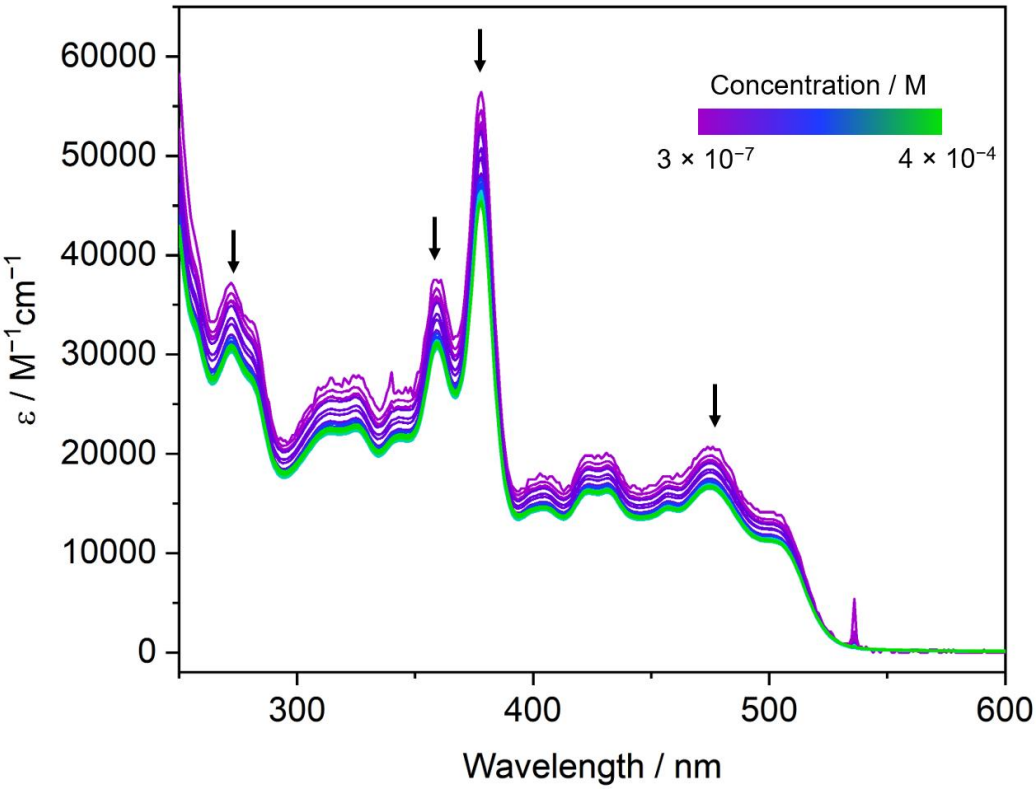

Figure S5. Absorption spectra of **aPDI-CF$_3$** recorded at various concentrations, between *ca.* 3×10^{-7} M and *ca.* 4×10^{-4} M, in $CHCl_3$ exhibiting a substantial concentration dependence of the apparent molar absorption coefficient values (ε)

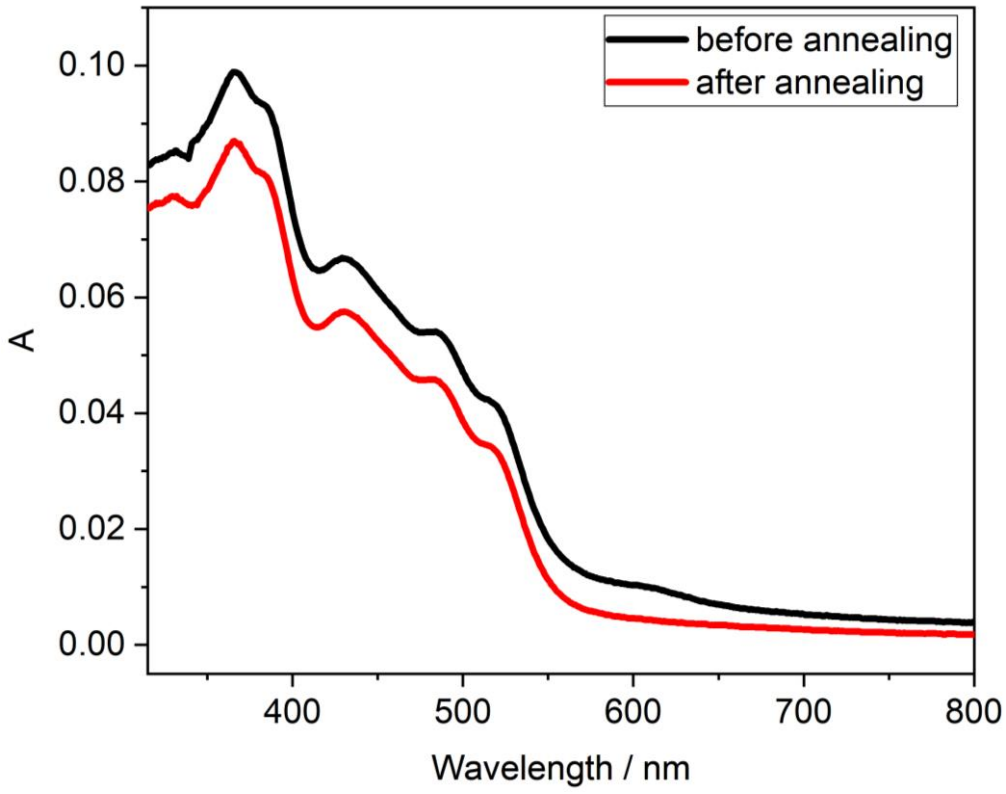

Figure S6. Absorption spectra of the thin film of **aPDI-CF$_3$** before (black line) and after (red line) annealing

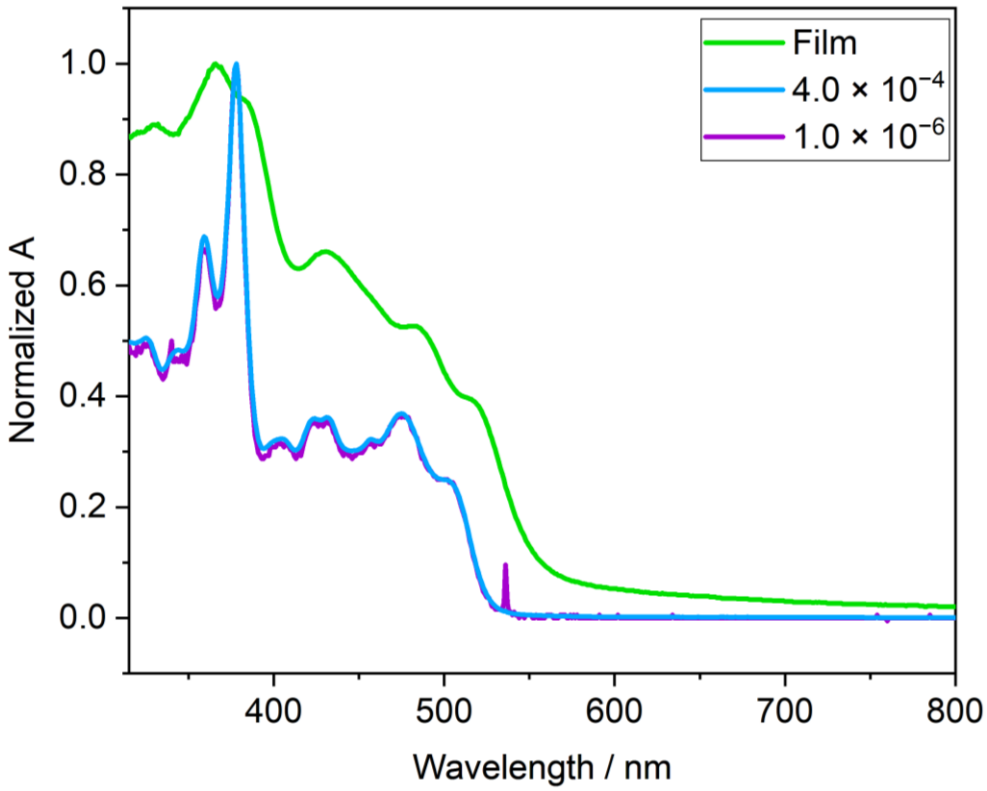

Figure S7. Comparison between the normalized absorption spectra of **aPDI-CF₃** in $CHCl_3$ solution at concentrations of 1.0×10^{-6} M (purple line) and 4.0×10^{-4} M (blue line) and as a thin film after annealing (green line)

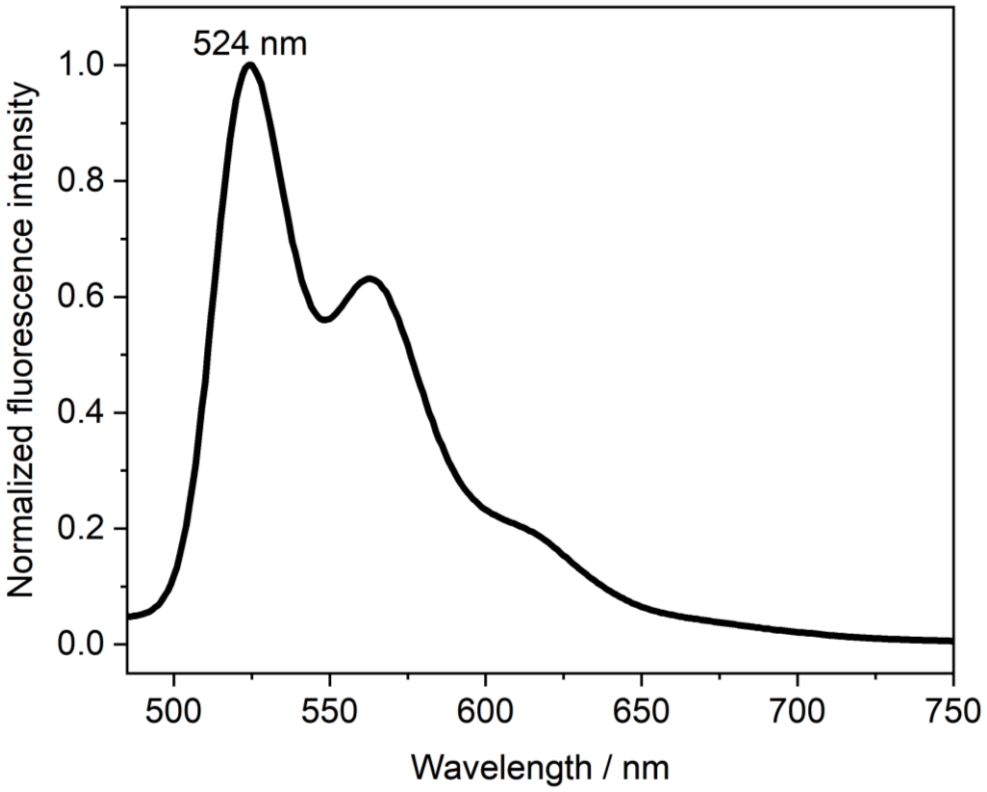

Figure S8. Normalized emission spectra (λ_{exc} = 475 nm) of **aPDI-CF₃** recorded in $CHCl_3$

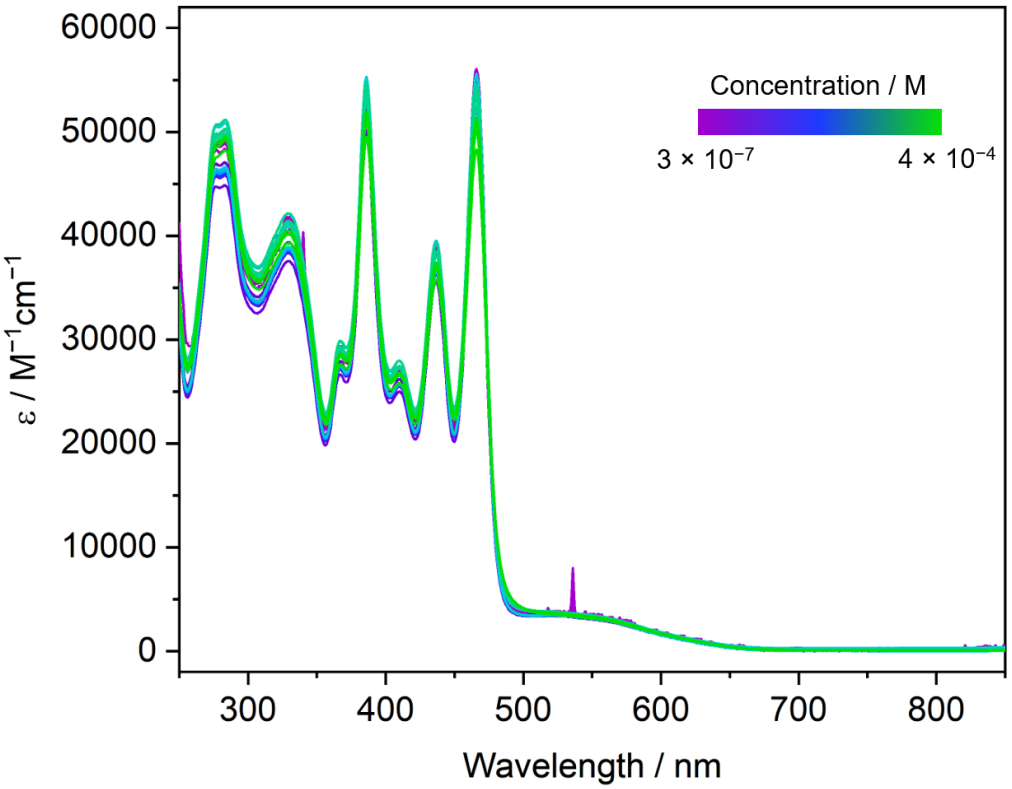

Figure S9. Absorption spectra of **aPDI-OMe** recorded at various concentrations, between *ca.* 3×10^{-7} M and *ca.* 4×10^{-4} M, in $CHCl_3$ exhibiting a minor concentration dependence of the apparent molar absorption coefficient values (ε)

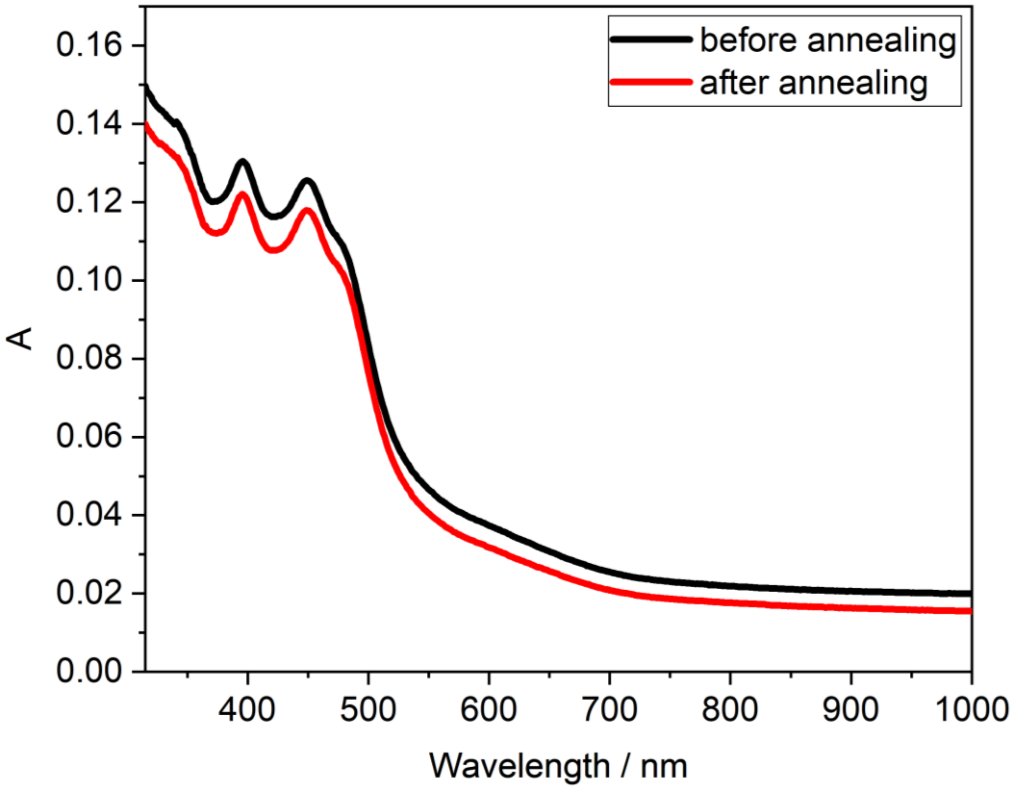

Figure S10. Absorption spectra of the thin film of **aPDI-OMe** before (black line) and after (red line) annealing

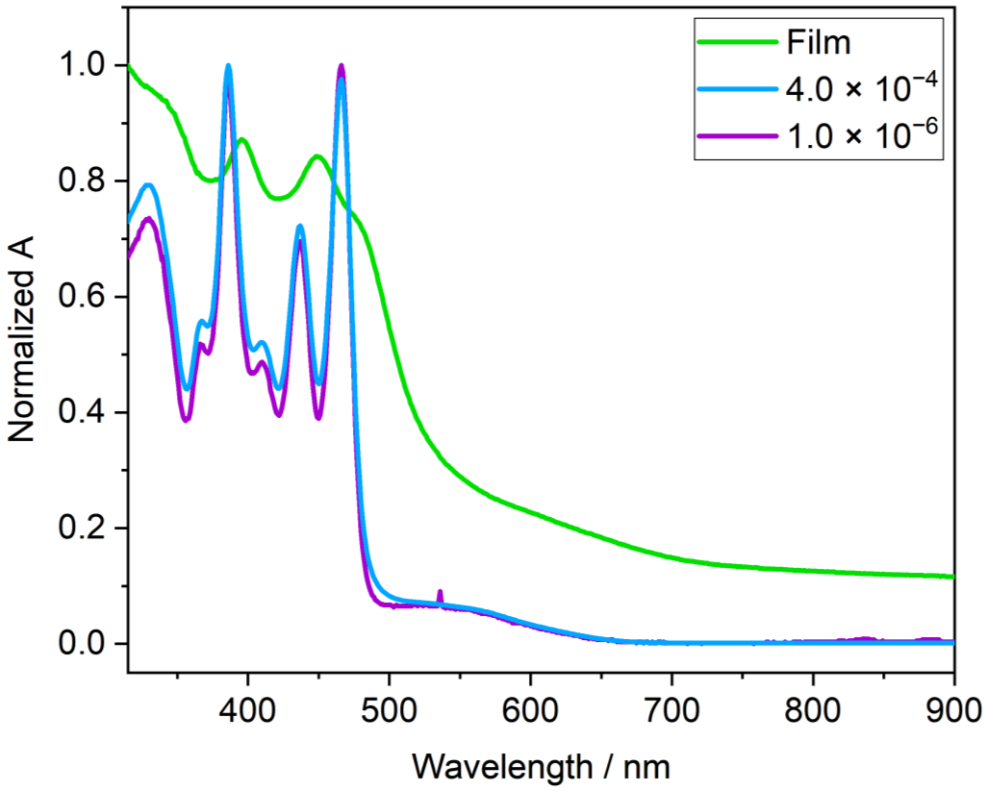

Figure S11. Comparison between the normalized absorption spectra of **aPDI-OMe** in $CHCl_3$ solution at concentrations of 1.0×10^{-6} M (purple line) and 4.0×10^{-4} M (blue line) and as a thin film after annealing (green line)

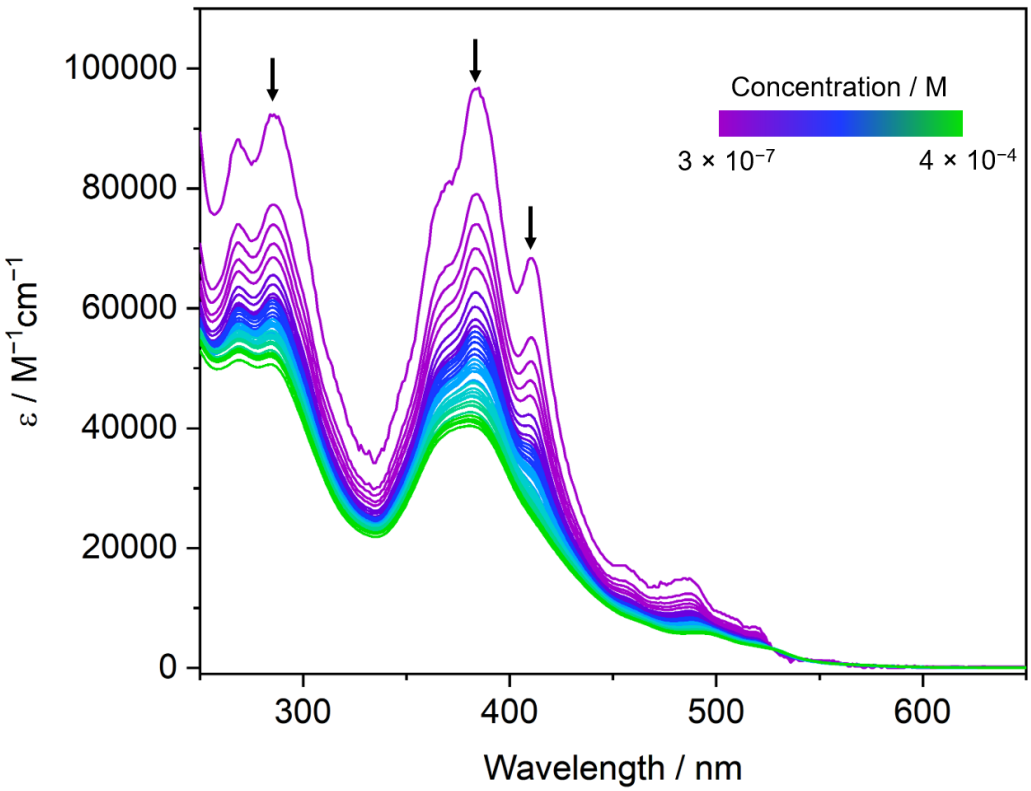

Figure S12. Absorption spectra of **1,6-Ph** recorded at various concentrations, between *ca.* 3×10^{-7} M and *ca.* 4×10^{-4} M, in $CHCl_3$ exhibiting a strong concentration dependence of the apparent molar absorption coefficient values (ε)

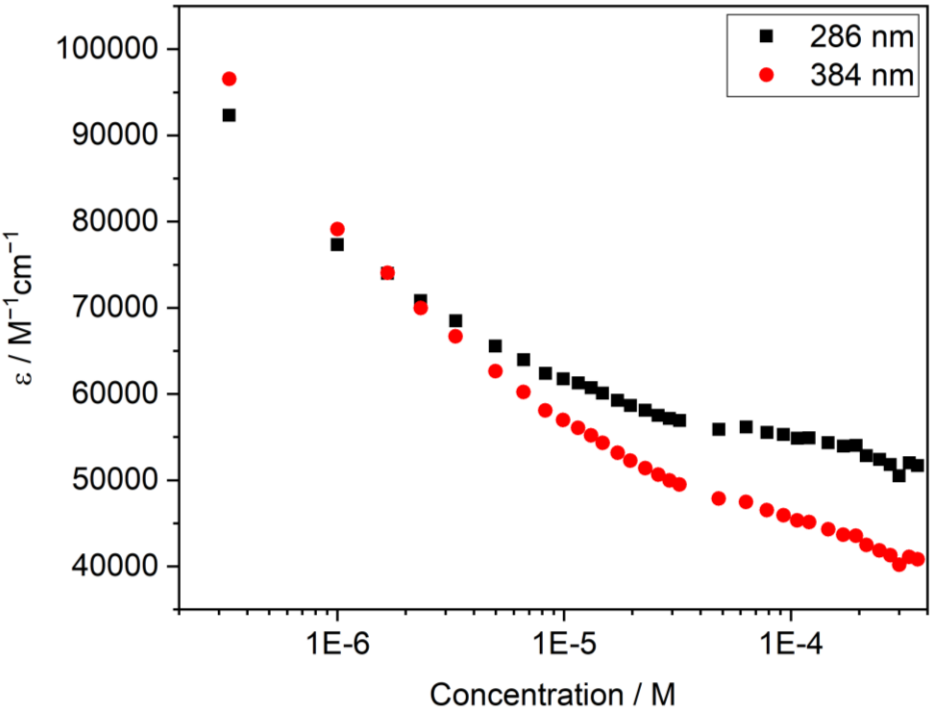

Figure S13. Plot of the apparent molar absorption coefficient ε of **1,6-Ph** at λ = 286 nm (black square), and λ = 384 nm (red dot) vs. concentration exhibiting a strong concentration dependence of the apparent molar absorption coefficient value. The apparent molar absorption coefficient of **1,6-Ph** decreases when increasing its concentration.

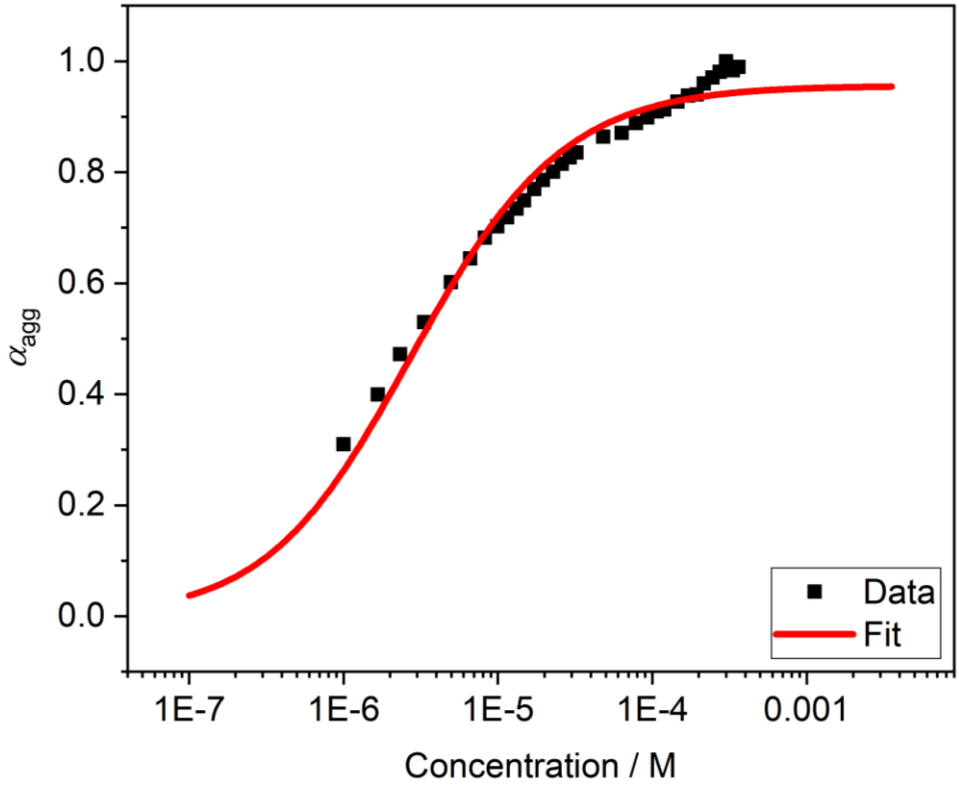

Figure S14. Non-linear least-squares fitting of the changes in the of the fraction of aggregated molecules (α_{agg}), calculated at λ = 384 nm, upon concentration increase of **1,6-Ph** in $CHCl_3$ using the isodesmic model. K_a = (2.0 ± 0.2) × 10^5 M^{-1}

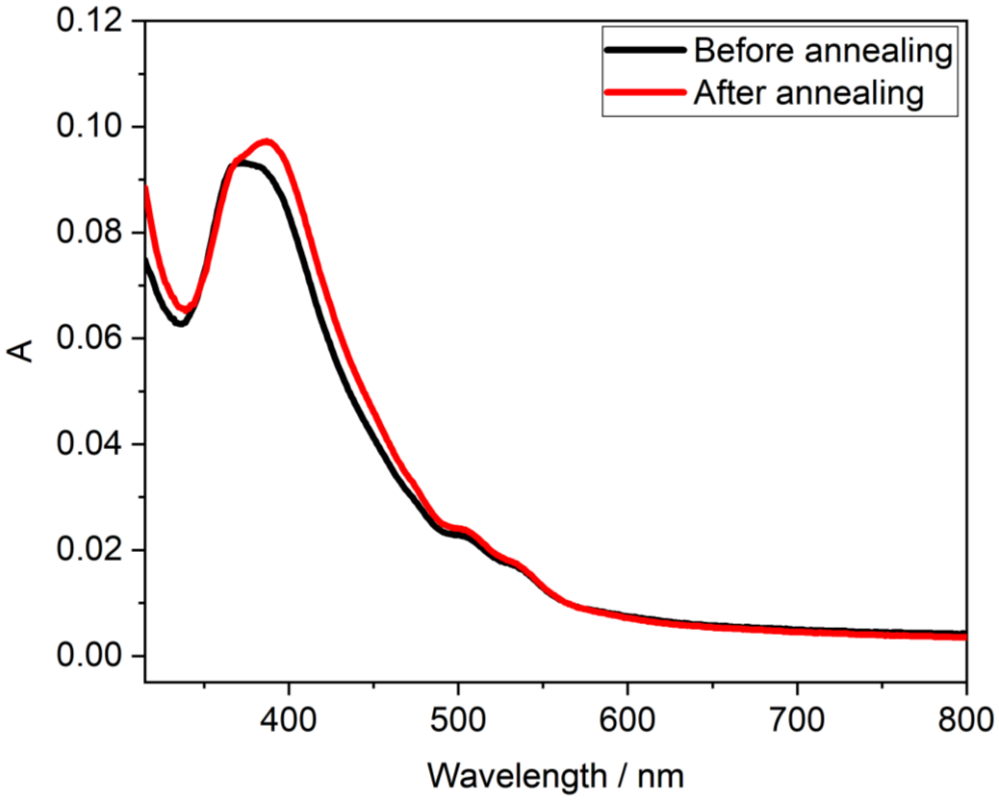

Figure S15. Absorption spectra of the thin film of **1,6-Ph** before (black line) and after (red line) annealing

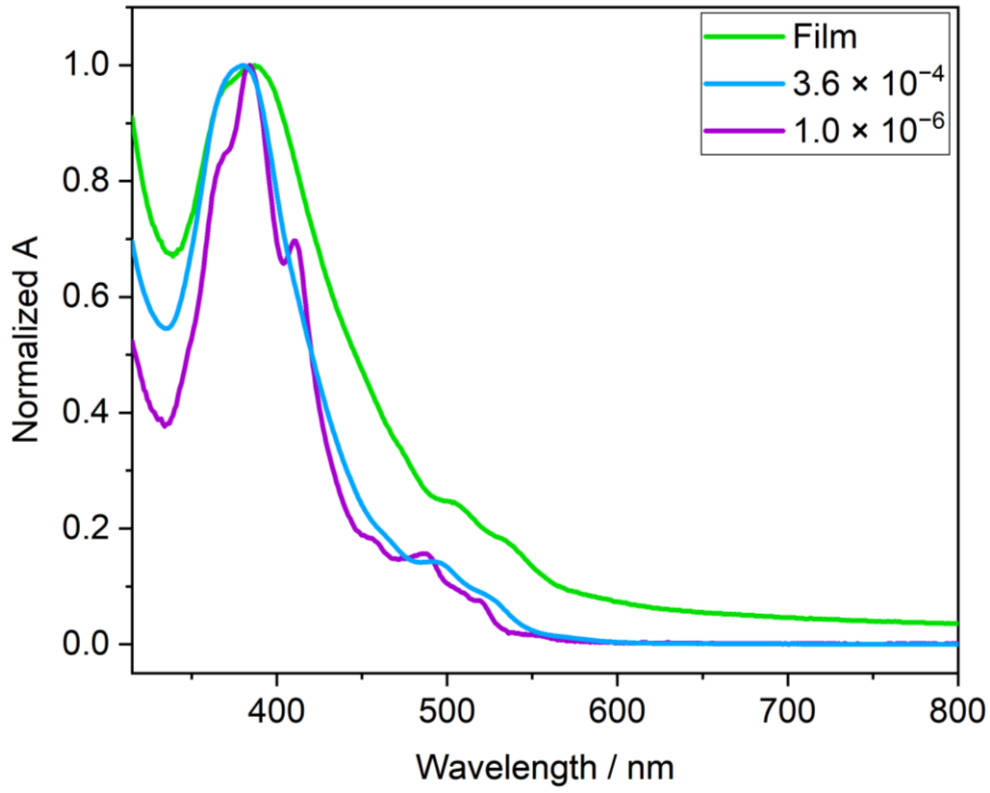

Figure S16. Comparison between the normalized absorption spectra of **1,6-Ph** in $CHCl_3$ solution at concentrations of 1.0×10^{-6} M (purple line) and 3.6×10^{-4} M (blue line) and as a thin film after annealing (green line)

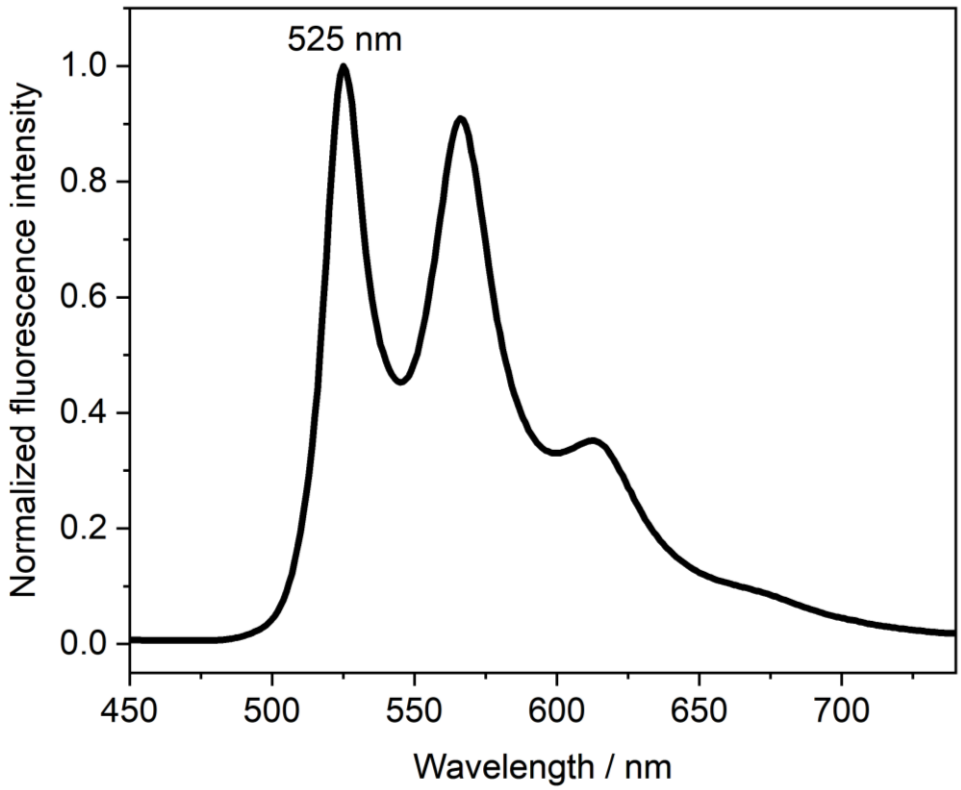

Figure S17. Normalized emission spectra (λ_{exc} = 380 nm) of **1,6-Ph** recorded in $CHCl_3$

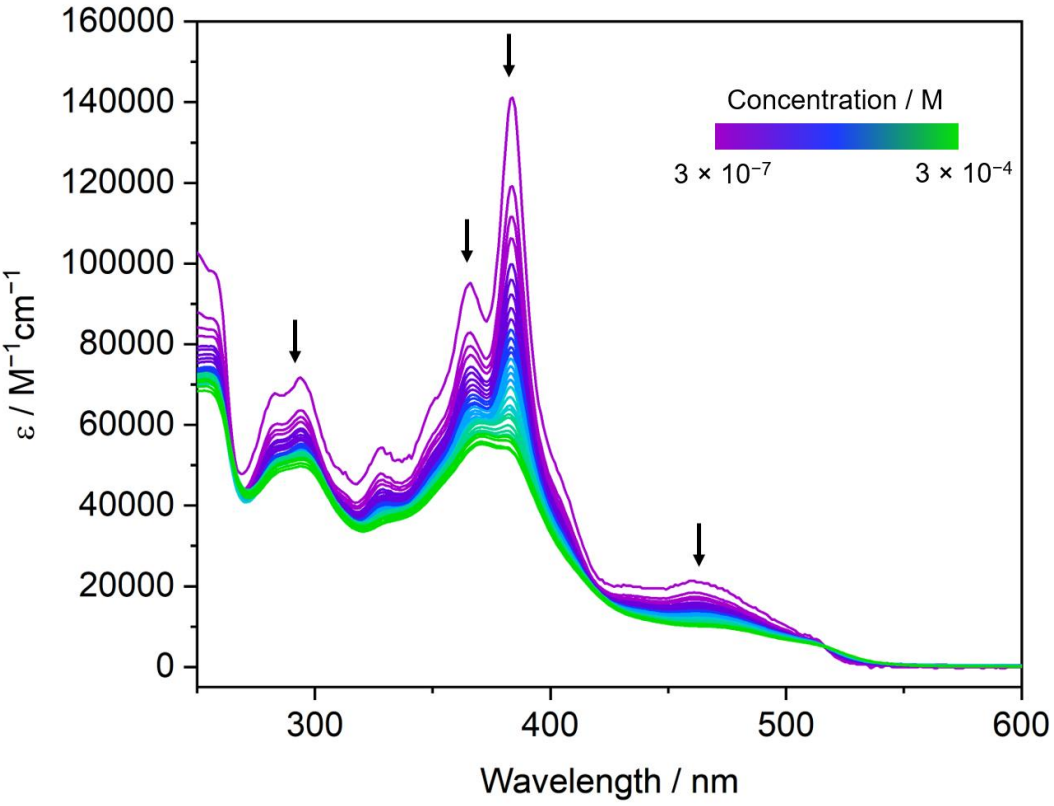

Figure S18. Absorption spectra of **1,7-Ph** recorded at various concentrations, between *ca.* 3×10^{-7} M and *ca.* 3×10^{-4} M, in $CHCl_3$ exhibiting a strong concentration dependence of the apparent molar absorption coefficient values (ε)

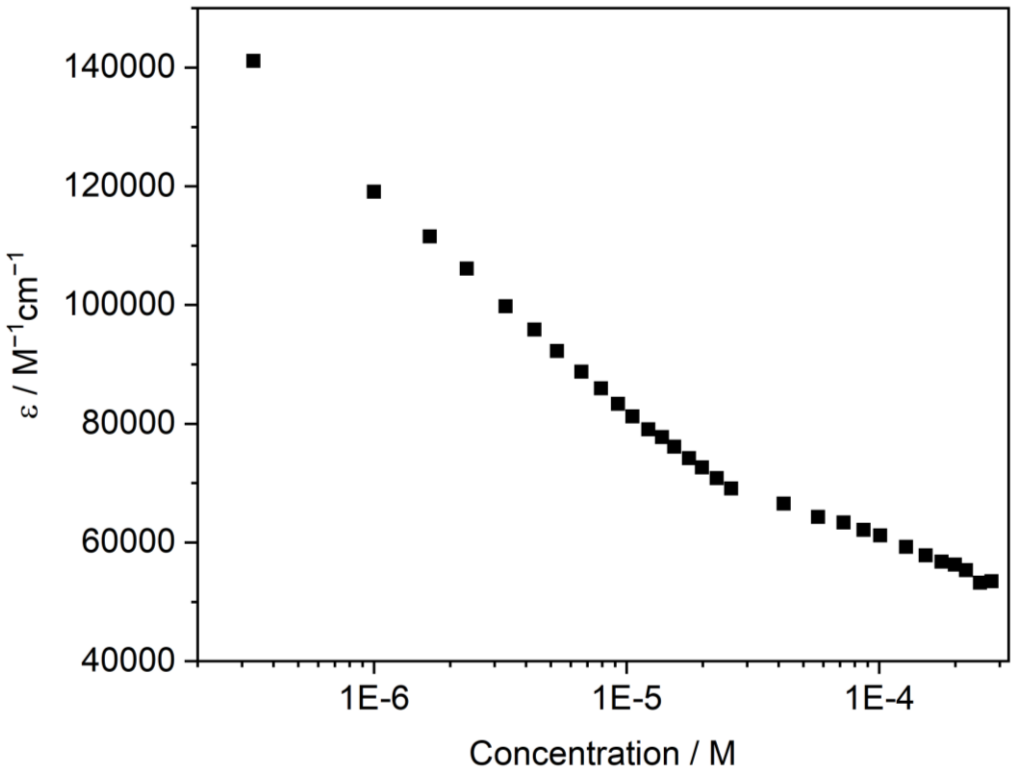

Figure S19. Plot of the apparent molar absorption coefficient ε of **1,7-Ph** at λ = 384 nm vs. concentration exhibiting a strong concentration dependence of the apparent molar absorption coefficient value. The apparent molar absorption coefficient of **1,7-Ph** decreases when increasing its concentration.

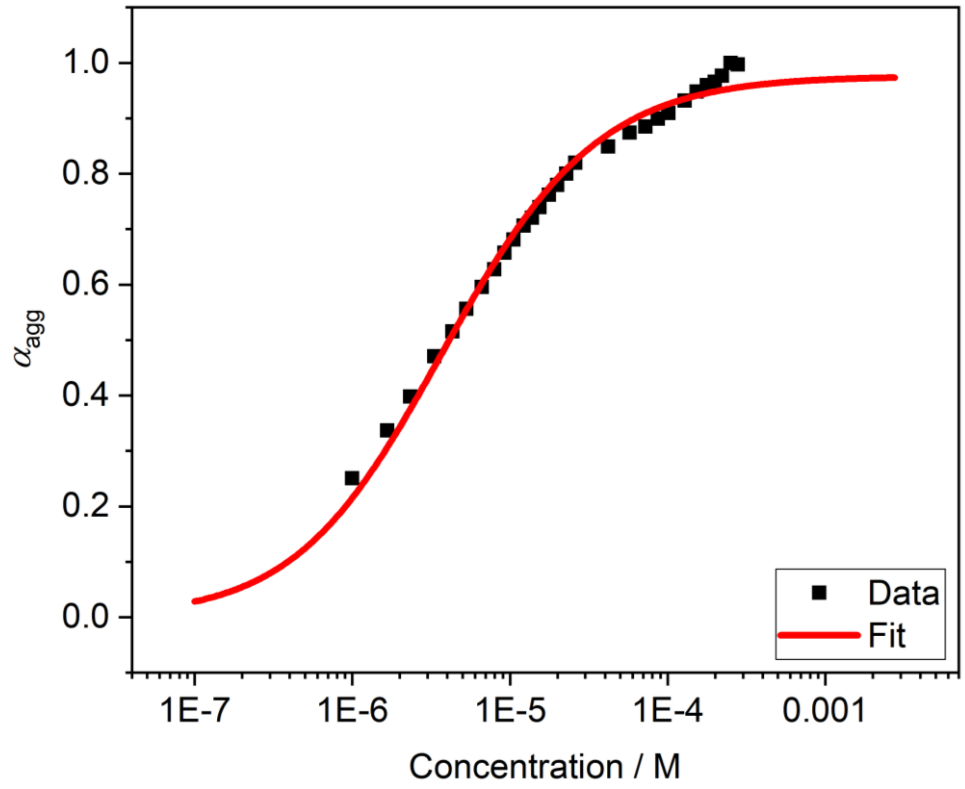

Figure S20. Non-linear least-squares fitting of the changes in the of the fraction of aggregated molecules (α_{agg}), calculated at λ = 384 nm, upon concentration increase of **1,7-Ph** in $CHCl_3$ using the isodesmic model. $K_a = (1.5 \pm 0.1) \times 10^5$ M^{-1}

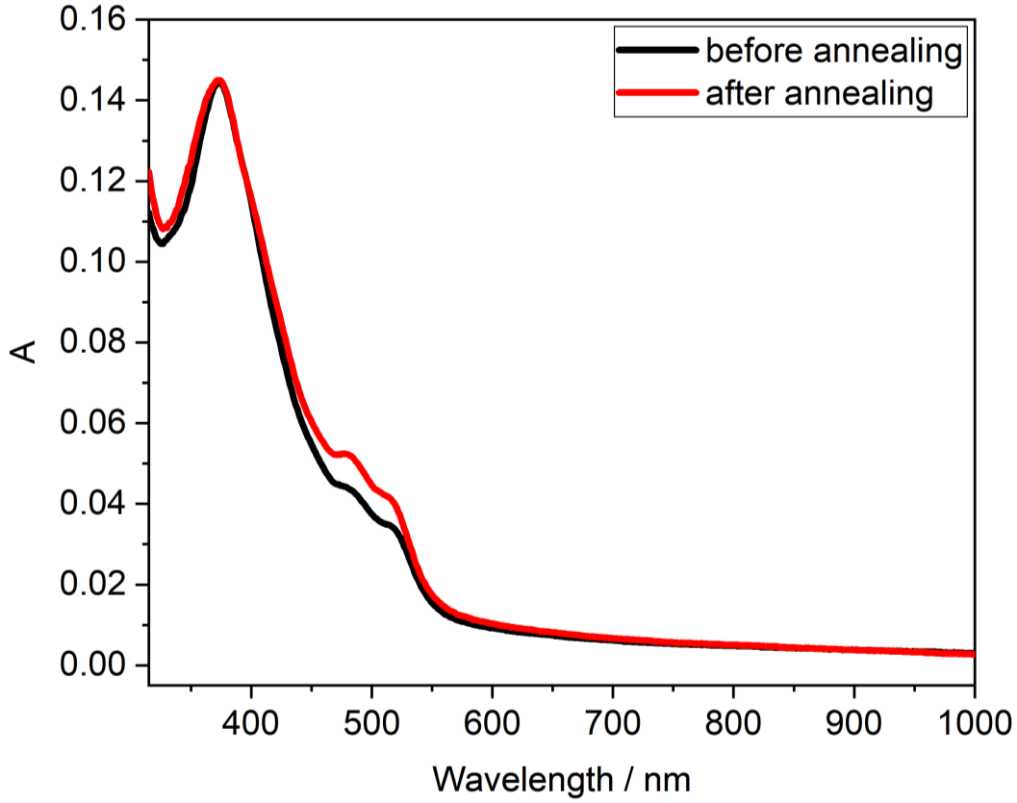

Figure S21. Absorption spectra of the thin film of **1,7-Ph** before (black line) and after (red line) annealing

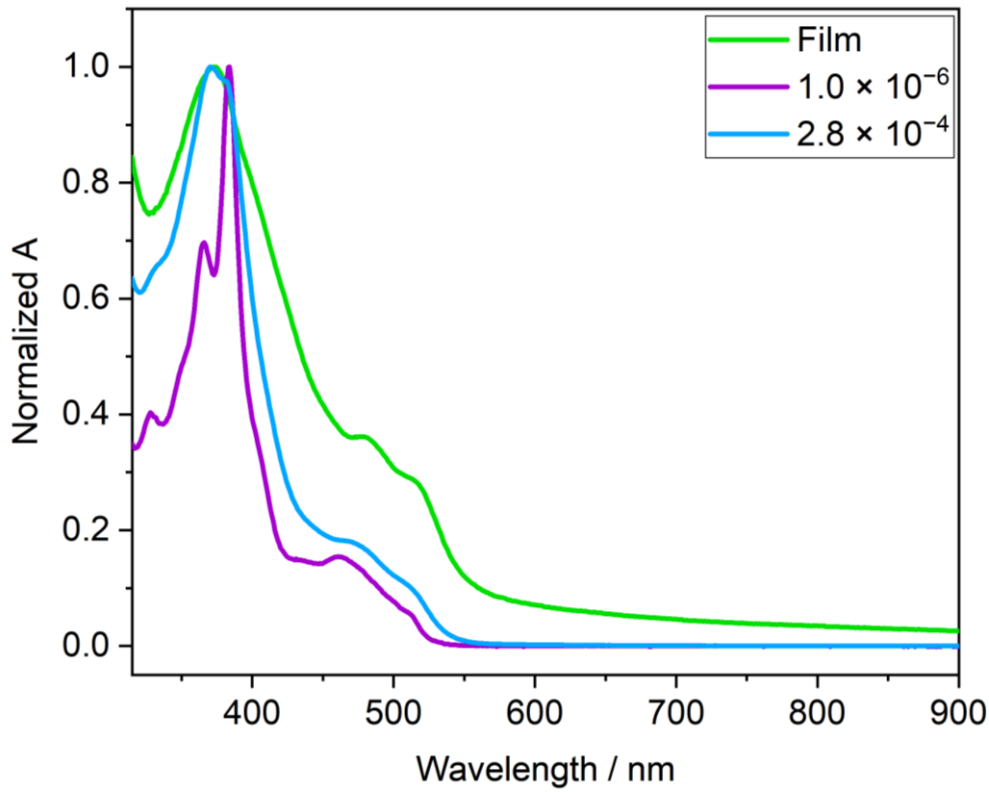

Figure S22. Comparison between the normalized absorption spectra of **1,7-Ph** in $CHCl_3$ solution at concentrations of 1.0×10^{-6} M (purple line) and 2.8×10^{-4} M (blue line) and as a thin film after annealing (green line)

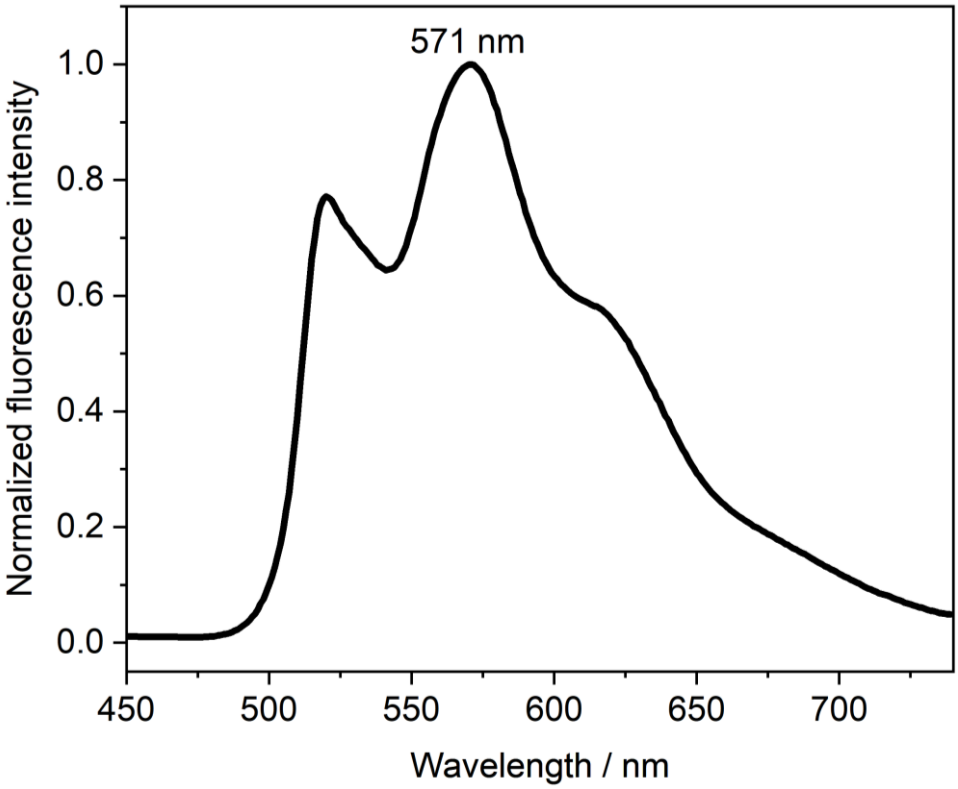

Figure S23. Normalized emission spectra (λ_{exc} = 380 nm) of **1,7-Ph** recorded in $CHCl_3$

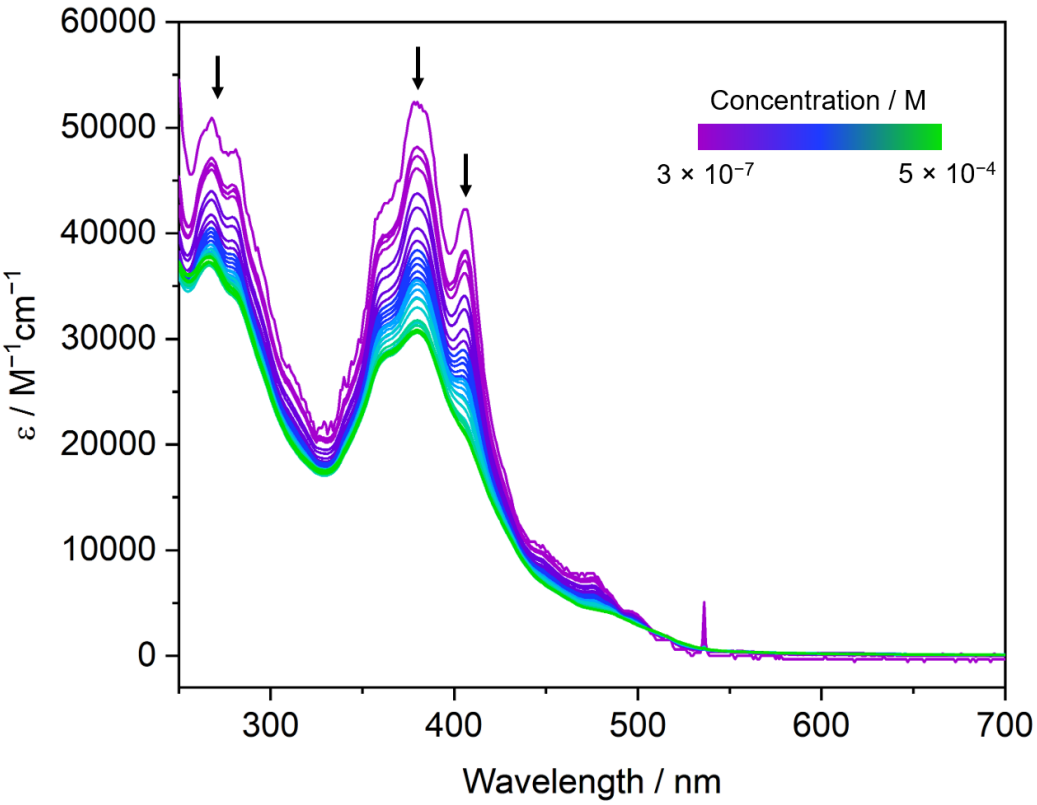

Figure S24. Absorption spectra of **1,6-CF_3** recorded at various concentrations, between *ca.* 3×10^{-7} M and *ca.* 5×10^{-4} M, in $CHCl_3$ exhibiting a strong concentration dependence of the apparent molar absorption coefficient values (ε)

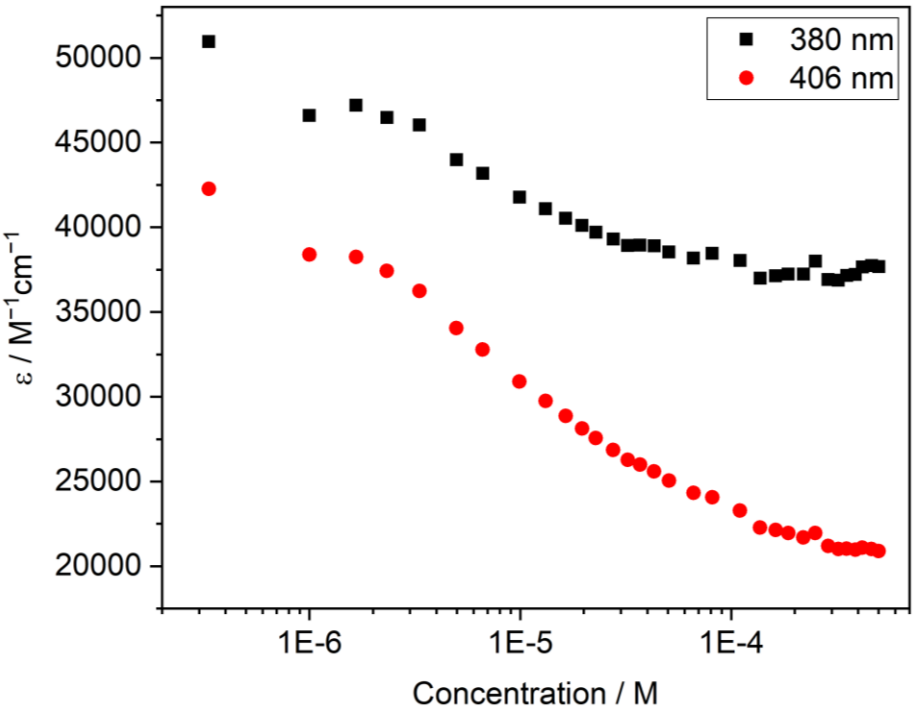

Figure S25. Plot of the apparent molar absorption coefficient ε of **1,6-CF₃** at λ = 380 nm (black square), and λ = 406 nm (red dot) vs. concentration exhibiting a strong concentration dependence of the apparent molar absorption coefficient value. The apparent molar absorption coefficient of **1,6-CF₃** decreases when increasing its concentration.

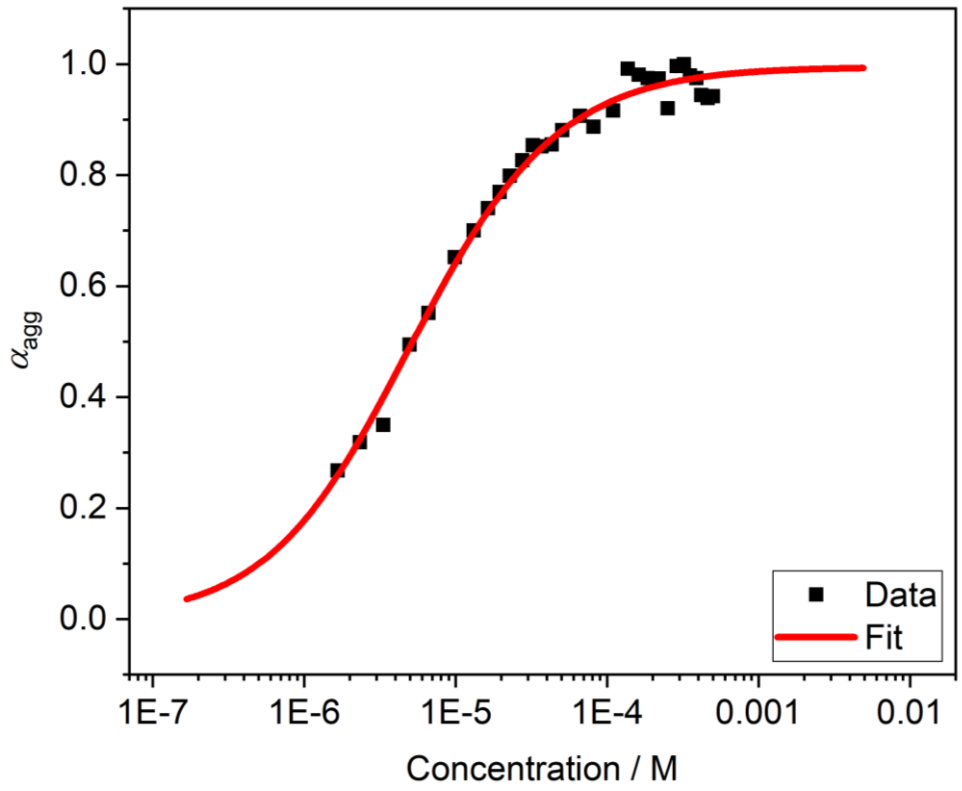

Figure S26. Non-linear least-squares fitting of the changes in the of the fraction of aggregated molecules (α_{agg}), calculated at λ = 380 nm, upon concentration increase of **1,6-CF₃** in $CHCl_3$ using the isodesmic model. $K_a = (1.1 \pm 0.1) \times 10^5$ M^{-1}

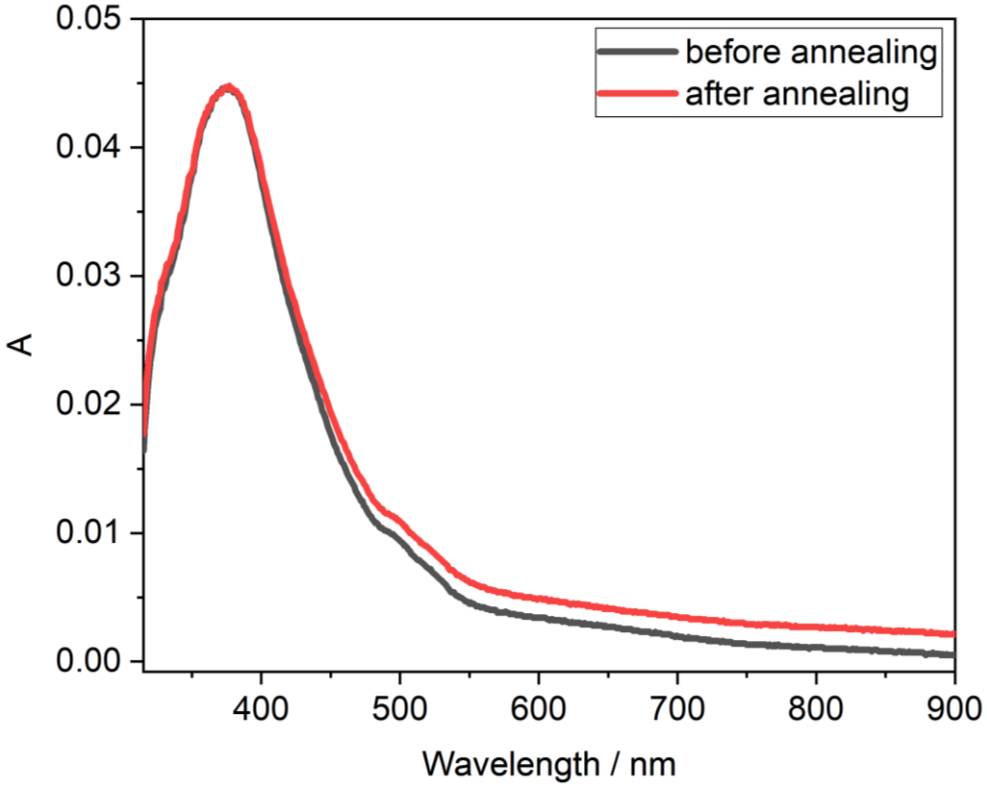

Figure S27. Absorption spectra of the thin film of **1,6-CF$_3$** before (black line) and after (red line) annealing

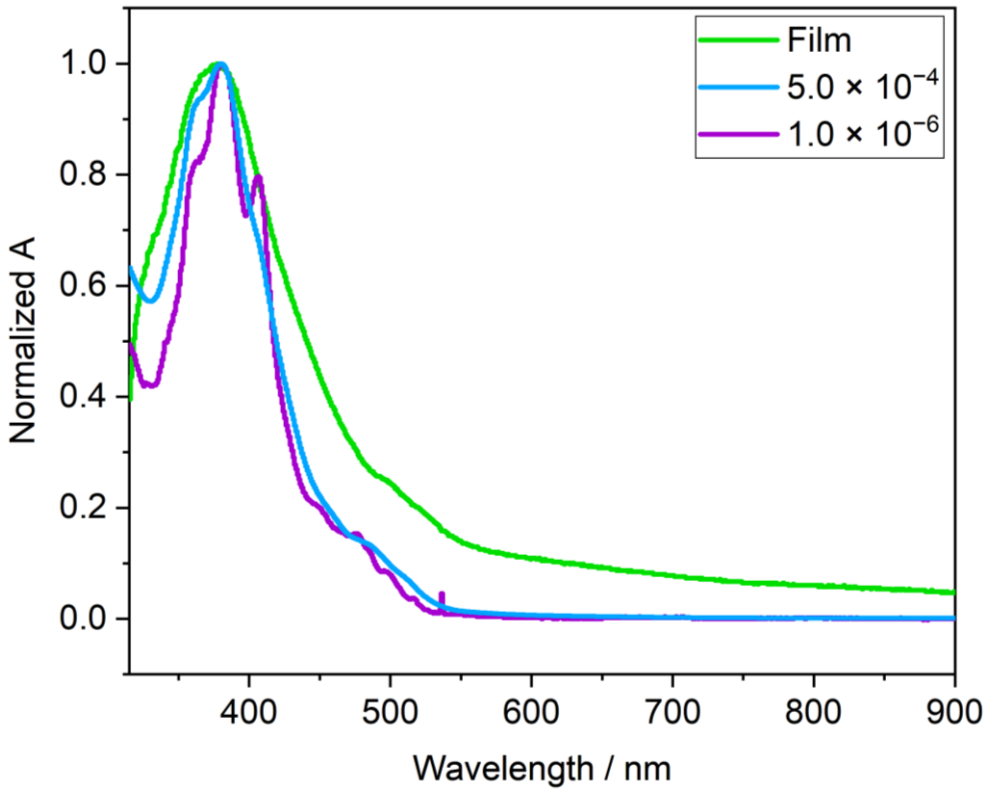

Figure S28. Comparison between the normalized absorption spectra of **1,6-CF$_3$** in $CHCl_3$ solution at concentrations of 1.0×10^{-6} M (purple line) and 5.0×10^{-4} M (blue line) and as a thin film after annealing (green line)

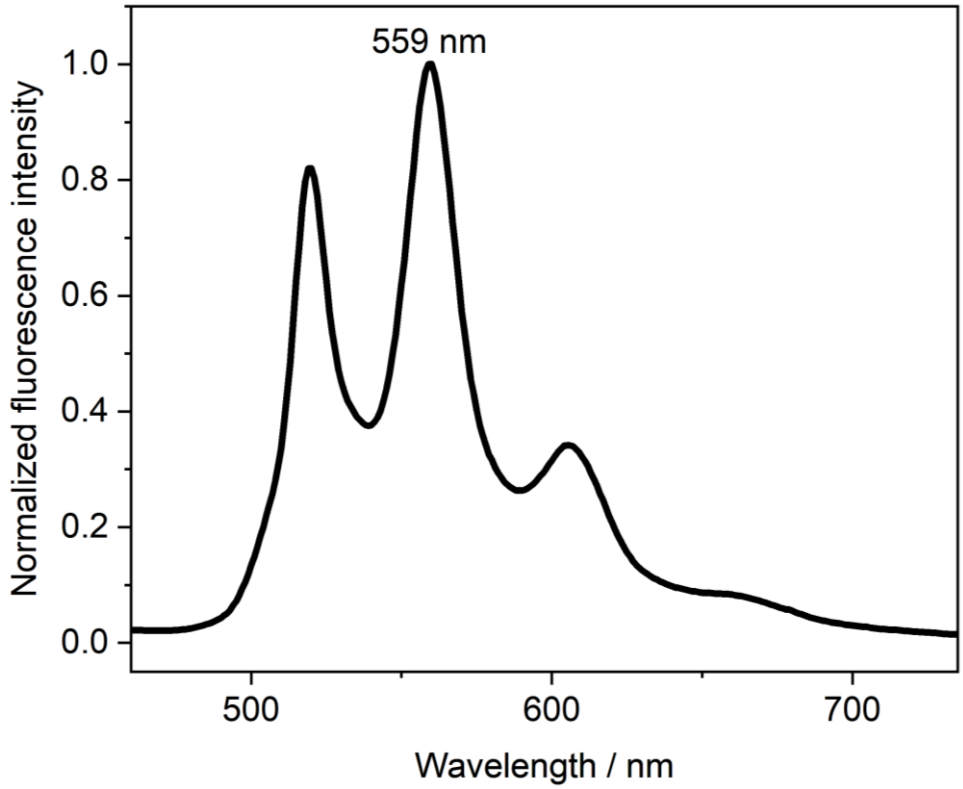

Figure S29. Normalized emission spectra (λ_{exc} = 380 nm) of **1,6-CF$_3$** recorded in $CHCl_3$

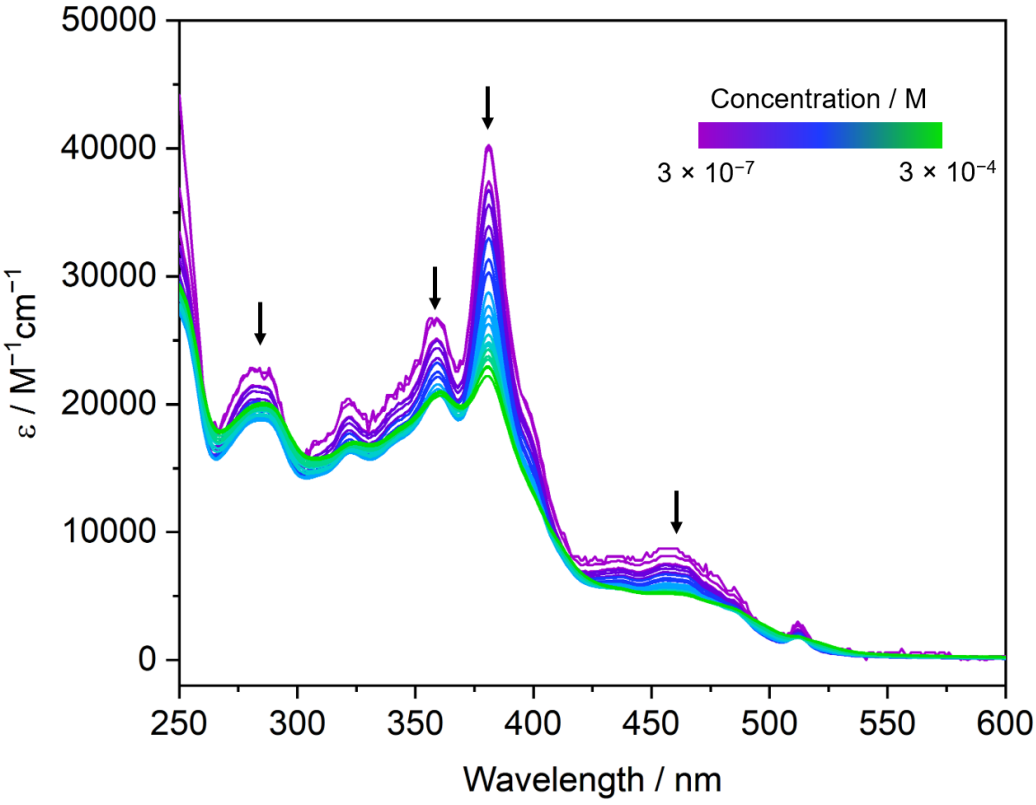

Figure S30. Absorption spectra of **1,7-CF$_3$** recorded at various concentrations, between *ca.* 3×10^{-7} M and *ca.* 3×10^{-4} M, in $CHCl_3$ exhibiting a strong concentration dependence of the apparent molar absorption coefficient values (ε)

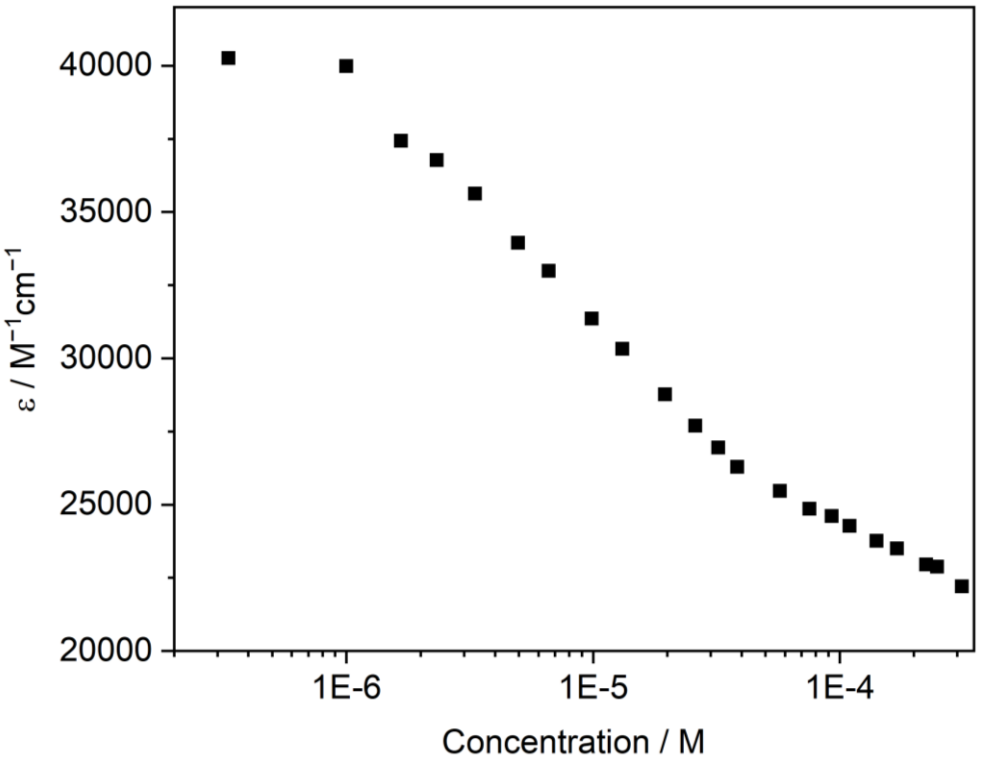

Figure S31. Plot of the apparent molar absorption coefficient ε of **1,7-CF₃** at λ = 381 nm vs. concentration exhibiting a strong concentration dependence of the apparent molar absorption coefficient value. The apparent molar absorption coefficient of **1,7-CF₃** decreases when increasing its concentration.

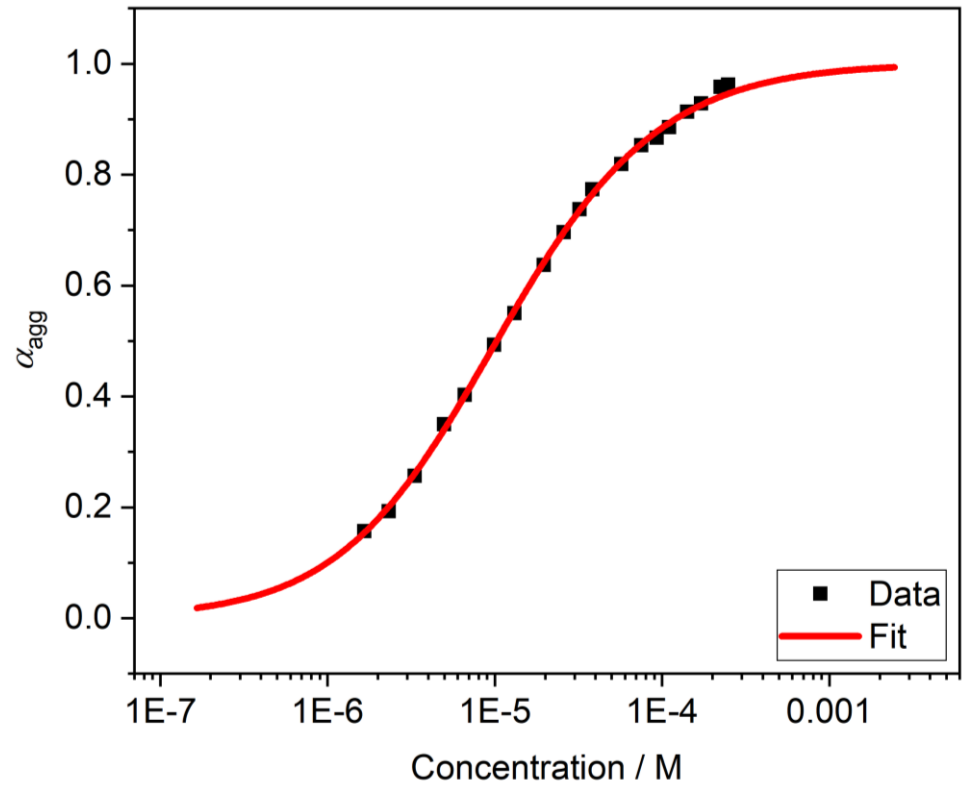

Figure S32. Non-linear least-squares fitting of the changes in the of the fraction of aggregated molecules (α_{agg}), calculated at λ = 381 nm, upon concentration increase of **1,7-CF₃** in $CHCl_3$ using the isodesmic model. K_a = (5.7 ± 0.1) × 10^4 M^{-1}

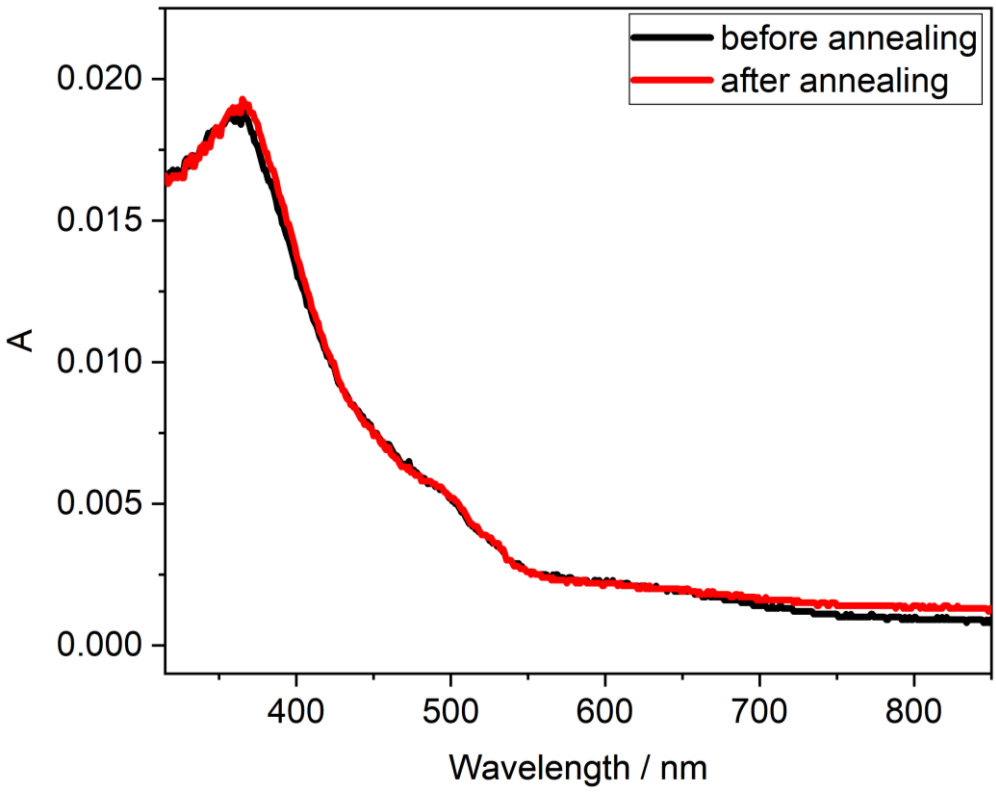

Figure S33. Absorption spectra of the thin film of **1,7-CF$_3$** before (black line) and after (red line) annealing

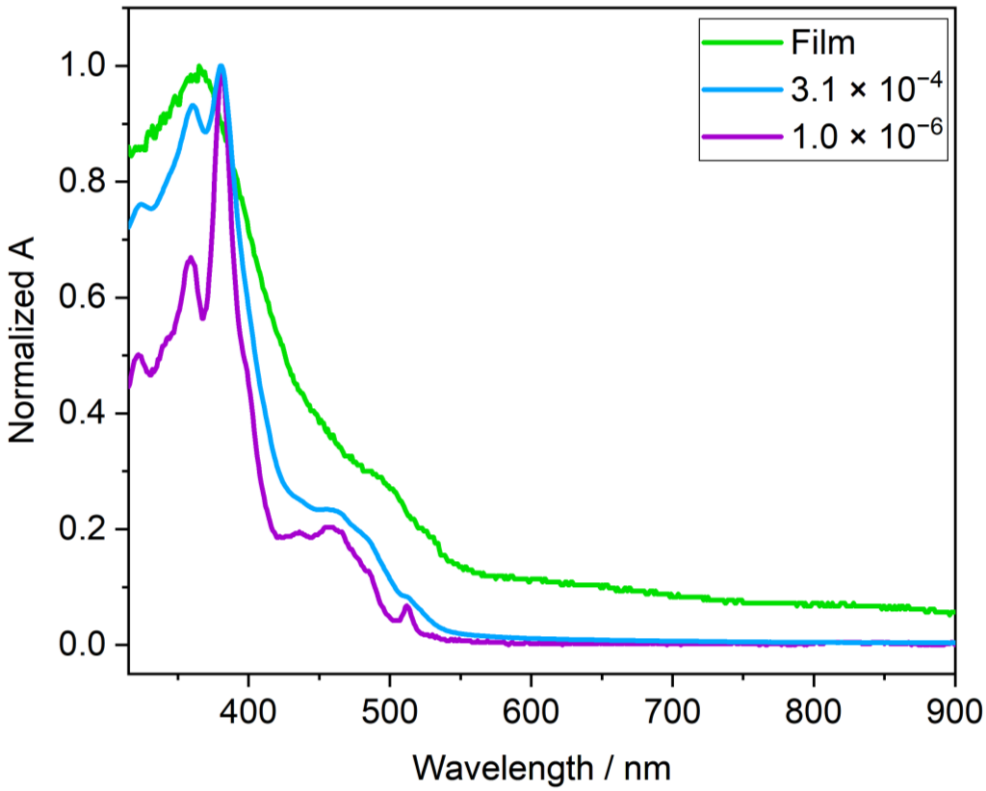

Figure S34. Comparison between the normalized absorption spectra of **1,7-CF$_3$** in $CHCl_3$ solution at concentrations of 1.0×10^{-6} M (purple line) and 3.1×10^{-4} M (blue line) and as a thin film after annealing (green line)

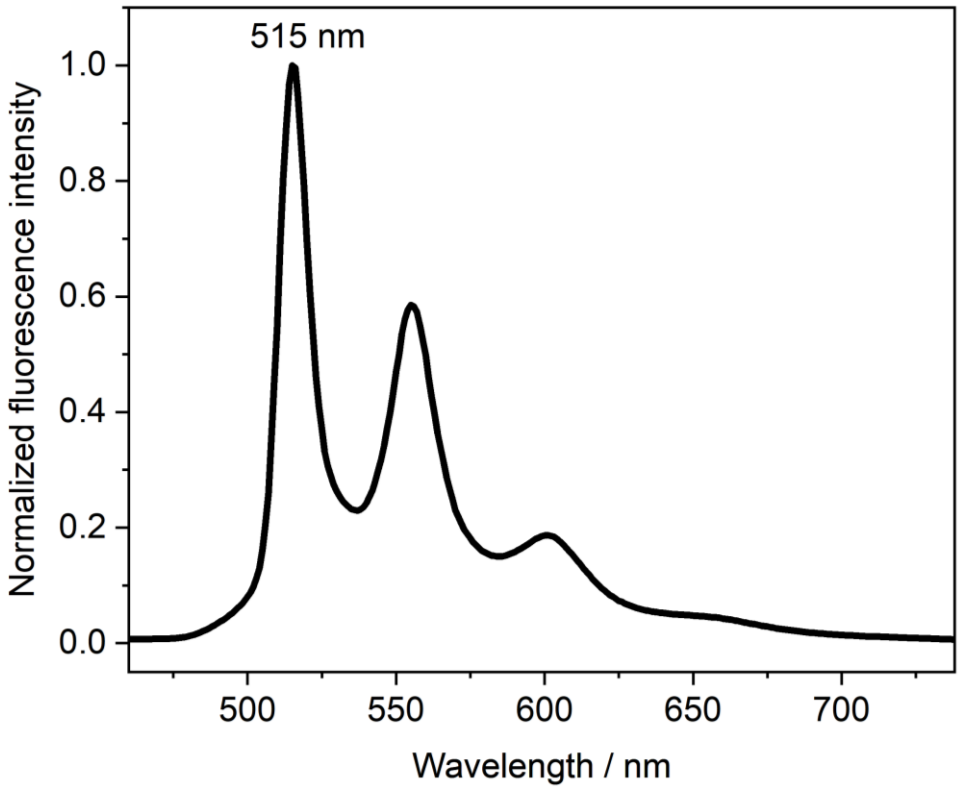

Figure S35. Normalized emission spectra (λ_{exc} = 380 nm) of **1,7-CF$_3$** recorded in $CHCl_3$

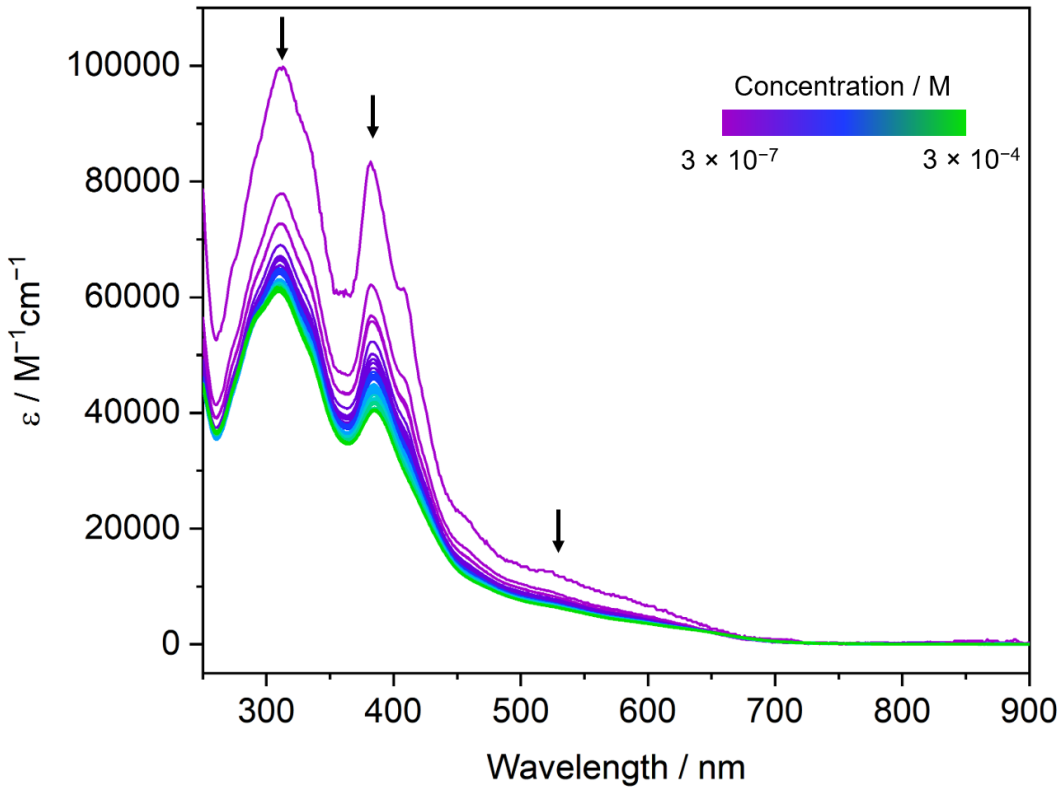

Figure S36. Absorption spectra of **1,6-OMe** recorded at various concentrations, between *ca.* 3×10^{-7} M and *ca.* 3×10^{-4} M, in $CHCl_3$ exhibiting a strong concentration dependence of the apparent molar absorption coefficient values (ε)

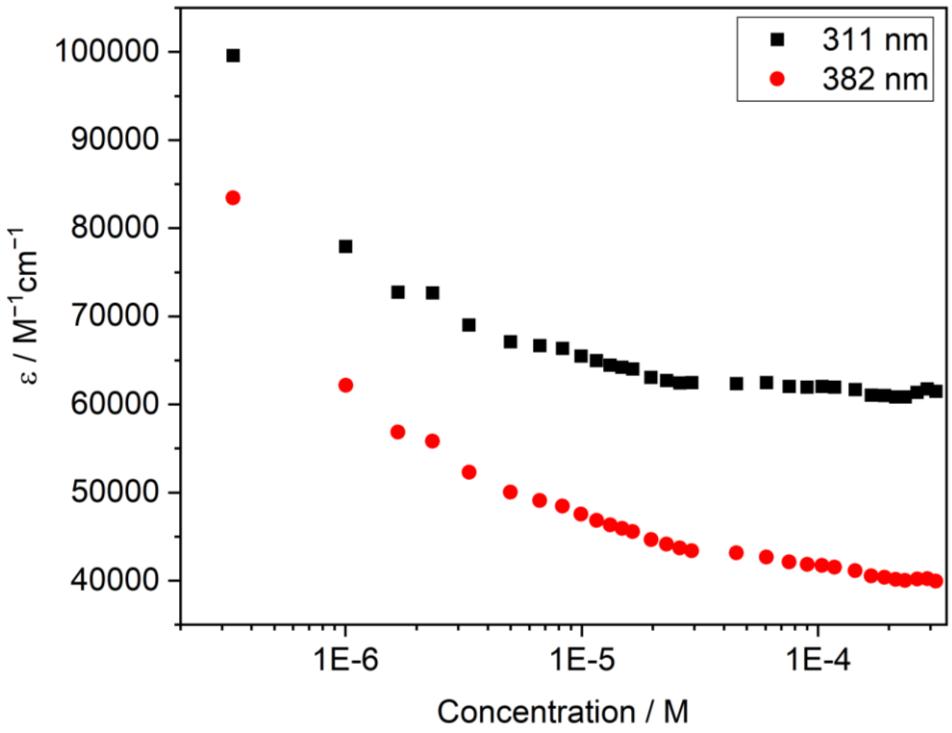

Figure S37. Plot of the apparent molar absorption coefficient ε of **1,6-OMe** at λ = 311 nm (black square), and λ = 382 nm (red dot) vs. concentration exhibiting a strong concentration dependence of the apparent molar absorption coefficient value. The apparent molar absorption coefficient of **1,6-OMe** decreases when increasing its concentration.

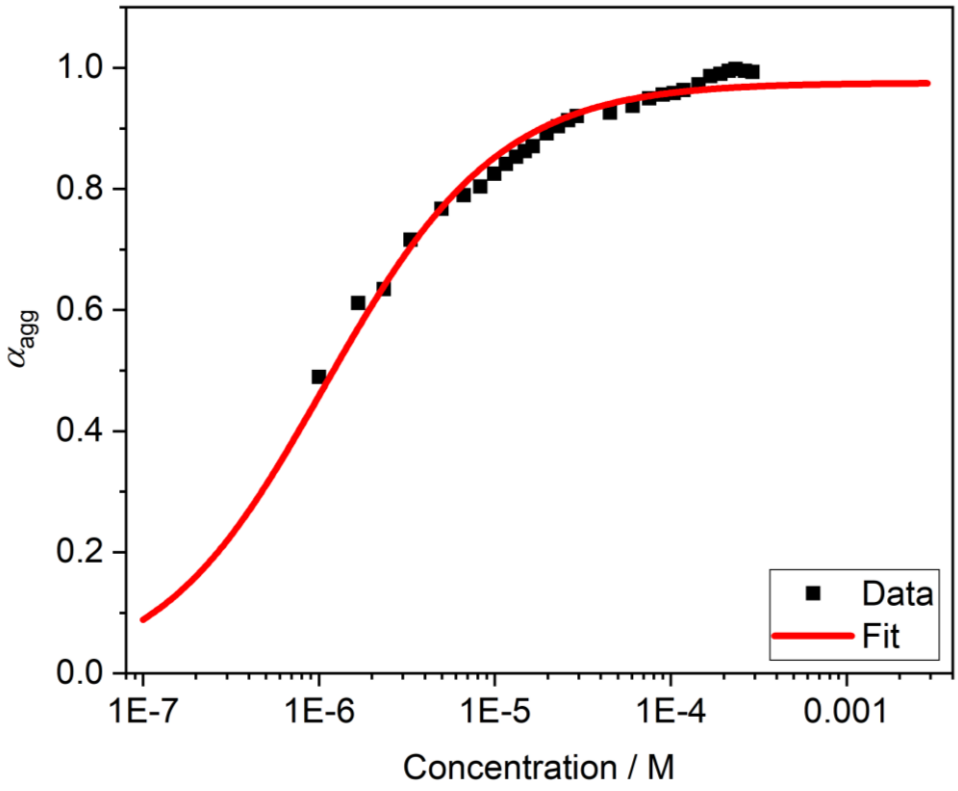

Figure S38. Non-linear least-squares fitting of the changes in the of the fraction of aggregated molecules (α_{agg}), calculated at λ = 382 nm, upon concentration increase of **1,6-OMe** in $CHCl_3$ using the isodesmic model. K_a = (5.1 ± 0.1) × 10^5 M^{-1}

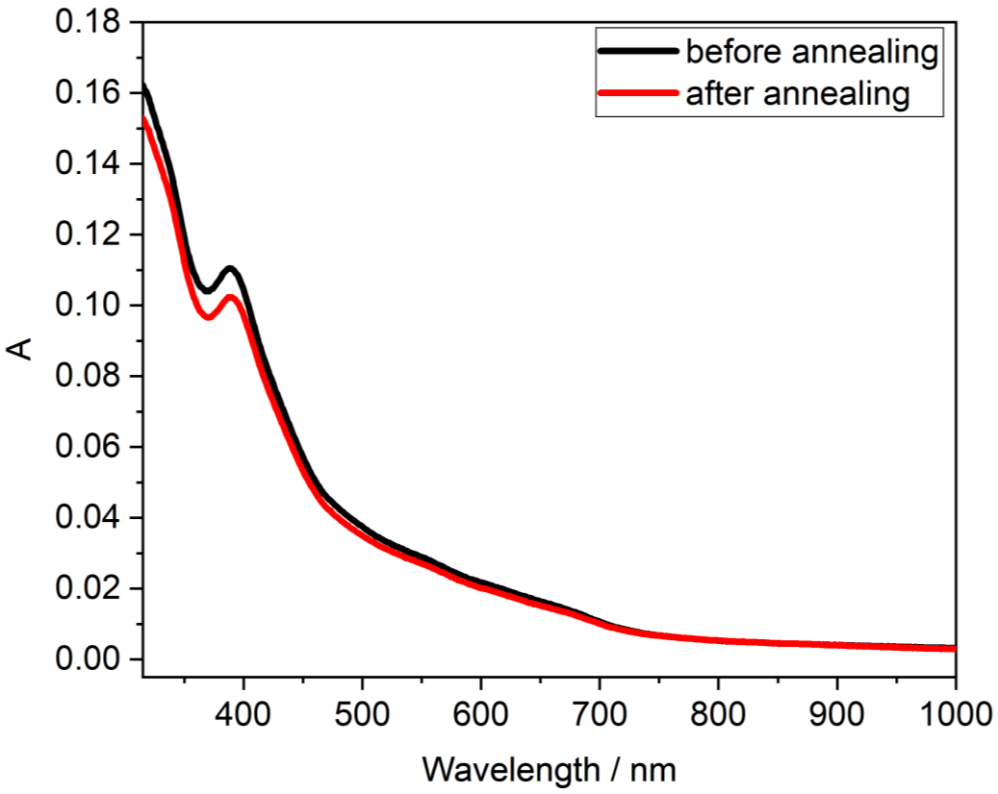

Figure S39. Absorption spectra of the thin film of **1,6-OMe** before (black line) and after (red line) annealing

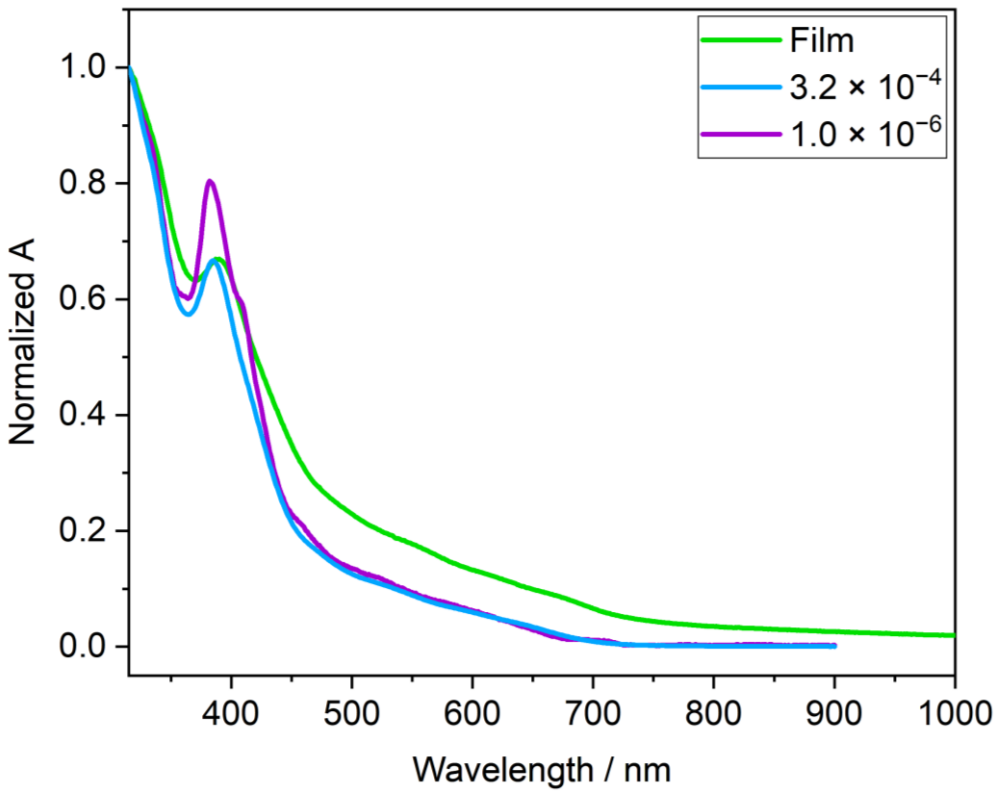

Figure S40. Comparison between the normalized absorption spectra of **1,6-OMe** in $CHCl_3$ solution at concentrations of 1.0×10^{-6} M (purple line) and 3.2×10^{-4} M (blue line) and as a thin film after annealing (green line)

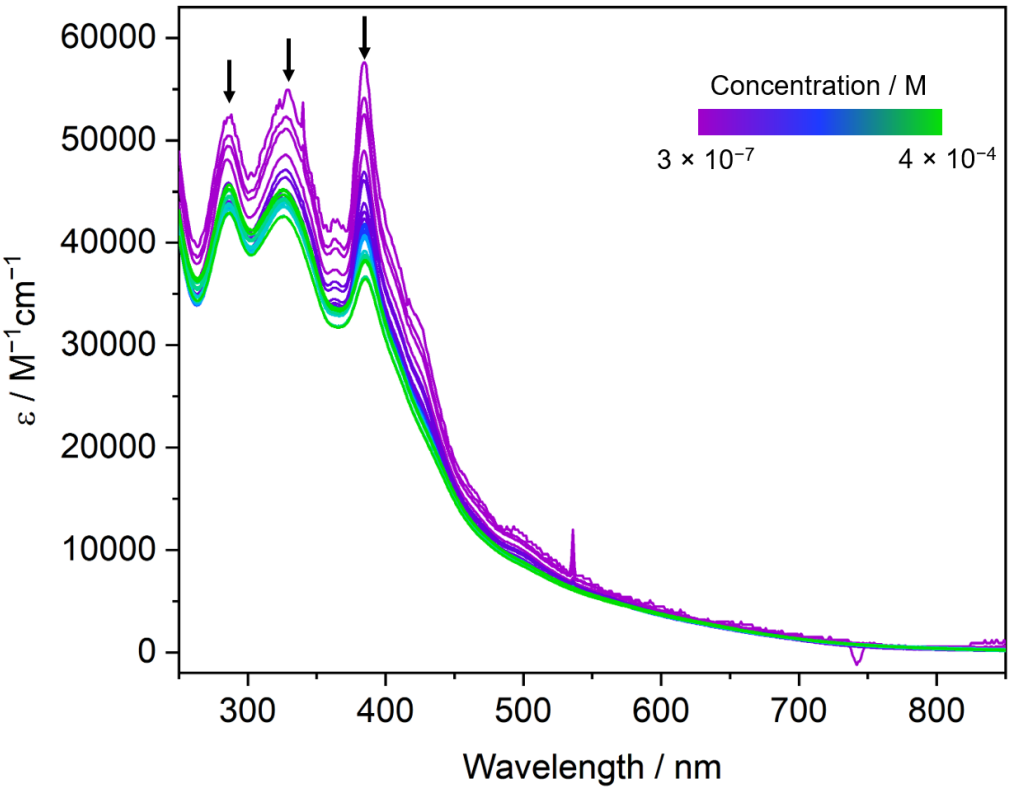

Figure S41. Absorption spectra of **1,7-OMe** recorded at various concentrations, between *ca.* 3×10^{-7} M and *ca.* 4×10^{-4} M, in $CHCl_3$ exhibiting a strong concentration dependence of the apparent molar absorption coefficient values (ε)

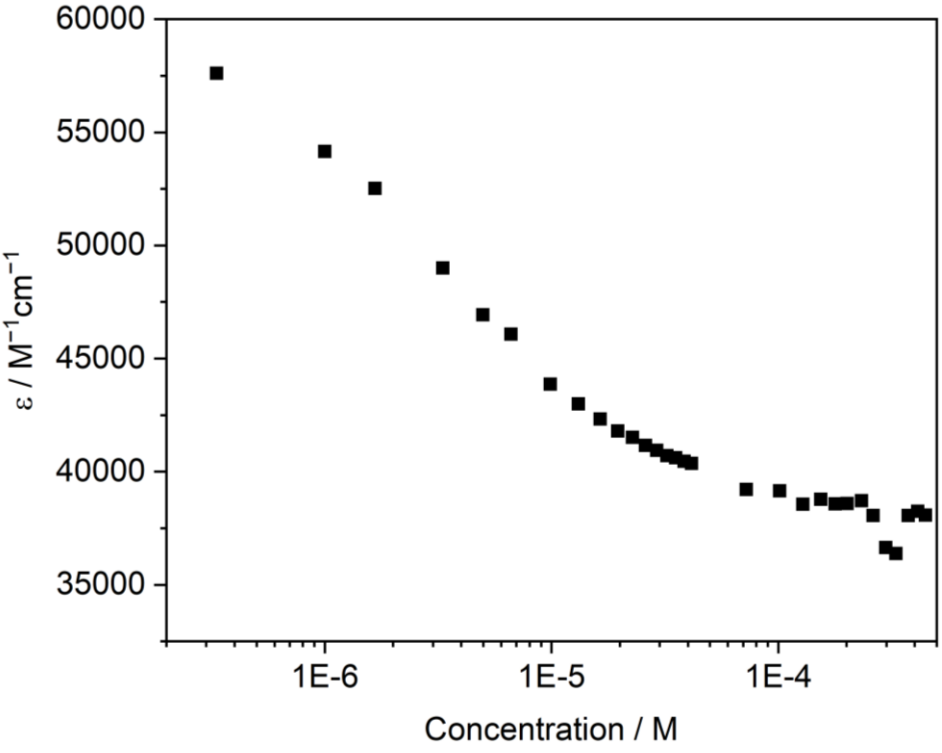

Figure S42. Plot of the apparent molar absorption coefficient ε of **1,7-OMe** at λ = 384 nm vs. concentration exhibiting a strong concentration dependence of the apparent molar absorption coefficient value. The apparent molar absorption coefficient of **1,7-OMe** decreases when increasing its concentration.

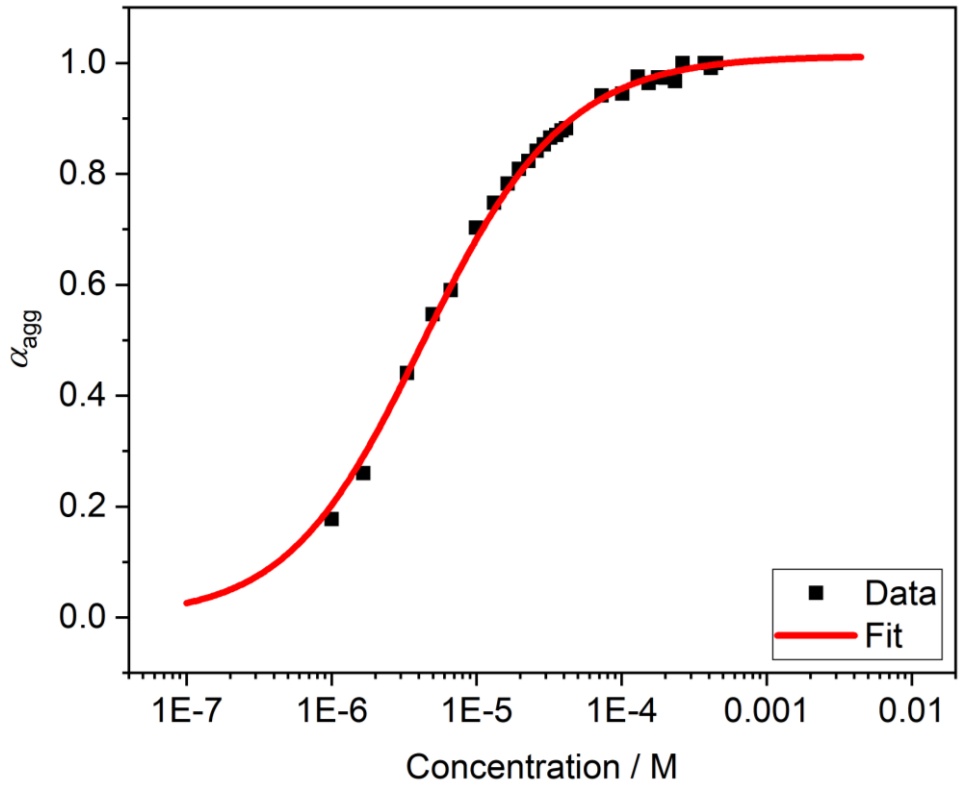

Figure S43. Non-linear least-squares fitting of the changes in the of the fraction of aggregated molecules (α_{agg}), calculated at λ = 384 nm, upon concentration increase of **1,7-OMe** in $CHCl_3$ using the isodesmic model. $K_a = (1.3 \pm 0.1) \times 10^5$ M^{-1}

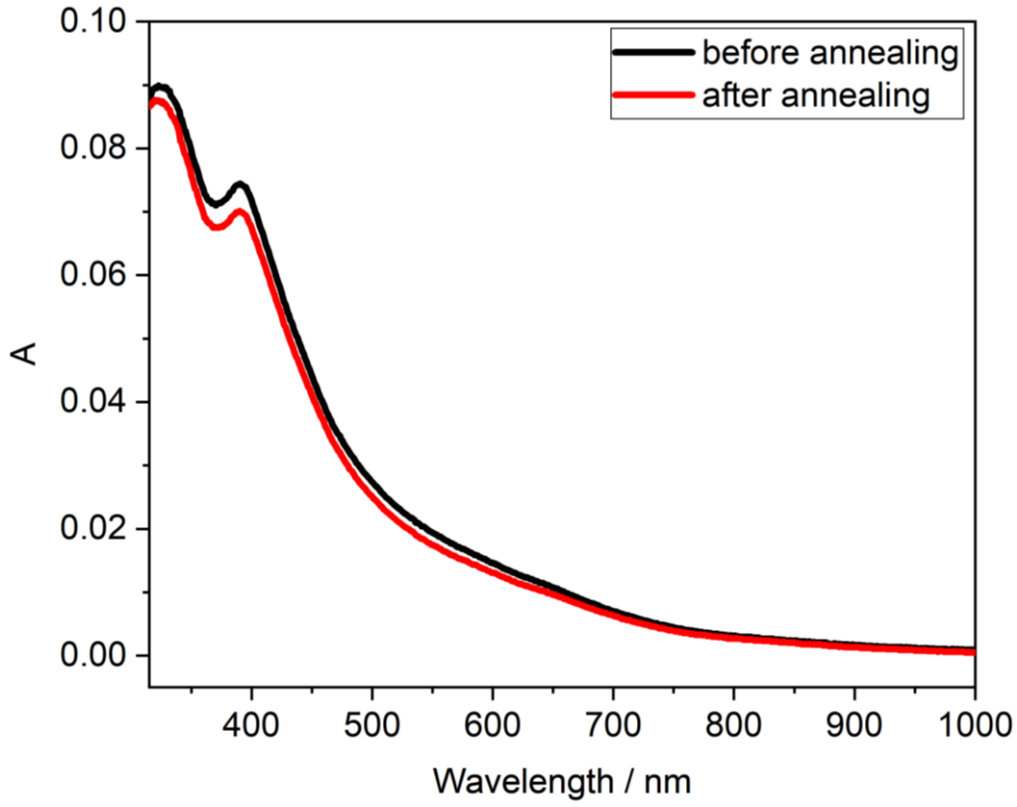

Figure S44. Absorption spectra of the thin film of **1,7-OMe** before (black line) and after (red line) annealing

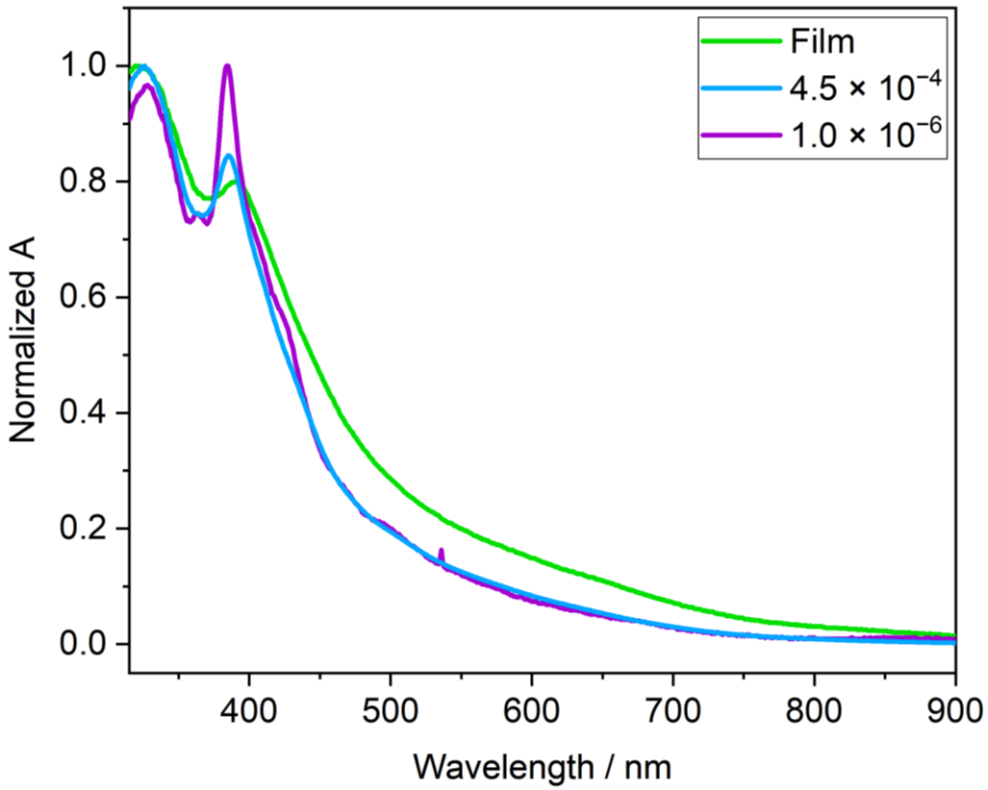

Figure S45. Comparison between the normalized absorption spectra of **1,7-OMe** in $CHCl_3$ solution at concentrations of 1.0×10^{-6} M (purple line) and 4.5×10^{-4} M (blue line) and as a thin film after annealing (green line)

4. Electrochemistry

Cyclic voltammetry was carried out on a Bio-Logic SAS SP-150 potentiostat, driven by the EC-Lab software, with a three electrodes configuration, using a silver wire as the reference electrode (calibrated to the Fc/Fc^+ couple after measurements), a Pt wire as counter electrode, and a Pt electrode as working electrode. Samples were dissolved in a CH_2Cl_2 solution containing $^nBu_4NPF_6$ (0.1 M) and Fc (0.1 mM) which were used as supporting electrolyte and internal reference, respectively. The scan rate was 100 mV/s and the measurements were performed in an argon-filled glovebox. It must be noted that compounds **1,7-CF$_3$** and **C-1,7** were not studied by cyclic voltammetry on account of their extremely limited solubilities in the solvent mixture used for the cyclic voltammetry experiments. Deconvolution of the voltammograms were performed employing a custom MATLAB software developed in-house.

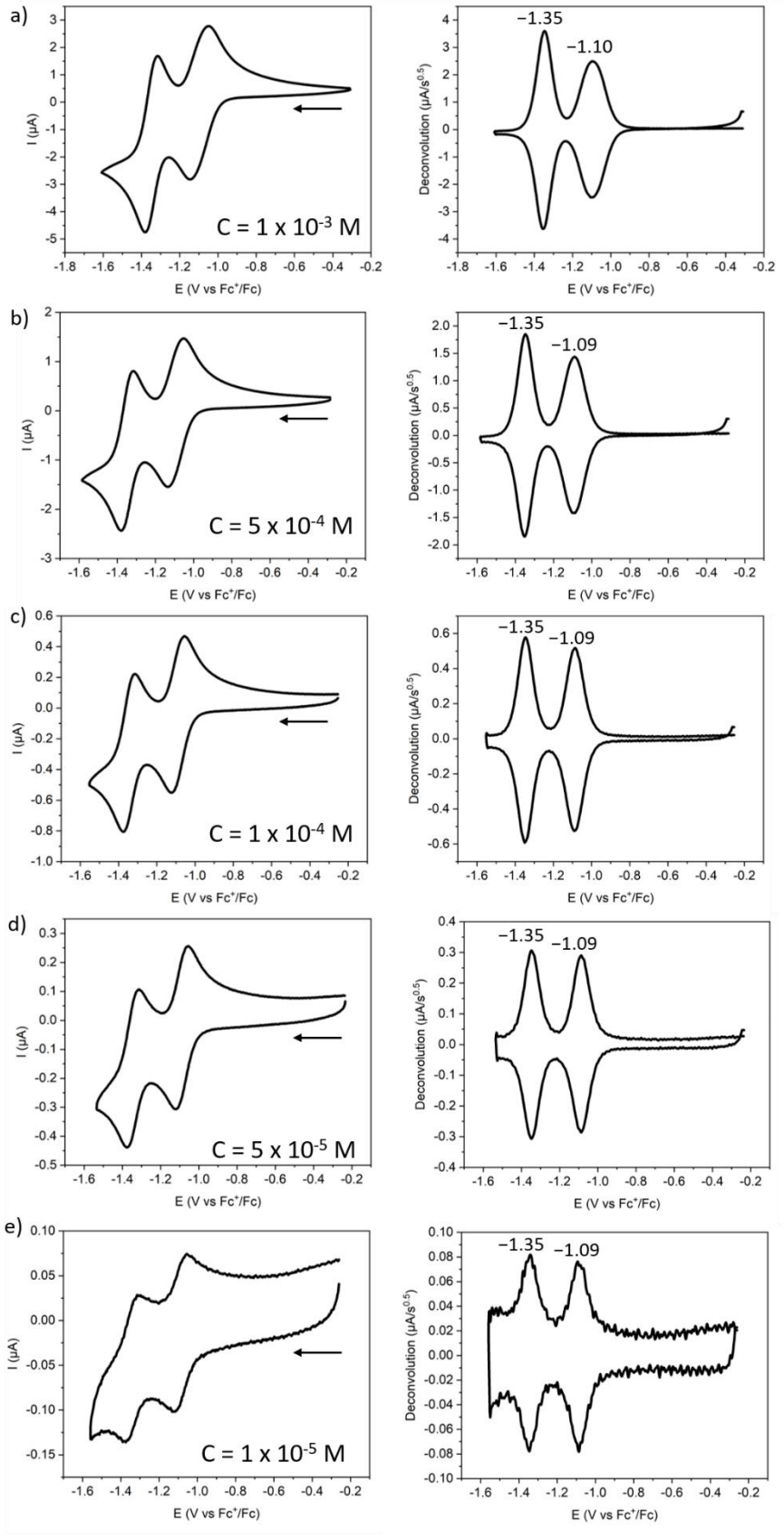

Figure S46. Cyclic voltammetry (left) and its deconvolution (right) of AzaBPDI **aPDI-Ph** recorded at various concentrations, i.e. (a) 1 mM, (b) 0.5 mM, (c) 0.1 mM, (d) 0.05 mM, and (e) 0.01 mM, in a CH_2Cl_2 solution containing $^{n}Bu_4NPF_6$ (0.1 M) as supporting electrolyte and Fc (0.1 mM) as internal reference.

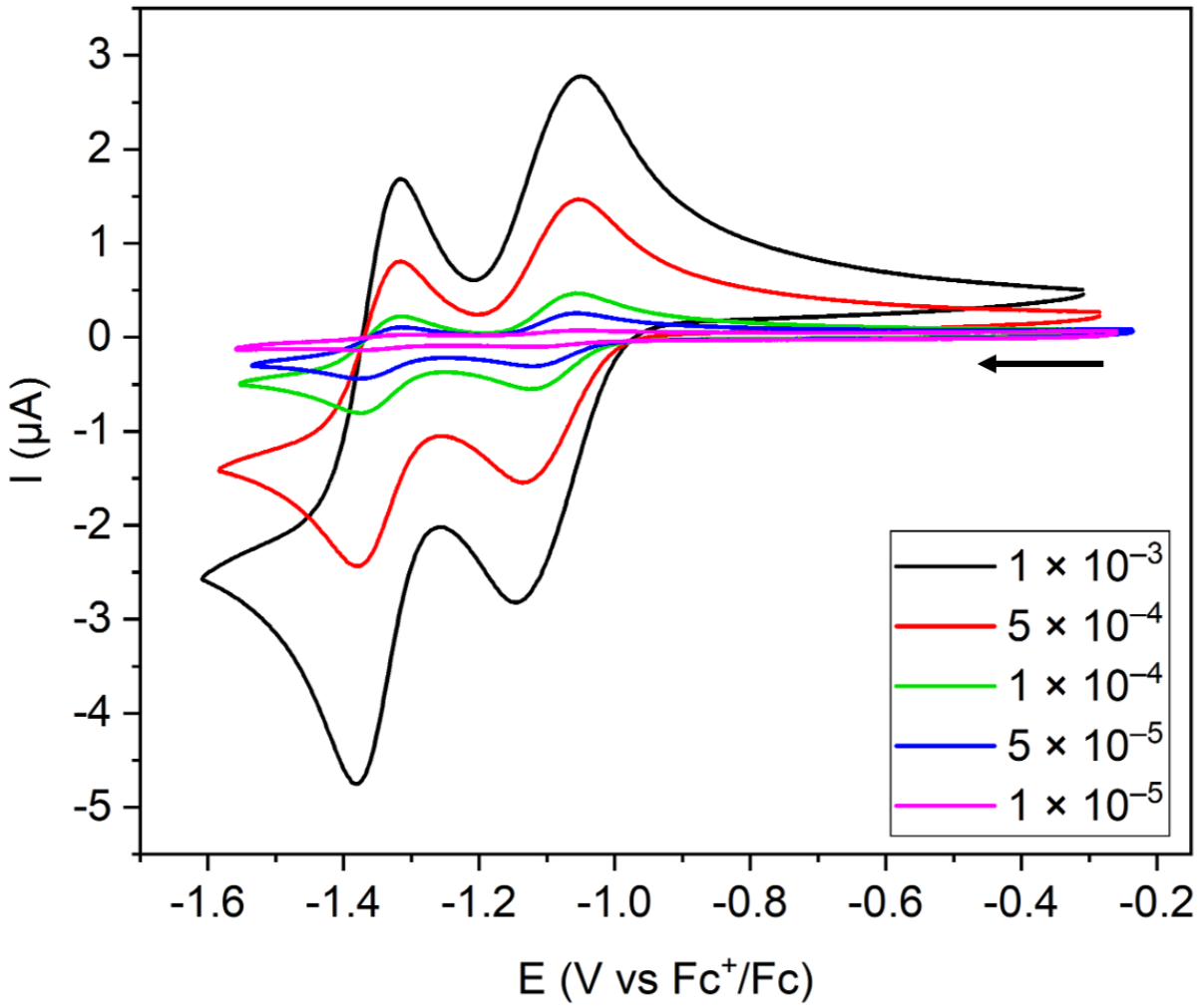

Figure S47. Cyclic voltammetry of AzaBPDI **aPDI-Ph** recorded at various concentrations (1 – 0.01 mM) in a CH_2Cl_2 solution containing $^nBu_4NPF_6$ (0.1 M) as supporting electrolyte and Fc (0.1 mM) as internal reference.

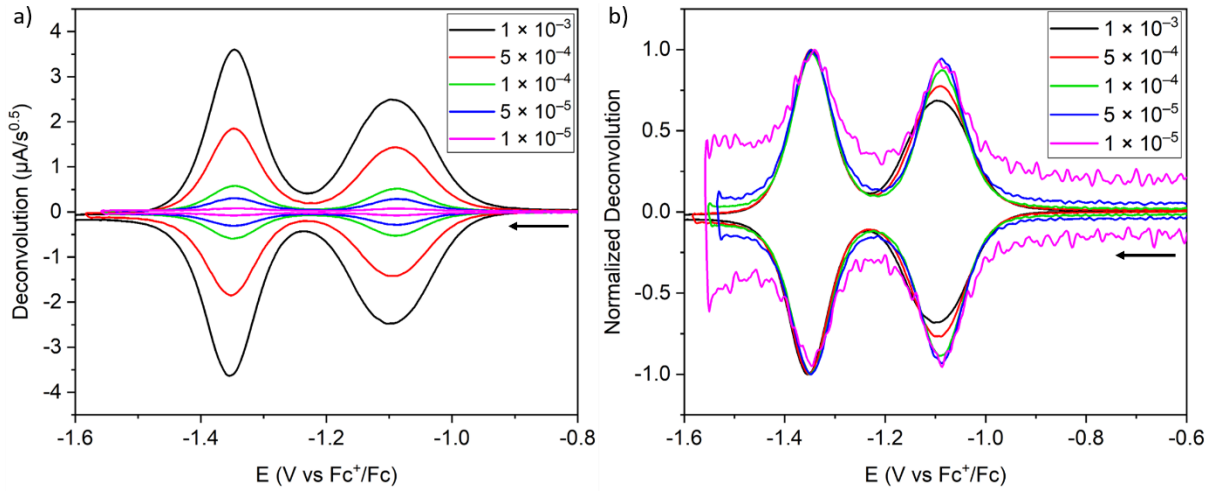

Figure S48. (a) Deconvolutions and (b) normalized deconvolutions of the cyclic voltammograms of AzaBPDI **aPDI-Ph** recorded at various concentrations (1 – 0.01 mM) in a CH_2Cl_2 solution containing $^nBu_4NPF_6$ (0.1 M) as supporting electrolyte and Fc (0.1 mM) as internal reference.

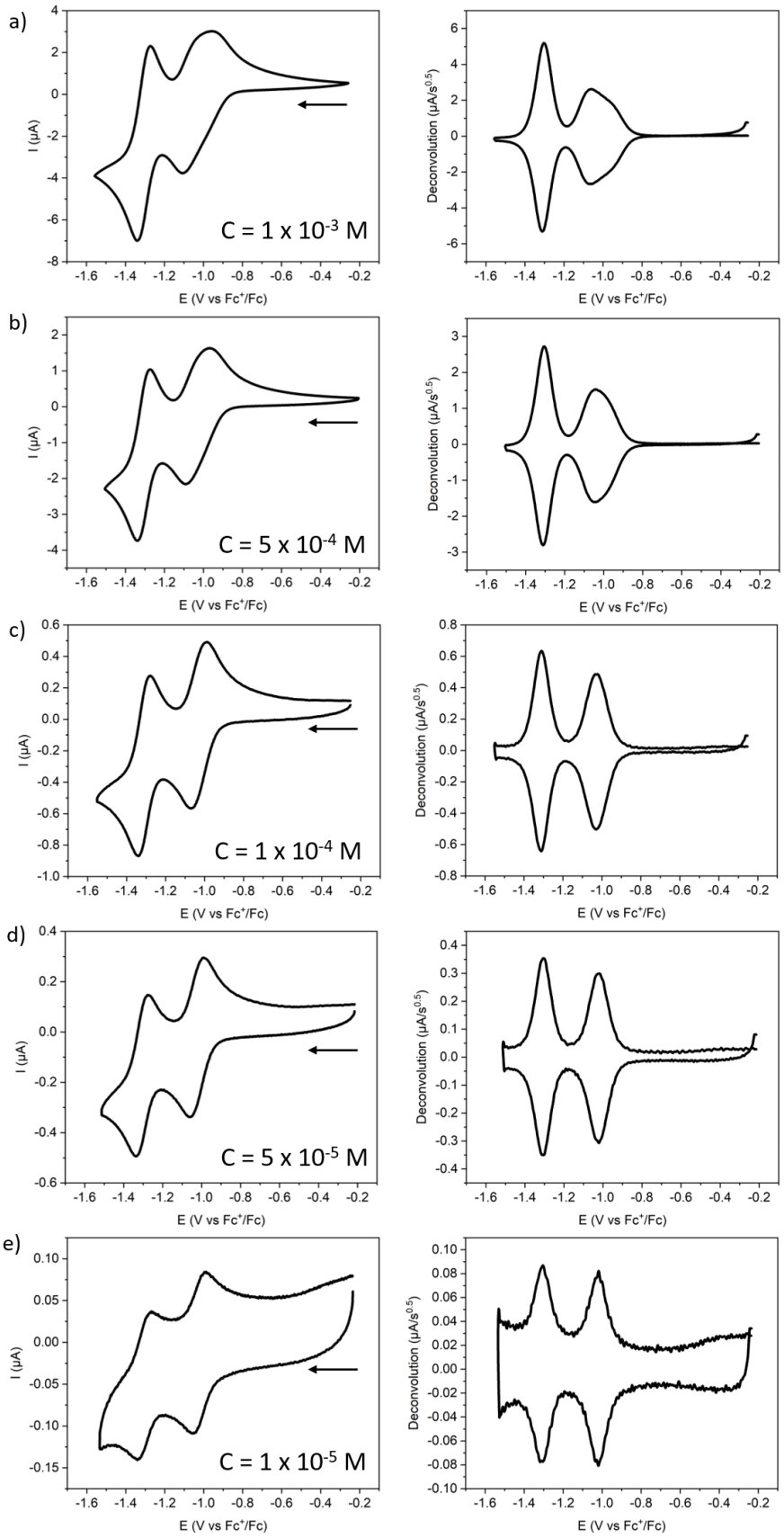

Figure S49. Cyclic voltammetry (left) and its deconvolution (right) of AzaBPDI **aPDI-CF$_3$** recorded at various concentrations, i.e. (a) 1 mM, (b) 0.5 mM, (c) 0.1 mM, (d) 0.05 mM, and (e) 0.01 mM, in a CH_2Cl_2 solution containing $^nBu_4NPF_6$ (0.1 M) as supporting electrolyte and Fc (0.1 mM) as internal reference.

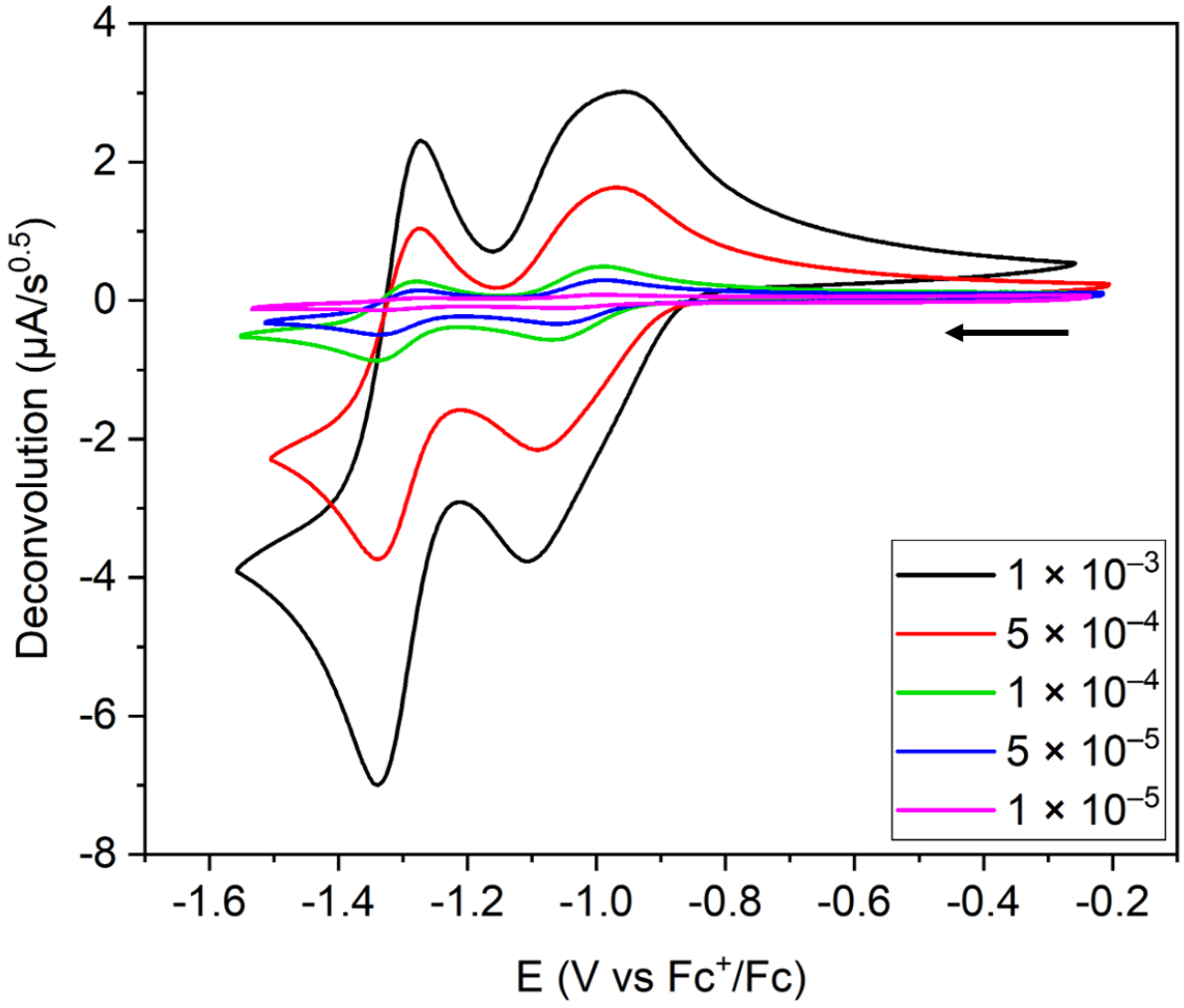

Figure S50. Cyclic voltammetry of AzaBPDI **aPDI-CF$_3$** recorded at various concentrations (1 – 0.01 mM) in a CH_2Cl_2 solution containing ^{n}Bu$_4$NPF$_6$ (0.1 M) as supporting electrolyte and Fc (0.1 mM) as internal reference.

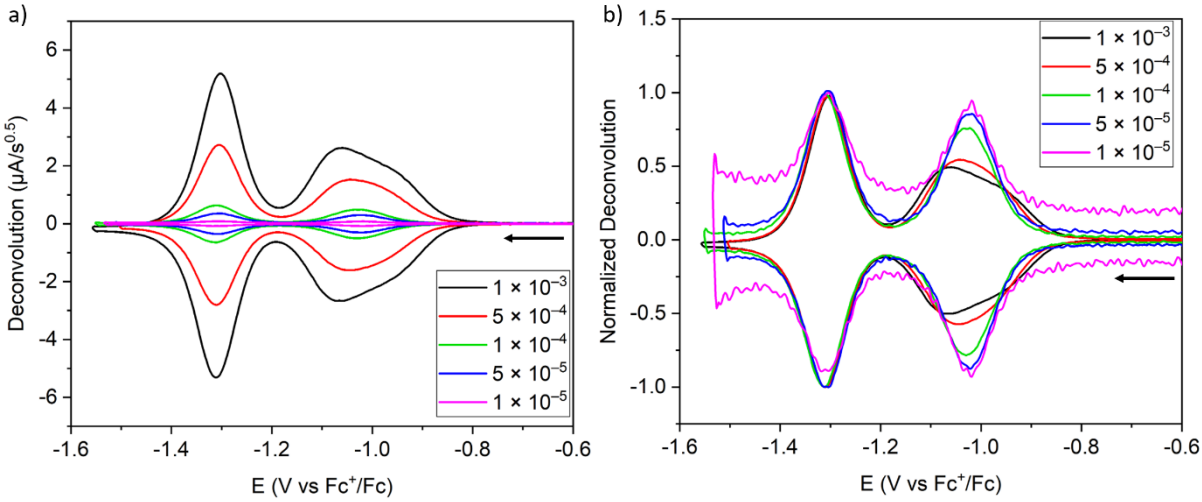

Figure S51. (a) Deconvolutions and (b) normalized deconvolutions of the cyclic voltammograms of AzaBPDI **aPDI-CF$_3$** recorded at various concentrations (1 – 0.01 mM) in a CH_2Cl_2 solution containing ^{n}Bu$_4$NPF$_6$ (0.1 M) as supporting electrolyte and Fc (0.1 mM) as internal reference.

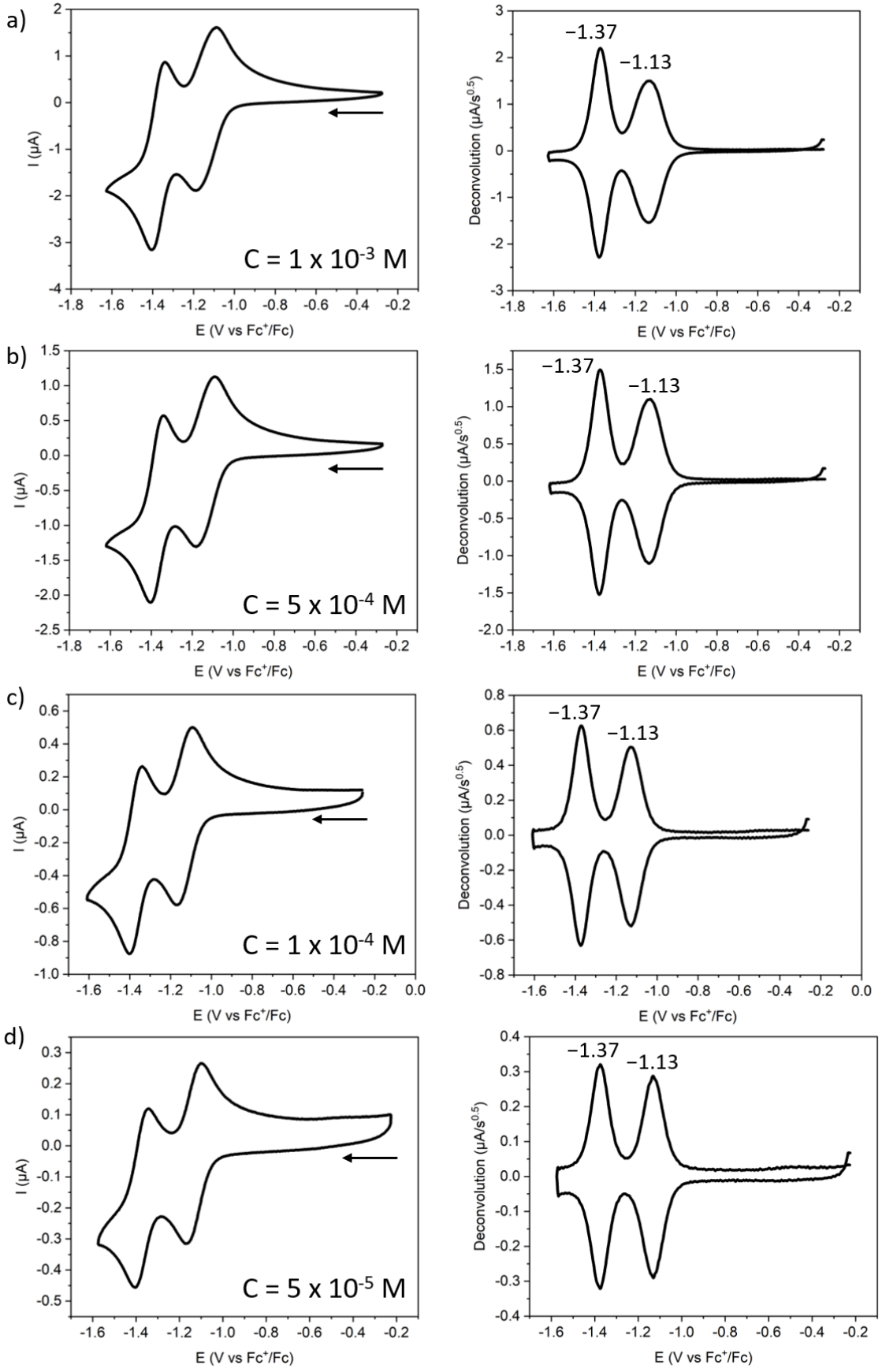

Figure S52. Cyclic voltammetry (left) and its deconvolution (right) of AzaBPDI **aPDI-OMe** recorded at various concentrations, i.e. (a) 1 mM, (b) 0.5 mM, (c) 0.1 mM, and (d) 0.05 mM, in a CH_2Cl_2 solution containing $^{n}Bu_4NPF_6$ (0.1 M) as supporting electrolyte and Fc (0.1 mM) as internal reference.

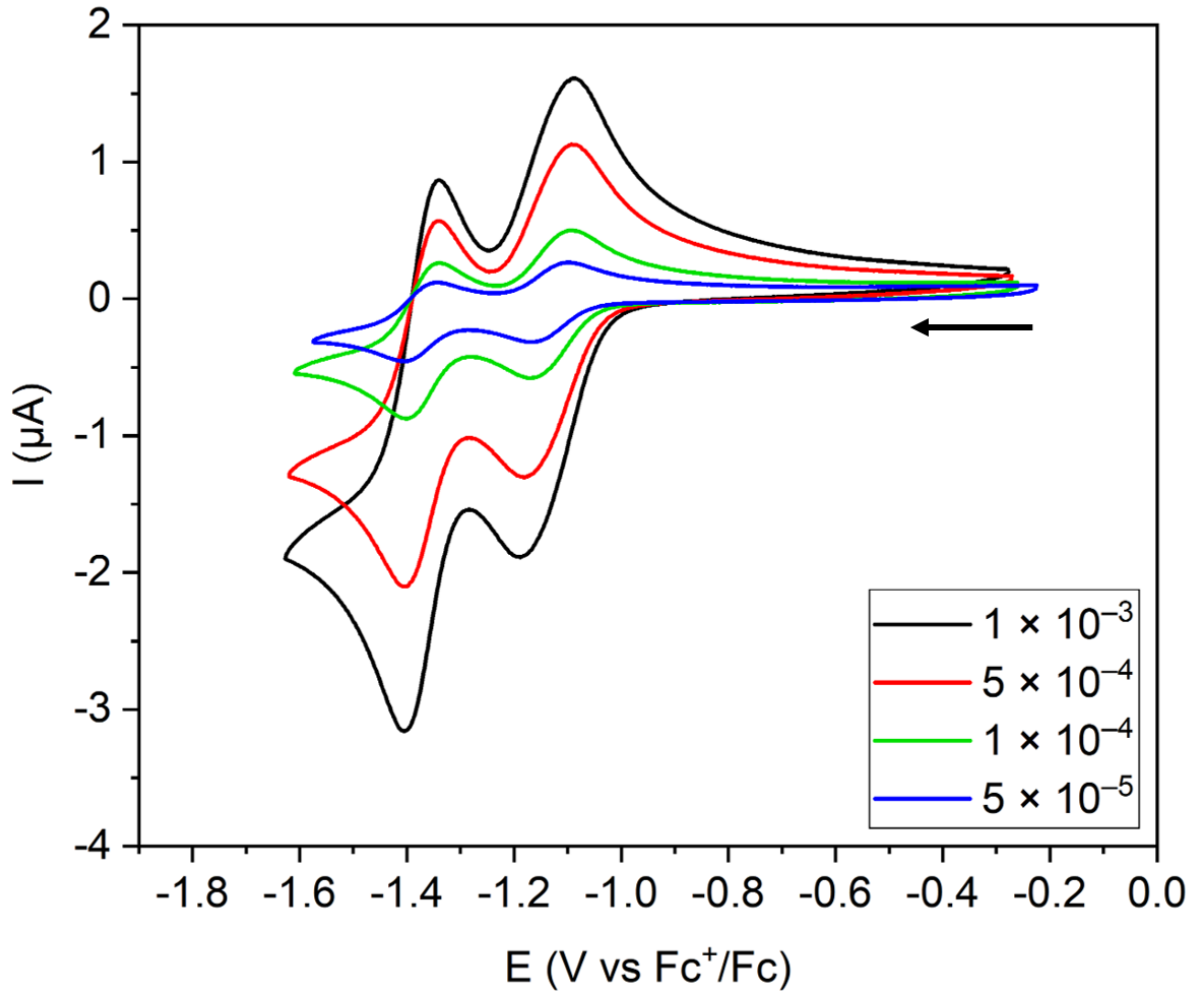

Figure S53. Cyclic voltammetry of AzaBPDI **aPDI-OMe** recorded at various concentrations (1 – 0.05 mM) in a CH_2Cl_2 solution containing $^nBu_4NPF_6$ (0.1 M) as supporting electrolyte and Fc (0.1 mM) as internal reference.

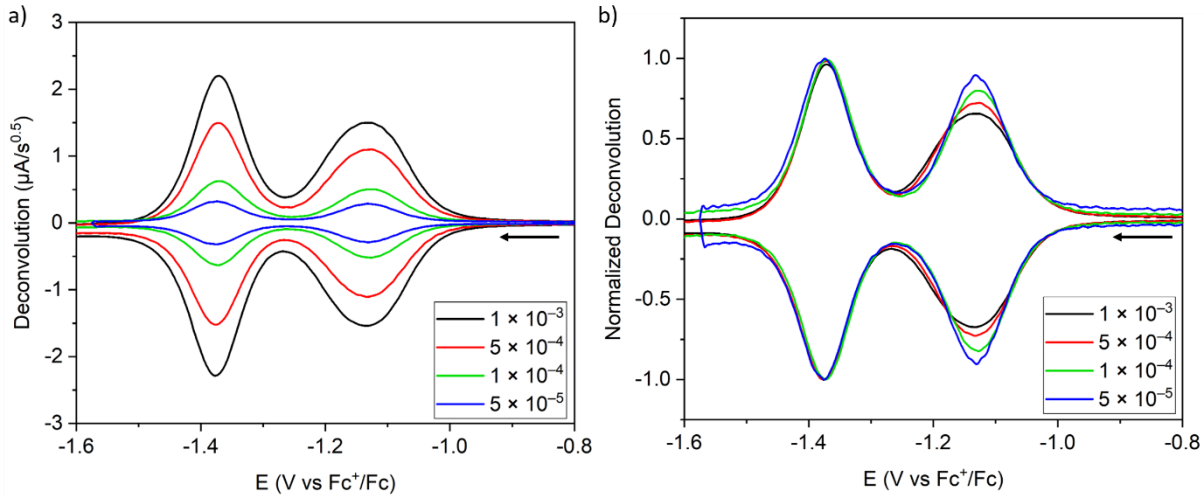

Figure S54. (a) Deconvolutions and (b) normalized deconvolutions of the cyclic voltammograms of AzaBPDI **aPDI-OMe** recorded at various concentrations (1 – 0.05 mM) in a CH_2Cl_2 solution containing $^nBu_4NPF_6$ (0.1 M) as supporting electrolyte and Fc (0.1 mM) as internal reference.

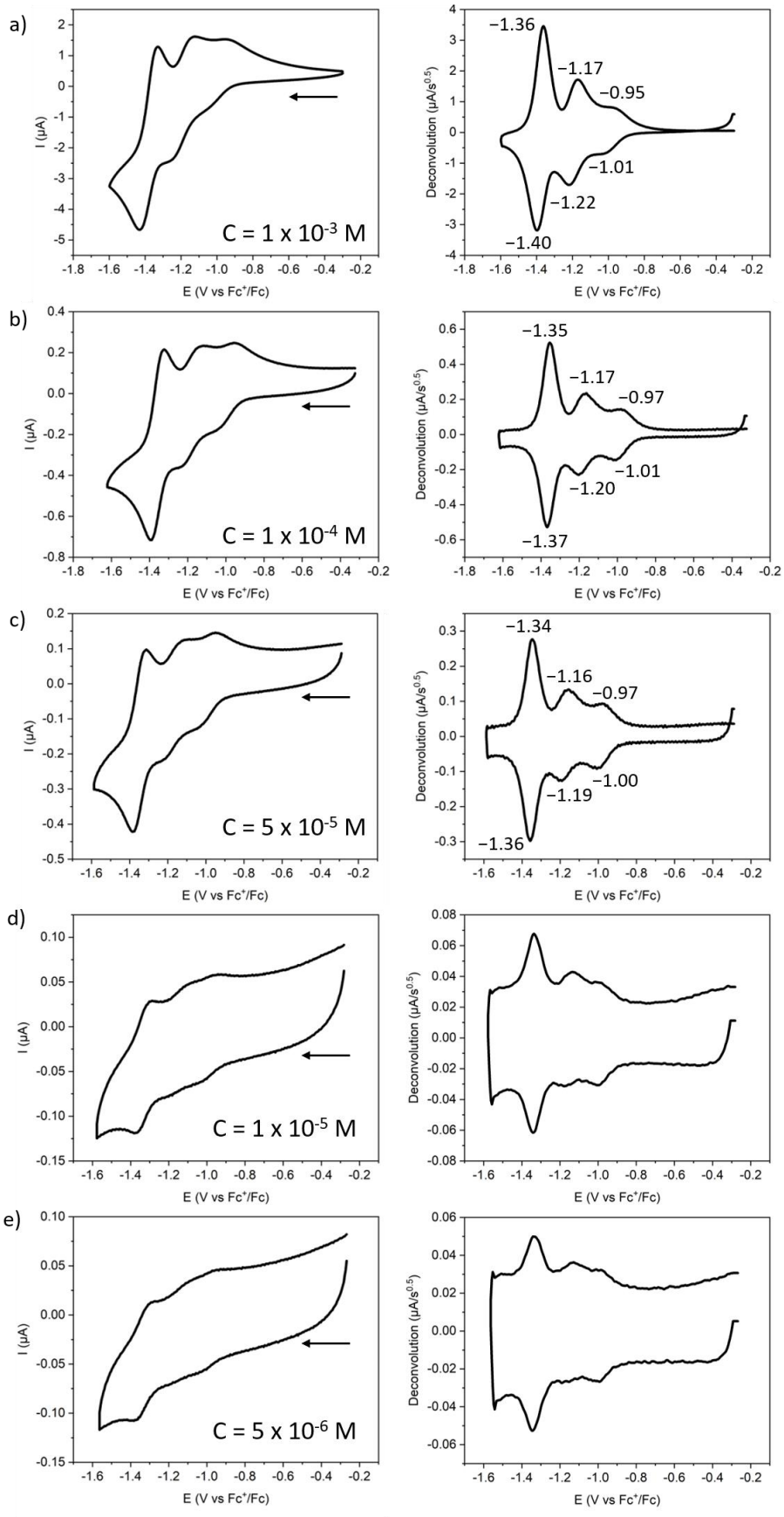

Figure S55. Cyclic voltammetry (left) and its deconvolution (right) of BACD **1,6-Ph** recorded at various concentrations, i.e. (a) 1 mM, (b) 0.1 mM, (c) 0.05 mM, (d) 0.01 mM, and (e) 0.005 mM, in a CH_2Cl_2 solution containing $^{n}Bu_4NPF_6$ (0.1 M) as supporting electrolyte and Fc (0.1 mM) as internal reference.

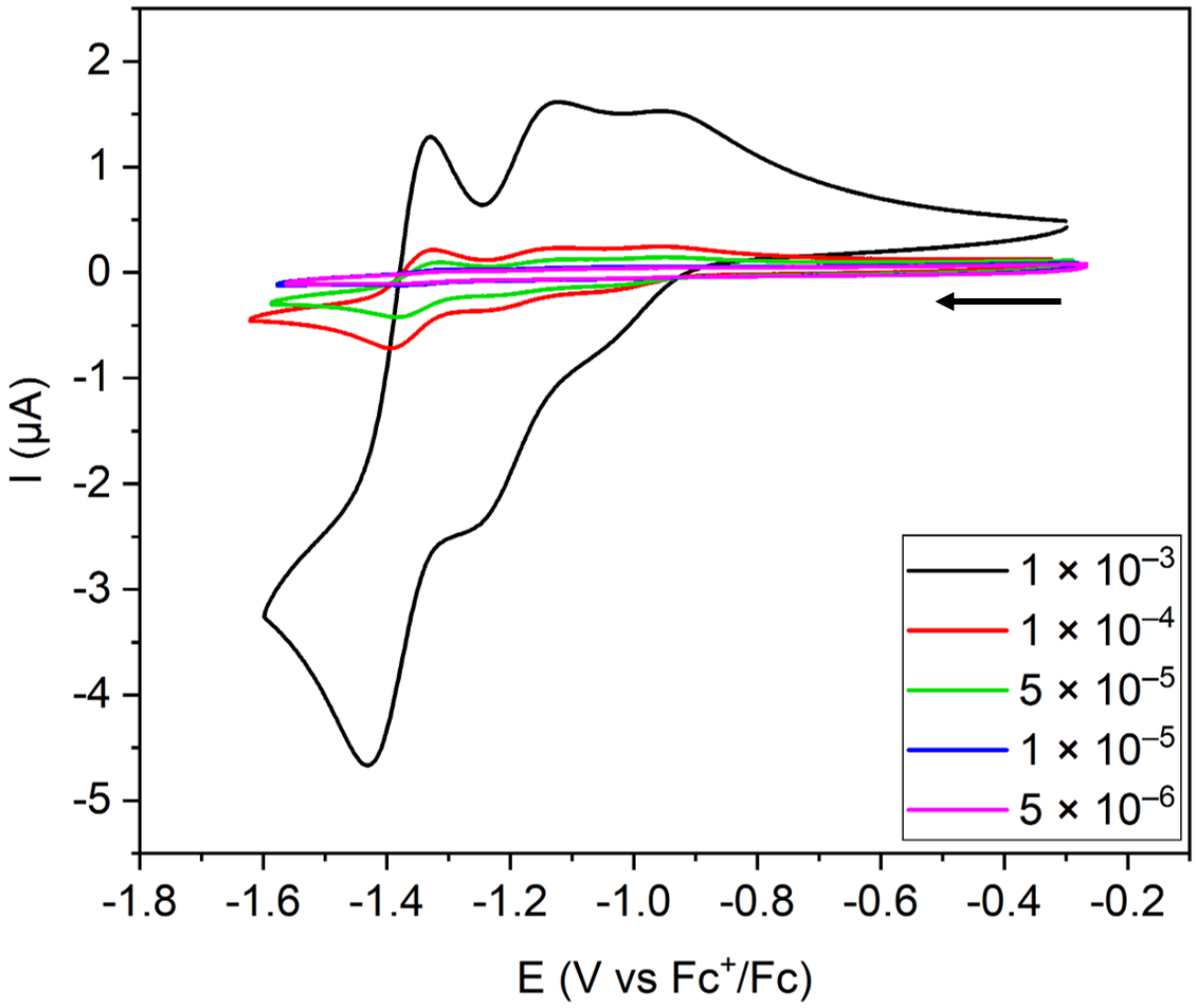

Figure S56. Cyclic voltammetry of BACD **1,6-Ph** recorded at various concentrations (1 – 0.005 mM) in a CH_2Cl_2 solution containing $^nBu_4NPF_6$ (0.1 M) as supporting electrolyte and Fc (0.1 mM) as internal reference.

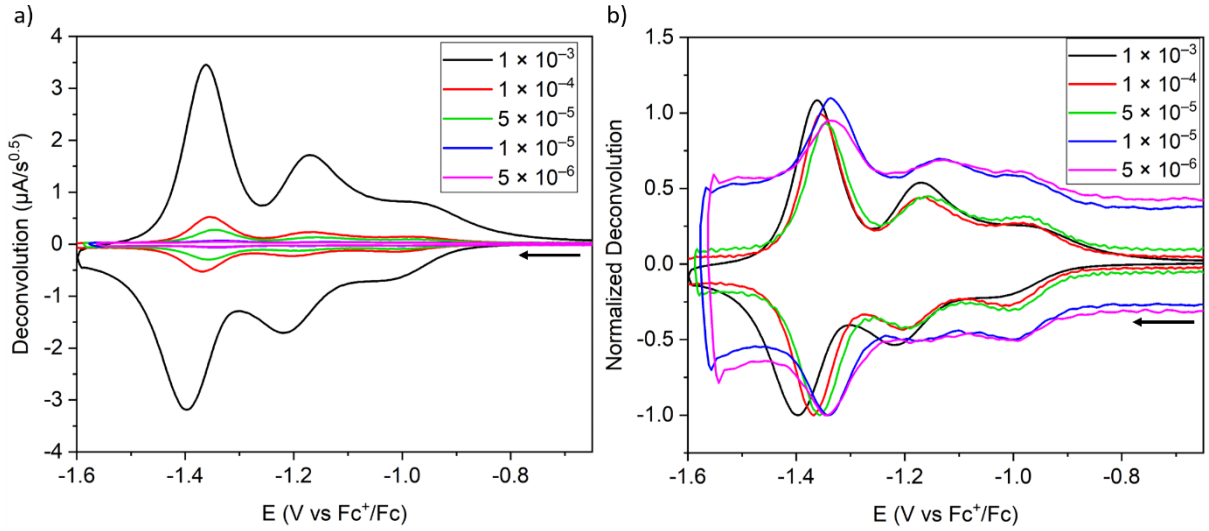

Figure S57. (a) Deconvolutions and (b) normalized deconvolutions of the cyclic voltammograms of BACD **1,6-Ph** recorded at various concentrations (1 – 0.005 mM) in a CH_2Cl_2 solution containing $^nBu_4NPF_6$ (0.1 M) as supporting electrolyte and Fc (0.1 mM) as internal reference.

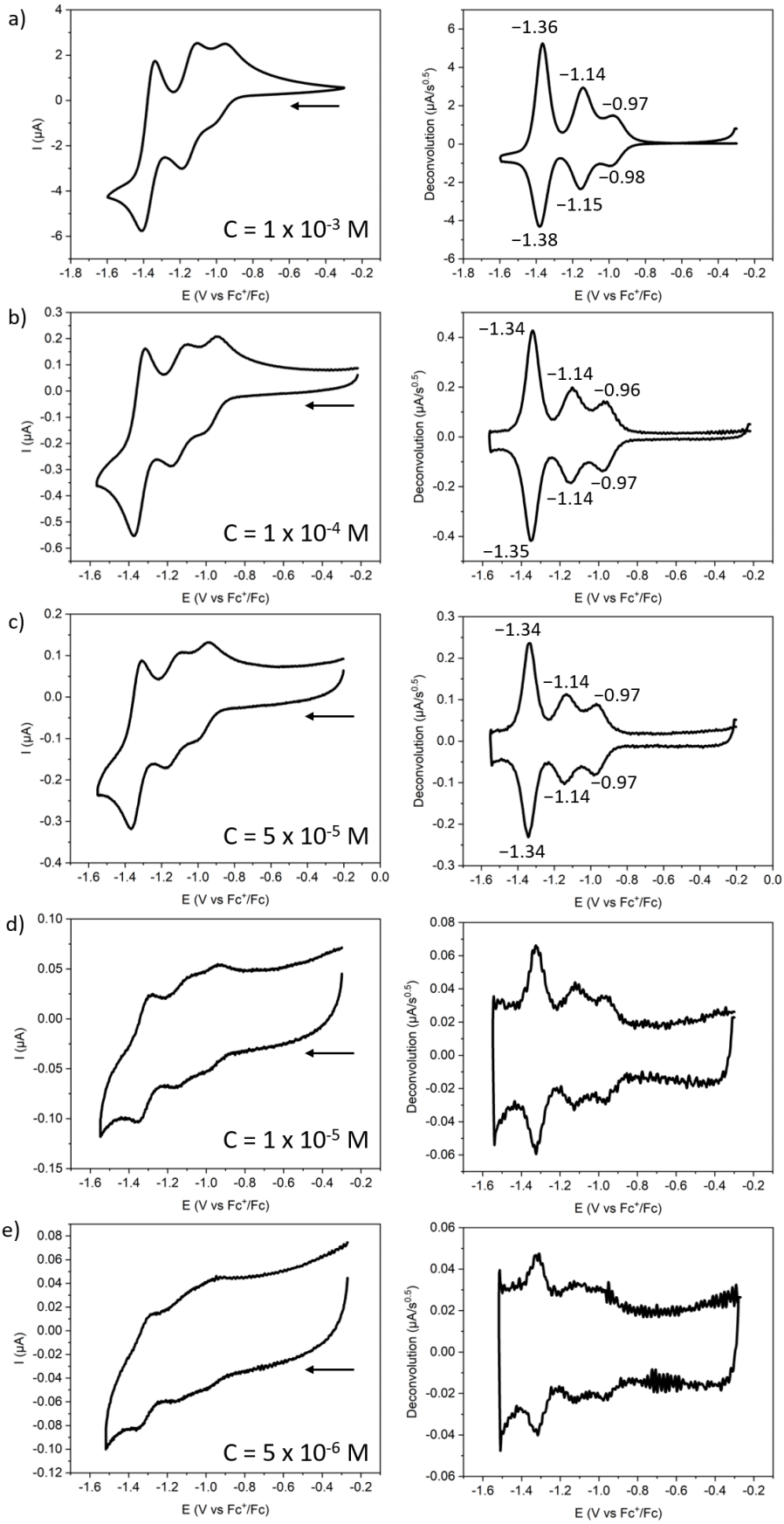

Figure S58. Cyclic voltammetry (left) and its deconvolution (right) of BACD **1,7-Ph** recorded at various concentrations, i.e. (a) 1 mM, (b) 0.1 mM, (c) 0.05 mM, (d) 0.01 mM, and (e) 0.005 mM, in a CH_2Cl_2 solution containing $^nBu_4NPF_6$ (0.1 M) as supporting electrolyte and Fc (0.1 mM) as internal reference.

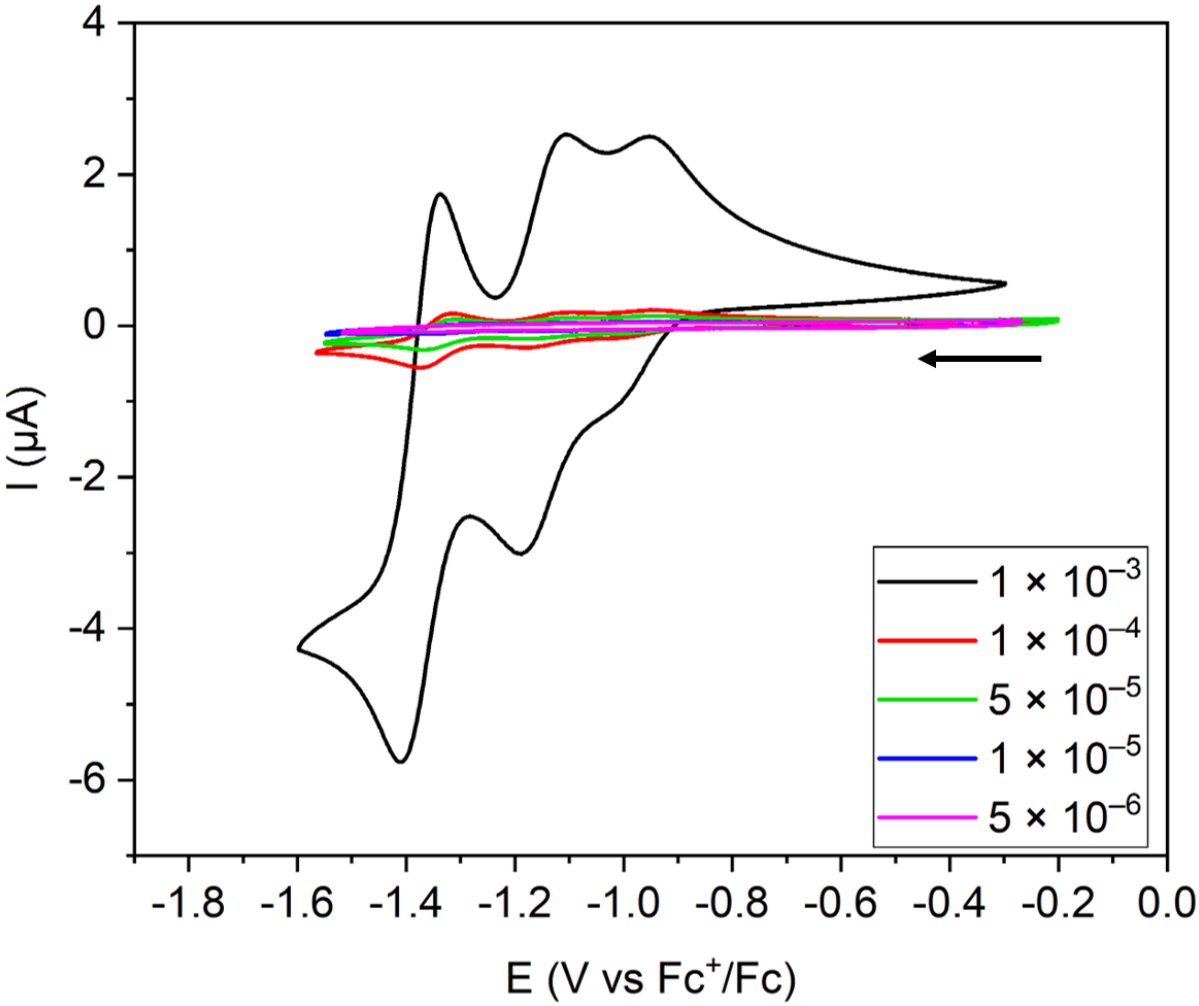

Figure S59. Cyclic voltammetry of BACD **1,7-Ph** recorded at various concentrations (1 – 0.005 mM) in a CH_2Cl_2 solution containing $^nBu_4NPF_6$ (0.1 M) as supporting electrolyte and Fc (0.1 mM) as internal reference.

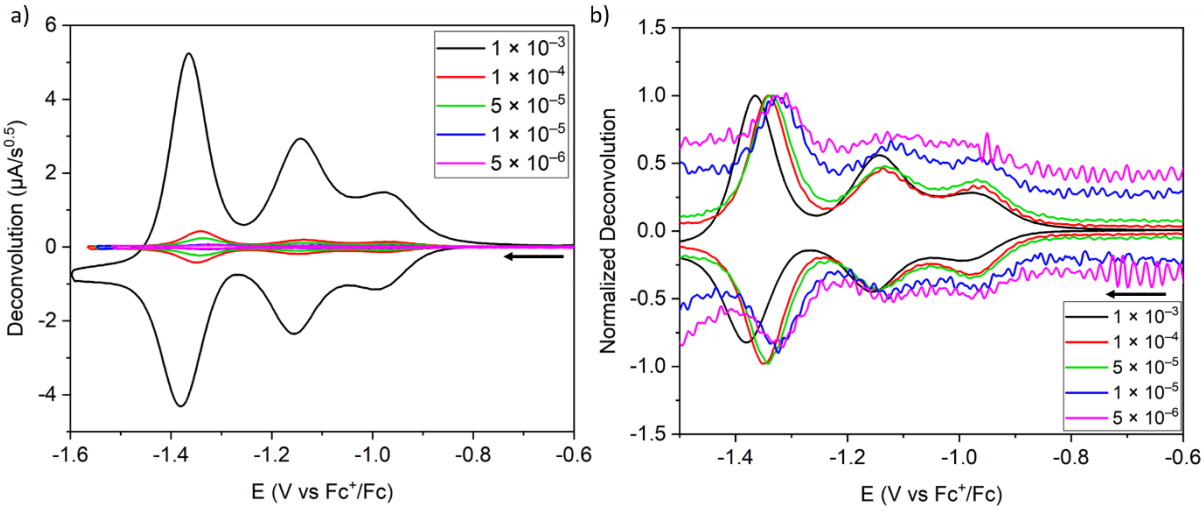

Figure S60. (a) Deconvolutions and (b) normalized deconvolutions of the cyclic voltammograms of BACD **1,7-Ph** recorded at various concentrations (1 – 0.005 mM) in a CH_2Cl_2 solution containing $^nBu_4NPF_6$ (0.1 M) as supporting electrolyte and Fc (0.1 mM) as internal reference.

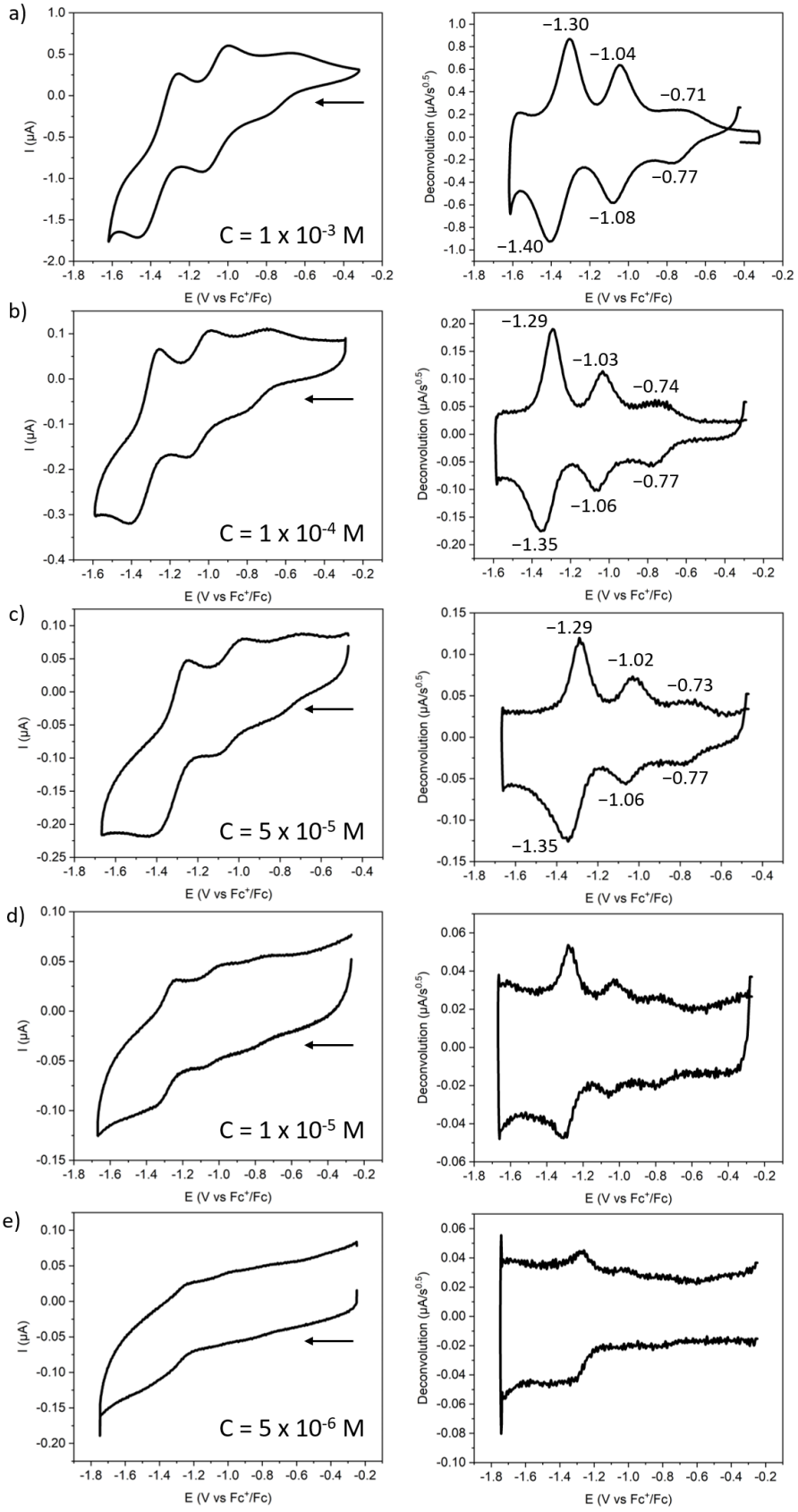

Figure S61. Cyclic voltammetry (left) and its deconvolution (right) of BACD **1,6-CF$_3$** recorded at various concentrations, i.e. (a) 1 mM, (b) 0.1 mM, (c) 0.05 mM, (d) 0.01 mM, and (e) 0.005 mM, in a CH_2Cl_2 solution containing $^nBu_4NPF_6$ (0.1 M) as supporting electrolyte and Fc (0.1 mM) as internal reference.

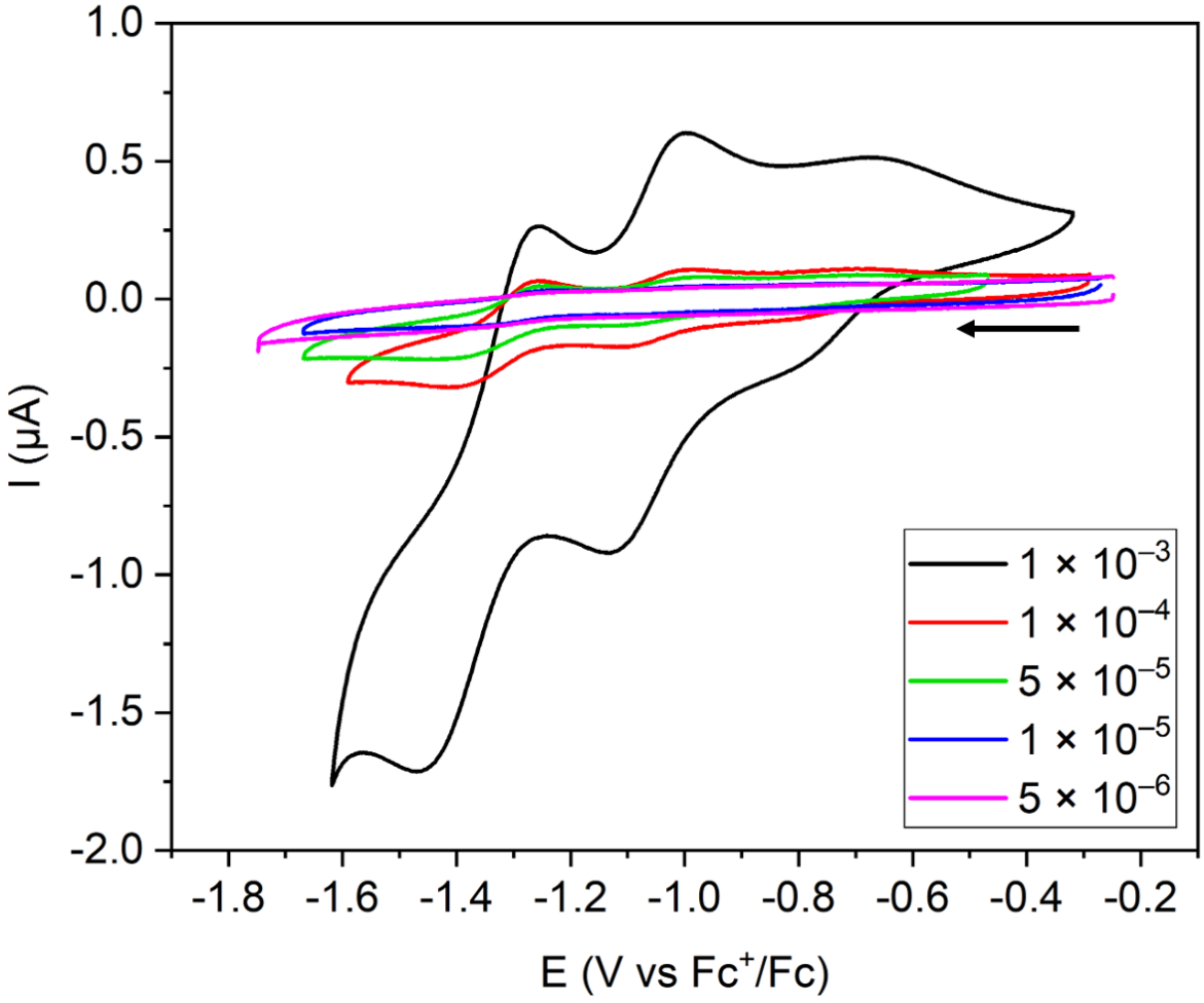

Figure S62. Cyclic voltammetry of BACD **1,6-CF$_3$** recorded at various concentrations (1 – 0.005 mM) in a CH_2Cl_2 solution containing $^nBu_4NPF_6$ (0.1 M) as supporting electrolyte and Fc (0.1 mM) as internal reference.

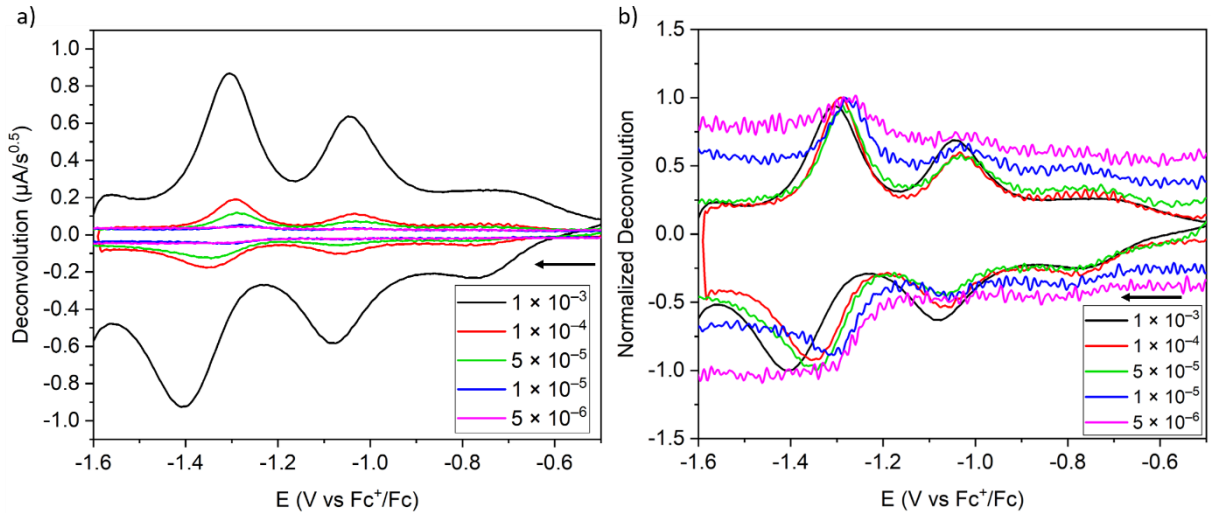

Figure S63. (a) Deconvolutions and (b) normalized deconvolutions of the cyclic voltammograms of BACD **1,6-CF$_3$** recorded at various concentrations (1 – 0.005 mM) in a CH_2Cl_2 solution containing $^nBu_4NPF_6$ (0.1 M) as supporting electrolyte and Fc (0.1 mM) as internal reference.

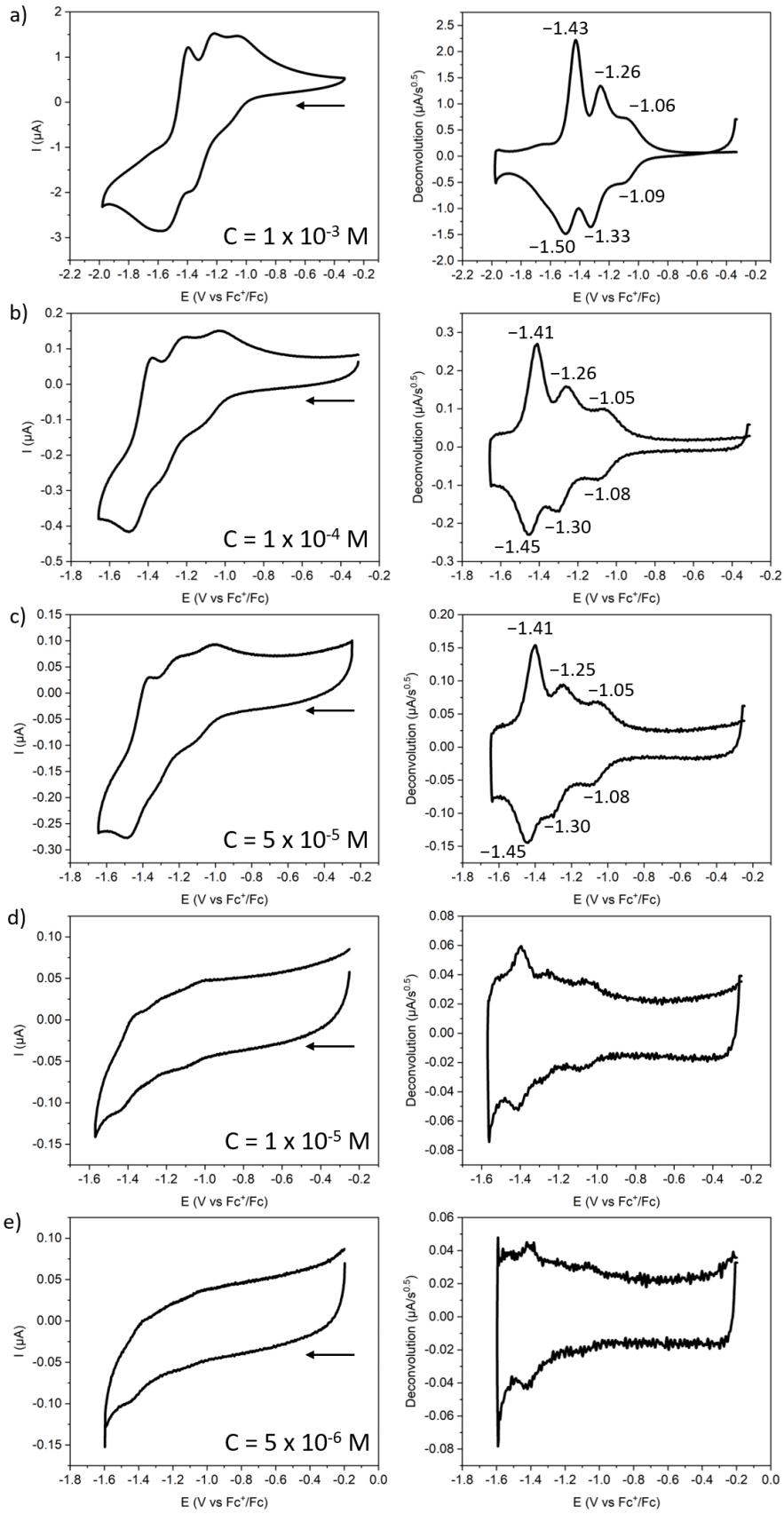

Figure S64. Cyclic voltammetry (left) and its deconvolution (right) of BACD **1,6-OMe** recorded at various concentrations, i.e. (a) 1 mM, (b) 0.1 mM, (c) 0.05 mM, (d) 0.01 mM, and (e) 0.005 mM, in a CH_2Cl_2 solution containing $^{n}Bu_4NPF_6$ (0.1 M) as supporting electrolyte and Fc (0.1 mM) as internal reference.

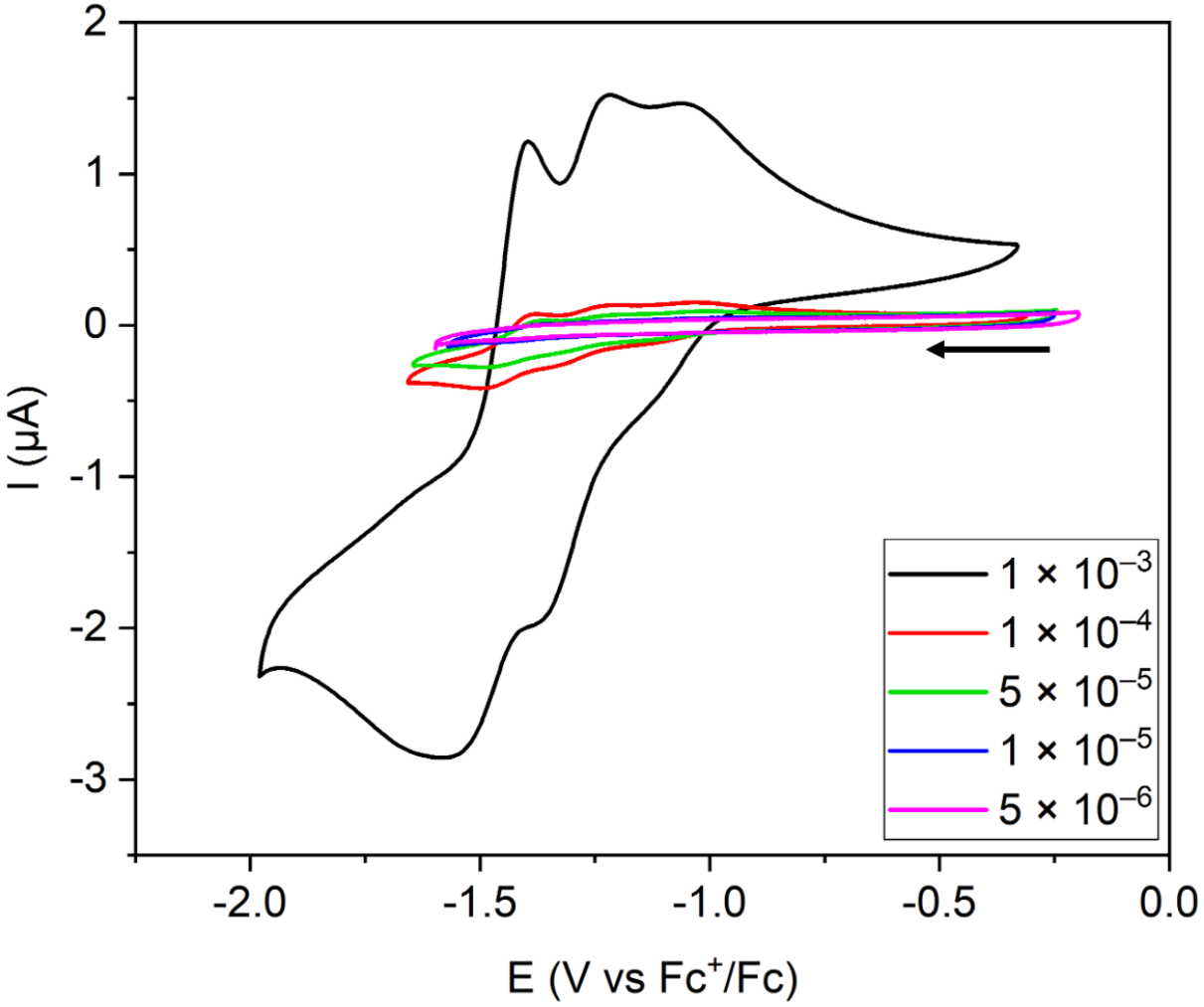

Figure S65. Cyclic voltammetry of BACD **1,6-OMe** recorded at various concentrations (1 – 0.005 mM) in a CH_2Cl_2 solution containing $^nBu_4NPF_6$ (0.1 M) as supporting electrolyte and Fc (0.1 mM) as internal reference.

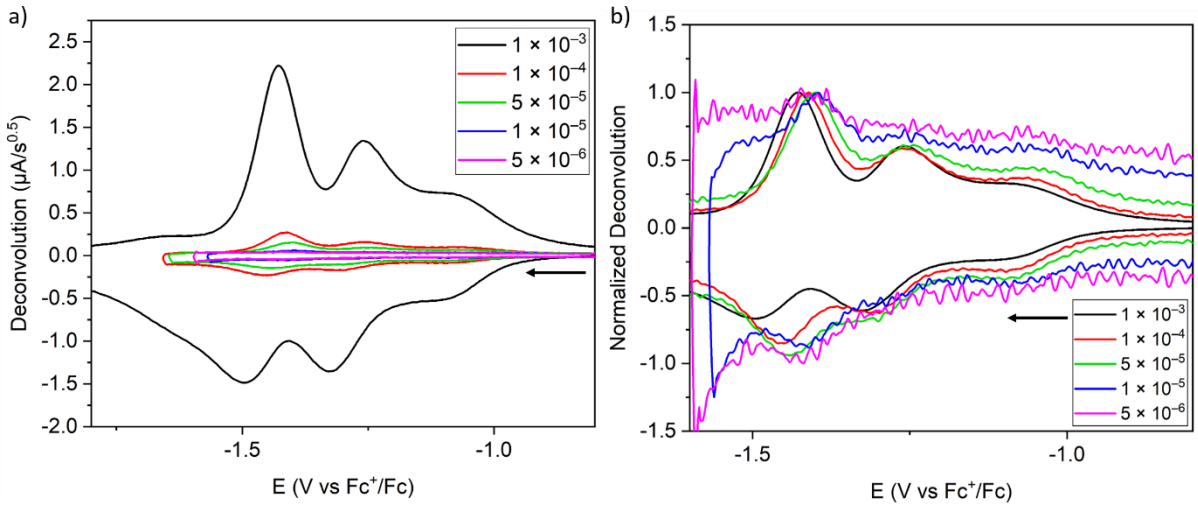

Figure S66. (a) Deconvolutions and (b) normalized deconvolutions of the cyclic voltammograms of BACD **1,6-OMe** recorded at various concentrations (1 – 0.005 mM) in a CH_2Cl_2 solution containing $^nBu_4NPF_6$ (0.1 M) as supporting electrolyte and Fc (0.1 mM) as internal reference.

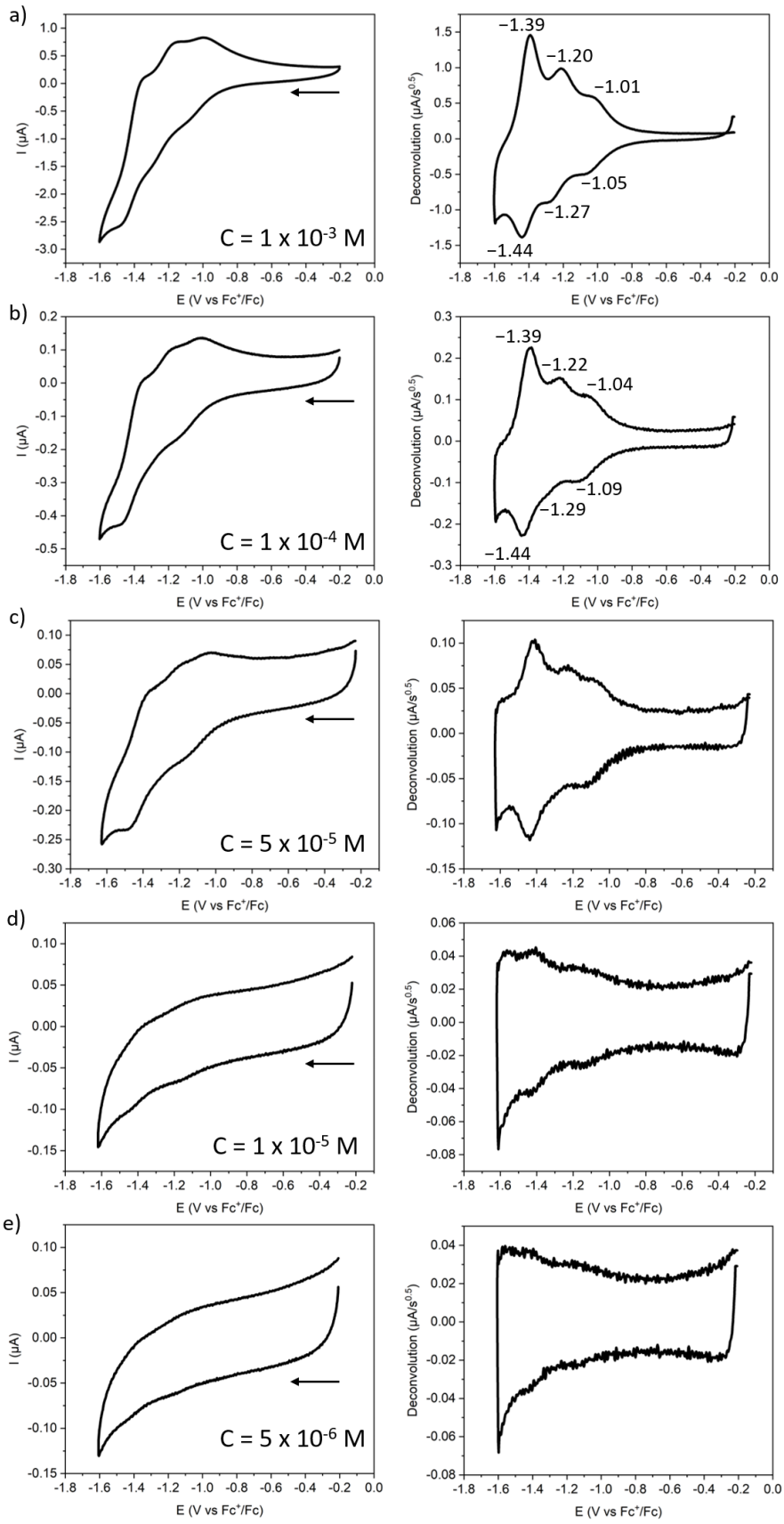

Figure S67. Cyclic voltammetry (left) and its deconvolution (right) of BACD **1,7-OMe** recorded at various concentrations, i.e. (a) 1 mM, (b) 0.1 mM, (c) 0.05 mM, (d) 0.01 mM, and (e) 0.005 mM, in a CH_2Cl_2 solution containing $^nBu_4NPF_6$ (0.1 M) as supporting electrolyte and Fc (0.1 mM) as internal reference.

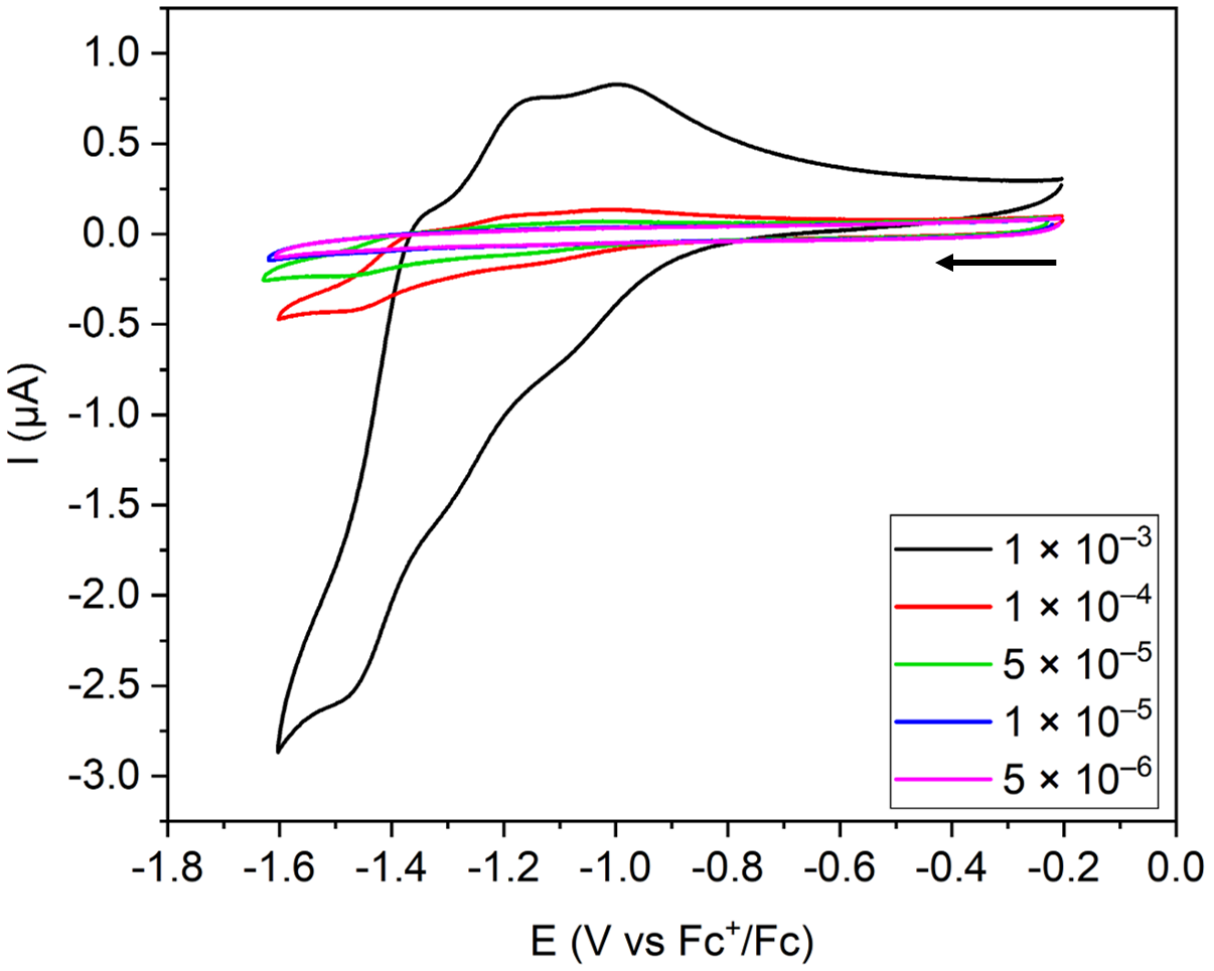

Figure S68. Cyclic voltammetry of BACD **1,7-OMe** recorded at various concentrations (1 – 0.005 mM) in a CH_2Cl_2 solution containing $^nBu_4NPF_6$ (0.1 M) as supporting electrolyte and Fc (0.1 mM) as internal reference.

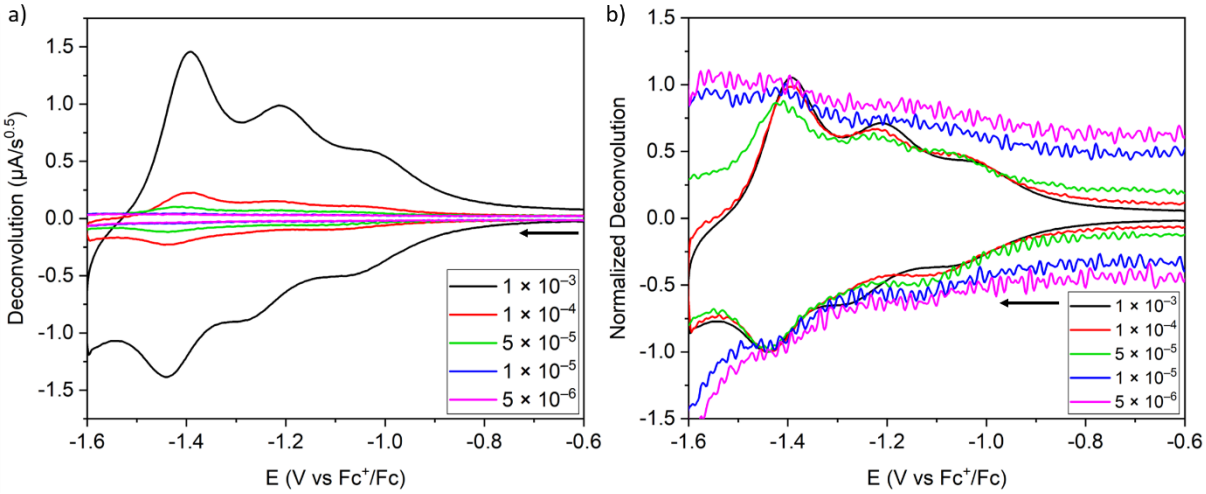

Figure S69. (a) Deconvolutions and (b) normalized deconvolutions of the cyclic voltammograms of BACD **1,7-OMe** recorded at various concentrations (1 – 0.005 mM) in a CH_2Cl_2 solution containing $^nBu_4NPF_6$ (0.1 M) as supporting electrolyte and Fc (0.1 mM) as internal reference.

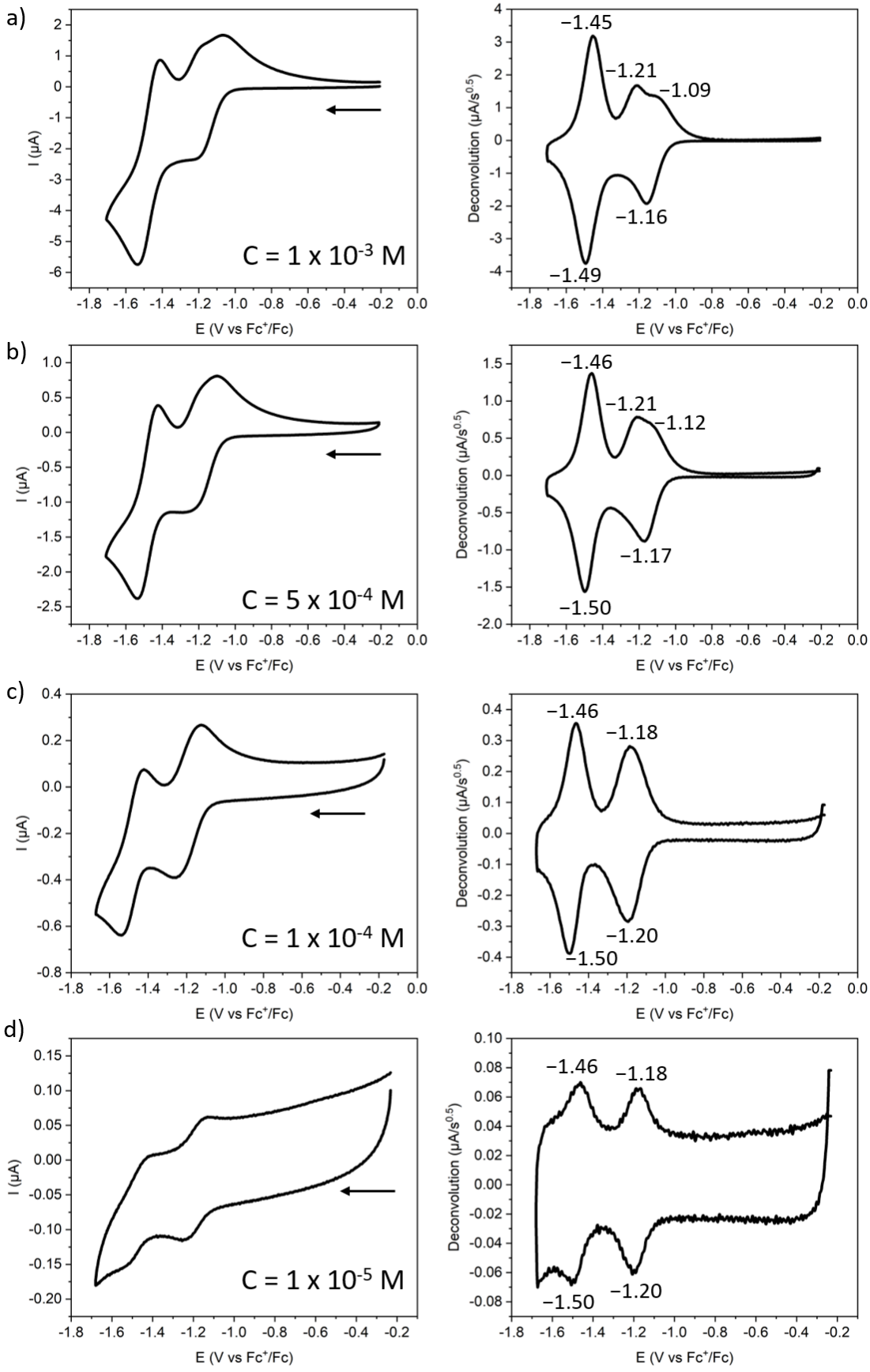

Figure S70. Cyclic voltammetry (left) and its deconvolution (right) of BACD **C-1,6** recorded at various concentrations, i.e. (a) 1 mM, (b) 0.5 mM, (c) 0.1 mM, and (d) 0.01 mM, in a CH_2Cl_2 solution containing $^{n}Bu_4NPF_6$ (0.1 M) as supporting electrolyte and Fc (0.1 mM) as internal reference.

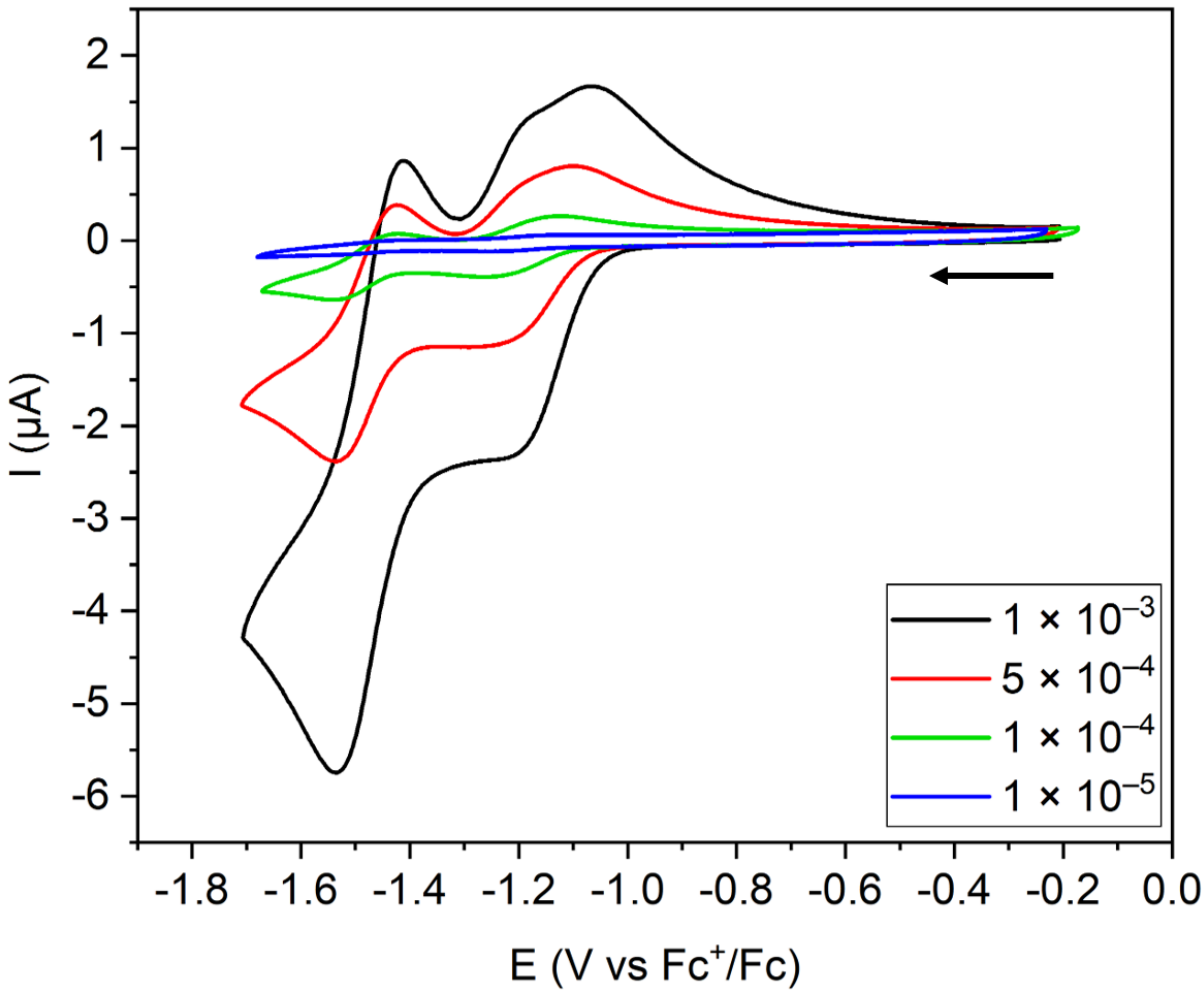

Figure S71. Cyclic voltammetry of BACD **C-1,6** recorded at various concentrations (1 – 0.01 mM) in a CH_2Cl_2 solution containing $^nBu_4NPF_6$ (0.1 M) as supporting electrolyte and Fc (0.1 mM) as internal reference.

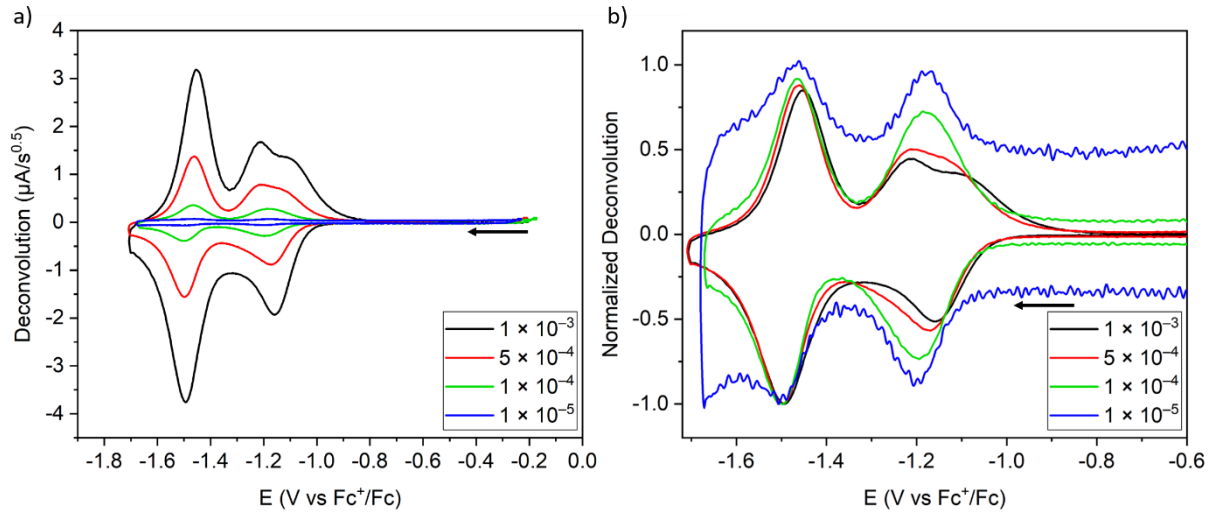

Figure S72. (a) Deconvolutions and (b) normalized deconvolutions of the cyclic voltammograms of BACD **C-1,6** recorded at various concentrations (1 – 0.01 mM) in a CH_2Cl_2 solution containing $^nBu_4NPF_6$ (0.1 M) as supporting electrolyte and Fc (0.1 mM) as internal reference.

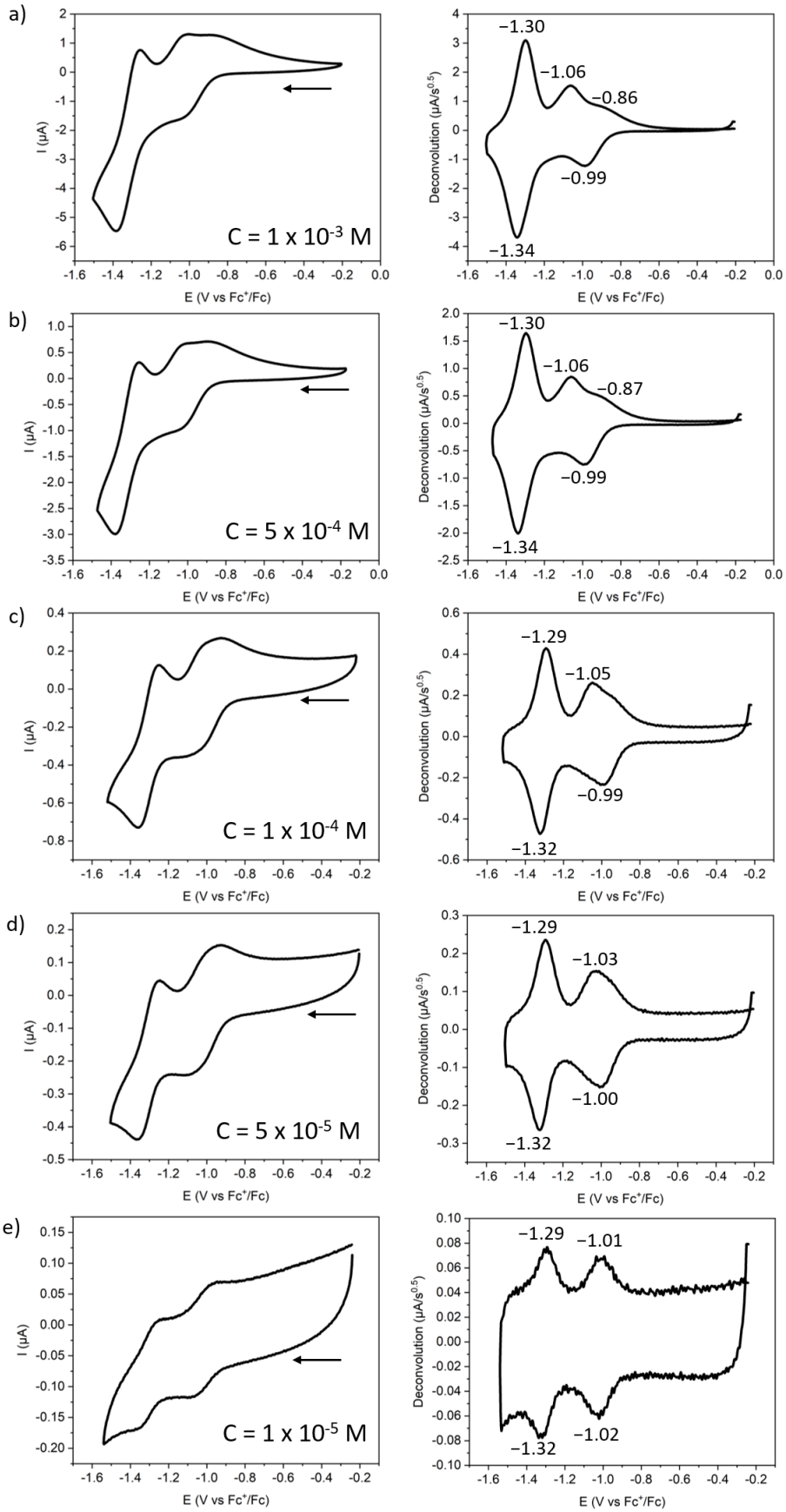

Figure S73. Cyclic voltammetry (left) and its deconvolution (right) of BACD **C-CF$_3$** recorded at various concentrations, i.e. (a) 1 mM, (b) 0.5 mM, (c) 0.1 mM, (e) 0.05 mM, and (d) 0.01 mM, in a CH_2Cl_2 solution containing $^nBu_4NPF_6$ (0.1 M) as supporting electrolyte and Fc (0.1 mM) as internal reference.

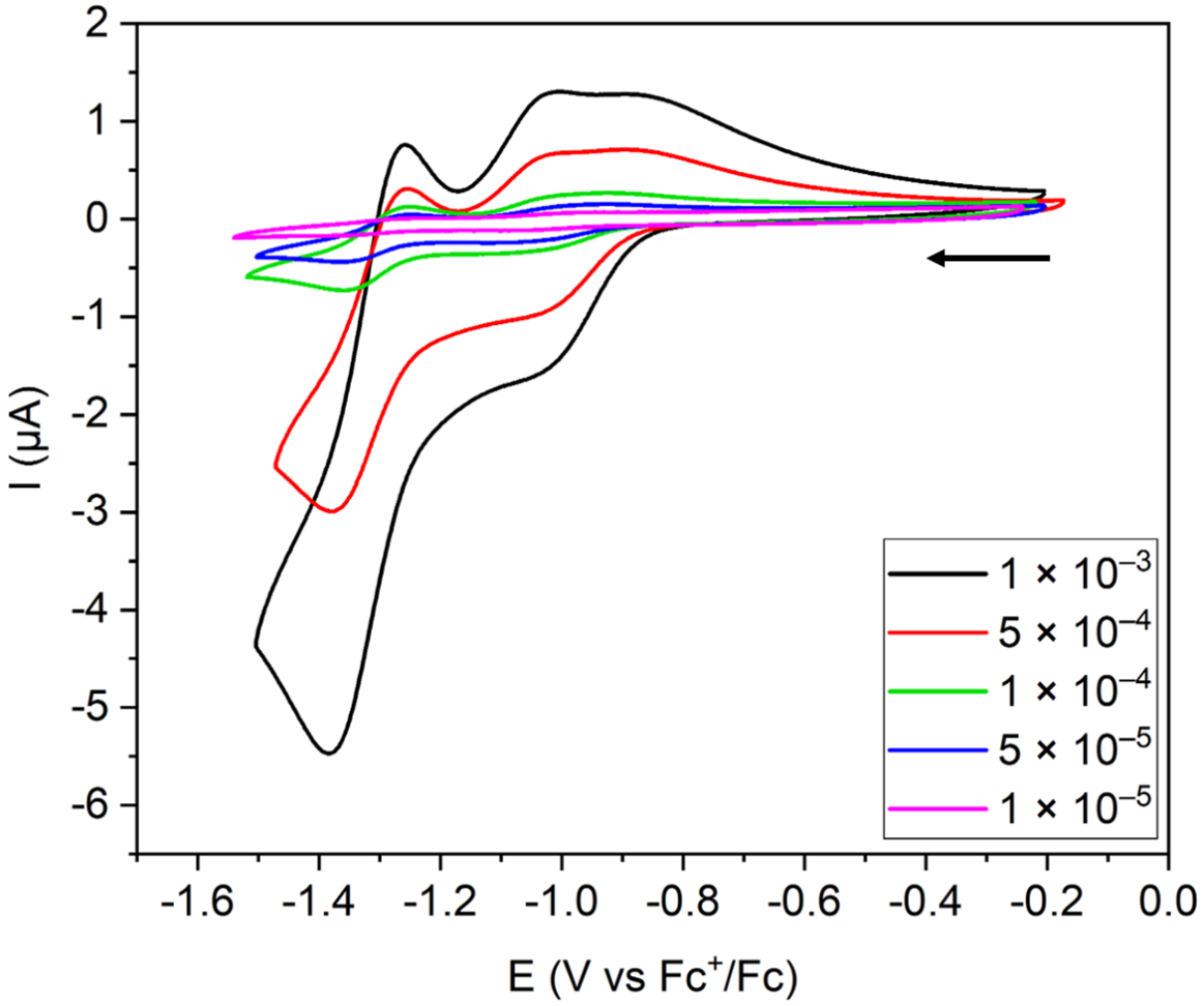

Figure S74. Cyclic voltammetry of BACD **C-CF$_3$** recorded at various concentrations (1 – 0.01 mM) in a CH_2Cl_2 solution containing $^nBu_4NPF_6$ (0.1 M) as supporting electrolyte and Fc (0.1 mM) as internal reference.

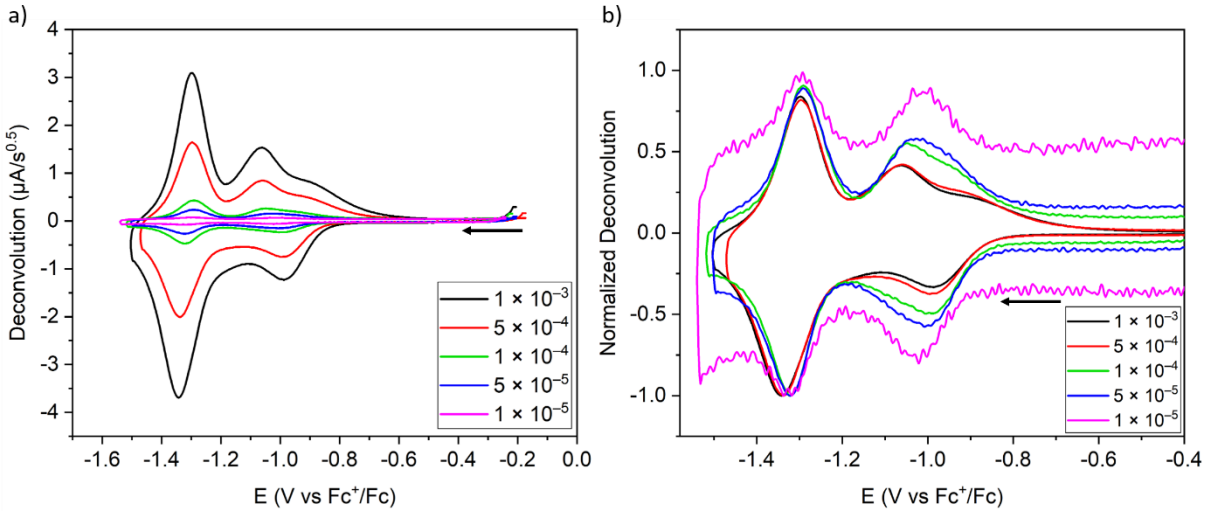

Figure S75. (a) Deconvolutions and (b) normalized deconvolutions of the cyclic voltammograms of BACD **C-CF$_3$** recorded at various concentrations (1 – 0.01 mM) in a CH_2Cl_2 solution containing $^nBu_4NPF_6$ (0.1 M) as supporting electrolyte and Fc (0.1 mM) as internal reference.

Simulated CVs via DIGIELCH 8F

Square scheme

$$\begin{array}{ccc} M + e^- & \overset{E_1}{\rightleftarrows} & M^{\cdot -} \\ \Updownarrow K_{MV} & & \Updownarrow K_{\pi D} \\ MV^{\cdot -} + e^- & \overset{E_2}{\rightleftarrows} & \pi D^{2-} \end{array}$$

Nernst equation : $E_1 + a\, ln\left(\frac{[M]}{[M^{\cdot -}]}\right) = E_2 + a\, ln\left(\frac{[MV^{\cdot -}]}{[\pi D^{2-}]}\right) \quad with\ a = \frac{RT}{F}$

Consequently, $\Delta E = E_1 - E_2 = a\, ln\left(\frac{K_{MV}}{K_{\pi D}}\right)$

If $K_{MV} > K_{\pi D}$, $\Delta E > 0$ and $E_1 > E_2$

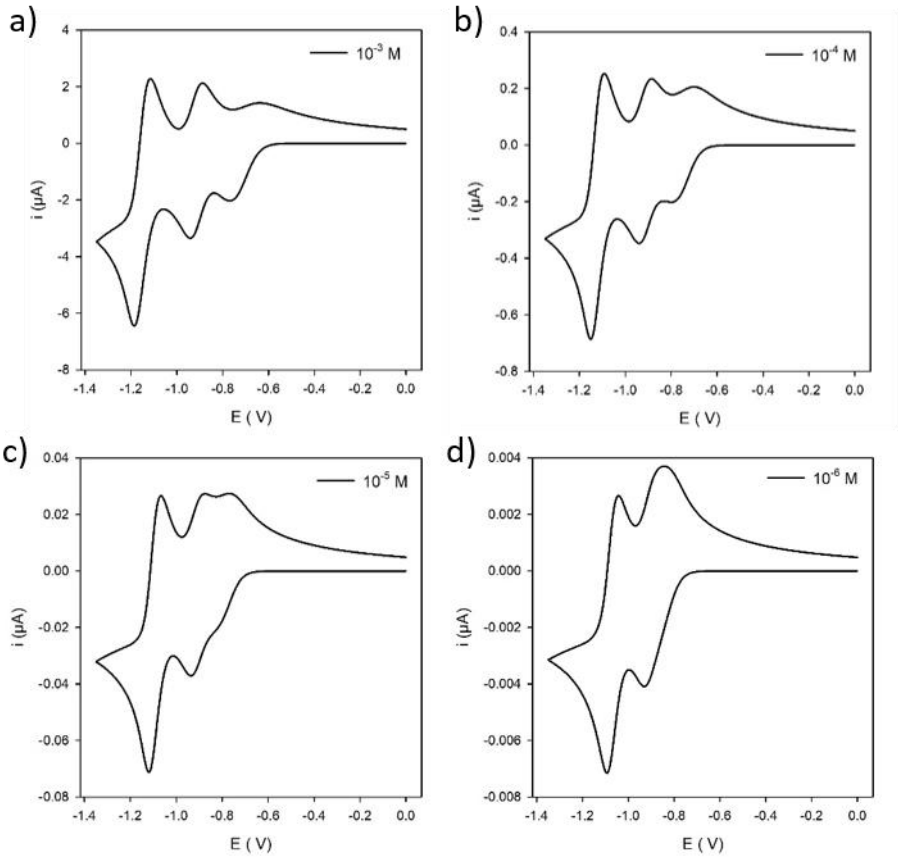

Figure S76. Simulated CVs for the extended BACD **1,7-Ph** at various concentrations: (a) 10^{-3} M, (b) 10^{-4} M, (c) 10^{-5} M, and (d) 10^{-6} M.

DigiElch parameters :

Diffusion: Semi-Infinite 1D ; Geometry: Planar ; Area (cm²): 0.0314

Ru (Ohm): 0 ; Cdl (F): 0 ; Temp. (K): 293 ; v (V/s): 0.1 ; D (cm^2/s) = 3 10^{-6} for all species

Splitting : E_1 (V) = −0.885 ; alpha = 0.5 ; ks (cm/s) = 0.05 and E_2 (V) = −0.915 ; alpha = 0.5 ; ks (cm/s) = 0.05

Second reduction : E_3 (V) = −1.05 ; alpha = 0.5 ; ks (cm/s) = 0.05

K_{MV} = 5 10^{+6} ; kf = 10^{+10} and $K_{\pi D}$ = 2.264 10^{+6} ; kf = 10^{+10}

5. Spectroelectrochemistry

Time-resolved spectroelectrochemistry was performed using the already described home self-made cell described elsewhere.[S5] A distance of 25-50 µm between the surface of the electrode and the optical window was typically used in our experiments. Electrochemical measurements were carried out using a platinum wire counter electrode and a silver wire as a quasi-reference electrode with a Biologic SP-300 potentiostat driven by the EC-Lab software including ohmic drop compensation. Experiments were recorded in dry HPLC-grade CH_2Cl_2 with $TBAPF_6$ (electrochemical grade, Fluka) as supporting electrolyte. All solutions were prepared and transferred into the spectroelectrochemical cell in a glove box containing dry, oxygen-free (<1 ppm) argon, at room temperature. Spectrophotometric measurements were carried out with a homemade bench composed of different PRINCETON INSTRUMENTS modules (light sources, fibers, monochromators, spectroscopy camera and software). To start the two experiments at the same time, the two benches are synchronized with TTL signals.

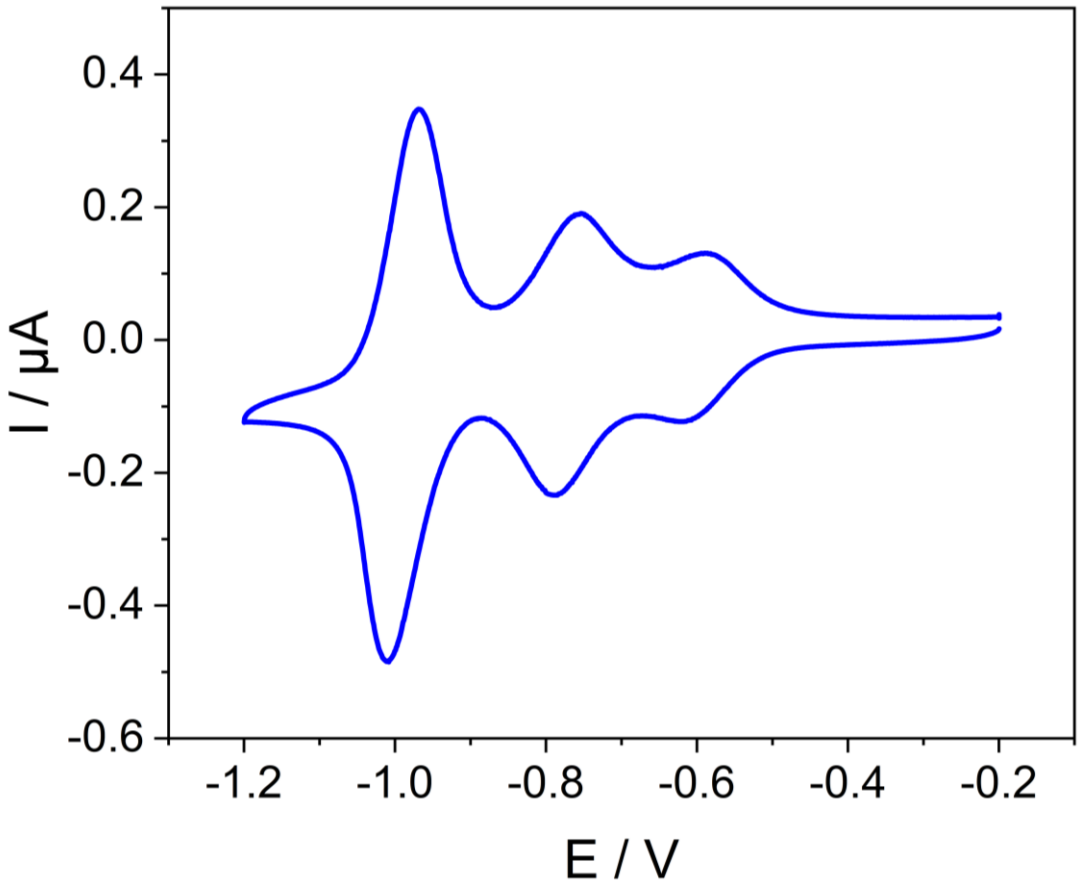

Figure S77. TLCV (CH_2Cl_2, 0.1 M $TBAPF_6$, 10 mV/s) of *ortho*-pentannulated BACD **1,6-Ph**

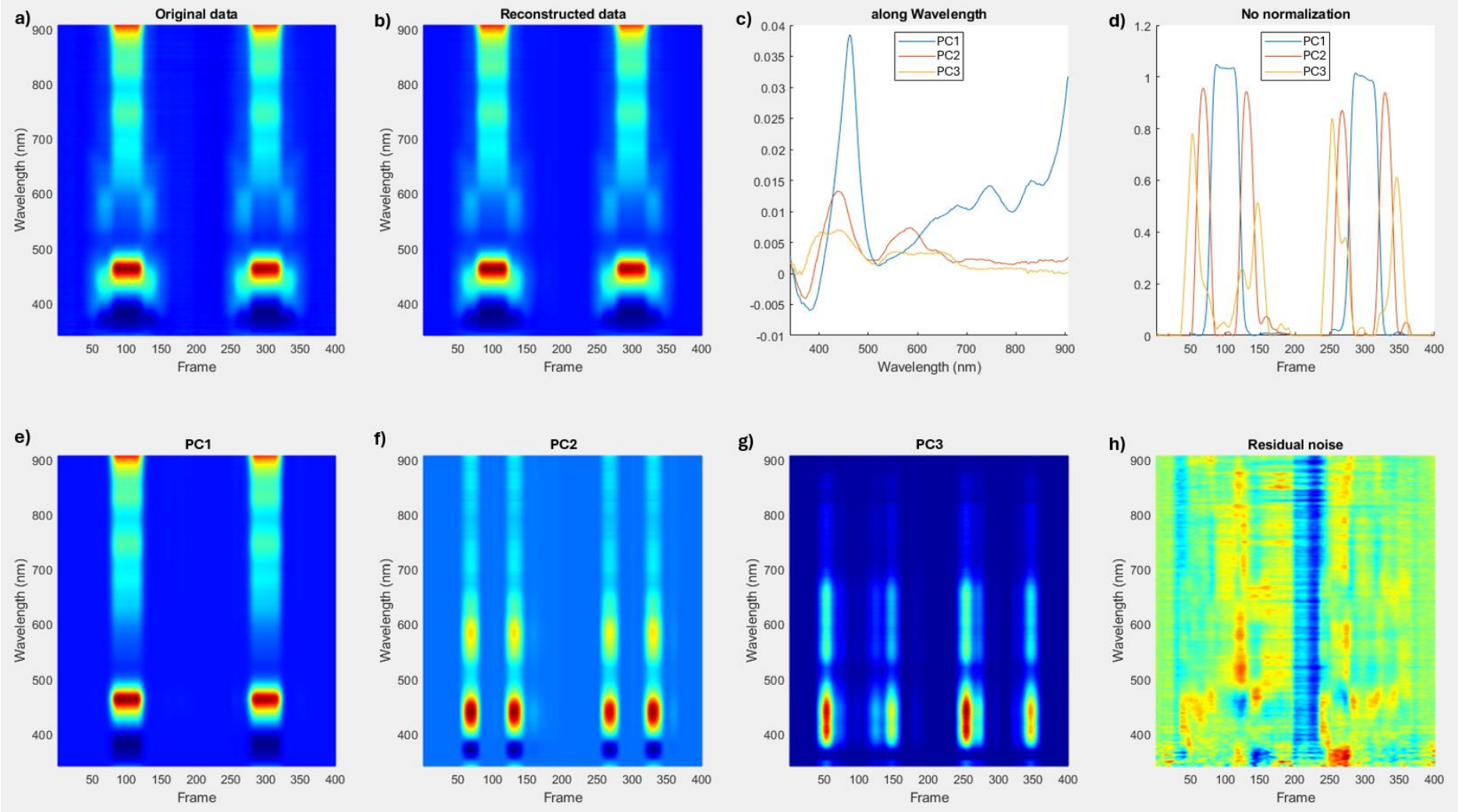

Figure S78. (a,b) Time-dependent variation of the optical response in the UV-visible range recorded during a cyclic voltammetry measurement in a 10^{-3} M solution of *ortho*-pentannulated BACD **1,6-Ph** (CH_2Cl_2, $TBAPF_6$ 0.1 M, 10 mV/s) under thin layer. (e,f,g) 3D spectra showing the principal components (PCs) of the three events and (c) their evolution-associated 2D spectra. (d) Population curves of the PCs. (h) Residual noise after mathematical extraction of the PCs of each event.

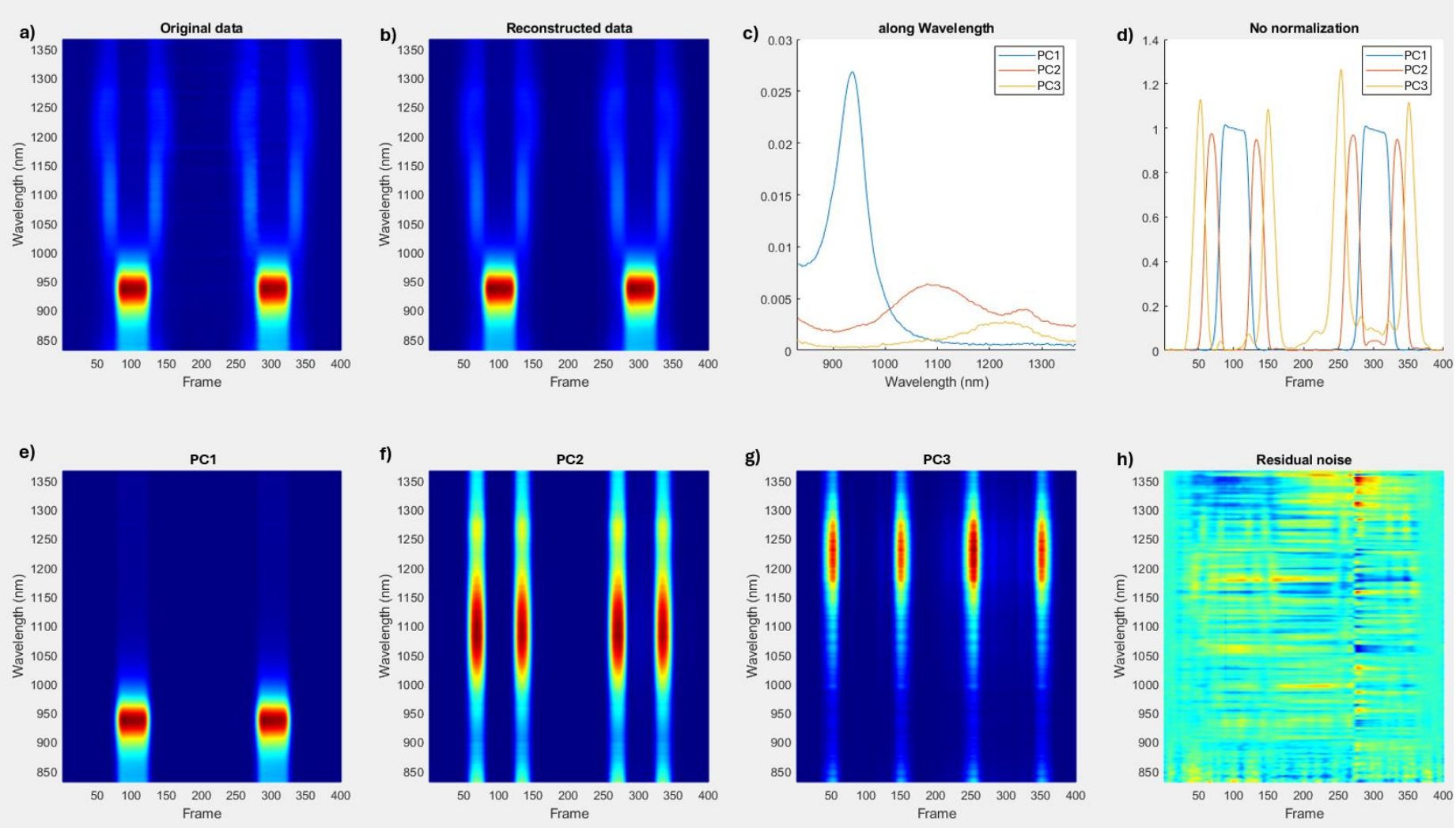

Figure S79. (a,b) Time-dependent variation of the optical response in the near-infrared range recorded during a cyclic voltammetry measurement in a 10^{-3} M solution of *ortho*-pentannulated BACD **1,6-Ph** (CH_2Cl_2, $TBAPF_6$ 0.1 M, 10 mV/s) under thin layer. (e,f,g) 3D spectra showing the principal components (PCs) of the three events and (c) their evolution-associated 2D spectra. (d) Population curves of the PCs. (h) Residual noise after mathematical extraction of the PCs of each event.

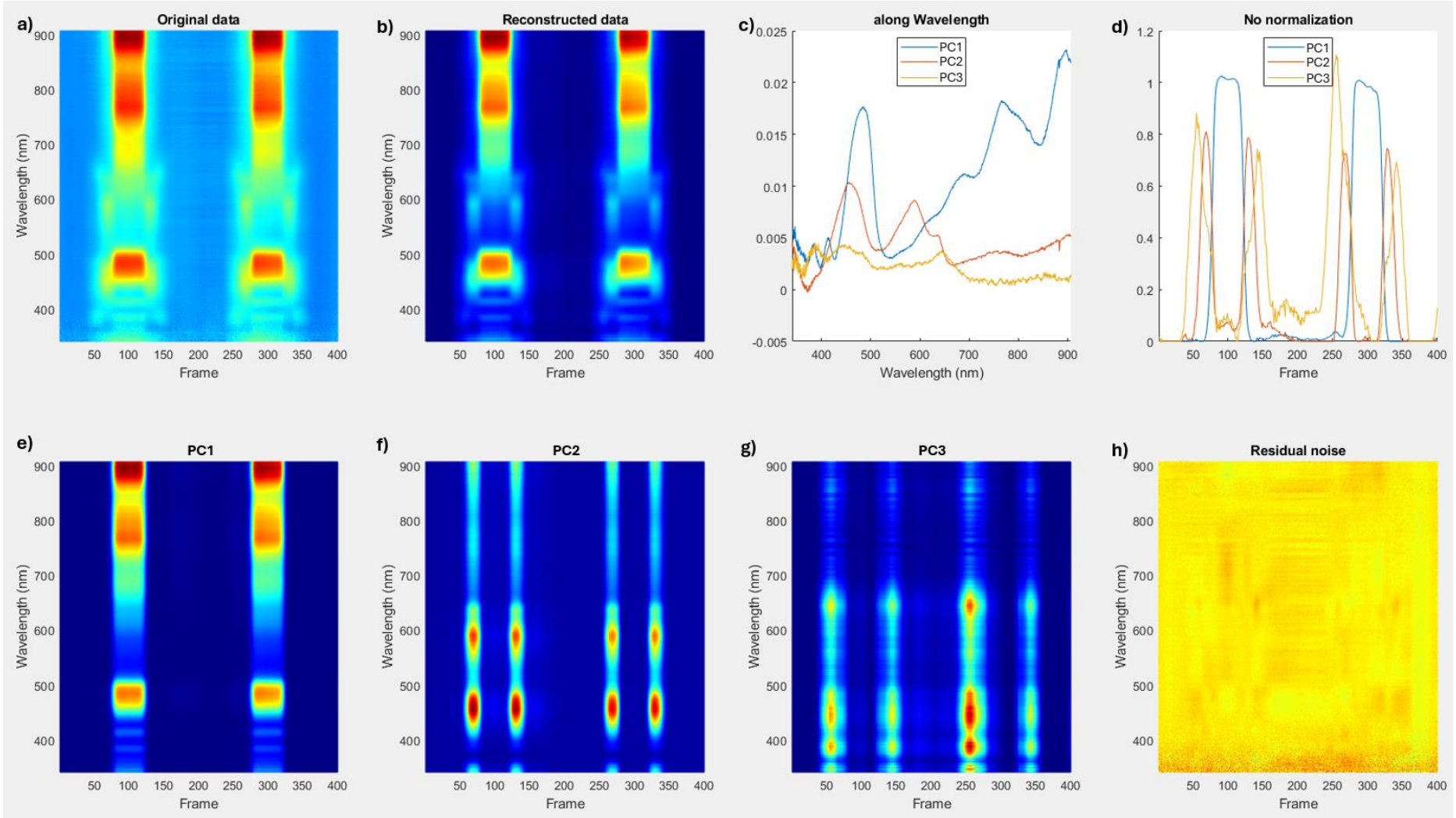

Figure S80. (a,b) Time-dependent variation of the optical response in the UV-visible range recorded during a cyclic voltammetry measurement in a 10^{-3} M solution of *ortho*-pentannulated BACD **1,7-Ph** (CH_2Cl_2, $TBAPF_6$ 0.1 M, 10 mV/s) under thin layer. (e,f,g) 3D spectra showing the principal components (PCs) of the three events and (c) their evolution-associated 2D spectra. (d) Population curves of the PCs. (h) Residual noise after mathematical extraction of the PCs of each event.

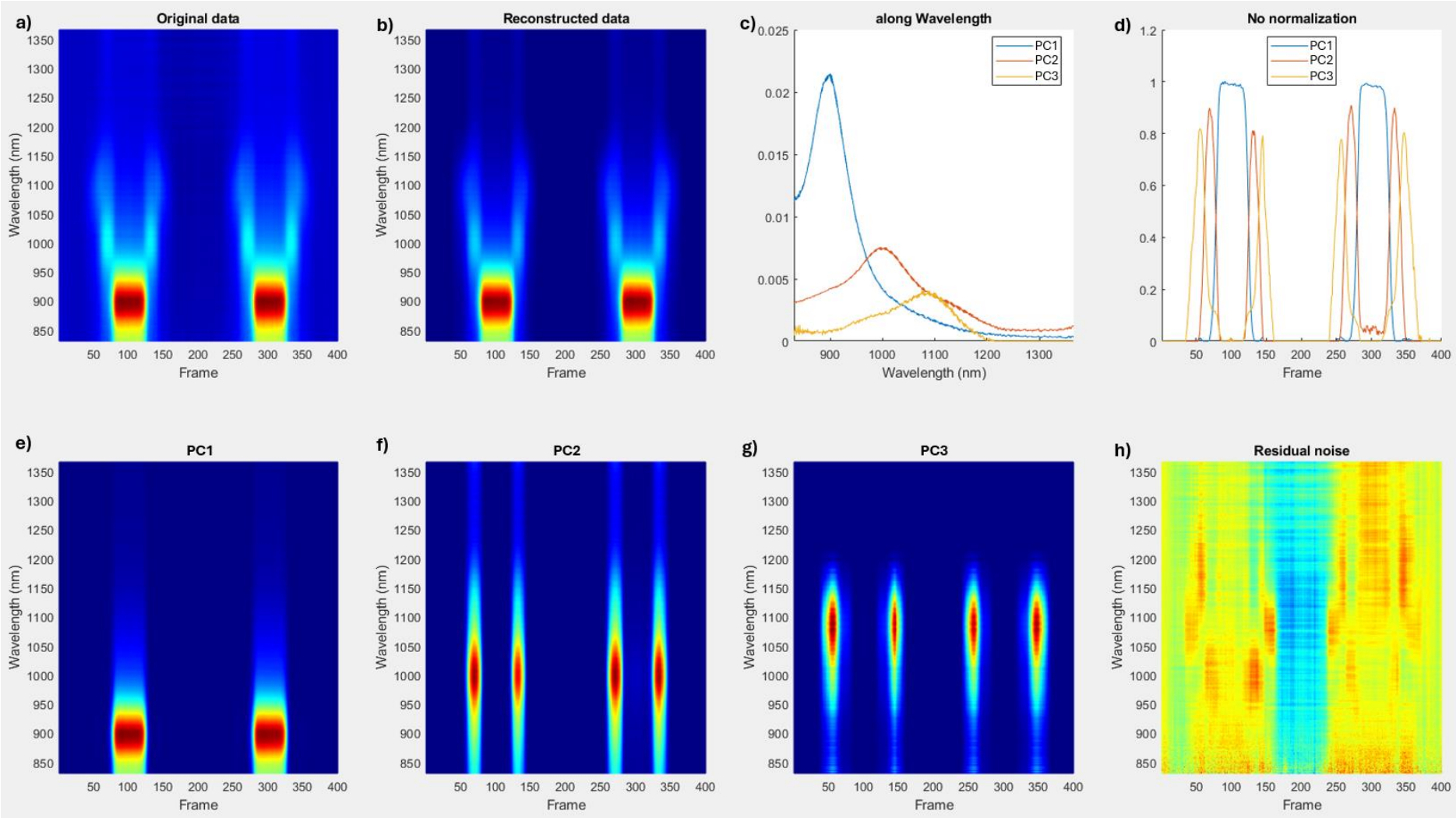

Figure S81. (a,b) Time-dependent variation of the optical response in the near-infrared range recorded during a cyclic voltammetry measurement in a 10^{-3} M solution of *ortho*-pentannulated BACD **1,7-Ph** (CH_2Cl_2, $TBAPF_6$ 0.1 M, 10 mV/s) under thin layer. (e,f,g) 3D spectra showing the principal components (PCs) of the three events and (c) their evolution-associated 2D spectra. (d) Population curves of the PCs. (h) Residual noise after mathematical extraction of the PCs of each event.

6. Computational Methods

Molecular Dynamics Simulations

Molecular dynamics simulations were done with GROMACS 2018.3 package.[S6] **1,7-Ph** and dichloromethane molecules have been described through the generalized AMBER force field (GAFF)[S7] and the conversion to GROMACS formalism was done with acpype script.[S8] Atomic charges were computed following the parametrization procedure based on the HF/6-31G(d) RESP charges. The size of the simulation box was approximatively 100 × 100 × 100 Å and has been filled with around 5000 dichloromethane molecules. Electrostatic interactions were considered by applying periodic boundary conditions with a cutoff of 10 Å and the use of the Particle Mesh Ewald method.[S9] The following procedure was applied :

- a minimization step using steepest descent method
- a first equilibration step in the NVT ensemble for 1000 ps at T = 298 K, ensured by the Berendsen weak coupling method[S10]
- a second equilibration step in the NPT ensemble for another 1000 ps, at P = 1 bar, ensured by the same Berendsen weak coupling method

The production phase was carried out in the NPT ensemble with a time step of 2 fs. The Nosé-Hoover thermostat[S11] and Parinello Rahman barostat,[S12] with both τ = 1 fs, were considered.

DFT and TD-DFT calculations

Ground state properties were computed at the B3LYP/6-311+G(d) (for singlet species, M, M^{2-}, D, and πD^{2-}) and UB3LYP/6-311+G(d) (for doublet species, $M^{\cdot-}$ and $MV^{\cdot-}$) level of theory, within an implicit solvation model for dichloromethane,[S13] using Gaussian09 software.[S14] For monomer species, 15 states have been computed to retrieve the UV-Vis absorption spectra while 30 states were considered for dimer species. Frequency calculations were systematically performed to ensure the molecules were in a true minimum of the potential energy surface. Gibbs free energies were also extracted from those frequency calculations to confirm the experimental reduction mechanism. Charge transfer calculations were performed applying the protocol described in a previous study.[S2]

Table S5. Experimental and calculated UV-Vis absorption properties (λ in nm) of a monomer and a dimer of **1,7-Ph**.

	λ_{exp} / nm	λ_{calc} / nm	*f*	Description	Attribution
M	460	482	0.21	H → L	$S_0 \rightarrow S_3$
	407[a]	410	0.21	H → L+1	$S_0 \rightarrow S_5$
	384	389[b]	0.99	H−2 → L+1	$S_0 \rightarrow S_6$
	366	375	0.48	H−3 → L	$S_0 \rightarrow S_8$
	351	356	0.28	H−1 → L+2	$S_0 \rightarrow S_{13}$
D	515[a]	512	0.11	H−1 → L+1	$S_0 \rightarrow S_9$
	479[a]	505	0.18	H−5 → L	$S_0 \rightarrow S_{10}$
	382	421	0.22	H−8 → L	$S_0 \rightarrow S_{17}$
	371	398[b]	0.51	H−4 → L	$S_0 \rightarrow S_{26}$

[a] Those values correspond to a shoulder in the experimental spectrum.
[b] Those values will be referred as λ_{max} since they exhibit the highest oscillator strength.

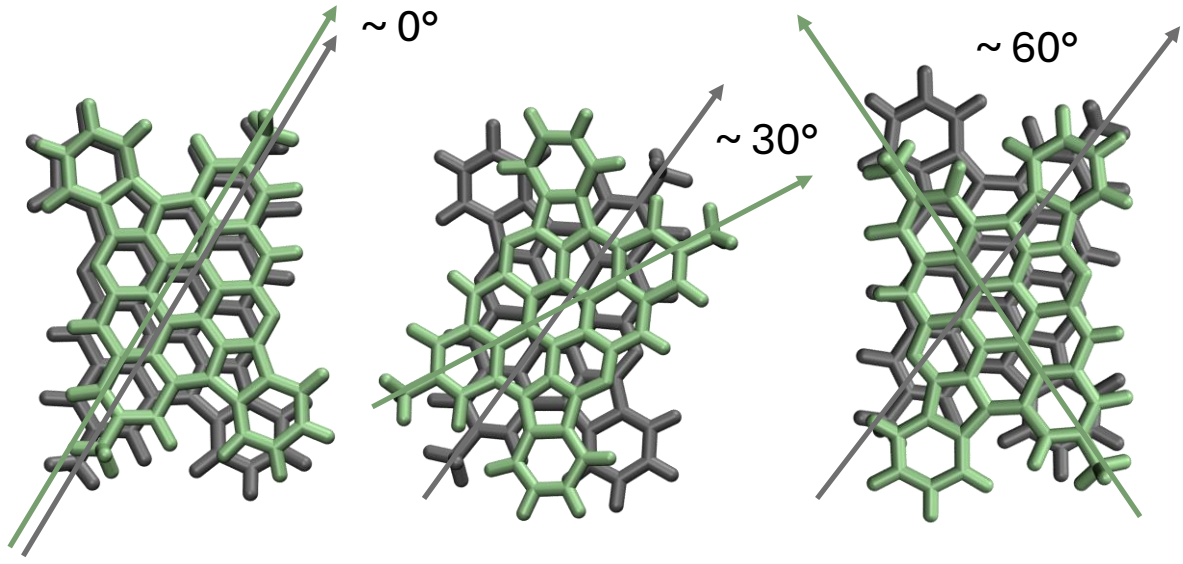

Figure S82. Illustration of the stacking pattern of **1,7-Ph** that have been observed during the 50 ns molecular dynamics simulation. The angle between the molecules has been highlighted with arrows and its value has also been provided. The structure with a 30 ° tilt is the most favorable one as it is the most observed during the simulations.

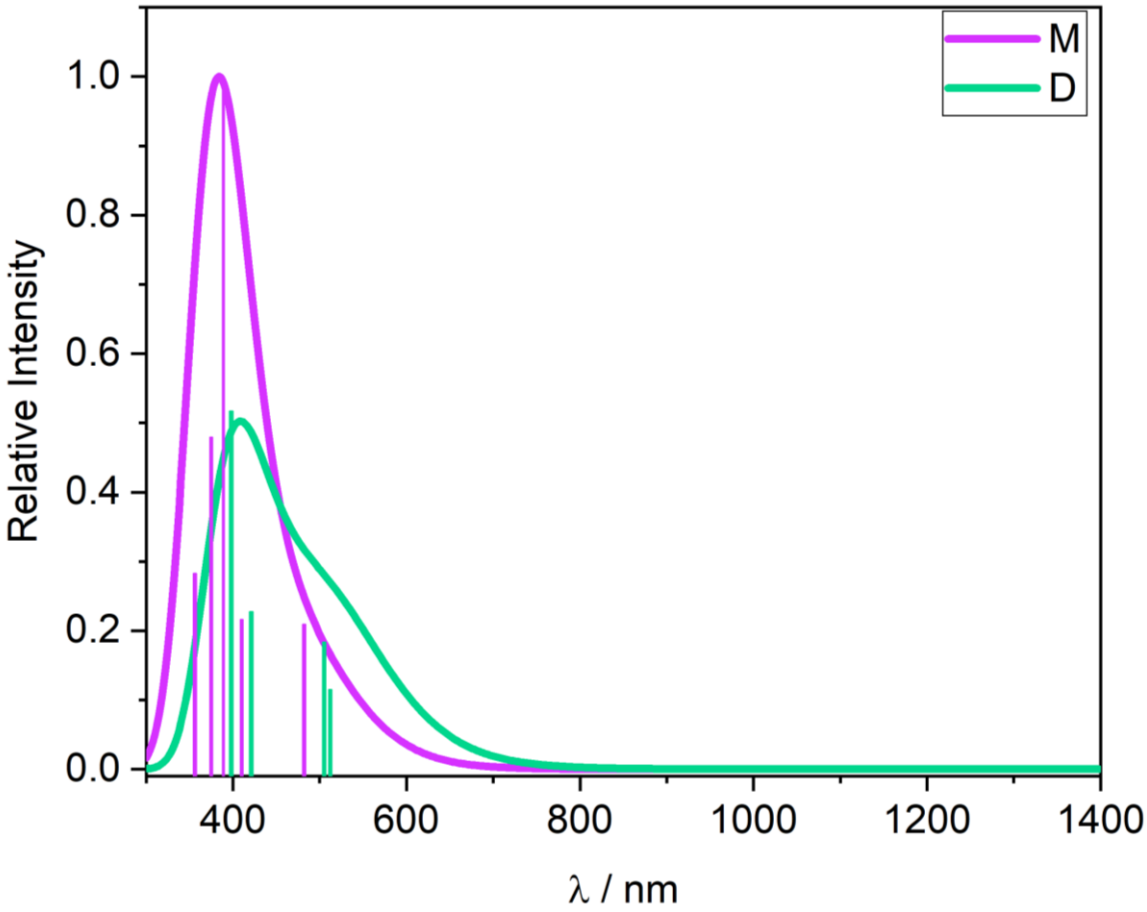

Figure S83. Calculated absorption spectra of a monomer (M, purple lines) and a dimer (D, green lines) of **1,7-Ph**. Calculated absorption peaks are also represented as sticks. FWHM = 0,2 eV.

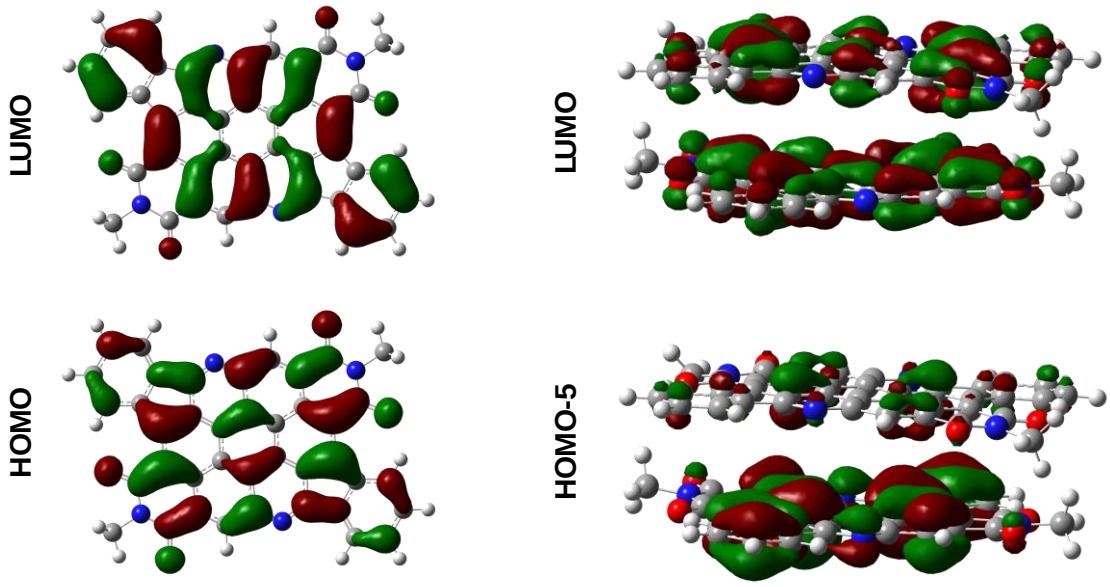

Figure S84. Representation of molecular orbitals of **1,7-Ph** corresponding to λ_{max} for a monomer (left) and a dimer (right). Isodensity = 0.0004 a.u.

Table S6. Gibbs free energy (ΔG) in kJ·mol^{-1} for a neutral (M), anionic radical (M$^{\cdot-}$), and dianionic monomer and a neutral (D), anionic radical (MV$^{\cdot-}$) and dianionic (πD^{2-}) dimer of **1,7-Ph**. For dimers, ΔG have been divided by two to obtain an average value for one molecule to allow the comparison with M.

	M	M$^{\cdot-}$	M^{2-}	D	MV$^{\cdot-}$	πD^{2-}
M	0	−266	−249	−14	−113	−142

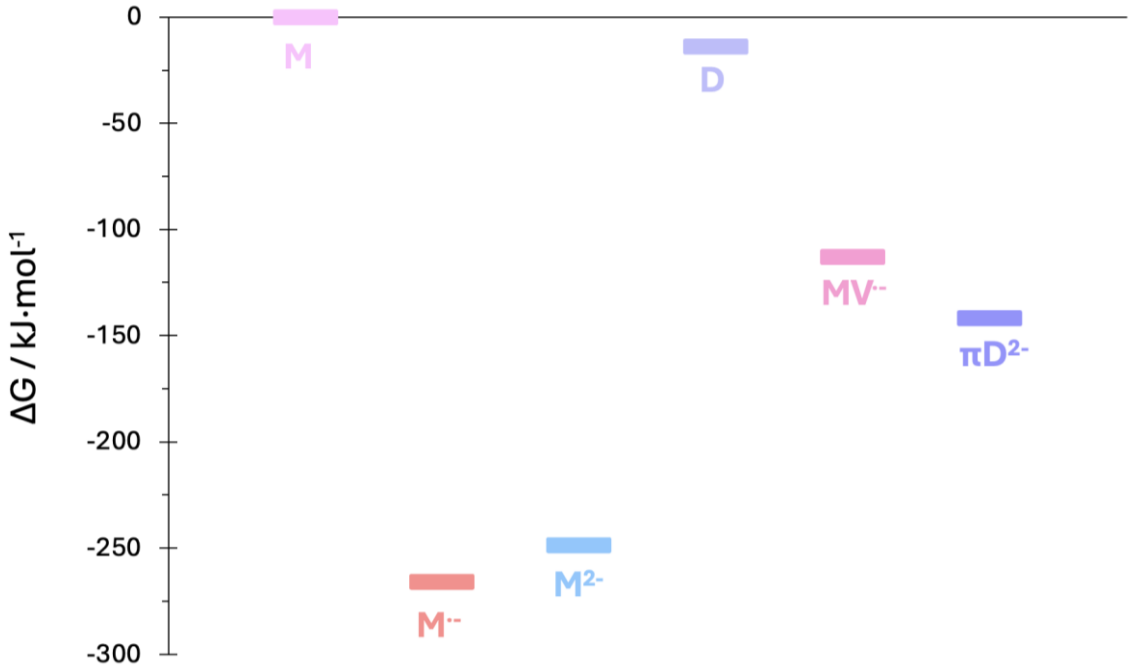

Figure S85. Gibbs free energy (ΔG) in kJ·mol^{-1} for a neutral (M), anionic radical (M$^{\cdot-}$), and dianionic monomer and a neutral (D), anionic radical (MV$^{\cdot-}$) and dianionic (πD^{2-}) dimer of **1,7-Ph**. For dimers, ΔG have been divided by two to obtain an average value for one molecule to allow the comparison with M.

7. NMR Spectroscopy

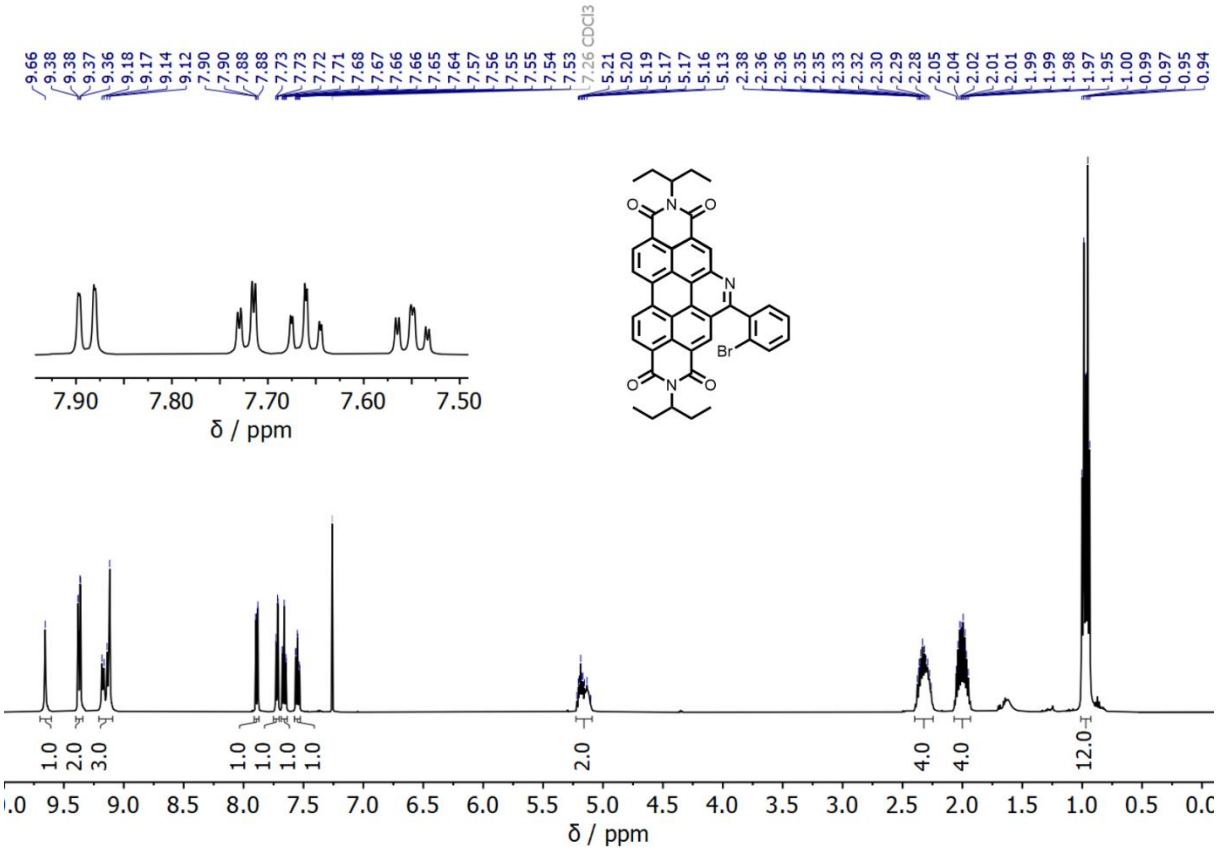

Figure S86. ^{1}H NMR (500 MHz, $CDCl_3$) spectrum of **Br-aPDI-Ph**

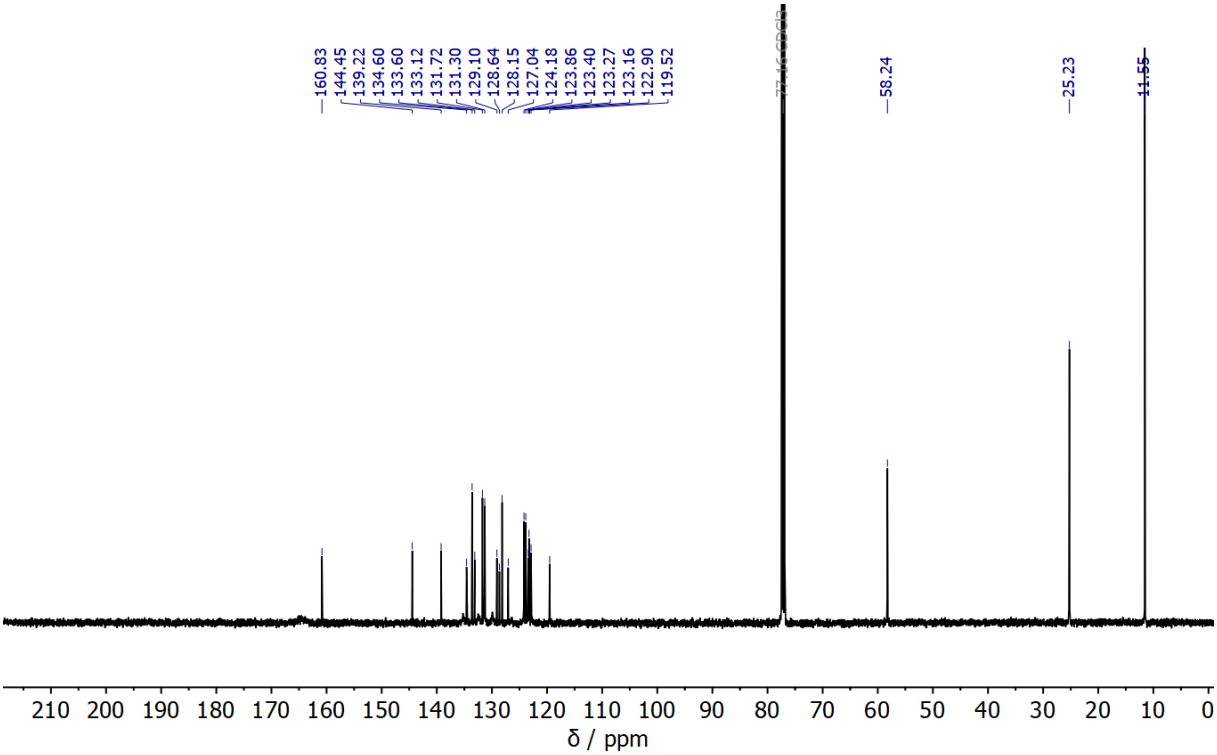

Figure S87. ^{13}C NMR (125 MHz, $CDCl_3$) spectrum of **Br-aPDI-Ph**

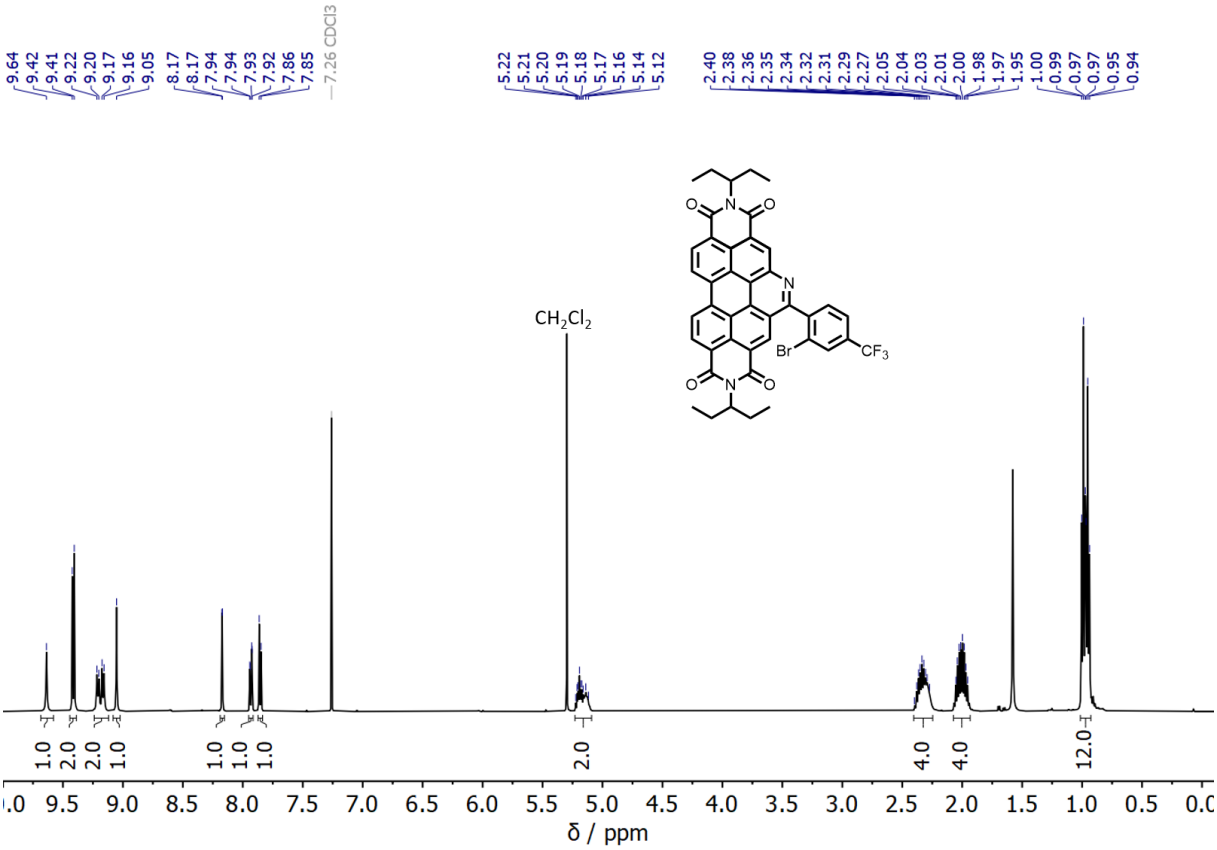

Figure S88. ^{1}H NMR (500 MHz, $CDCl_3$) spectrum of **Br-aPDI-CF$_3$**

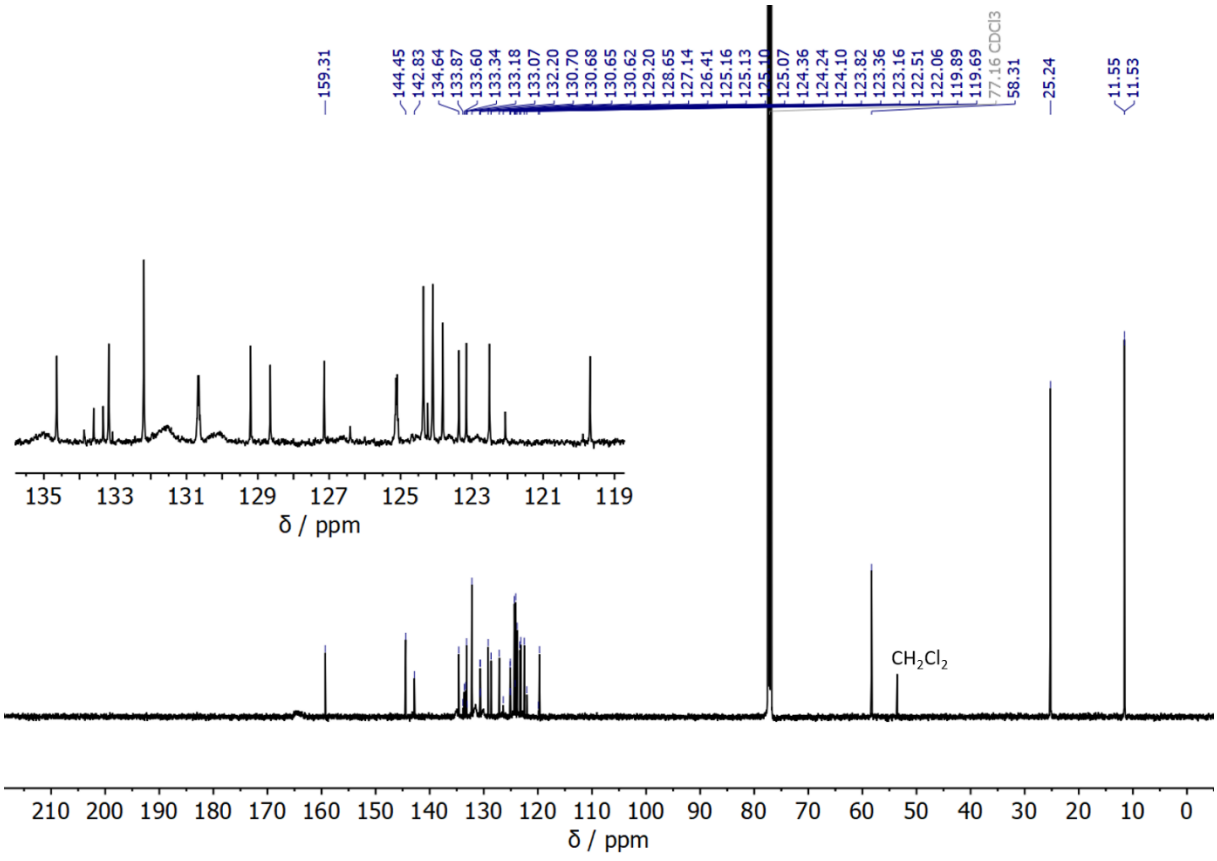

Figure S89. ^{13}C NMR (125 MHz, $CDCl_3$) spectrum of **Br-aPDI-CF$_3$**

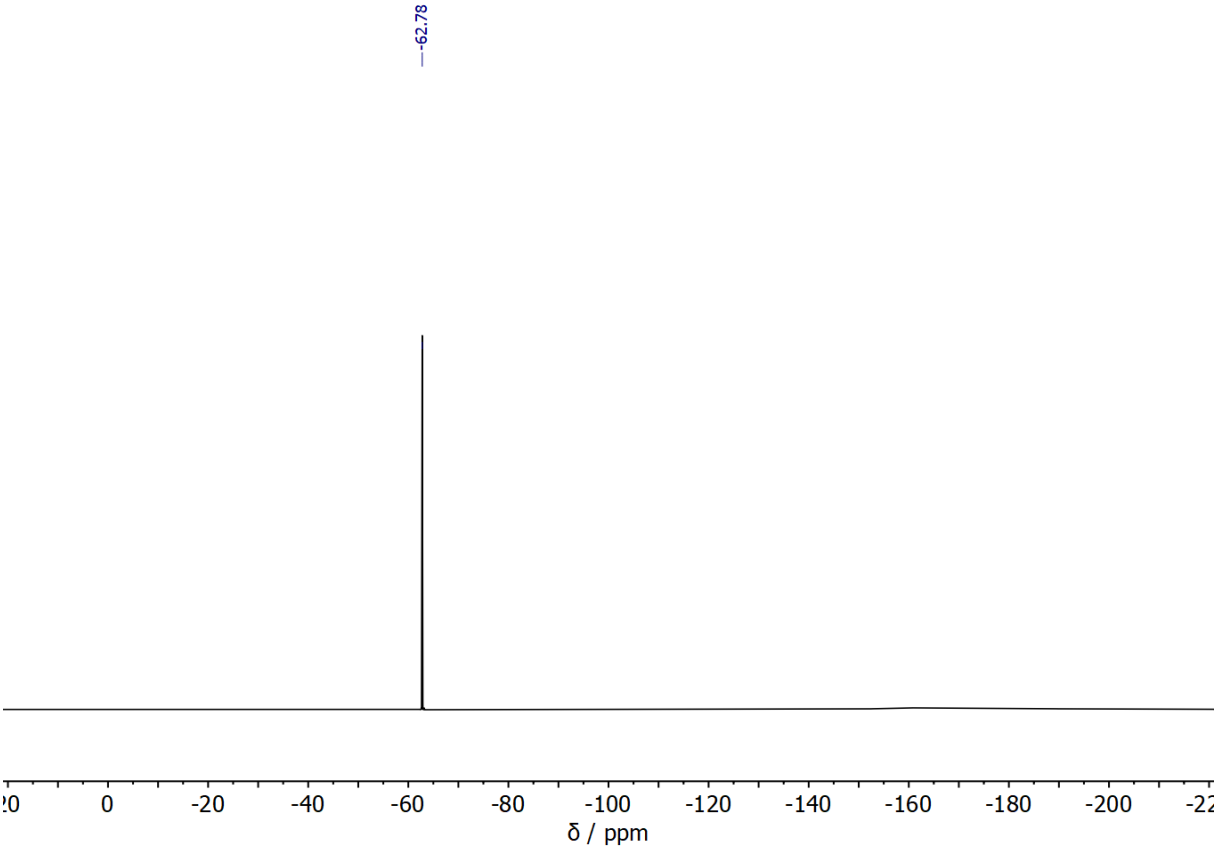

Figure S90. ^{19}F NMR (470 MHz, $CDCl_3$) spectrum of **Br-aPDI-CF$_3$**

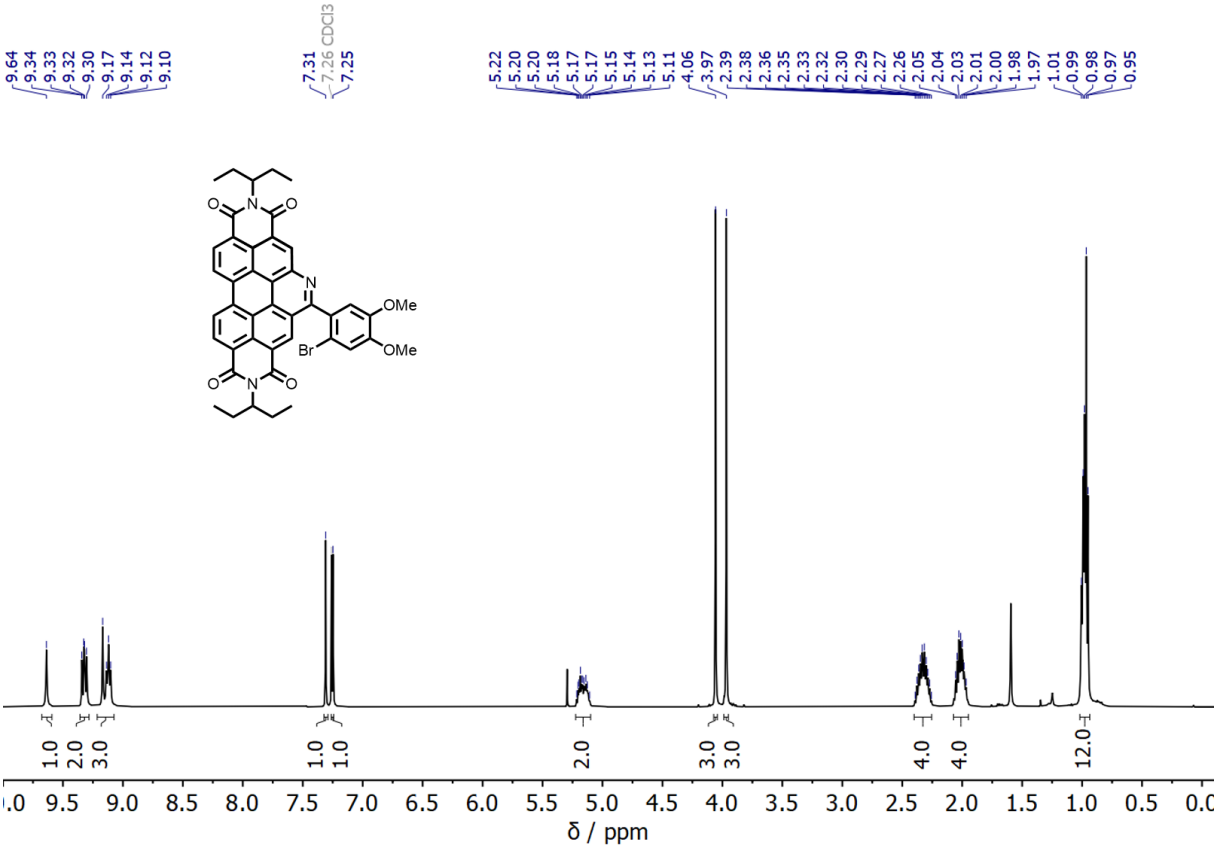

Figure S91. ^{1}H NMR (500 MHz, $CDCl_3$) spectrum of **Br-aPDI-OMe**

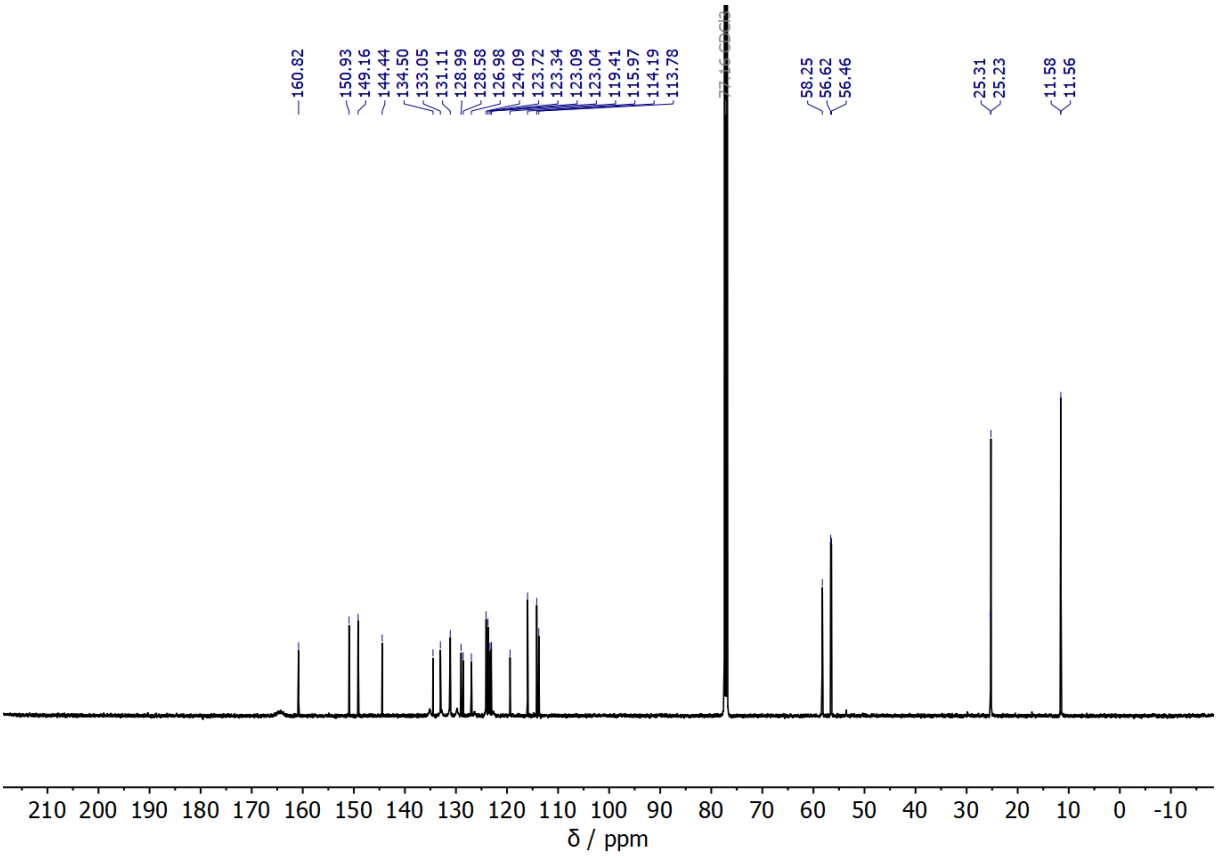

Figure S92. ^{13}C NMR (125 MHz, $CDCl_3$) spectrum of **Br-aPDI-OMe**

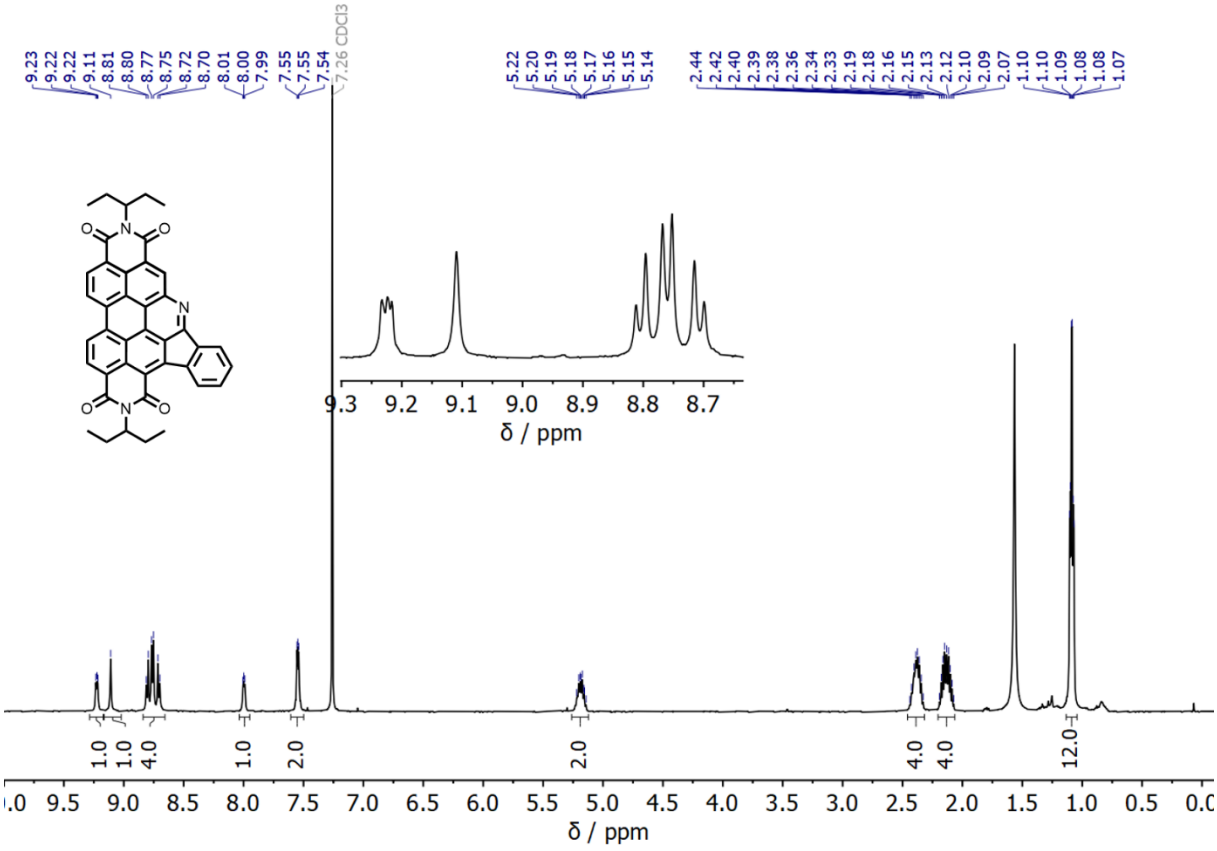

Figure S93. ^{1}H NMR (500 MHz, $CDCl_3$) spectrum of **aPDI-Ph**

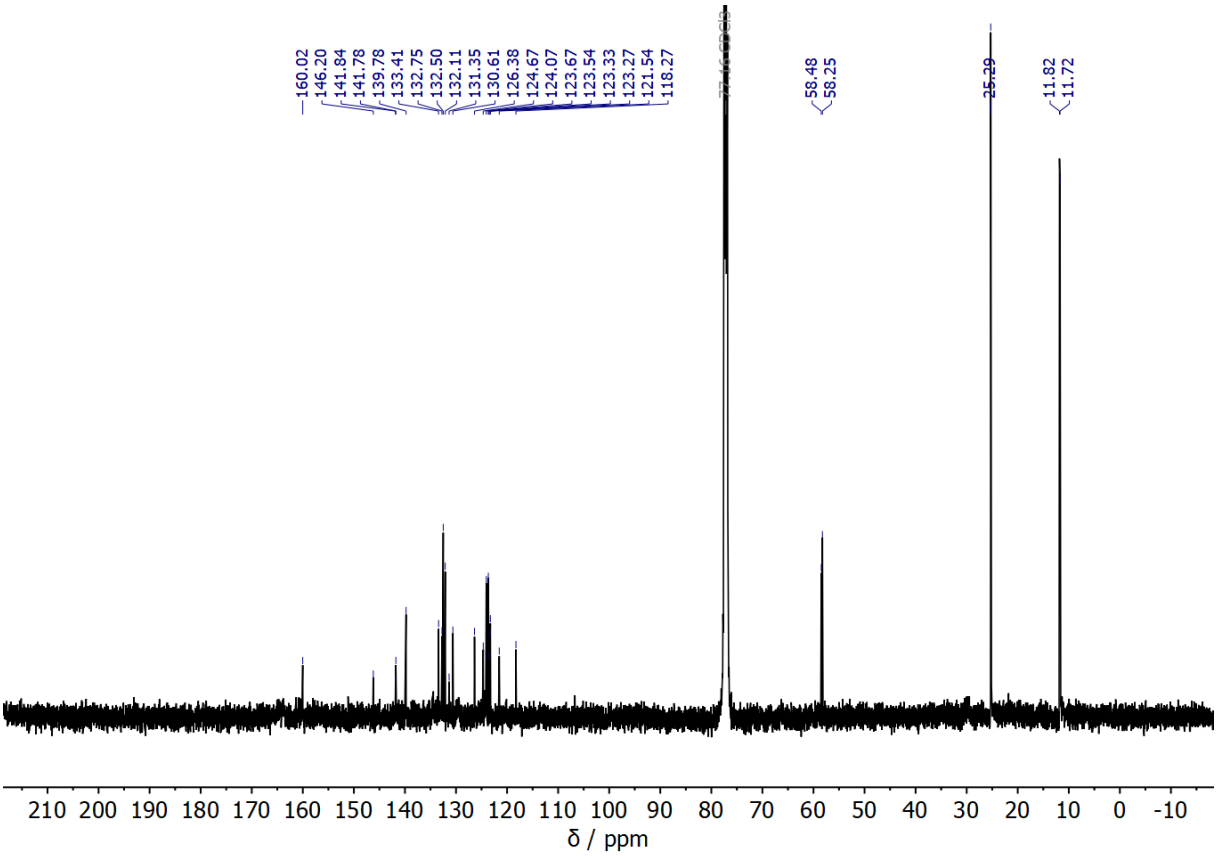

Figure S94. ^{13}C NMR (125 MHz, $CDCl_3$) spectrum of **aPDI-Ph**

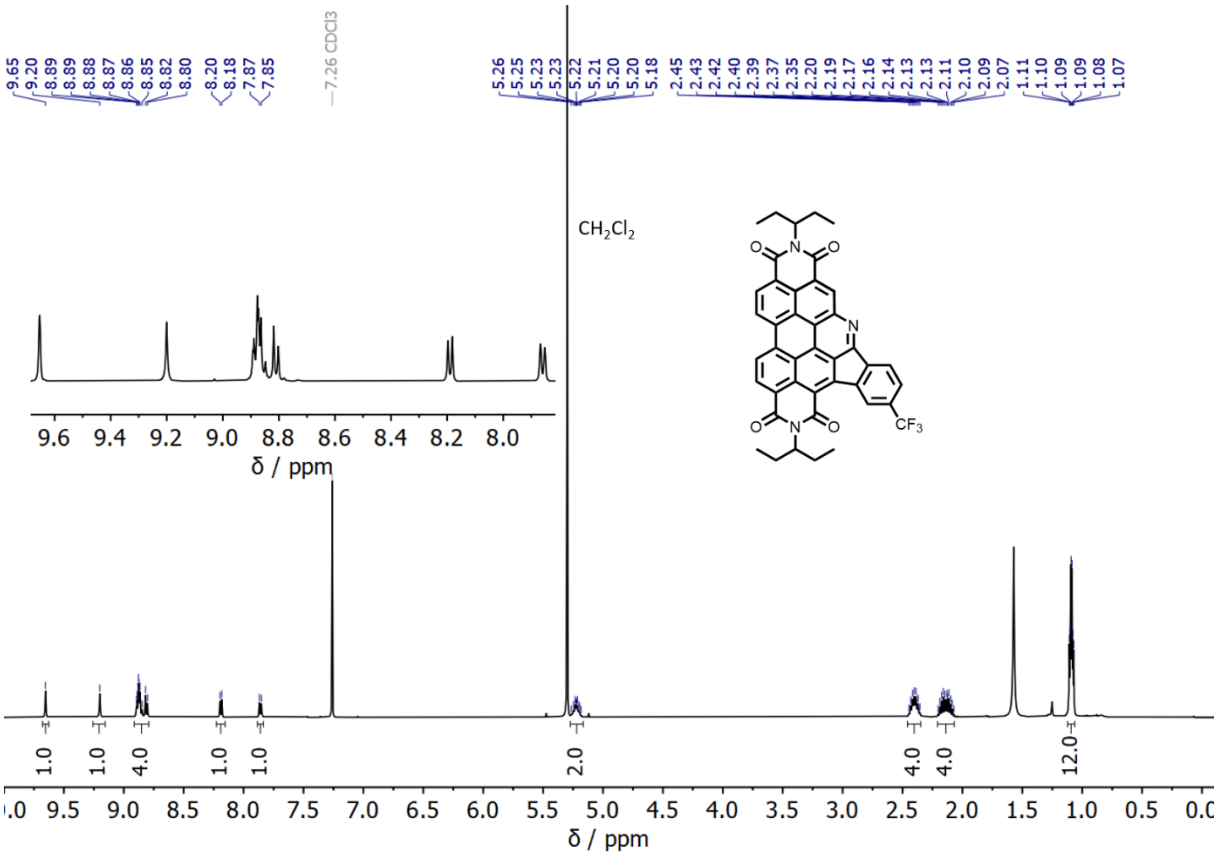

Figure S95. ^{1}H NMR (500 MHz, $CDCl_3$) spectrum of **aPDI-CF_3**

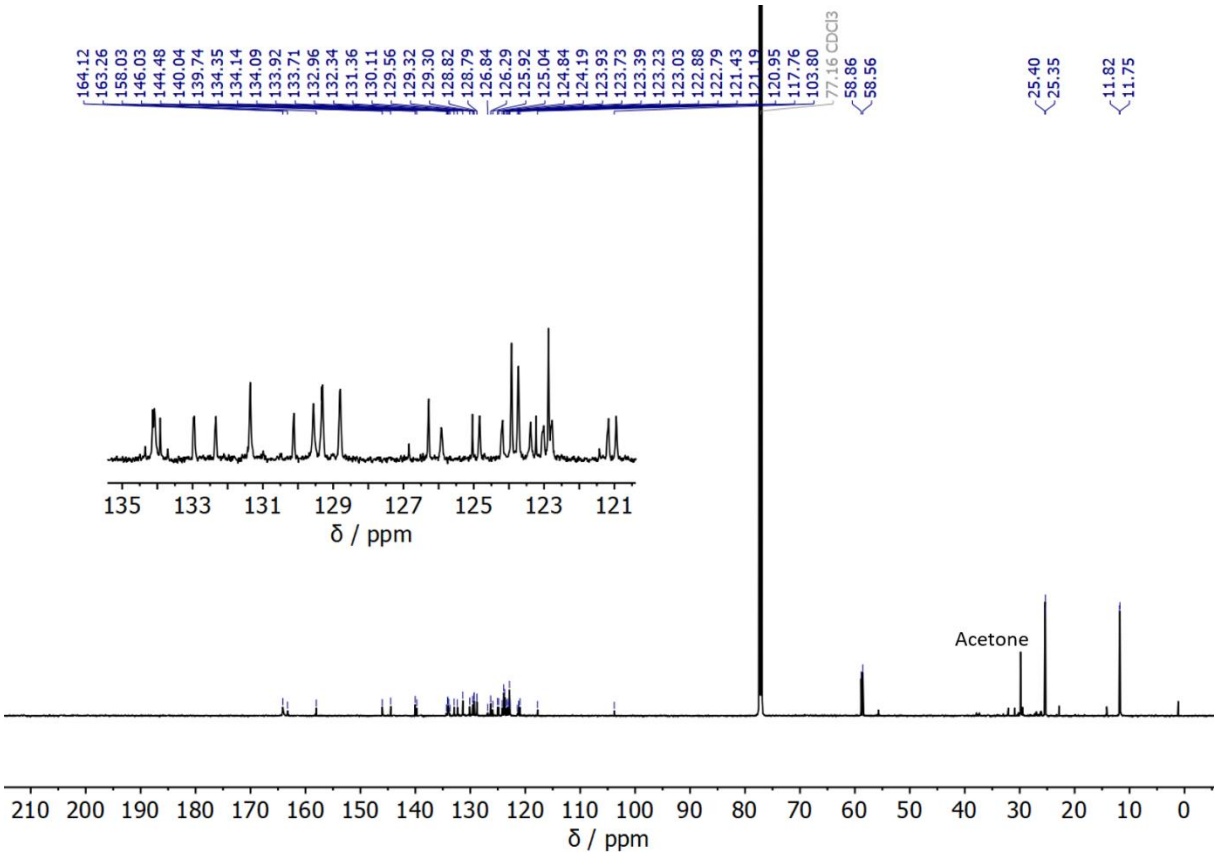

Figure S96. ^{13}C NMR (150 MHz, 328 K, $CDCl_3$) spectrum of **aPDI-CF_3**

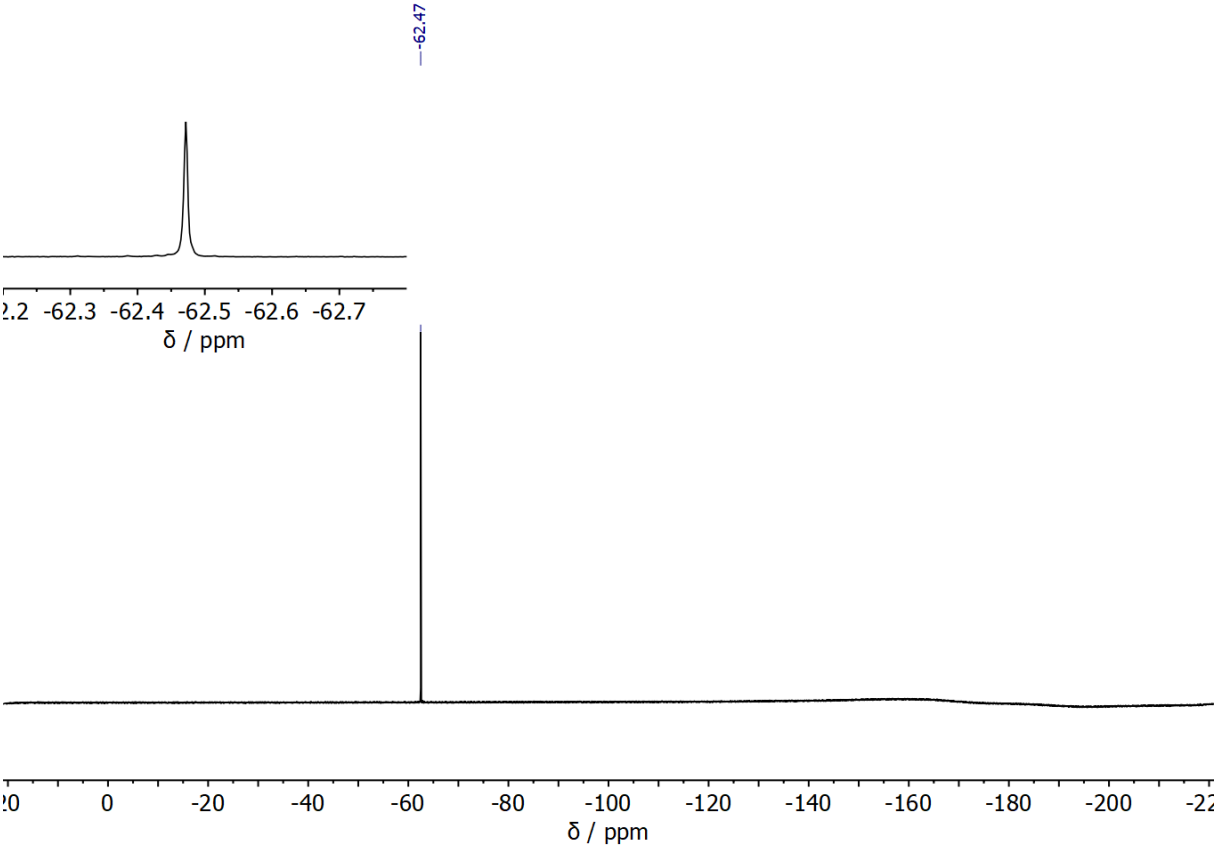

Figure S97. ^{19}F NMR (470 MHz, $CDCl_3$) spectrum of **aPDI-CF_3**

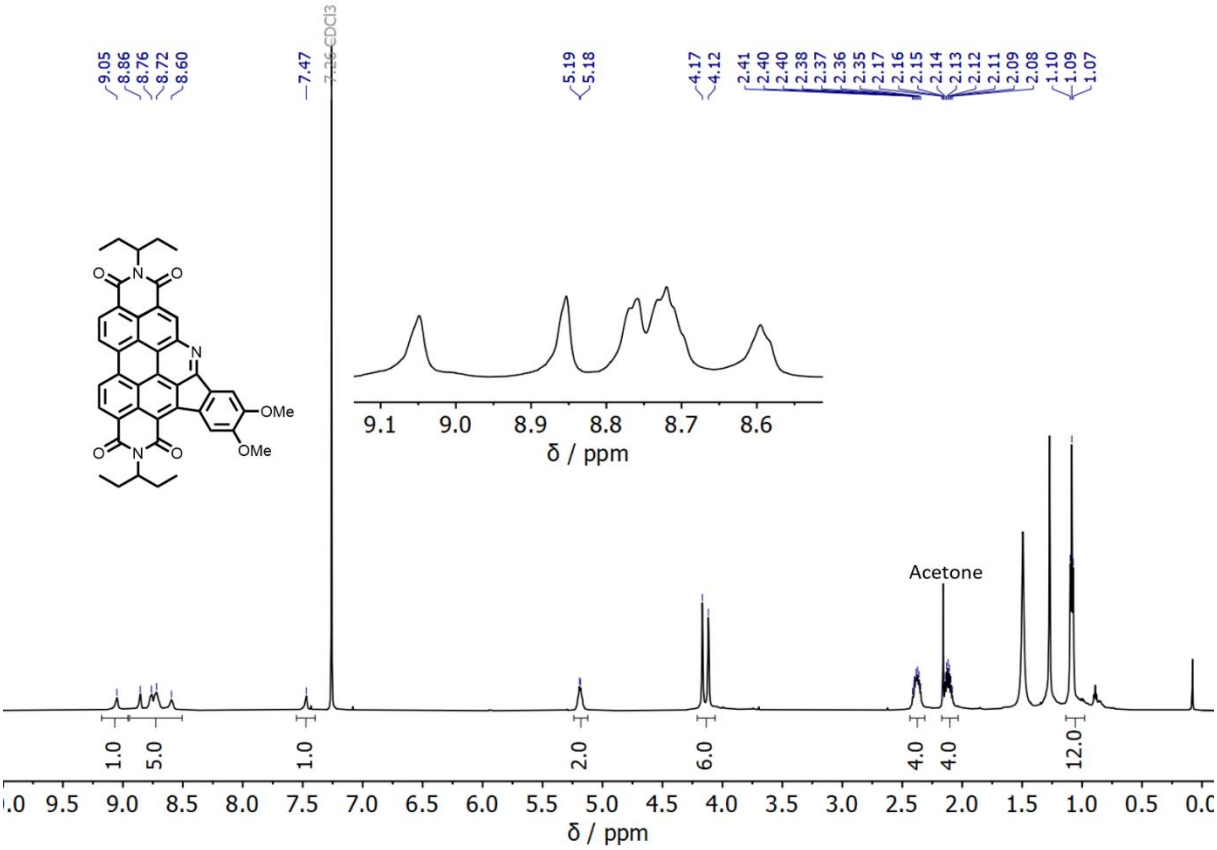

Figure S98. ^{1}H NMR (600 MHz, 328 K, $CDCl_3$) spectrum of **aPDI-OMe**

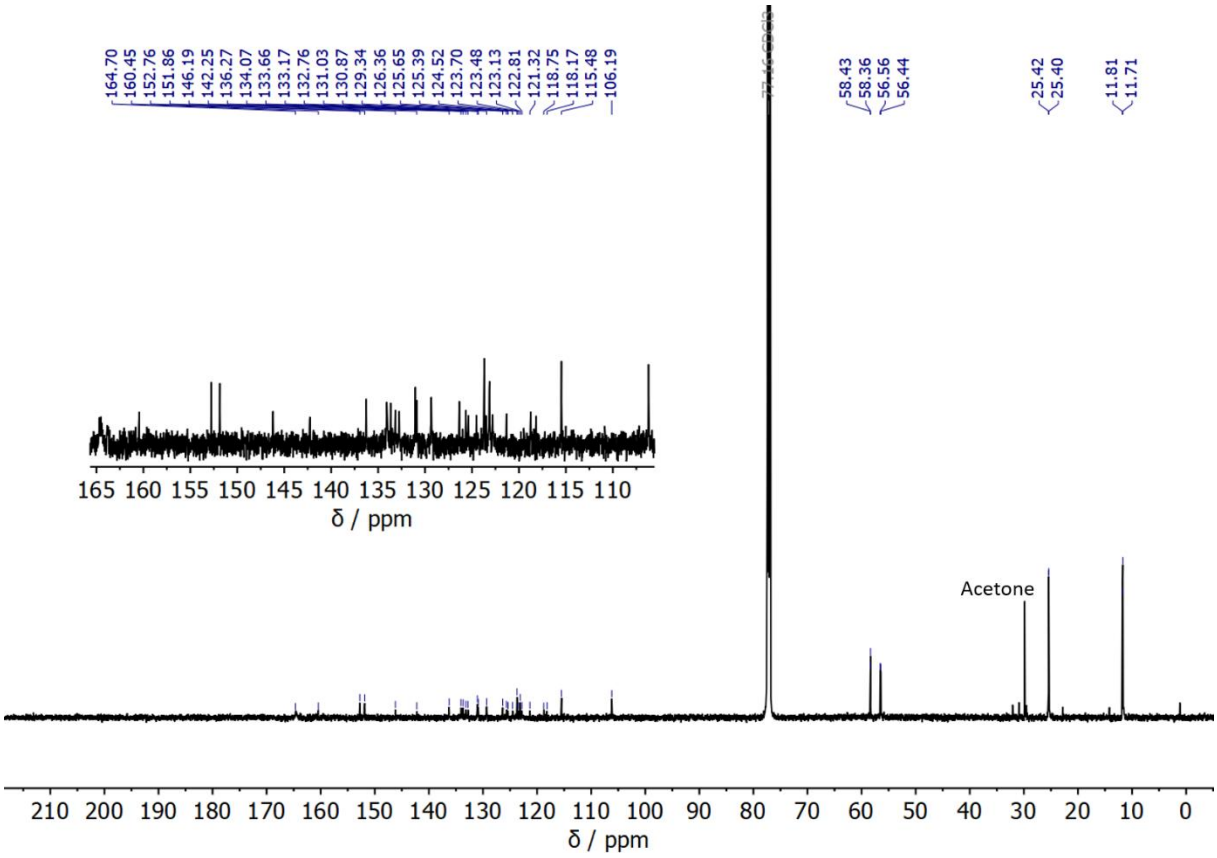

Figure S99. ^{13}C NMR (150 MHz, 328 K, $CDCl_3$) spectrum of **aPDI-OMe**

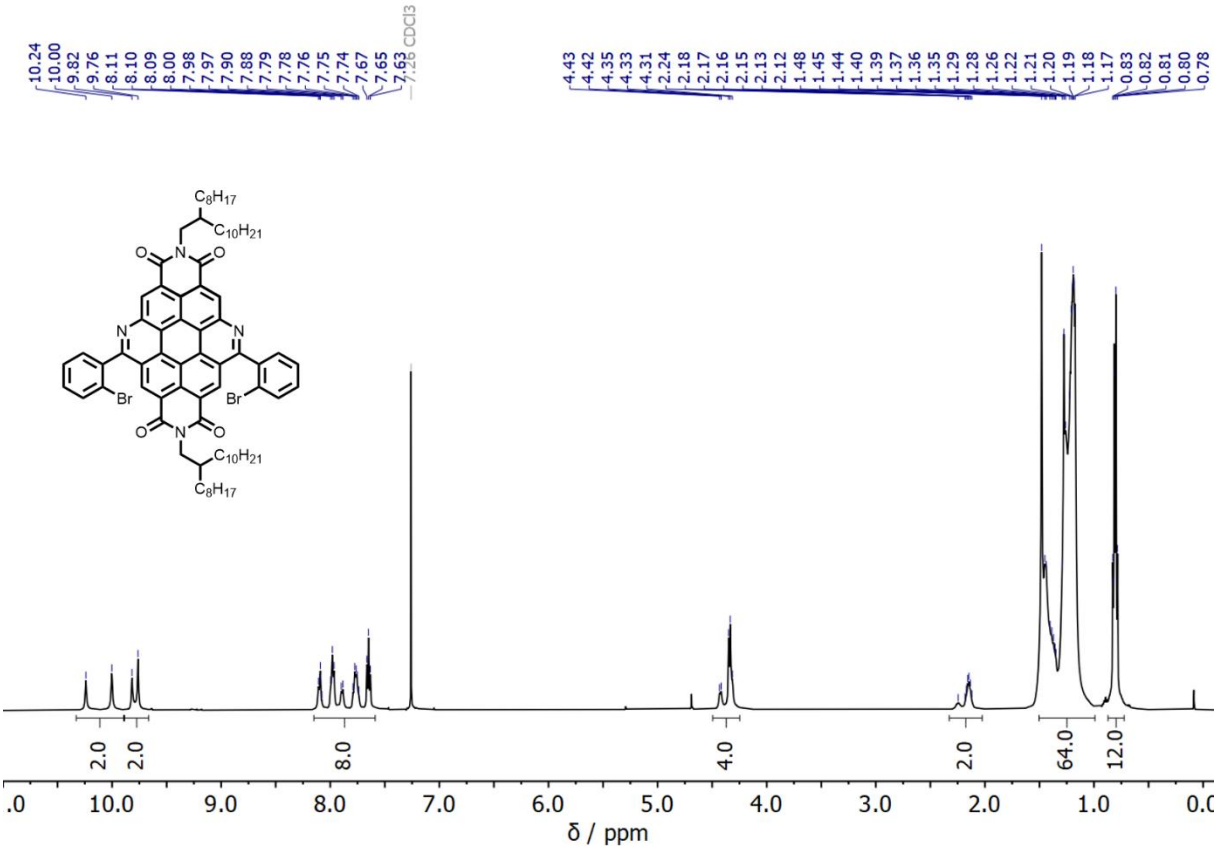

Figure S100. ^{1}H NMR (500 MHz, 328 K, $CDCl_3$) spectrum of **1,6-BACD-Ph**

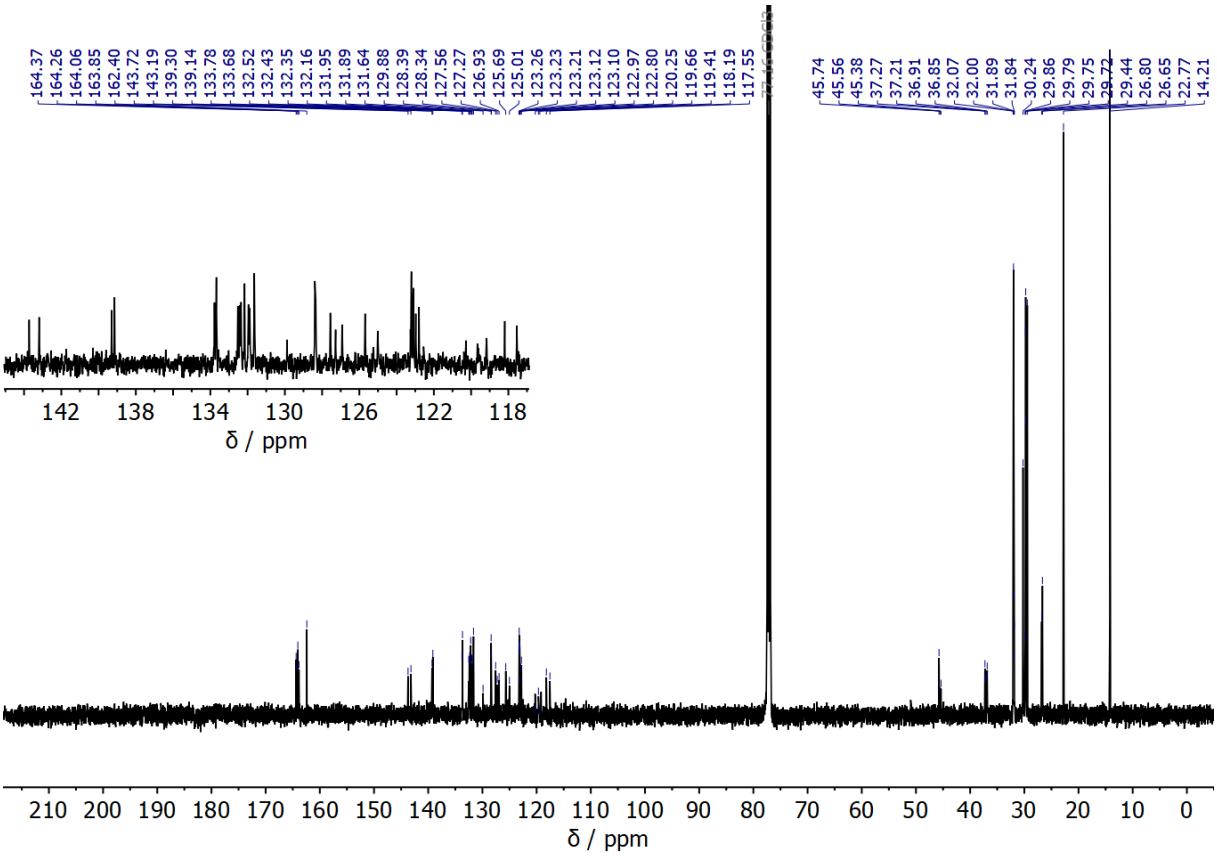

Figure S101. ^{13}C NMR (125 MHz, $CDCl_3$) spectrum of **1,6-BACD-Ph**

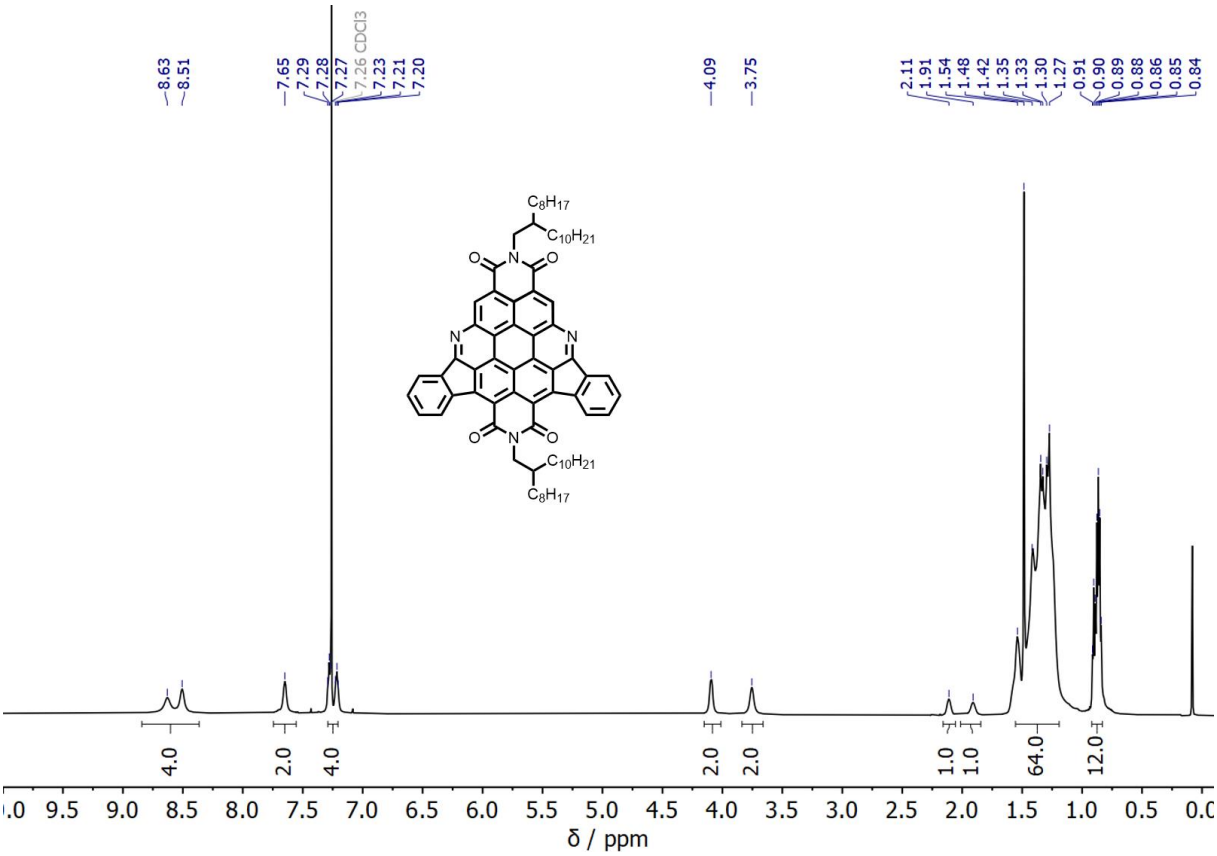

Figure S102. ^{1}H NMR (600 MHz, 328 K, $CDCl_3$) spectrum of **1,6-Ph**

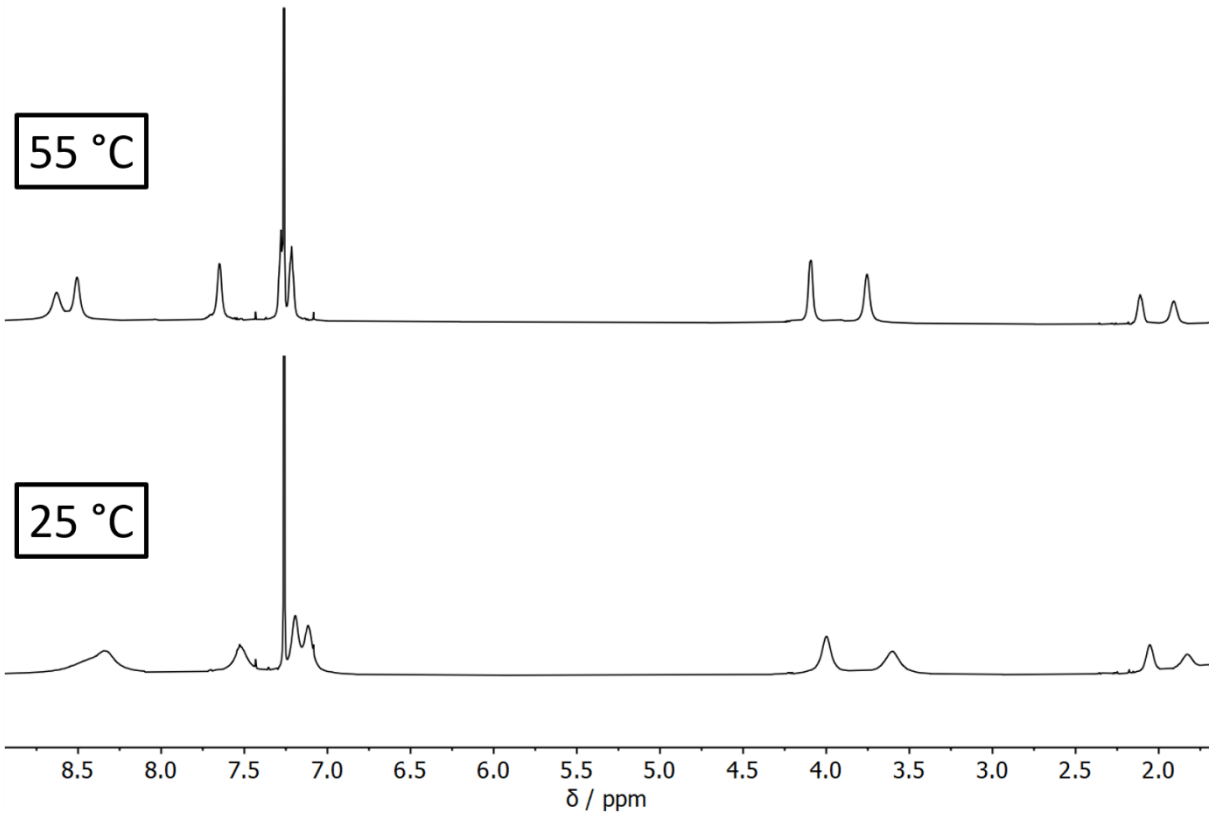

Figure S103. VT ^{1}H NMR (600 MHz, $CDCl_3$) spectrum of **1,6-Ph** exhibiting a temperature dependence on account of its self-association through strong π-π interactions

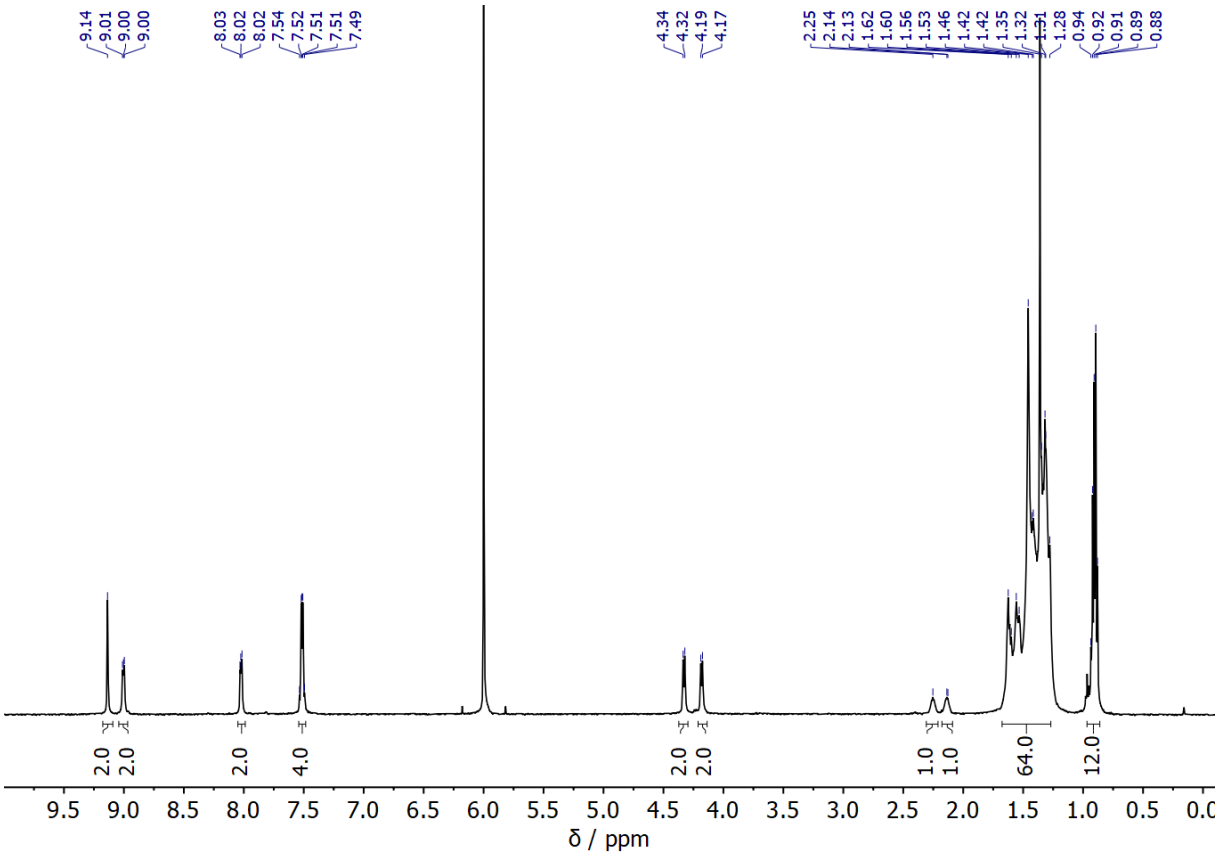

Figure S104. ^{1}H NMR (500 MHz, 393 K, $C_2D_2Cl_4$) spectrum of **1,6-Ph**

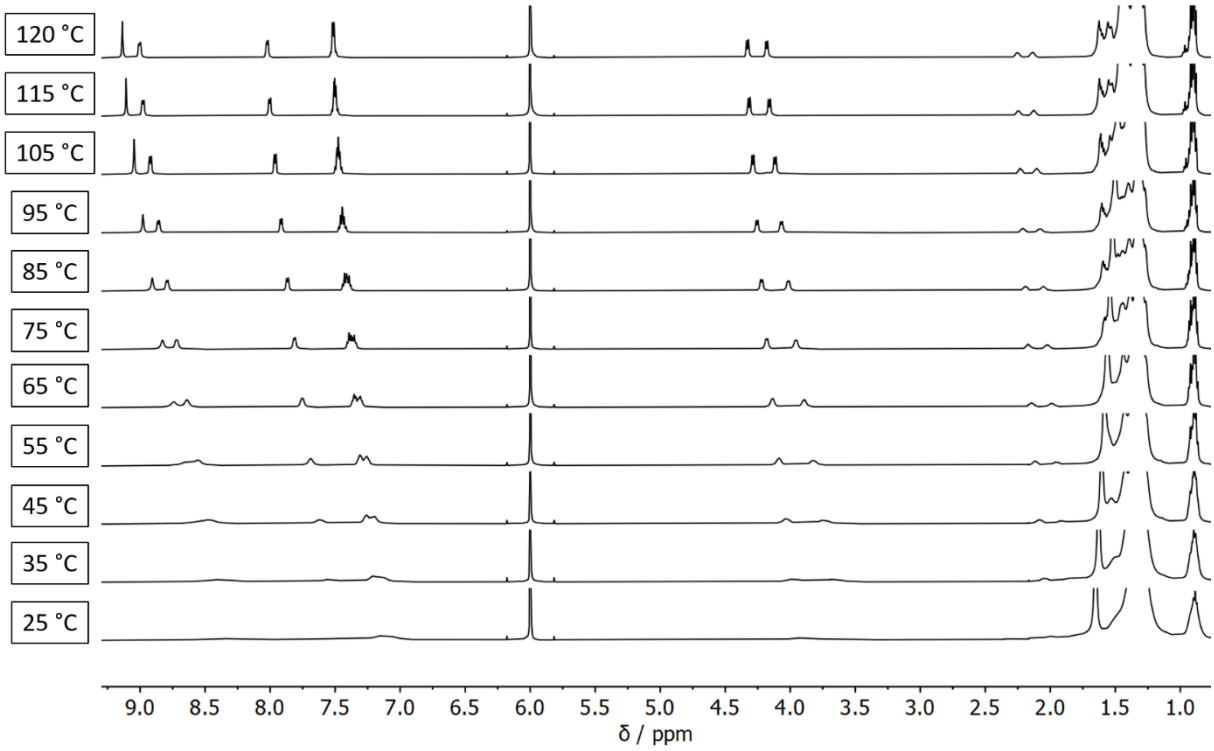

Figure S105. VT ^{1}H NMR (500 MHz, $C_2D_2Cl_4$) spectrum of **1,6-Ph**

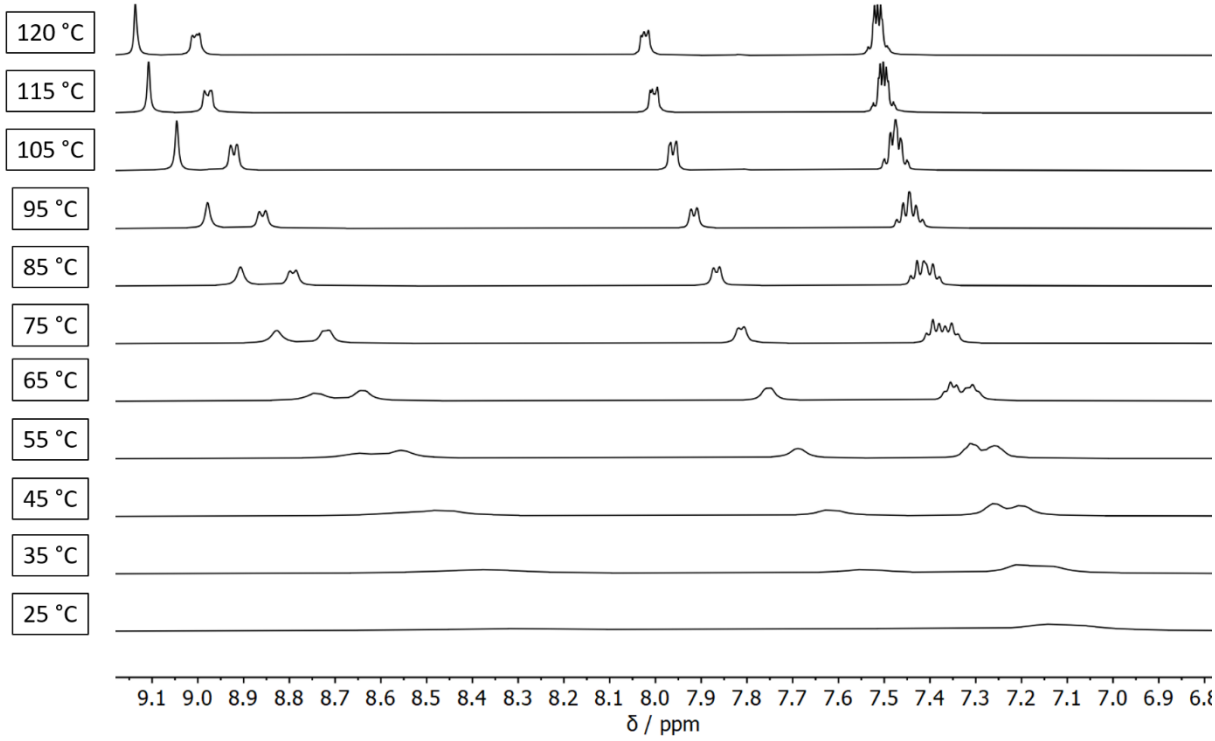

Figure S106. Zoom in the aromatic region of the VT ^{1}H NMR (500 MHz, $C_2D_2Cl_4$) spectrum of **1,6-Ph** exhibiting a temperature dependence of its self-association through strong π-π interactions

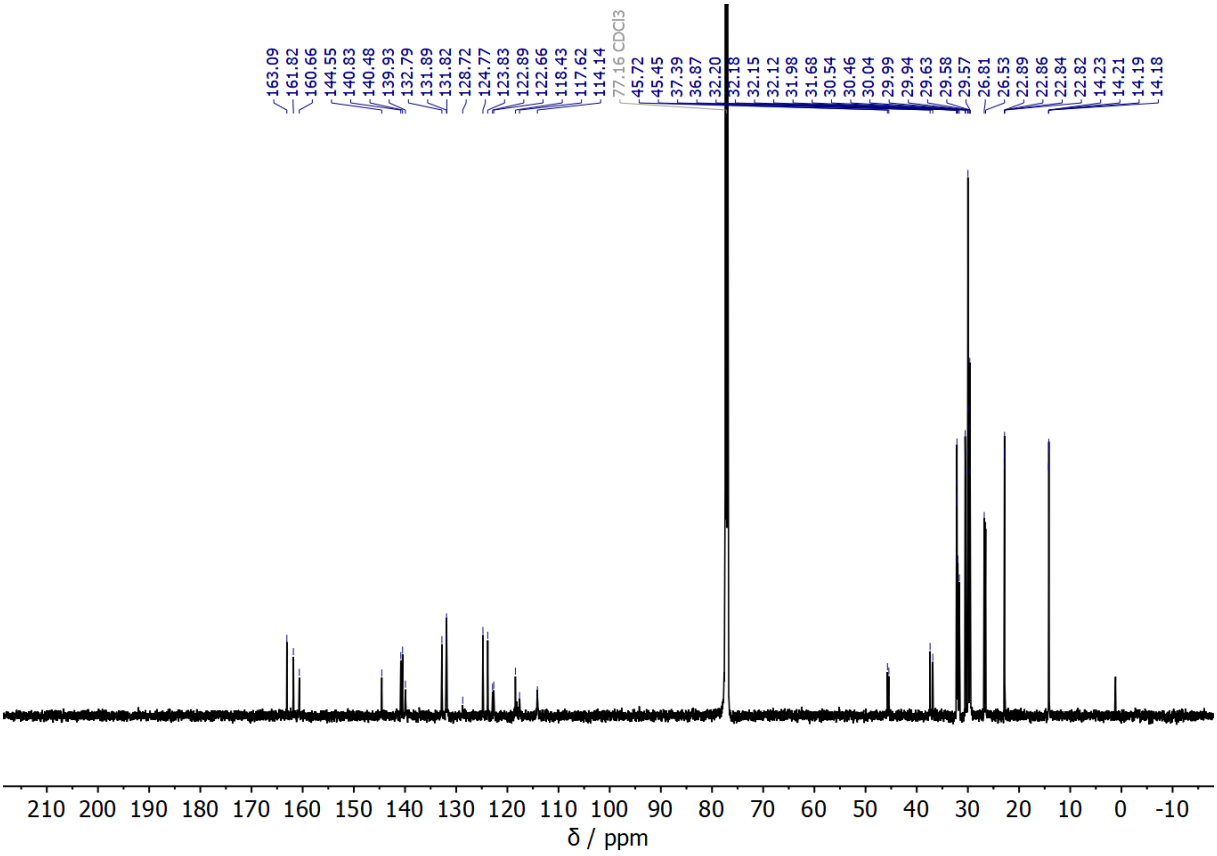

Figure S107. ^{13}C NMR (150 MHz, 328 K, $CDCl_3$) spectrum of **1,6-Ph**

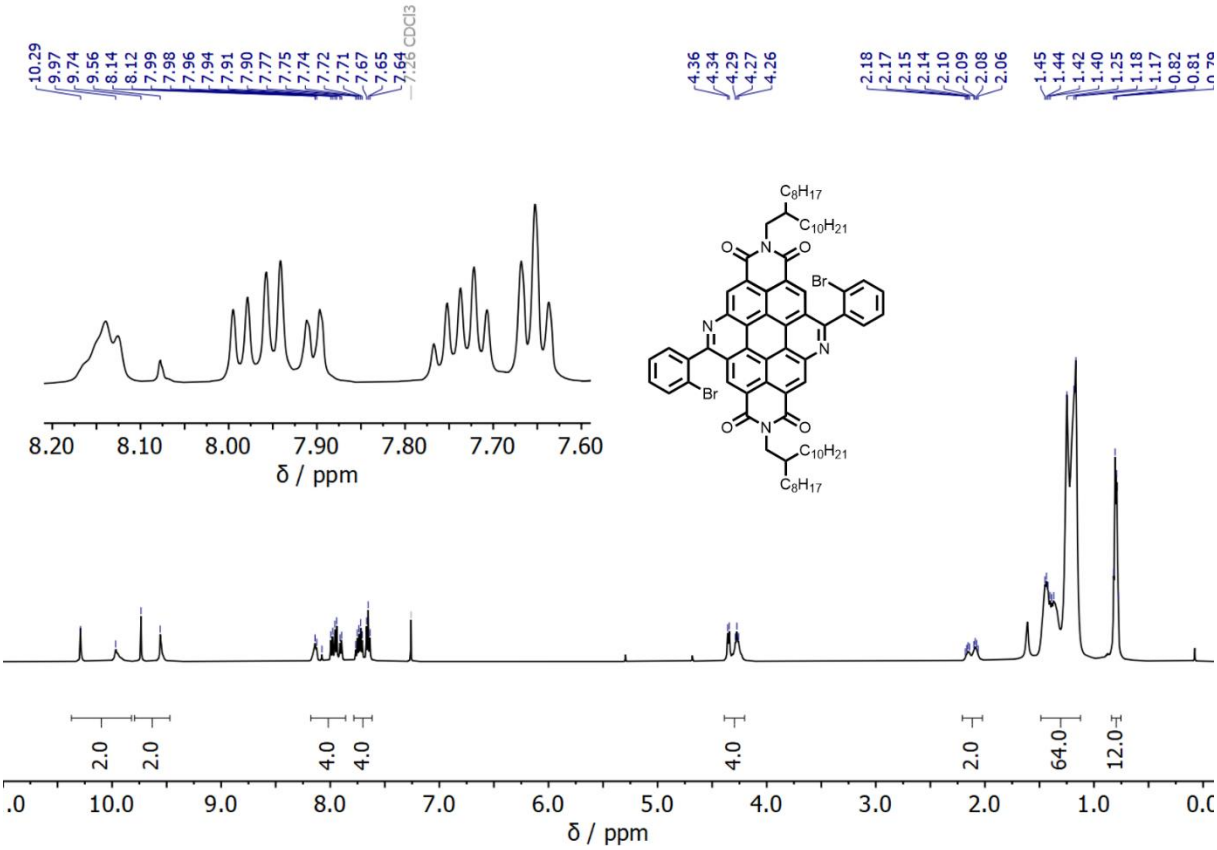

Figure S108. ^{1}H NMR (500 MHz, $CDCl_3$) spectrum of **1,7-BACD-Ph**

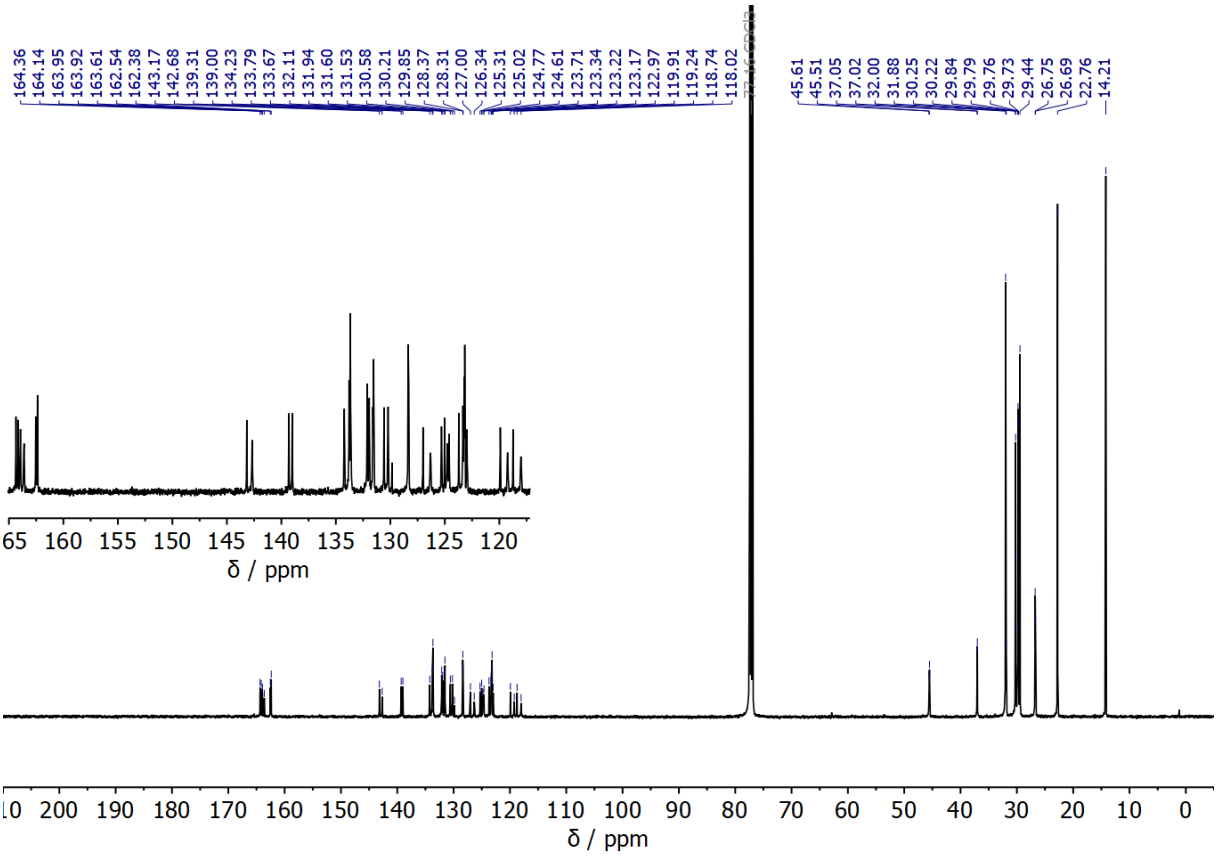

Figure S109. ^{13}C NMR (125 MHz, $CDCl_3$) spectrum of **1,7-BACD-Ph**

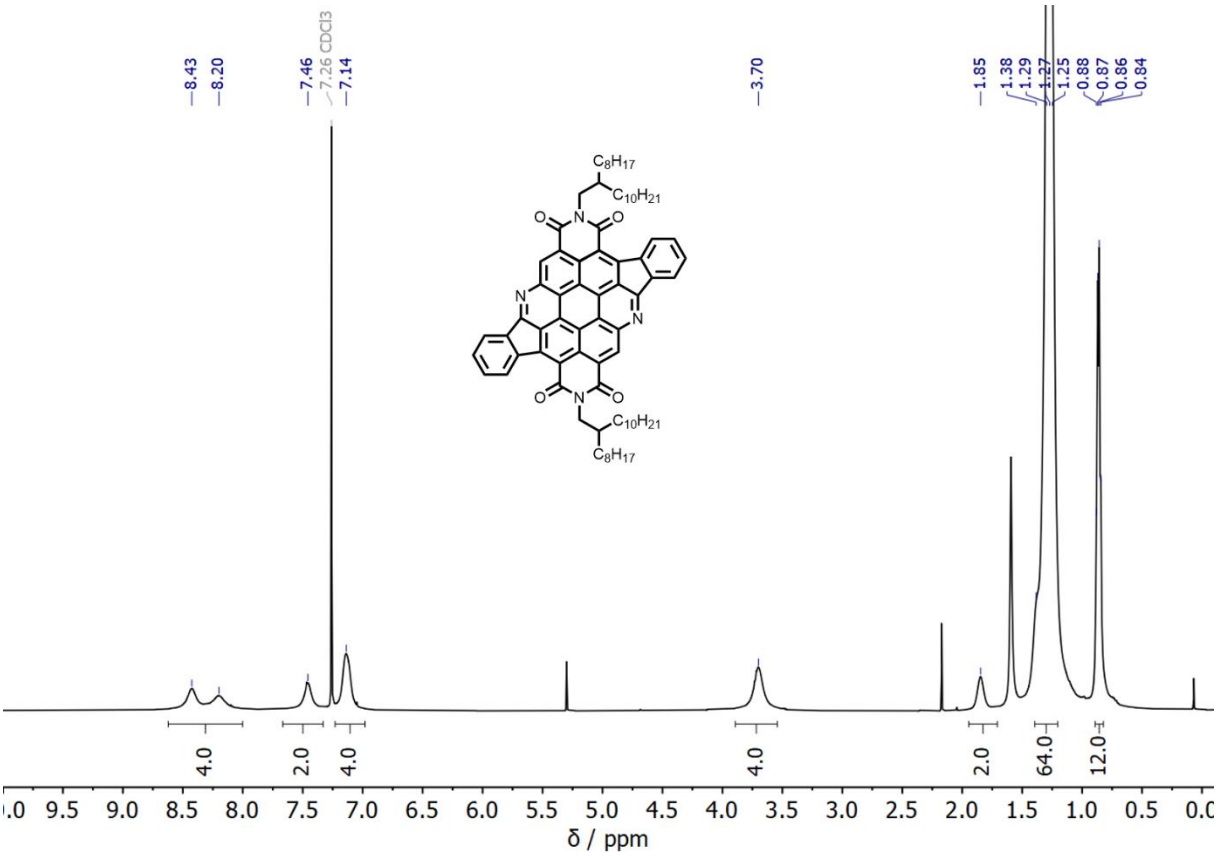

Figure S110. ^{1}H NMR (500 MHz, $CDCl_3$) spectrum of **1,7-Ph**

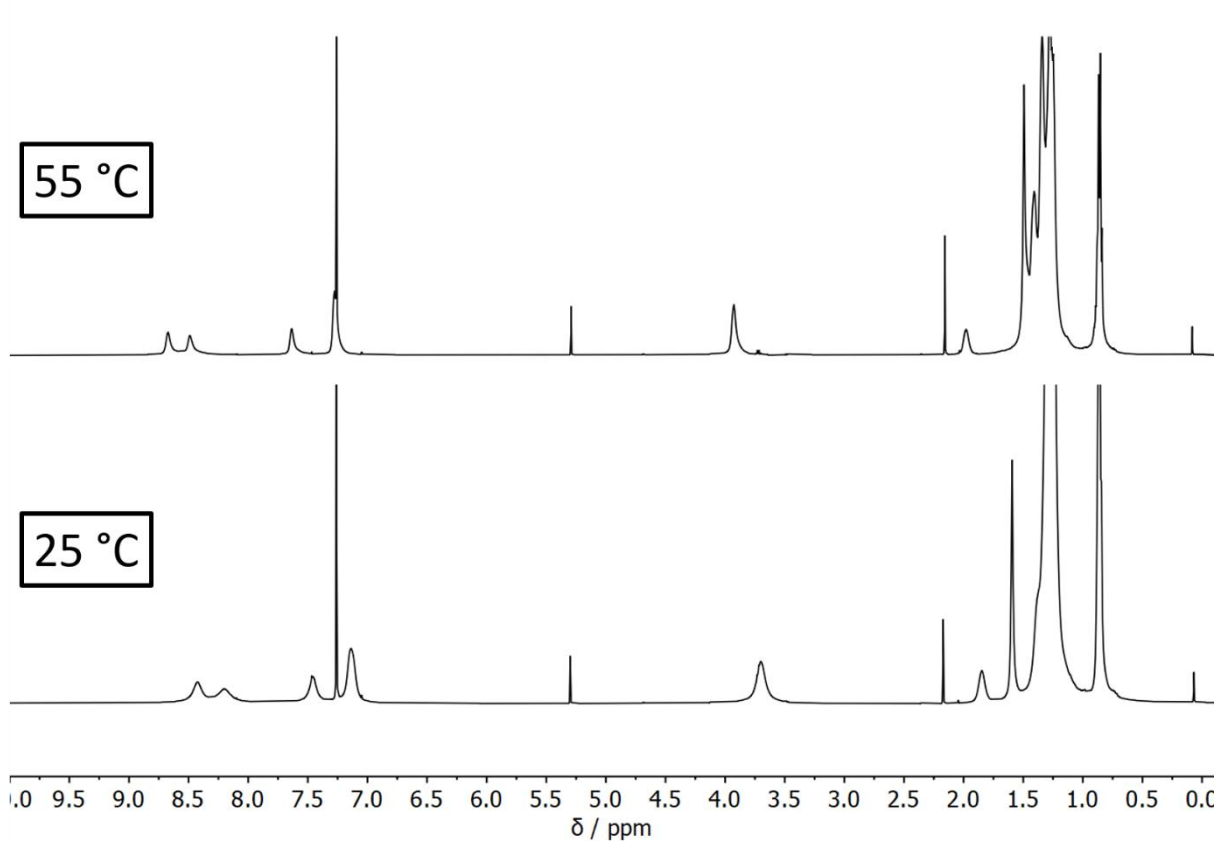

Figure S111. VT ^{1}H NMR (500 MHz, $CDCl_3$) spectrum of **1,7-Ph** exhibiting a temperature dependence on account of its self-association through strong π-π interactions

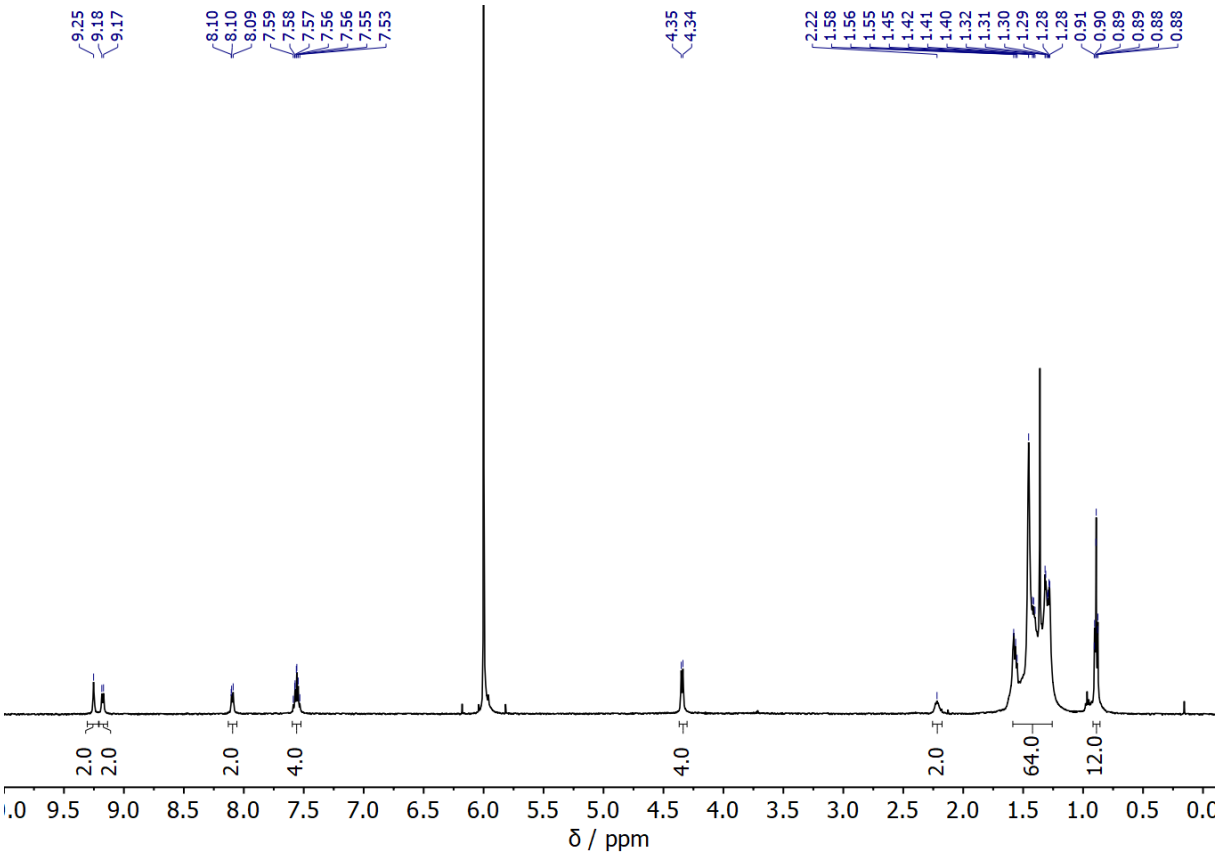

Figure S112. ^{1}H NMR (500 MHz, 393 K, $C_2D_2Cl_4$) spectrum of **1,7-Ph**

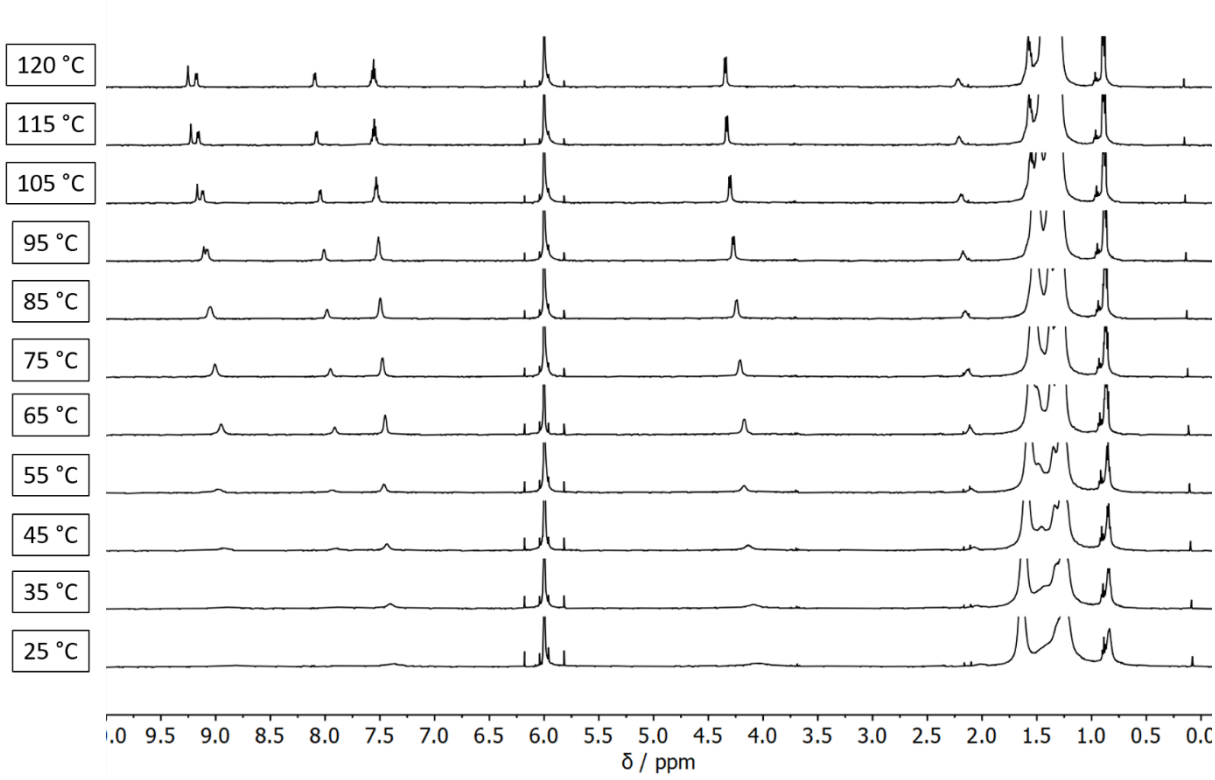

Figure S113. VT ^{1}H NMR (500 MHz, $C_2D_2Cl_4$) spectrum of **1,7-Ph**

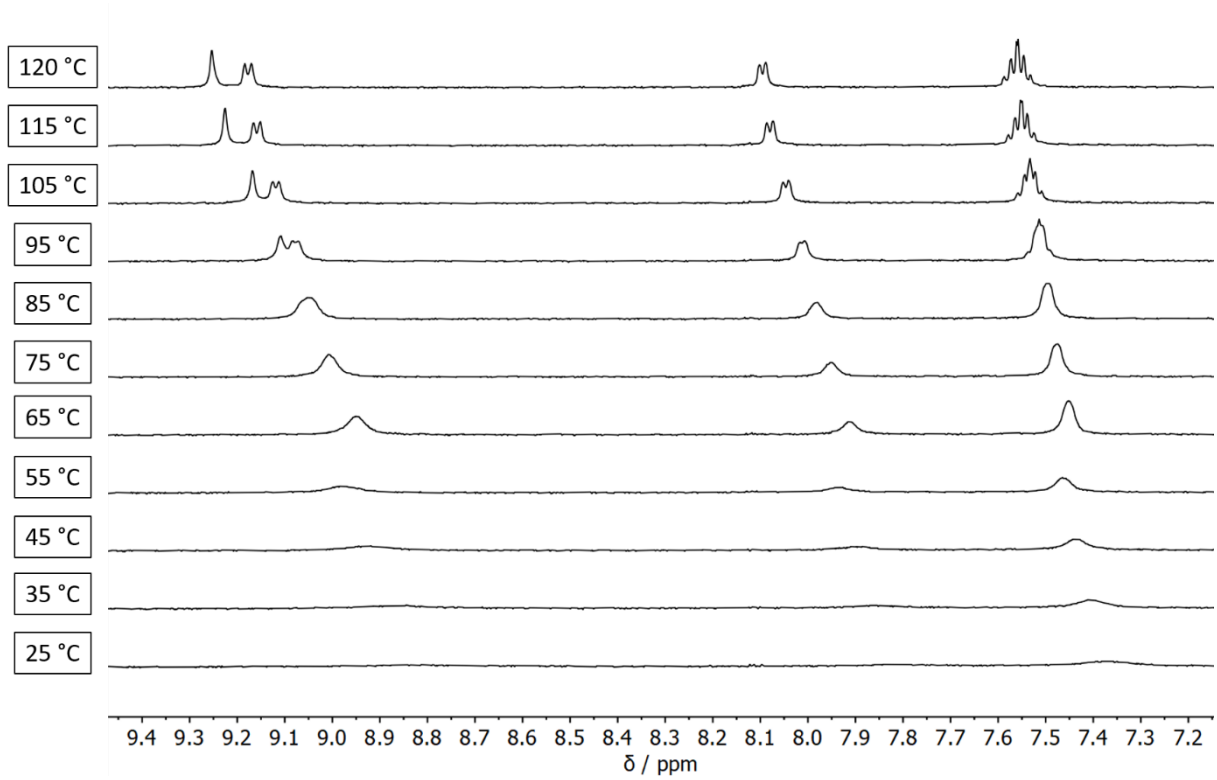

Figure S114. Zoom in the aromatic region of the VT ^{1}H NMR (500 MHz, $C_2D_2Cl_4$) spectrum of **1,7-Ph** exhibiting a temperature dependence of its self-association through strong π-π interactions

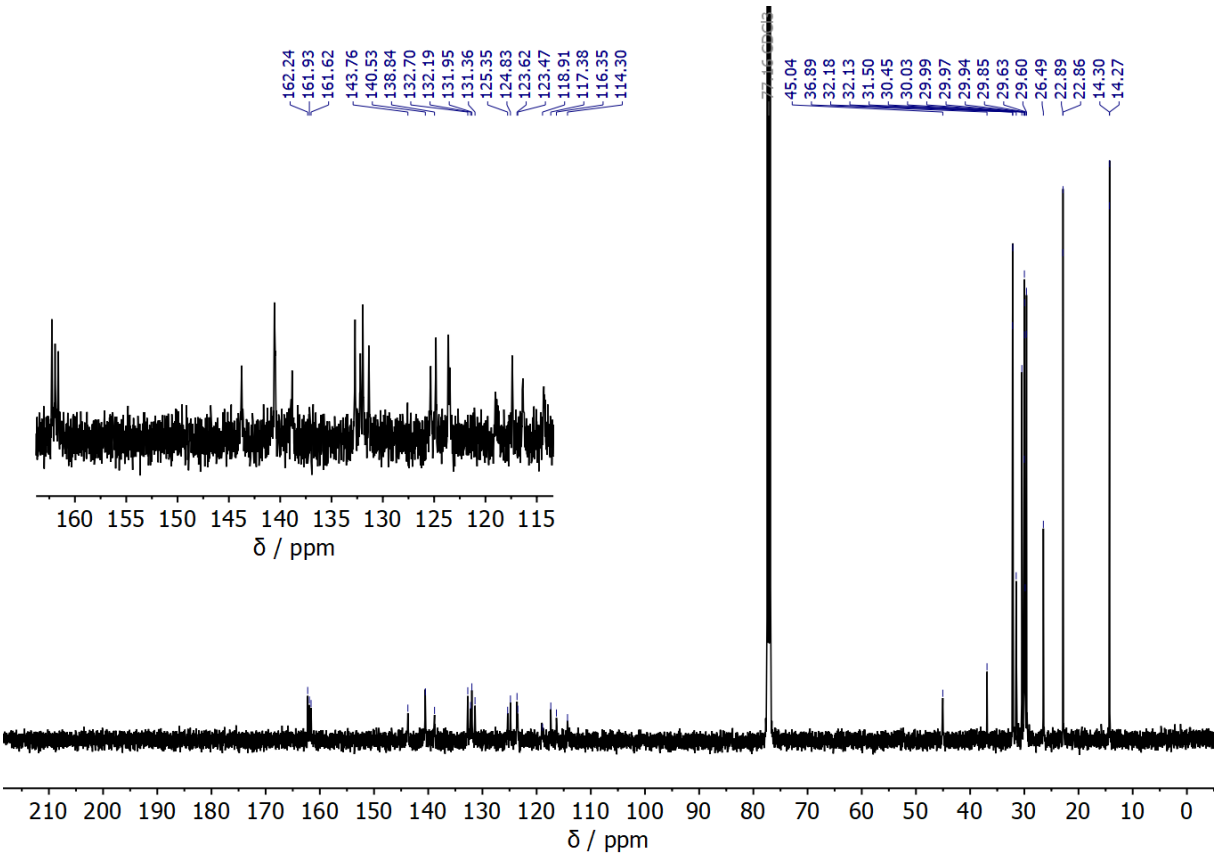

Figure S115. ^{13}C NMR (125 MHz, $CDCl_3$) spectrum of **1,7-Ph**

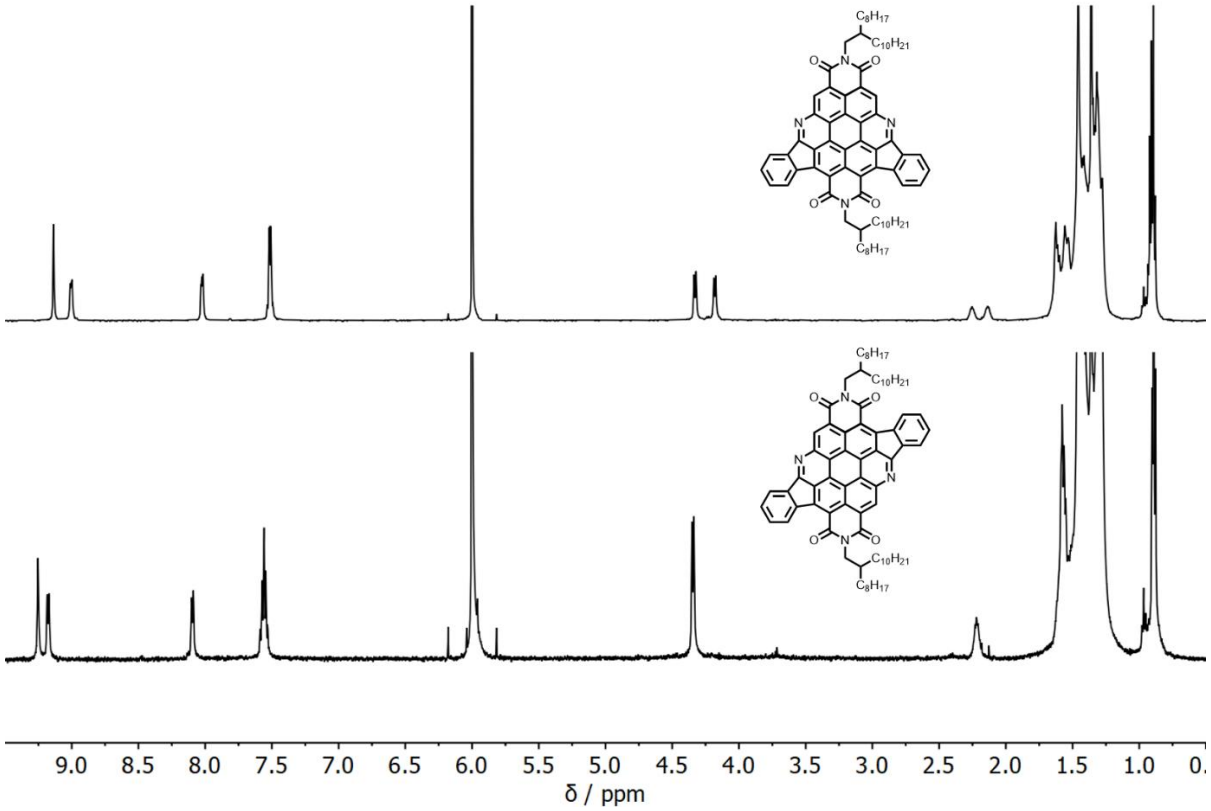

Figure S116. ^{1}H NMR (500 MHz, 393 K, $C_2D_2Cl_4$) spectrum of **1,6-Ph** (top) and **1,7-Ph** (bottom) showing their regiopurity and the differences of their proton resonances

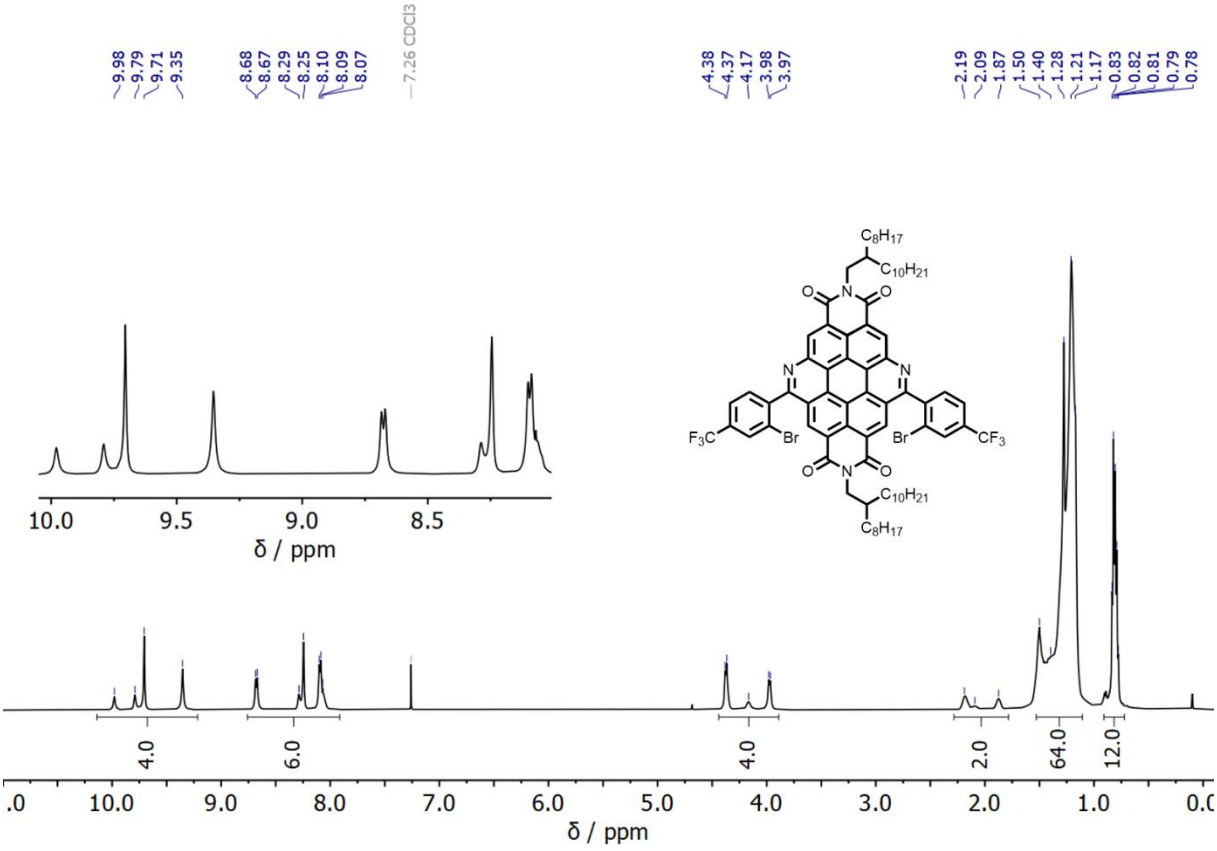

Figure S117. ^{1}H NMR (500 MHz, 328 K, $CDCl_3$) spectrum of **1,6-BACD-CF$_3$**

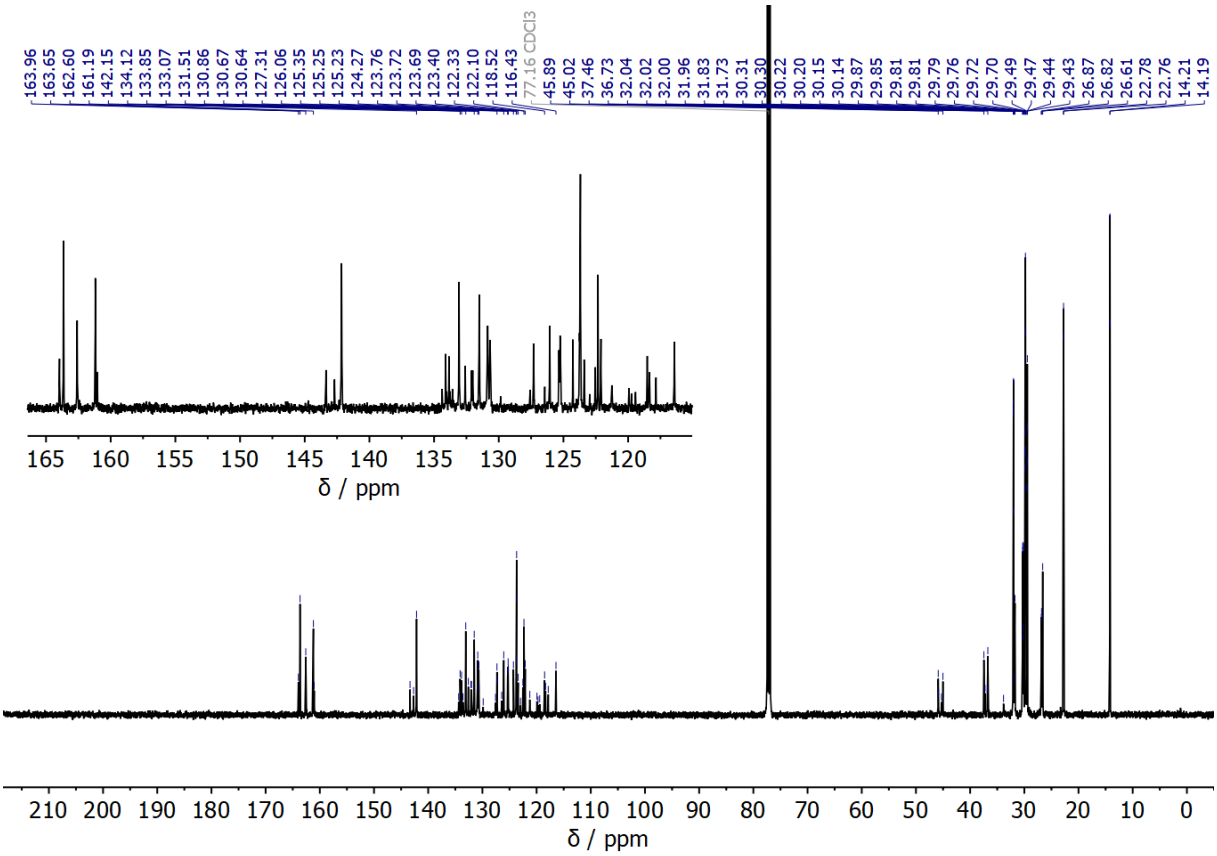

Figure S118. ^{13}C NMR (125 MHz, $CDCl_3$) spectrum of **1,6-BACD-CF₃**

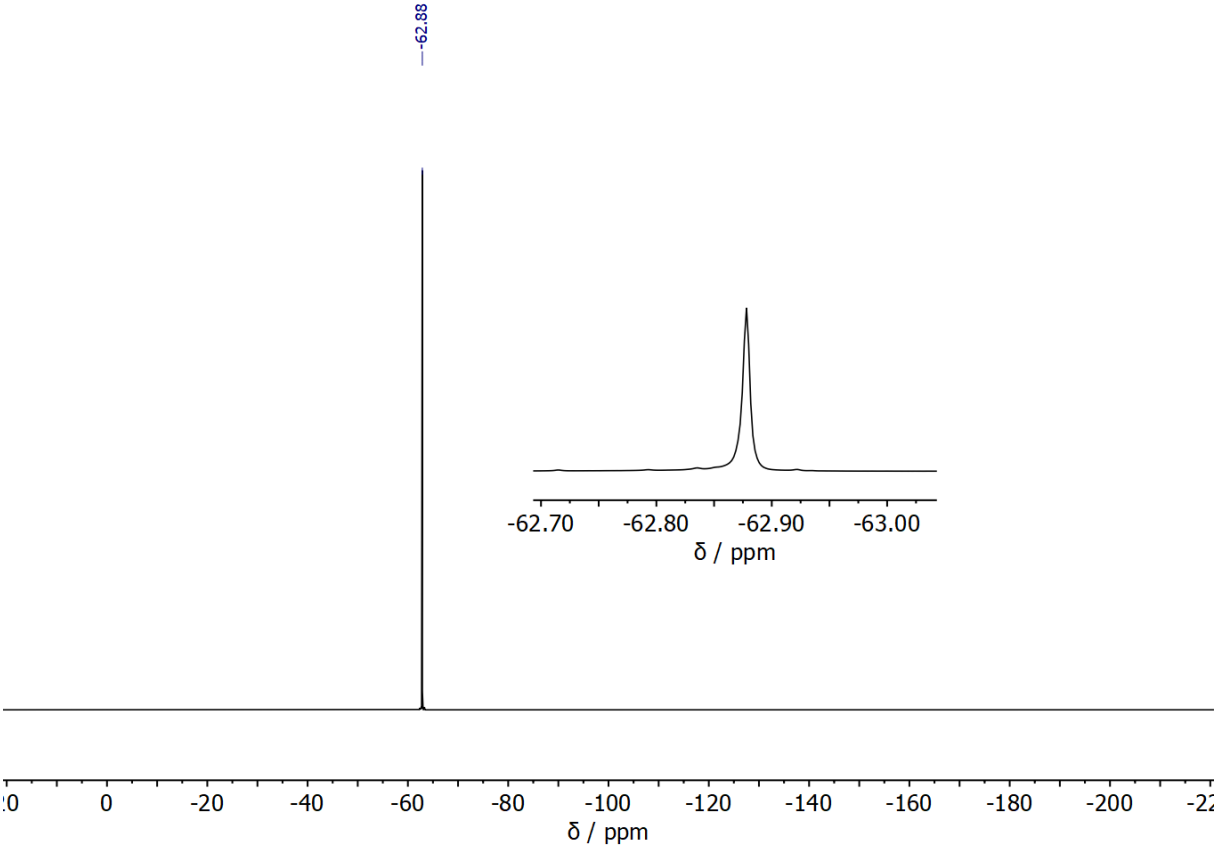

Figure S119. ^{19}F NMR (470 MHz, 328 K, $CDCl_3$) spectrum of **1,6-BACD-CF₃**

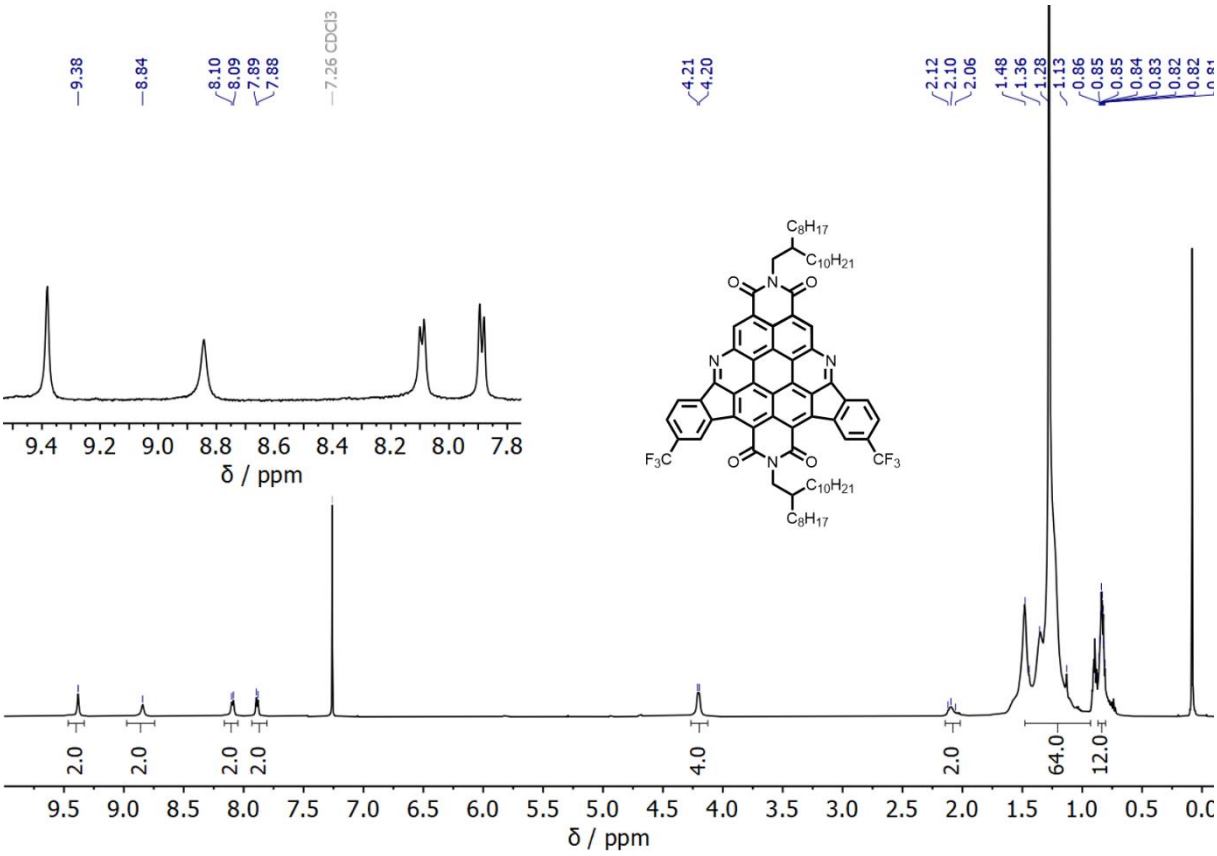

Figure S120. ^{1}H NMR (500 MHz, 328 K, $CDCl_3$) spectrum of **1,6-CF$_3$**

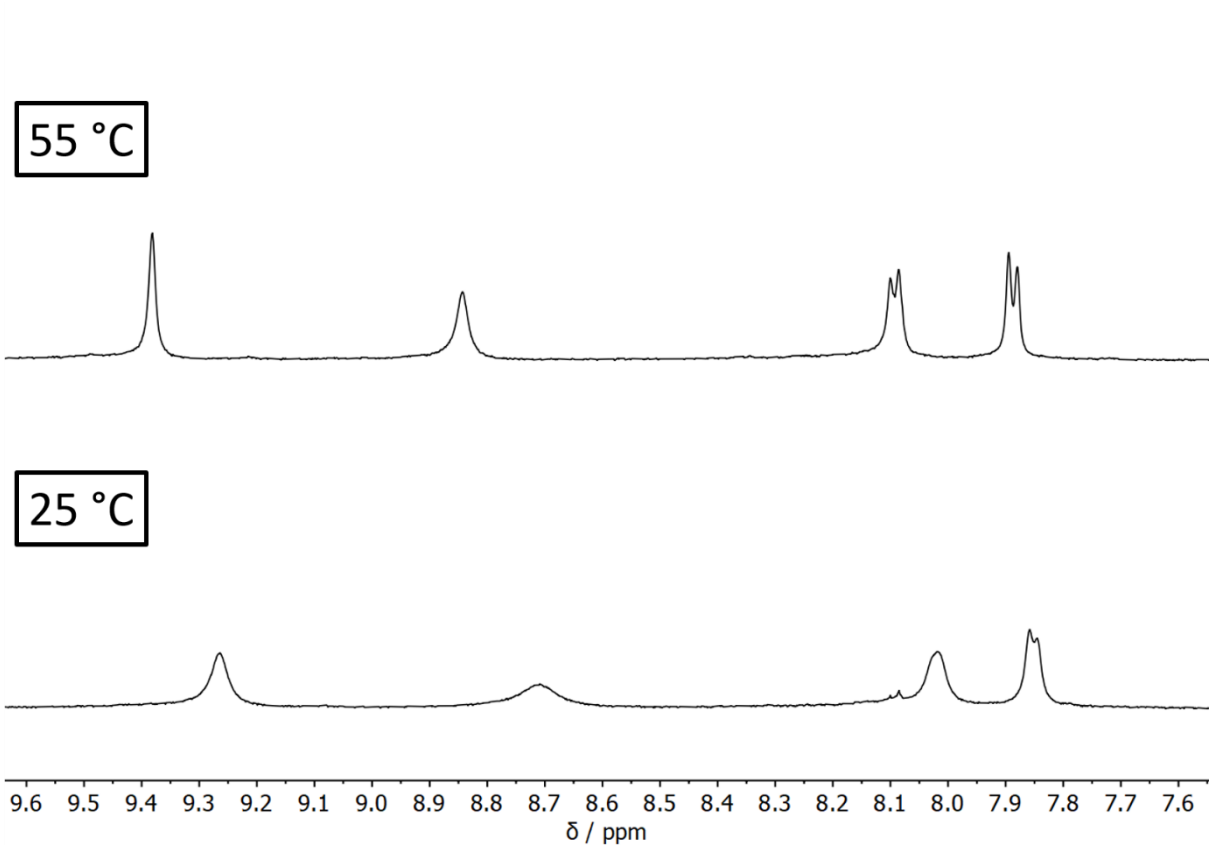

Figure S121. Zoom in the aromatic region of the VT ^{1}H NMR (500 MHz, $CDCl_3$) spectrum of **1,6-CF$_3$** exhibiting a temperature dependence of its self-association through strong π-π interactions

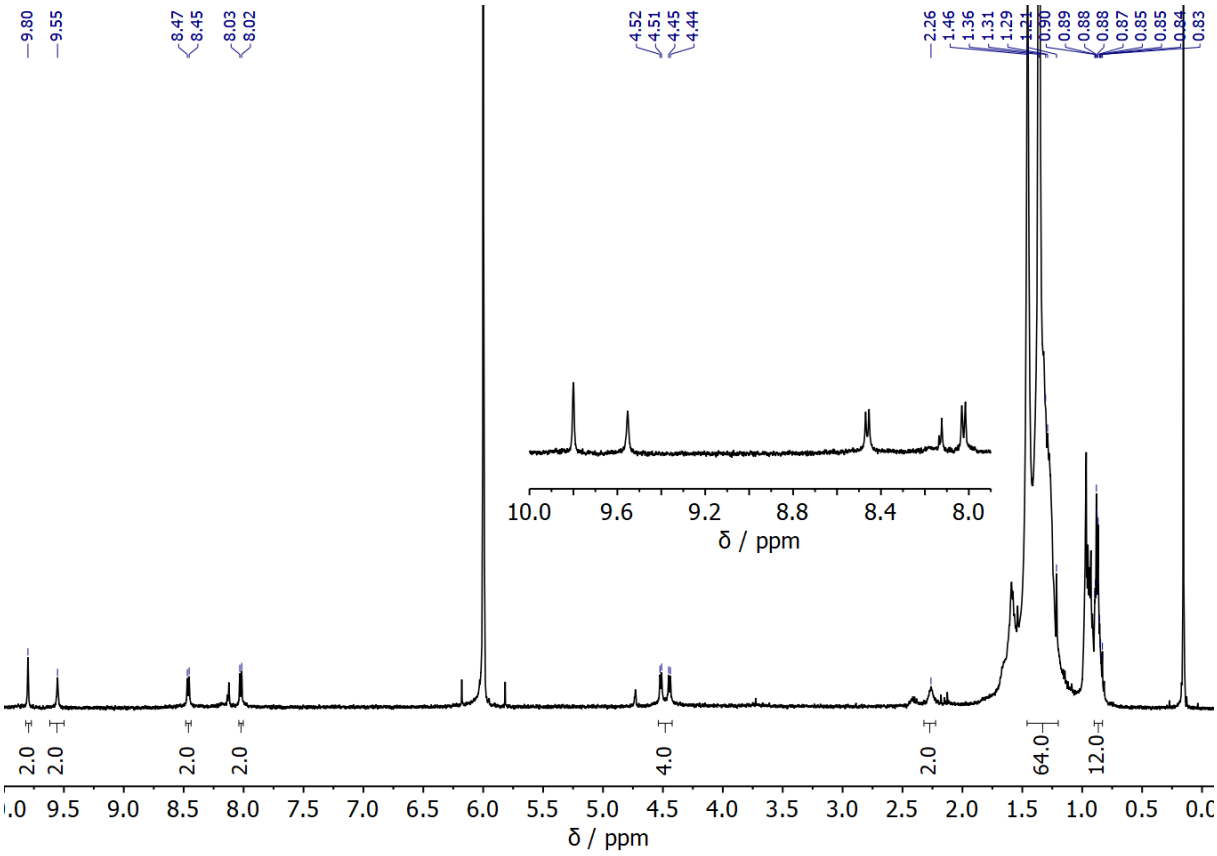

Figure S122. ^{1}H NMR (500 MHz, 393 K, $C_2D_2Cl_4$) spectrum of **1,6-CF$_3$**

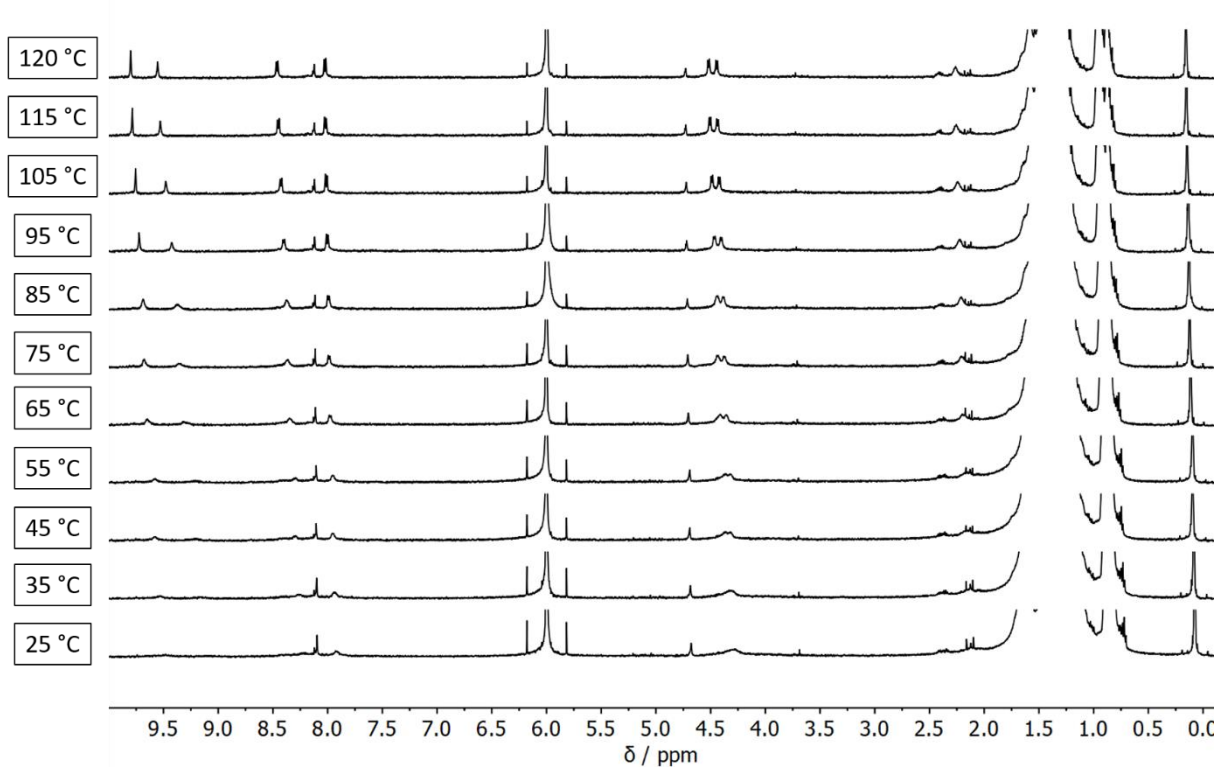

Figure S123. VT ^{1}H NMR (500 MHz, $C_2D_2Cl_4$) spectrum of **1,6-CF$_3$**

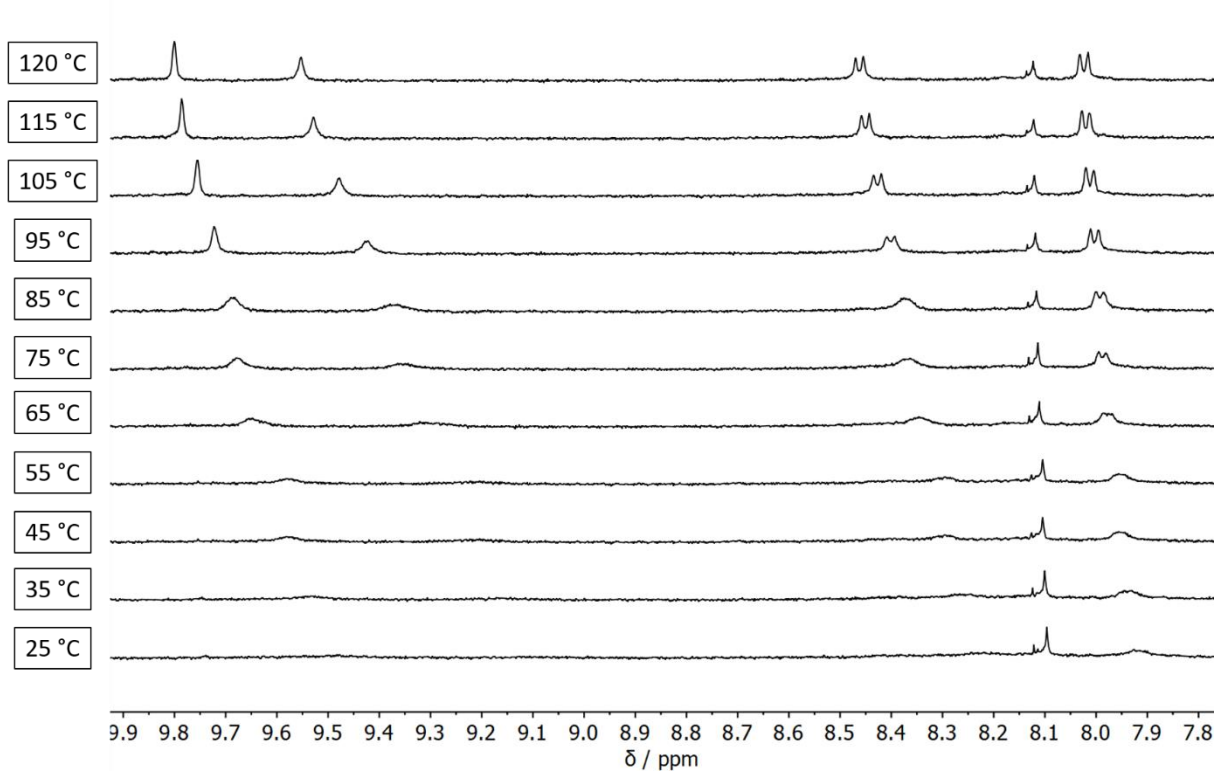

Figure S124. Zoom in the aromatic region of the VT ^{1}H NMR (500 MHz, $C_2D_2Cl_4$) spectrum of **1,6-CF_3** exhibiting a temperature dependence of its self-association through strong π-π interactions

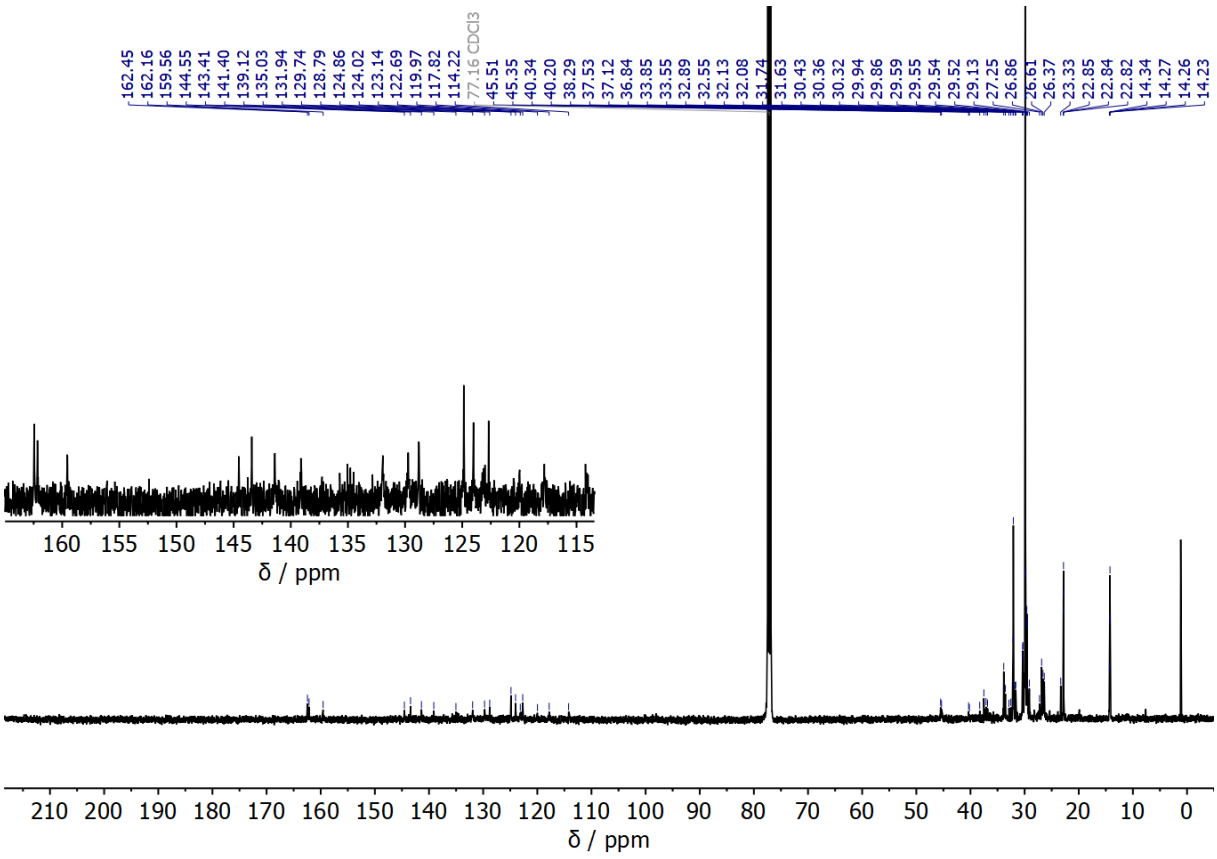

Figure S125. ^{13}C NMR (125 MHz, $CDCl_3$) spectrum of **1,6-CF_3**

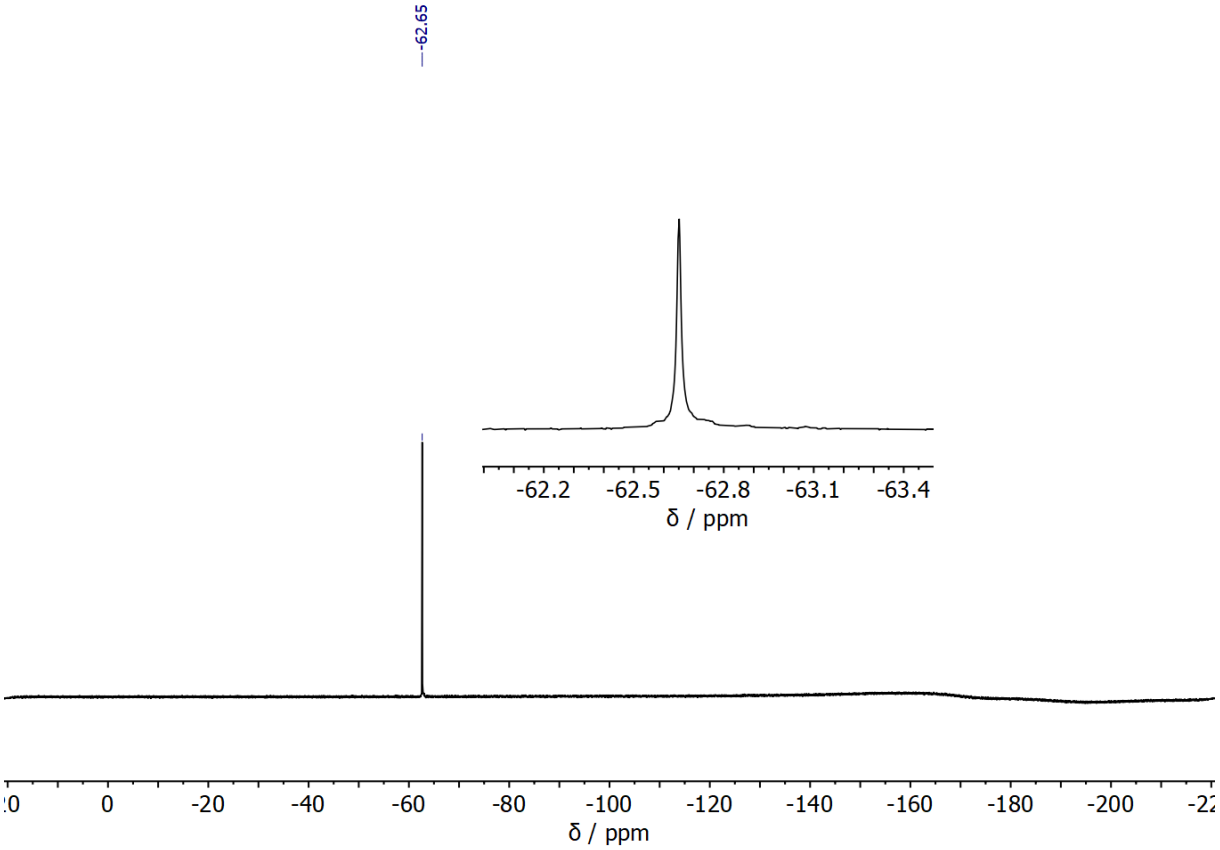

Figure S126. ^{19}F NMR (470 MHz, $CDCl_3$) spectrum of **1,6-CF$_3$**

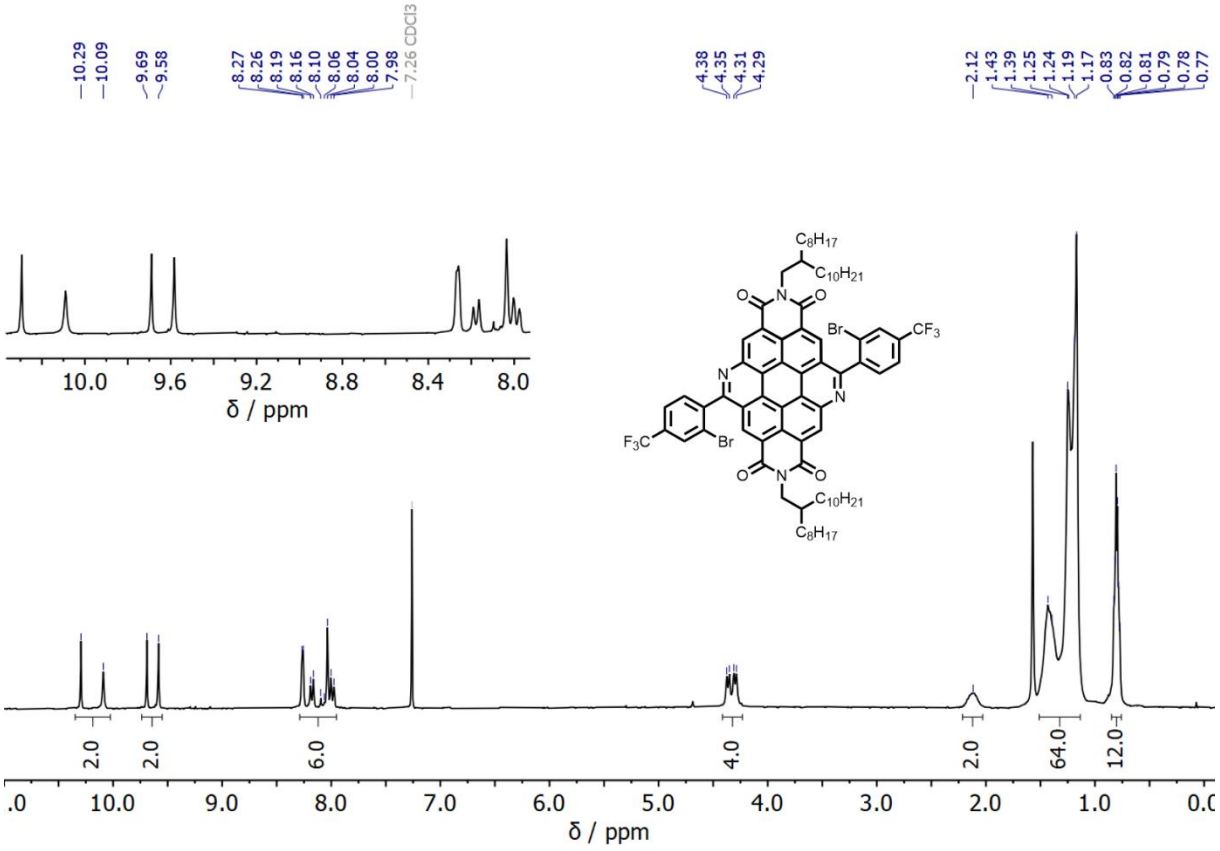

Figure S127. ^{1}H NMR (300 MHz, $CDCl_3$) spectrum of **1,7-BACD-CF$_3$**

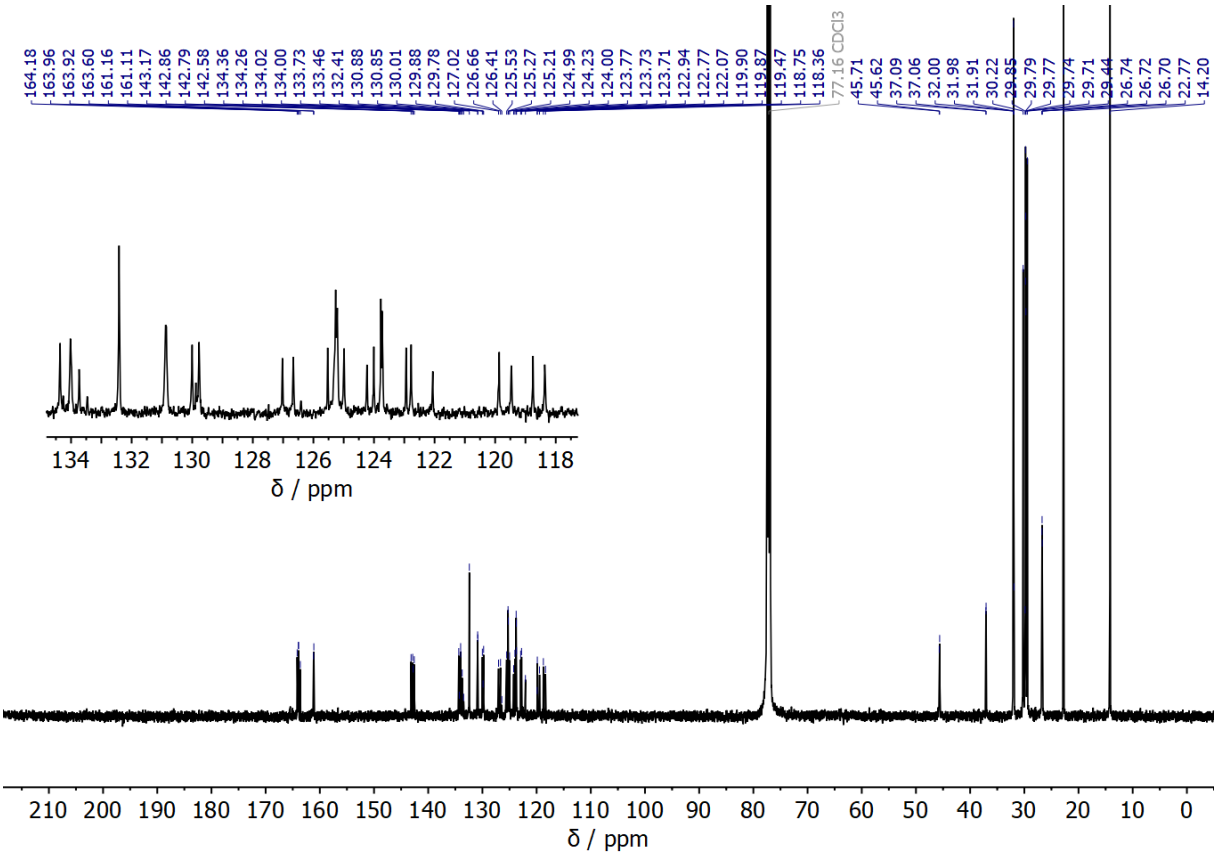

Figure S128. ^{13}C NMR (125 MHz, $CDCl_3$) spectrum of **1,7-BACD-CF₃**

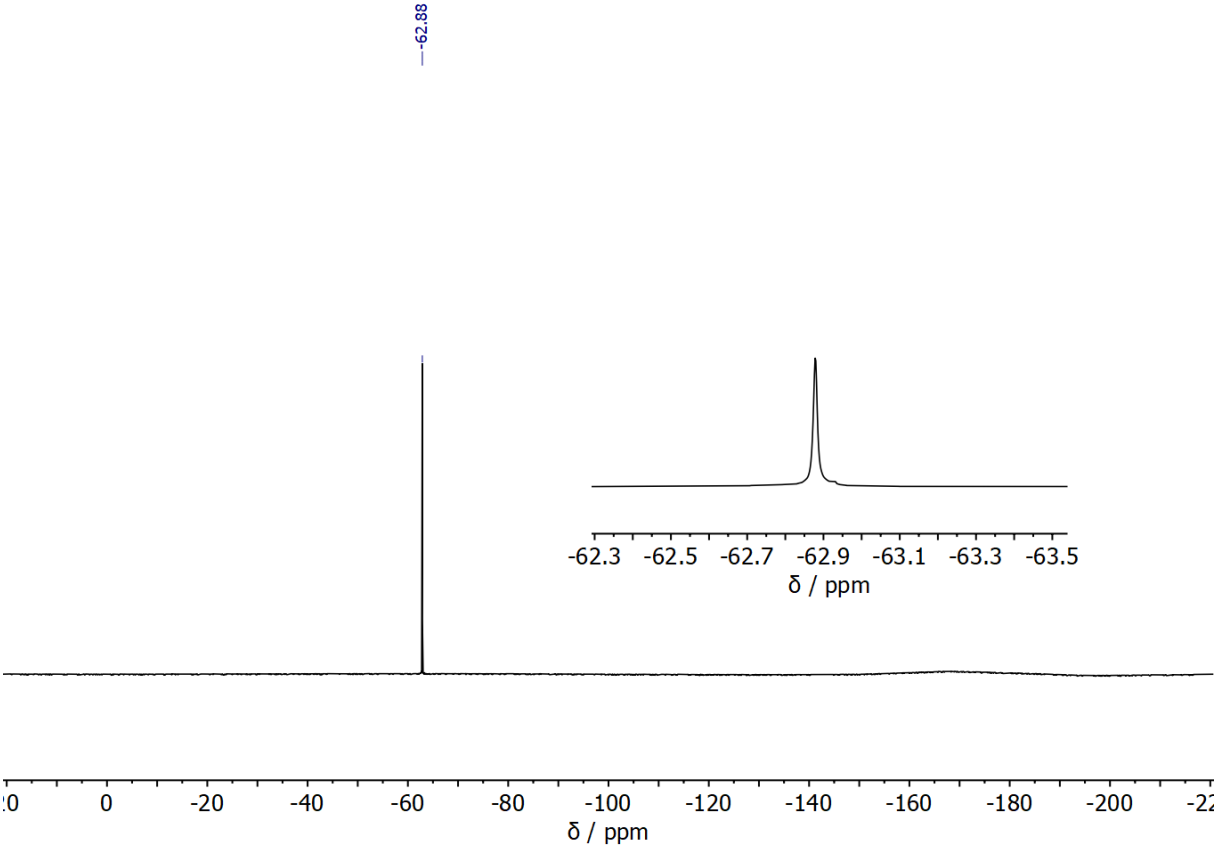

Figure S129. ^{19}F NMR (470 MHz, 328 K, $CDCl_3$) spectrum of **1,7-BACD-CF₃**

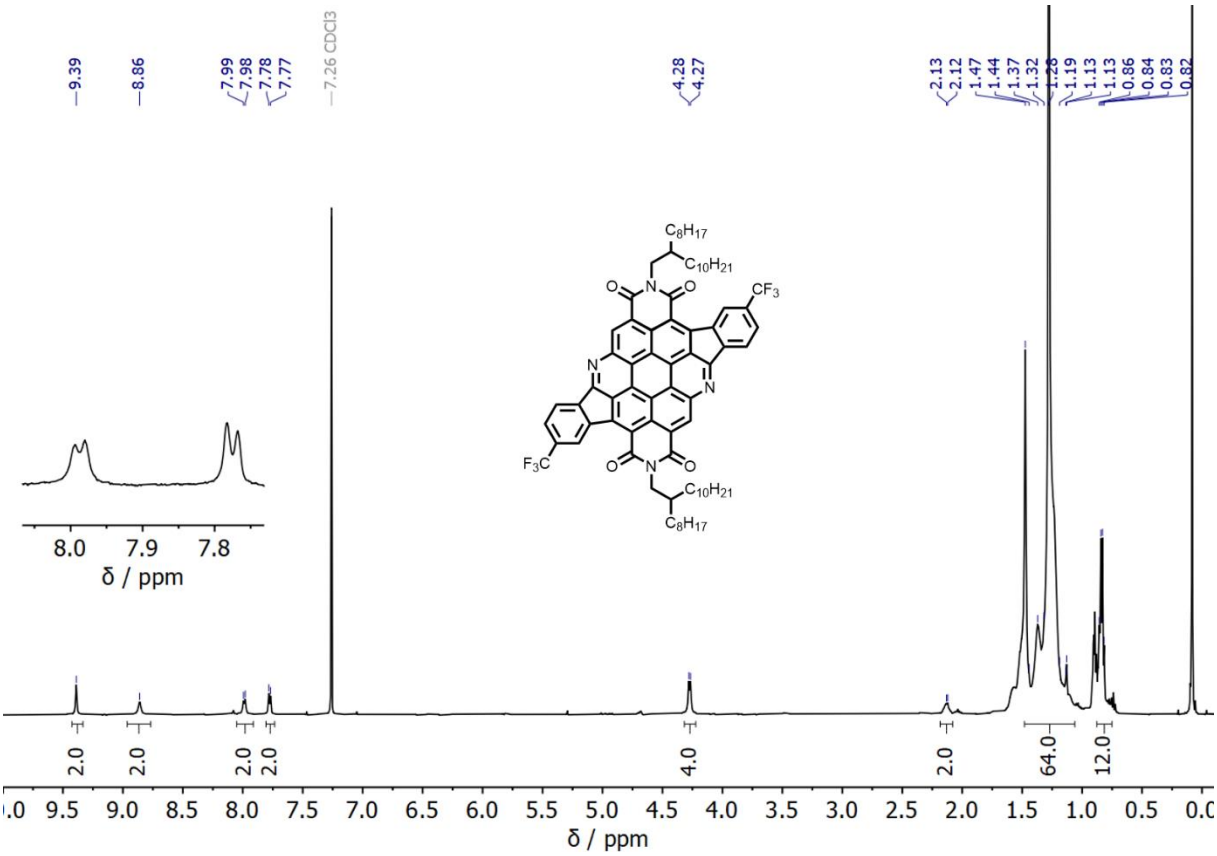

Figure S130. ^{1}H NMR (500 MHz, 328 K, $CDCl_3$) spectrum of **1,7-CF$_3$**

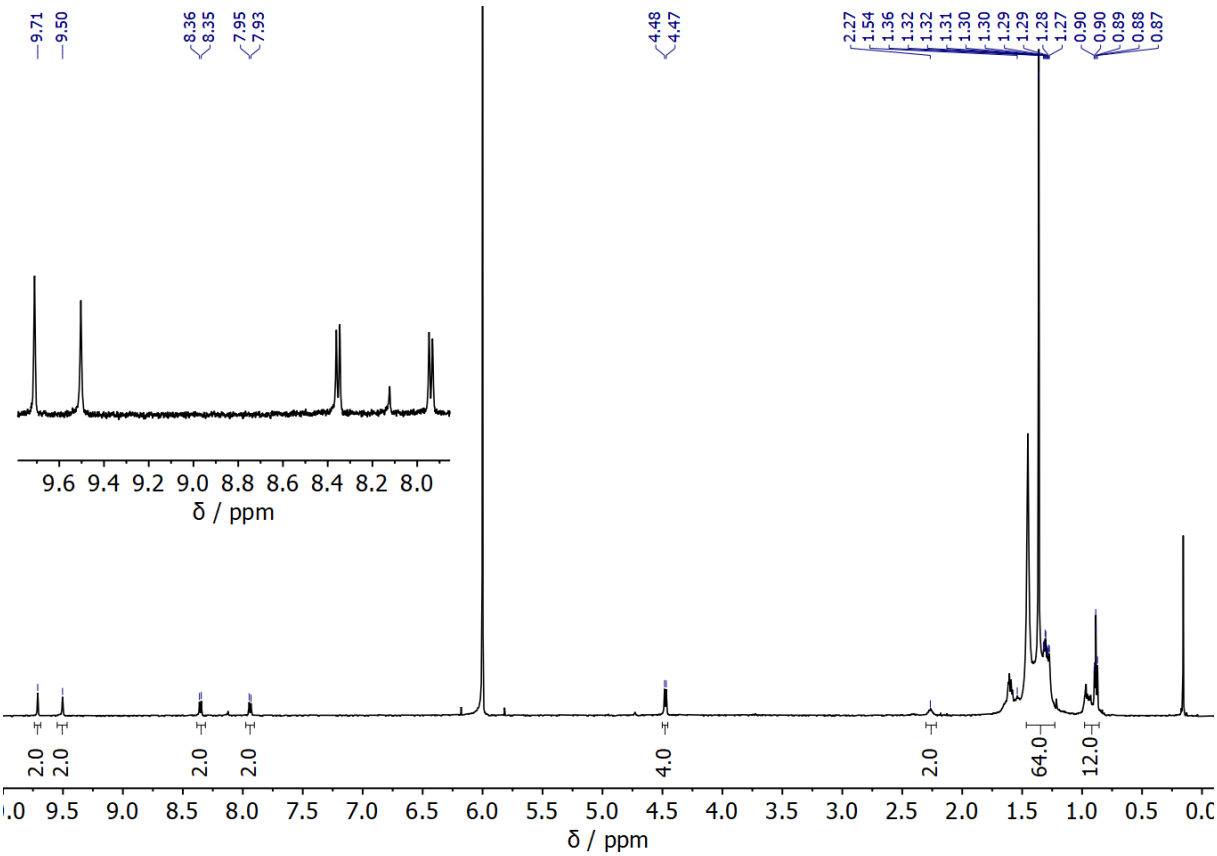

Figure S131. ^{1}H NMR (500 MHz, 393 K, $C_2D_2Cl_4$) spectrum of **1,7-CF$_3$**

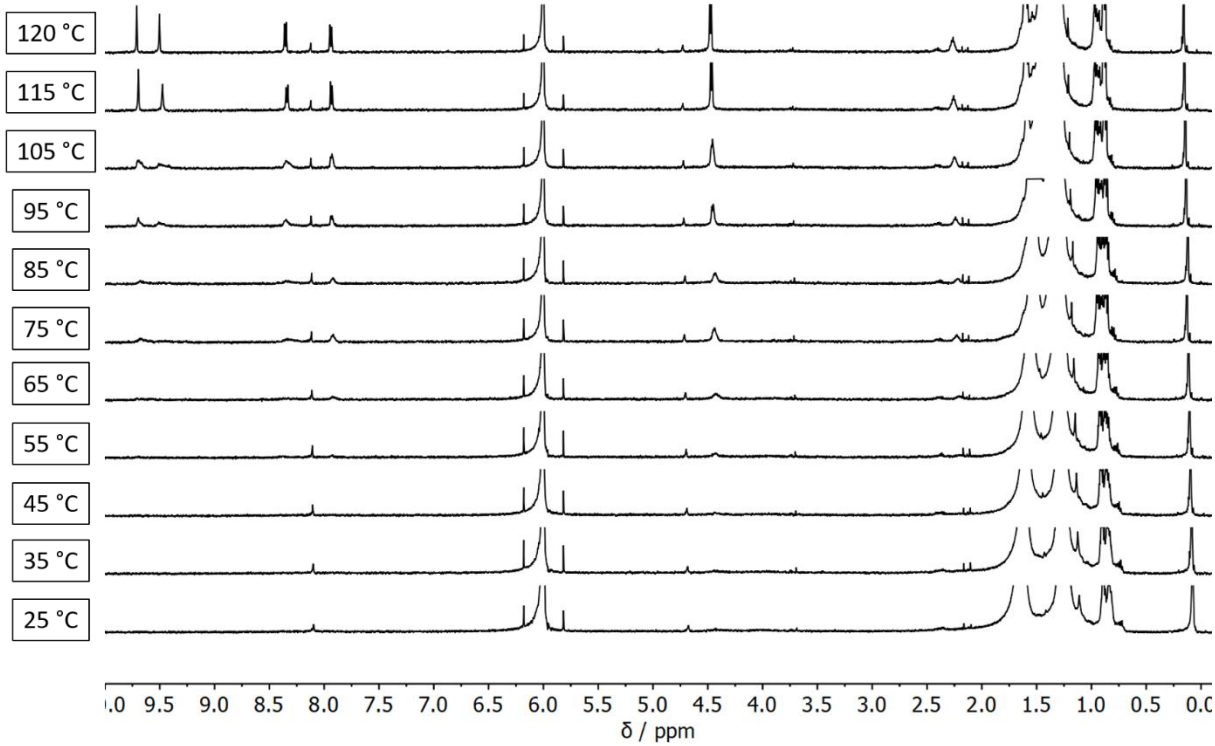

Figure S132. VT ^{1}H NMR (500 MHz, $C_2D_2Cl_4$) spectrum of **1,7-CF$_3$**. Note that compound **1,7-CF$_3$** was not soluble in $C_2D_2Cl_4$ at room temperature and dissolved during the VT NMR experiment.

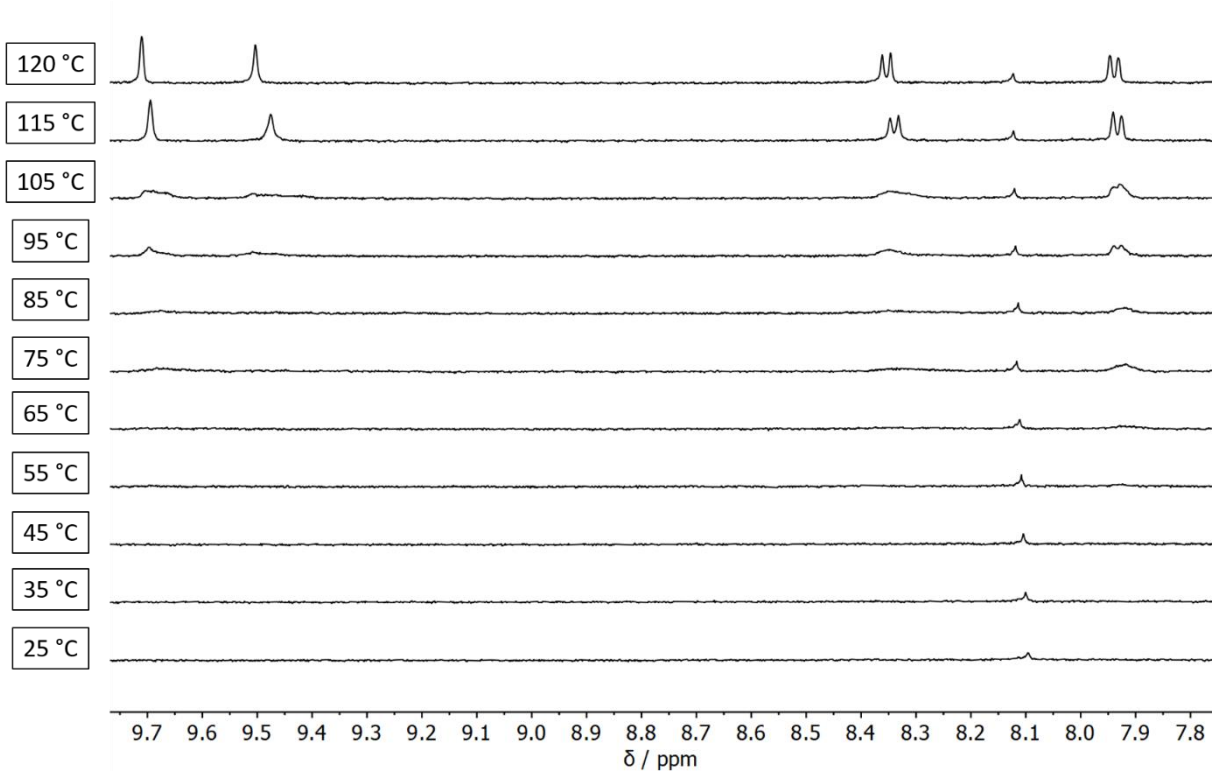

Figure S133. Zoom in the aromatic region of the VT ^{1}H NMR (500 MHz, $C_2D_2Cl_4$) spectrum of **1,7-CF$_3$** exhibiting a temperature dependence of its self-association through strong π-π interactions. Note that compound **1,7-CF$_3$** was not soluble in $C_2D_2Cl_4$ at room temperature and dissolved during the VT NMR experiment.

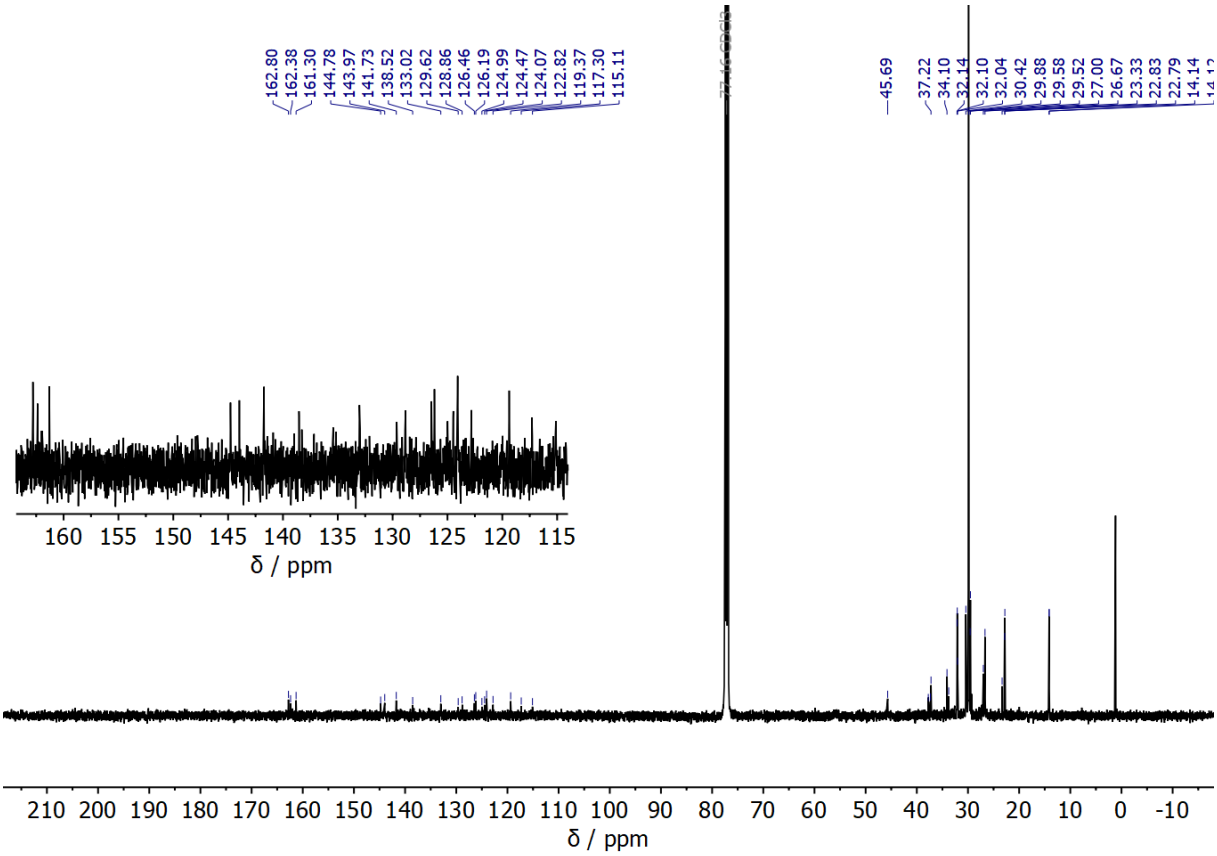

Figure S134. ^{13}C NMR (125 MHz, 328 K, $CDCl_3$) spectrum of **1,7-CF_3**

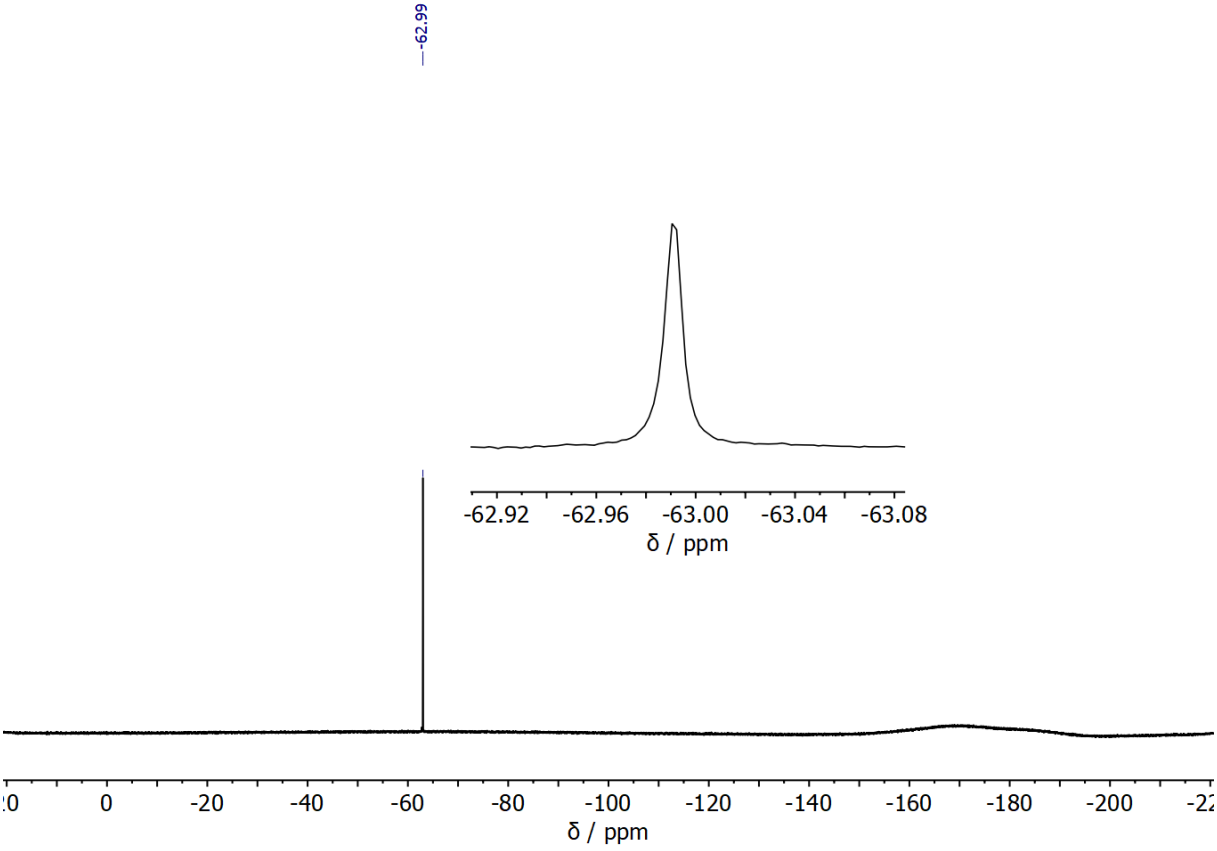

Figure S135. ^{19}F NMR (470 MHz, 328 K, $CDCl_3$) spectrum of **1,7-CF_3**

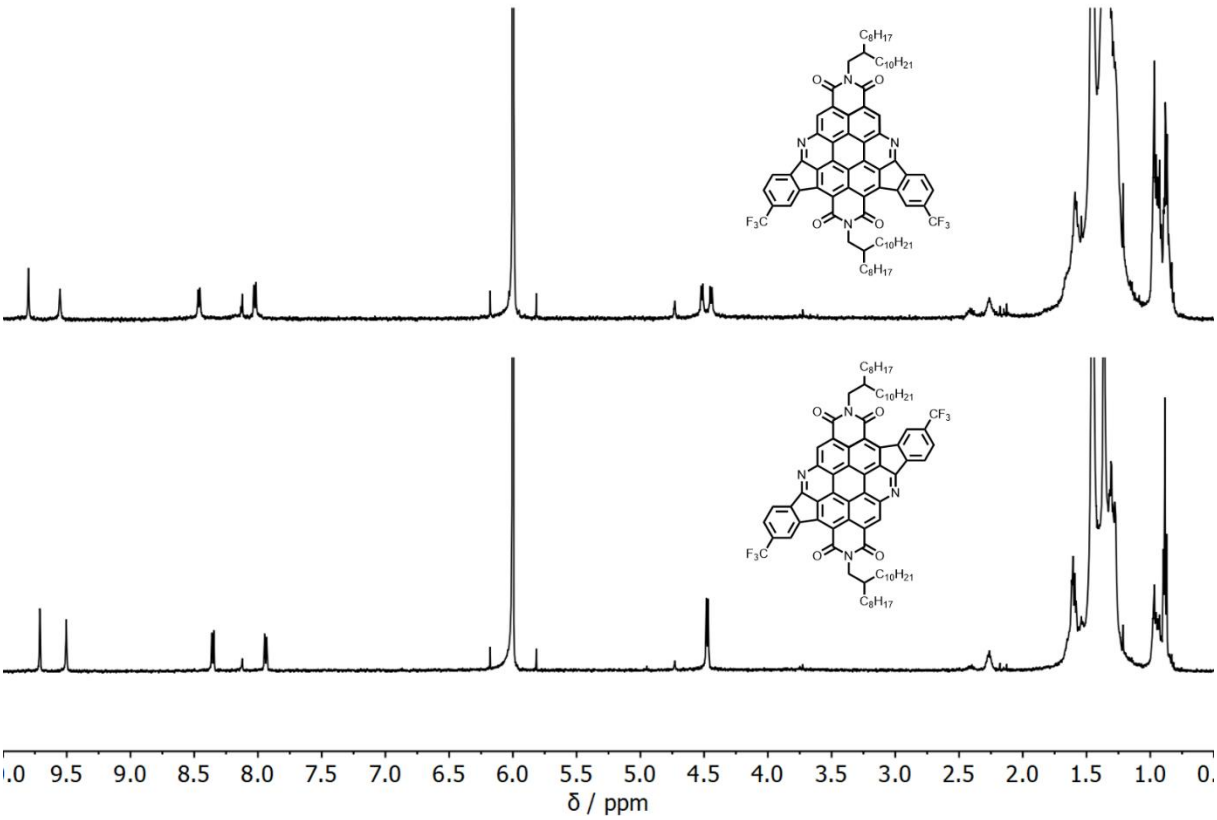

Figure S136. ^{1}H NMR (500 MHz, 393 K, $C_2D_2Cl_4$) spectrum of **1,6-CF$_3$** (top) and **1,7-CF$_3$** (bottom) showing their regiopurity and the differences of their proton resonances

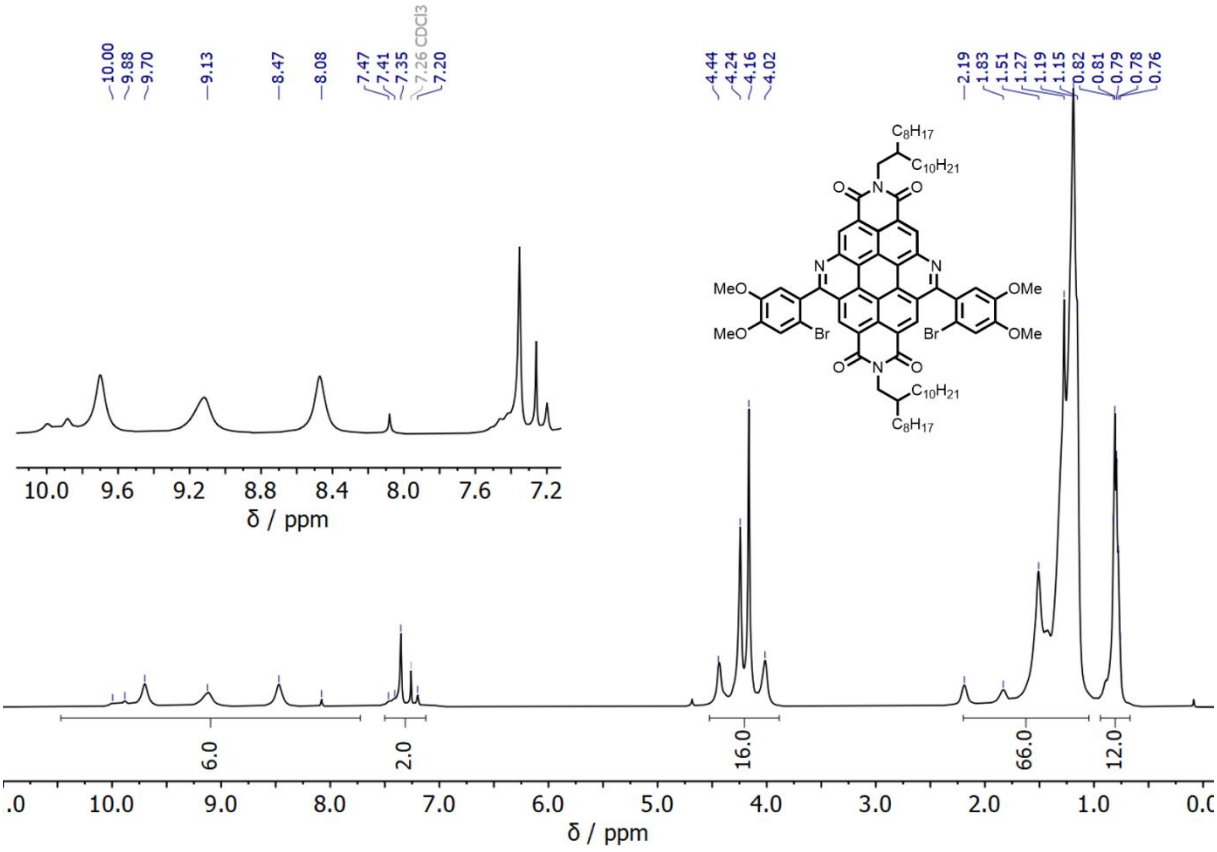

Figure S137. ^{1}H NMR (500 MHz, 328 K, $CDCl_3$) spectrum of **1,6-BACD-OMe**

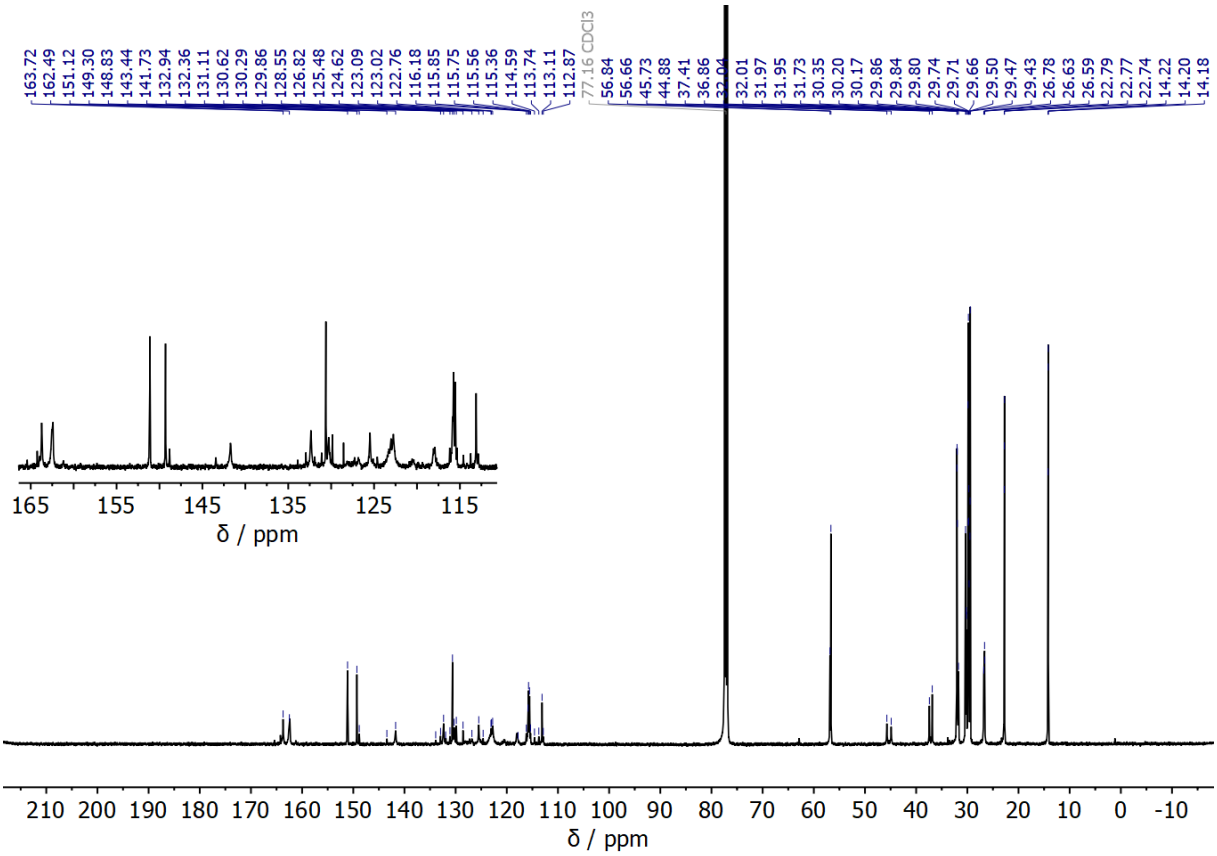

Figure S138. ^{13}C NMR (125 MHz, $CDCl_3$) spectrum of **1,6-BACD-OMe**

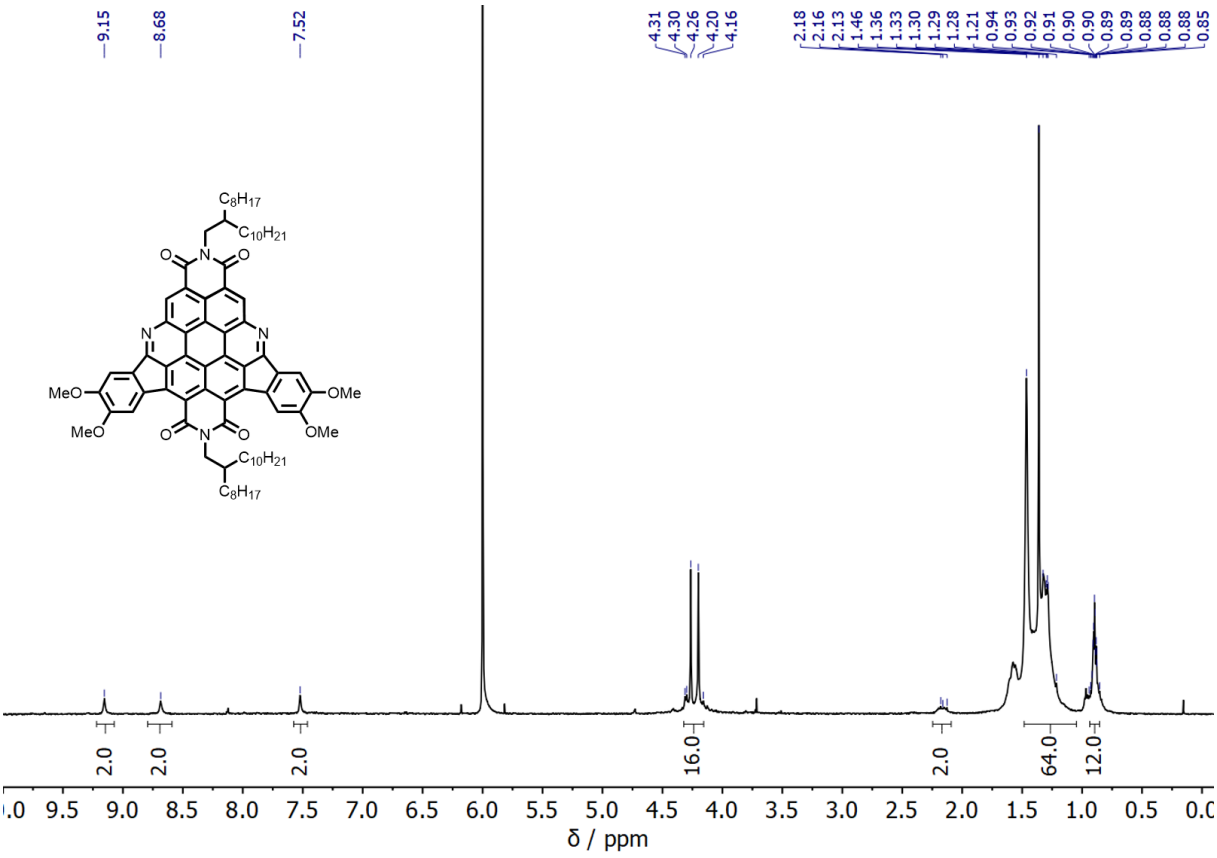

Figure S139. ^{1}H NMR (500 MHz, 393 K, $C_2D_2Cl_4$) spectrum of **1,6-OMe**

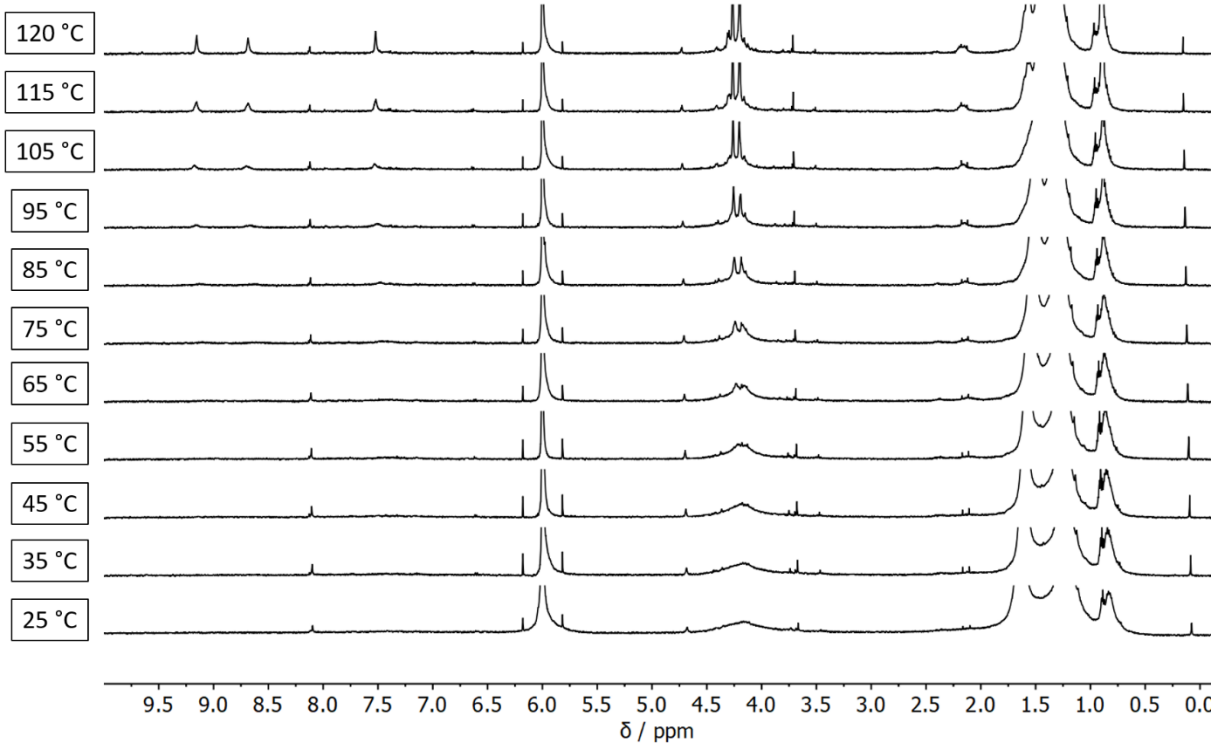

Figure S140. VT ^{1}H NMR (500 MHz, $C_2D_2Cl_4$) spectrum of **1,6-OMe**

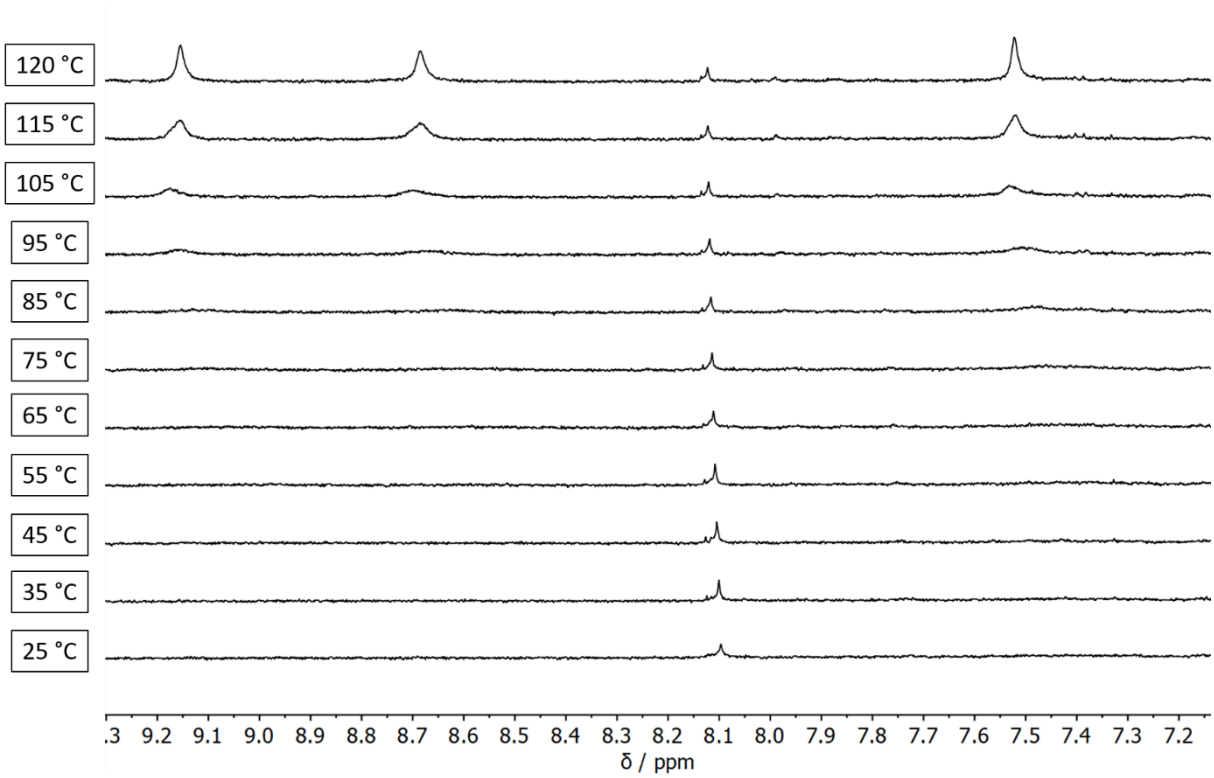

Figure S141. Zoom in the aromatic region of the VT ^{1}H NMR (500 MHz, $C_2D_2Cl_4$) spectrum of **1,6-OMe** exhibiting a temperature dependence of its self-association through strong π-π interactions

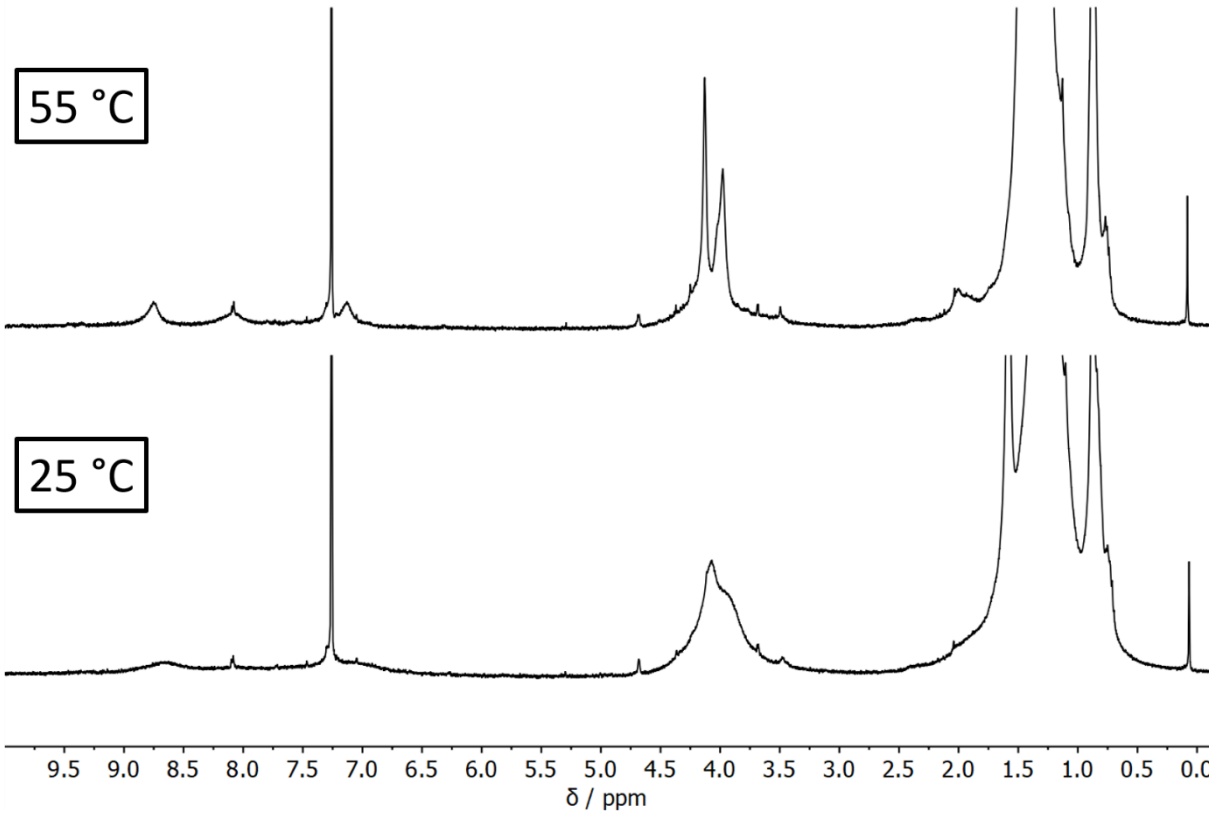

Figure S142. VT ^{1}H NMR (500 MHz, $CDCl_3$) spectrum of **1,6-OMe**

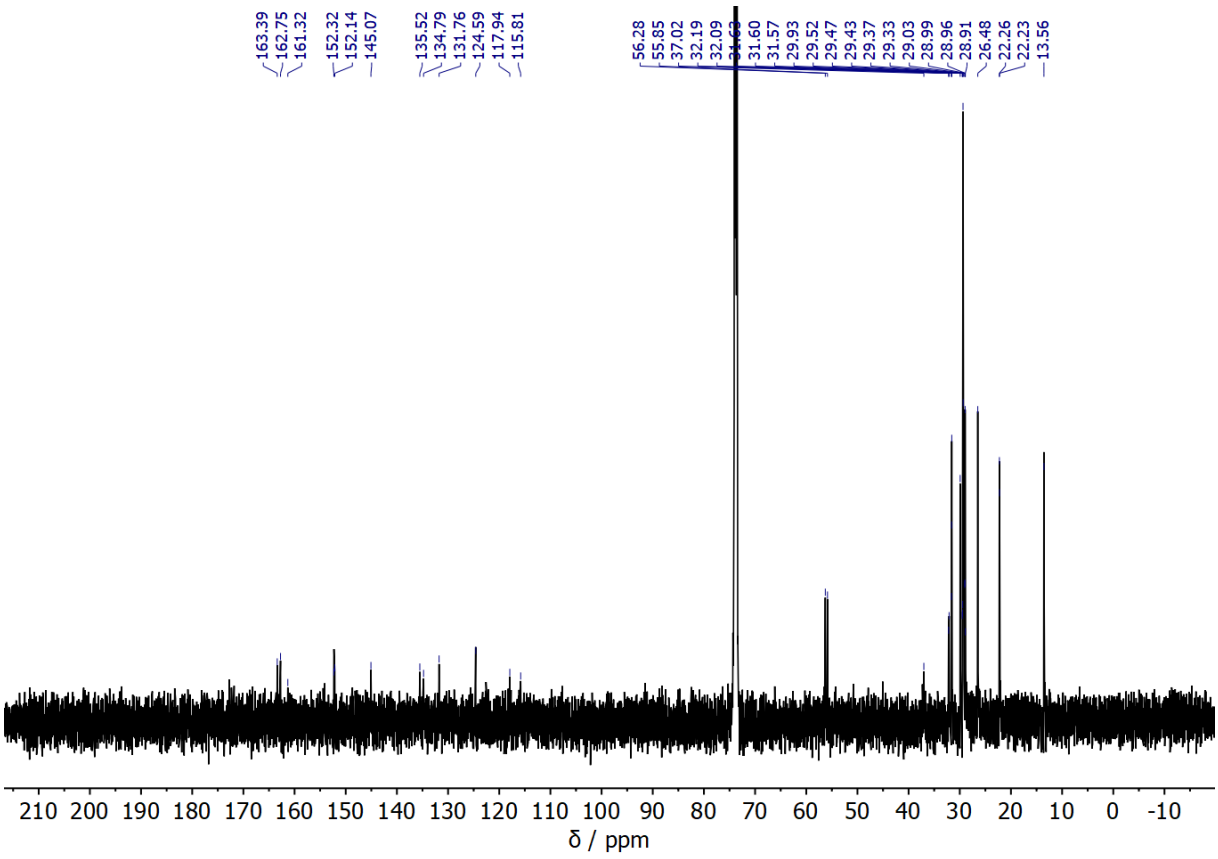

Figure S143. ^{13}C NMR (125 MHz, 393 K, $C_2D_2Cl_4$) spectrum of **1,6-OMe**

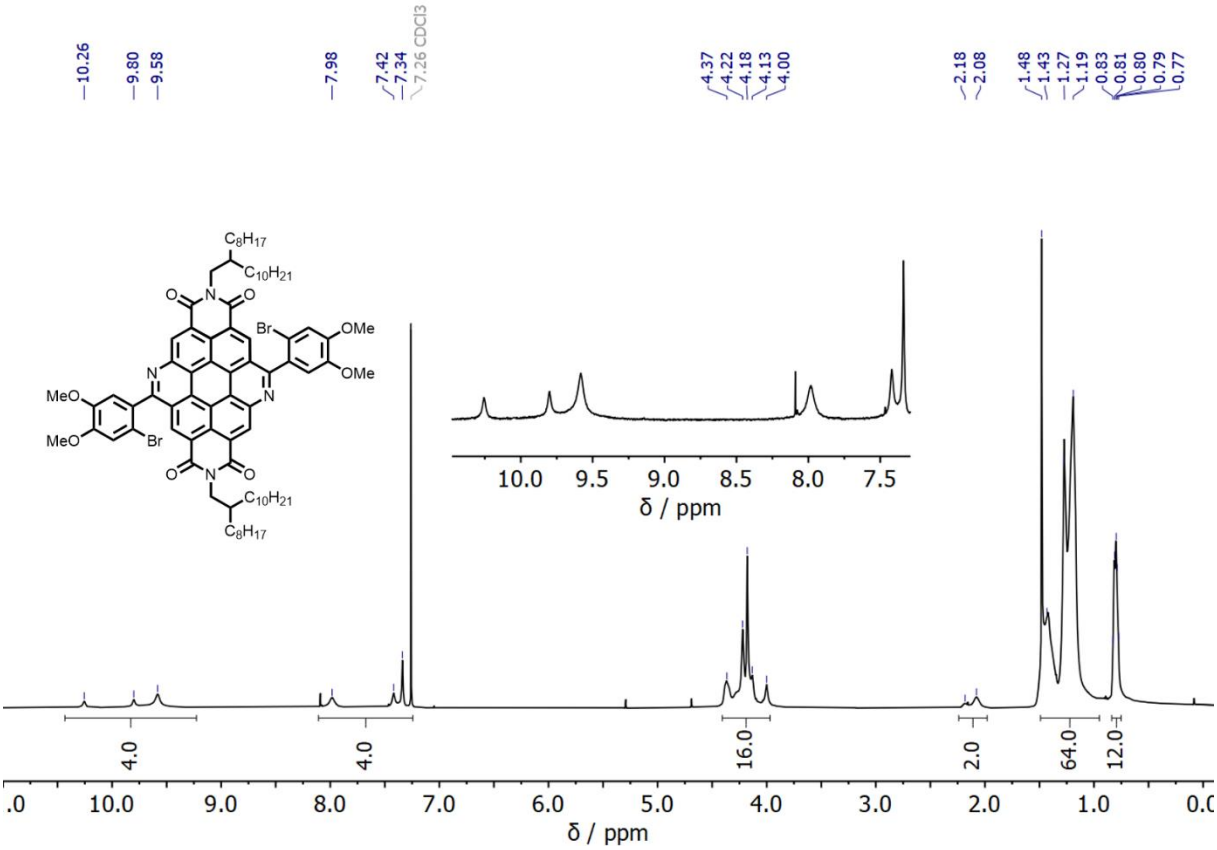

Figure S144. ^{1}H NMR (500 MHz, 328 K, $CDCl_3$) spectrum of **1,7-BACD-OMe**

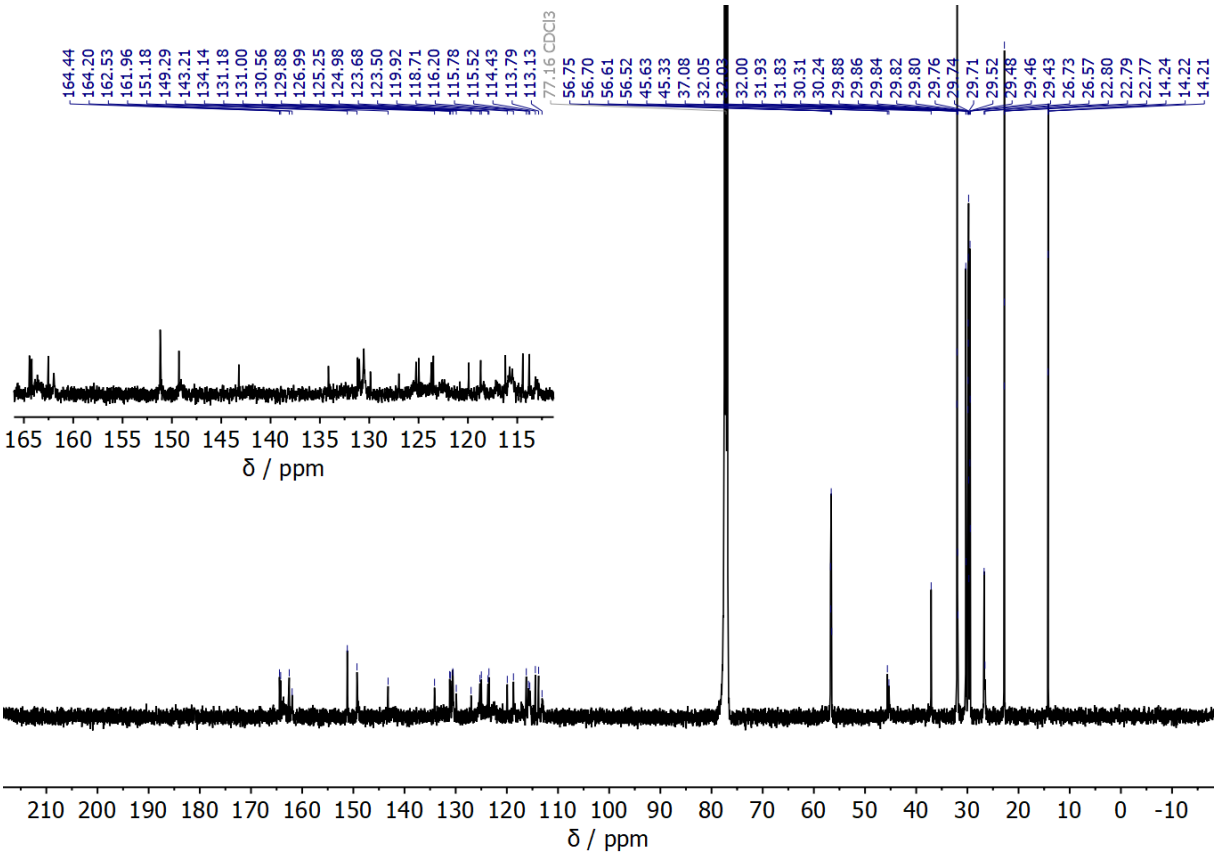

Figure S145. ^{13}C NMR (125 MHz, $CDCl_3$) spectrum of **1,7-BACD-OMe**

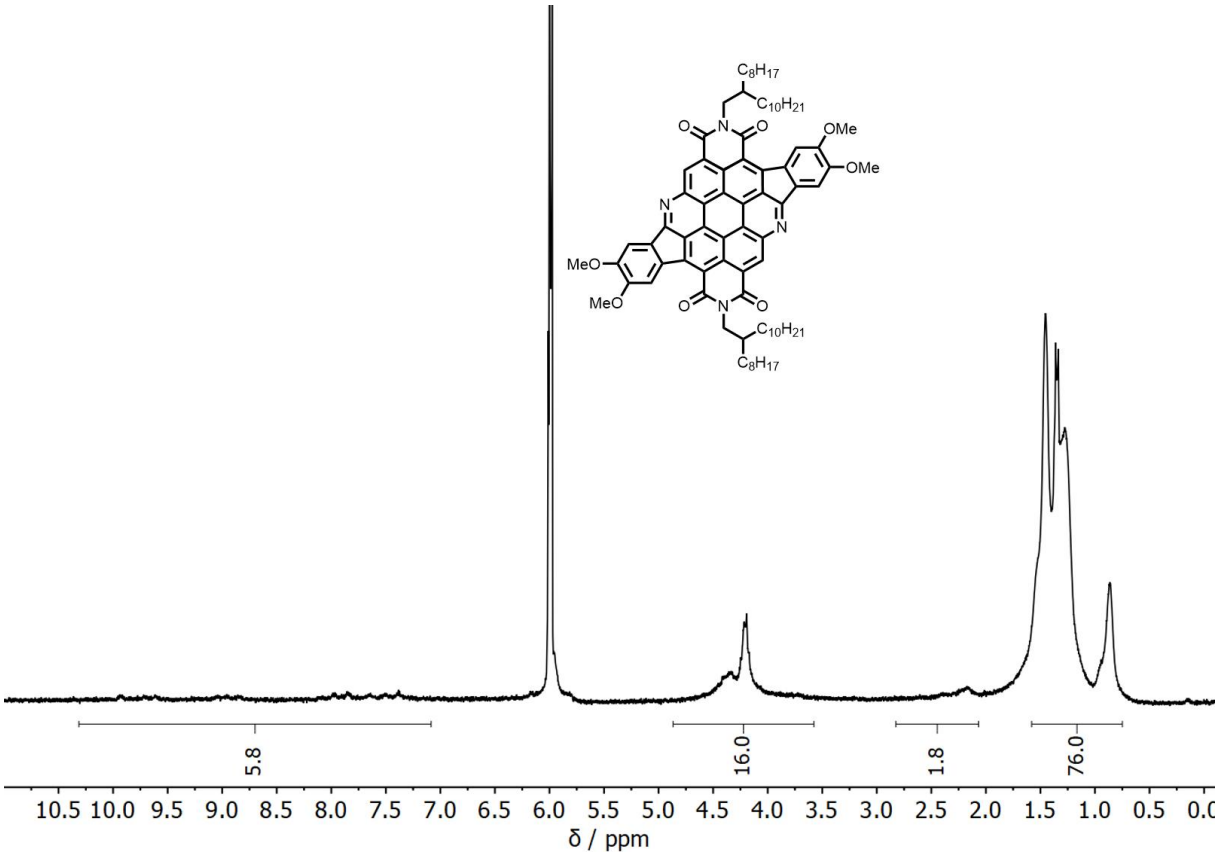

Figure S146. ^{1}H NMR (500 MHz, 393 K, $C_2D_2Cl_4$) spectrum of **1,7-OMe**

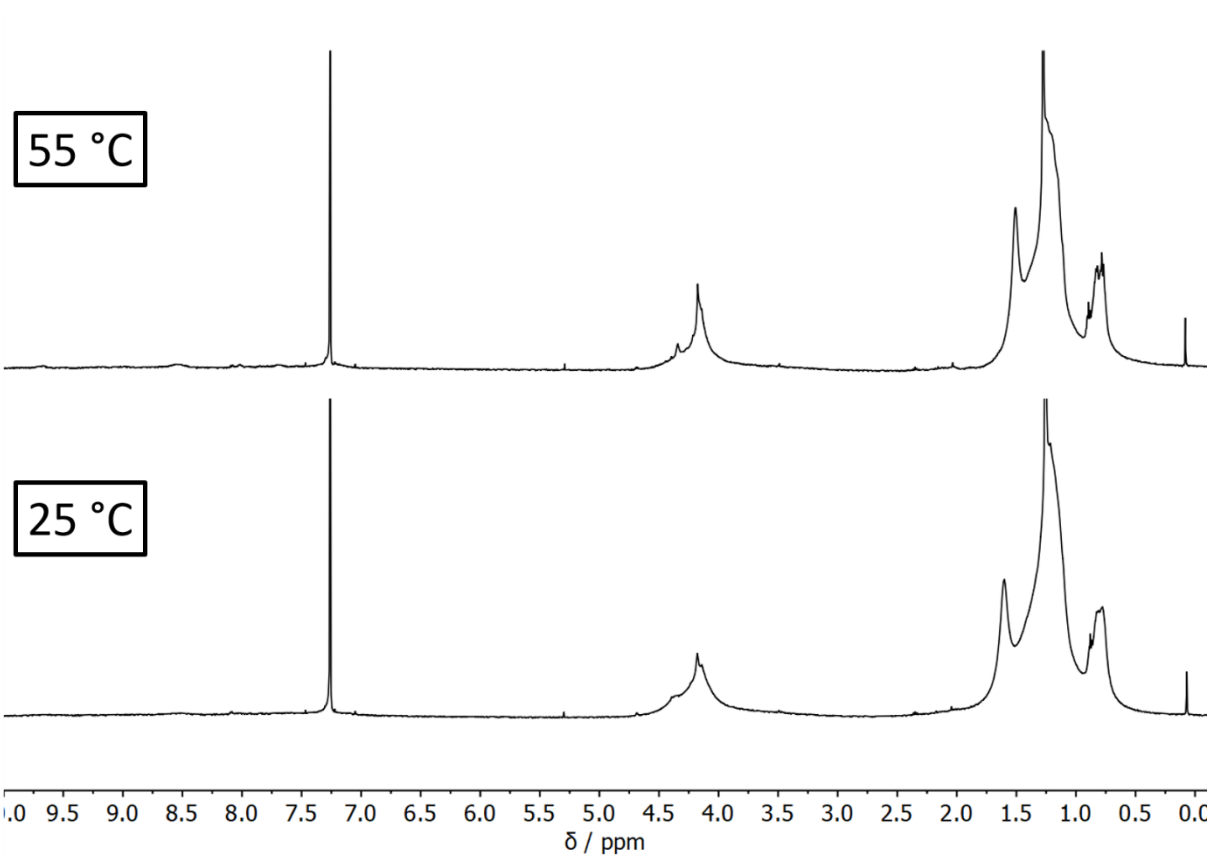

Figure S147. VT ^{1}H NMR (500 MHz, $CDCl_3$) spectrum of **1,7-OMe**

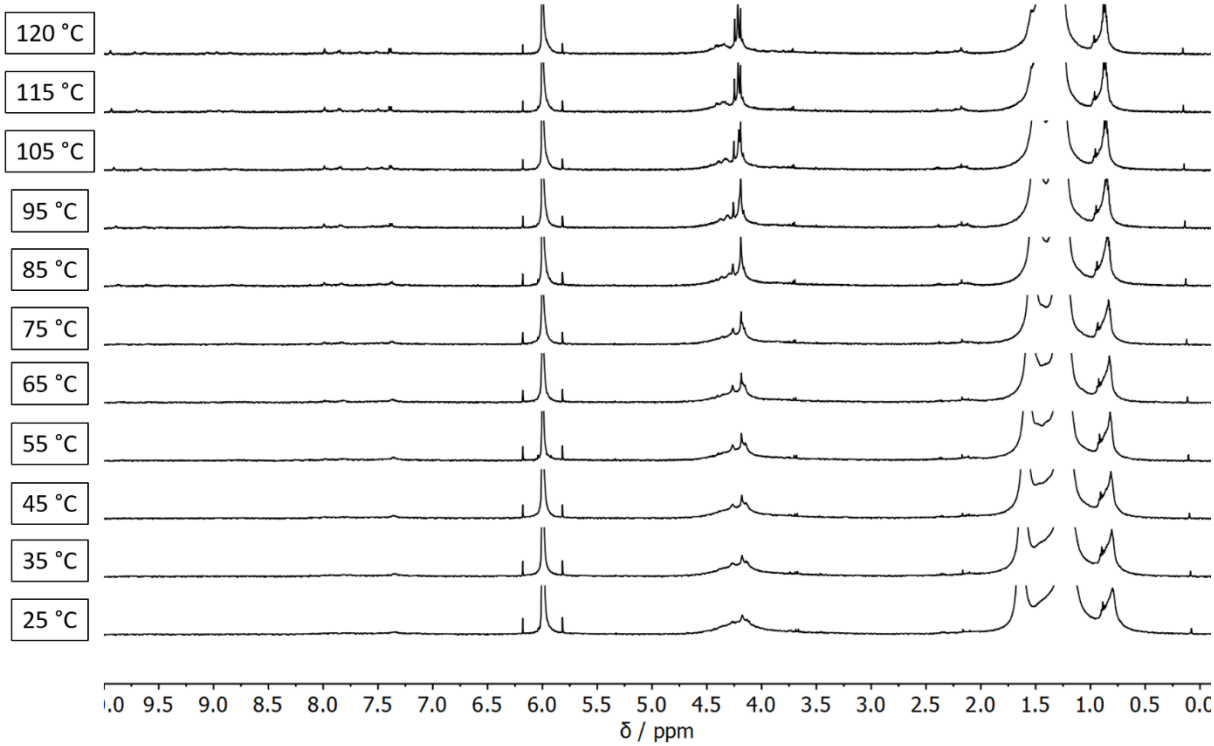

Figure S148. VT ^{1}H NMR (500 MHz, $C_2D_2Cl_4$) spectrum of **1,7-OMe**

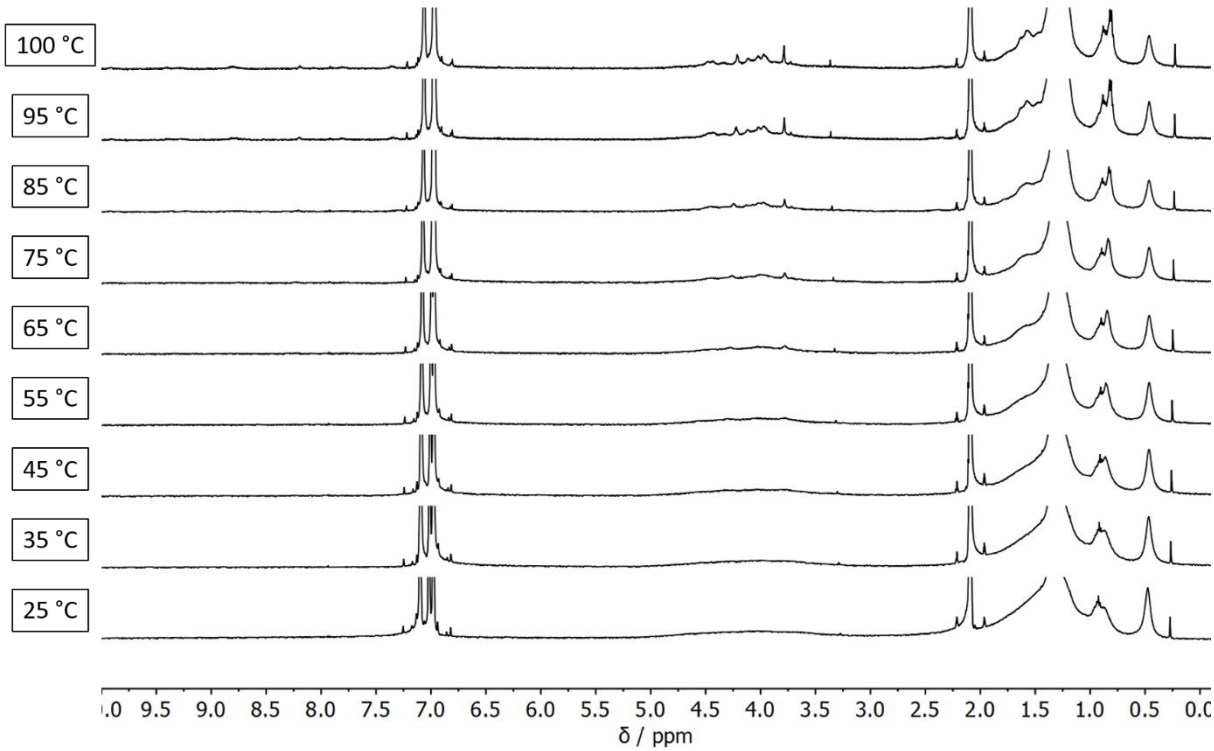

Figure S149. VT ^{1}H NMR (500 MHz, Toluene-d_8) spectrum of **1,7-OMe**

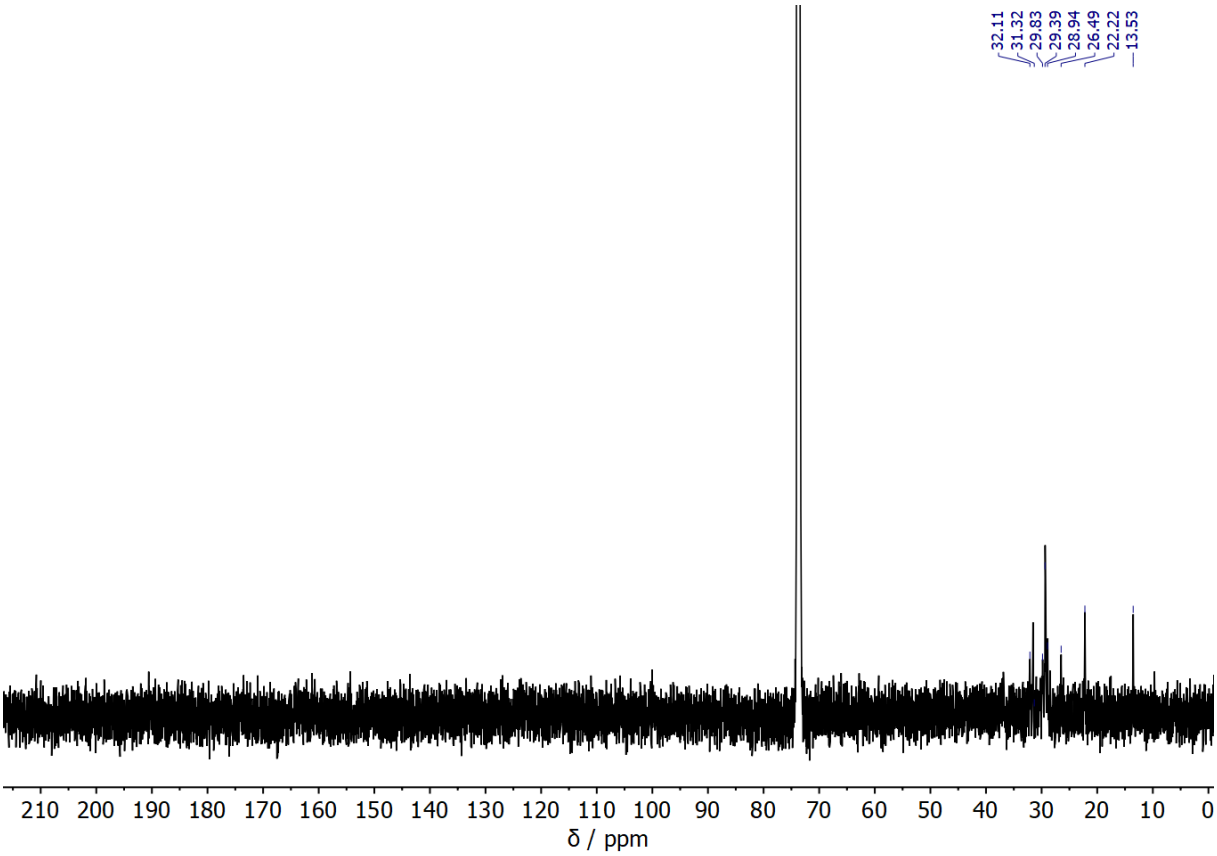

Figure S150. ^{13}C NMR (125 MHz, 393 K, $C_2D_2Cl_4$) spectrum of **1,7-OMe**

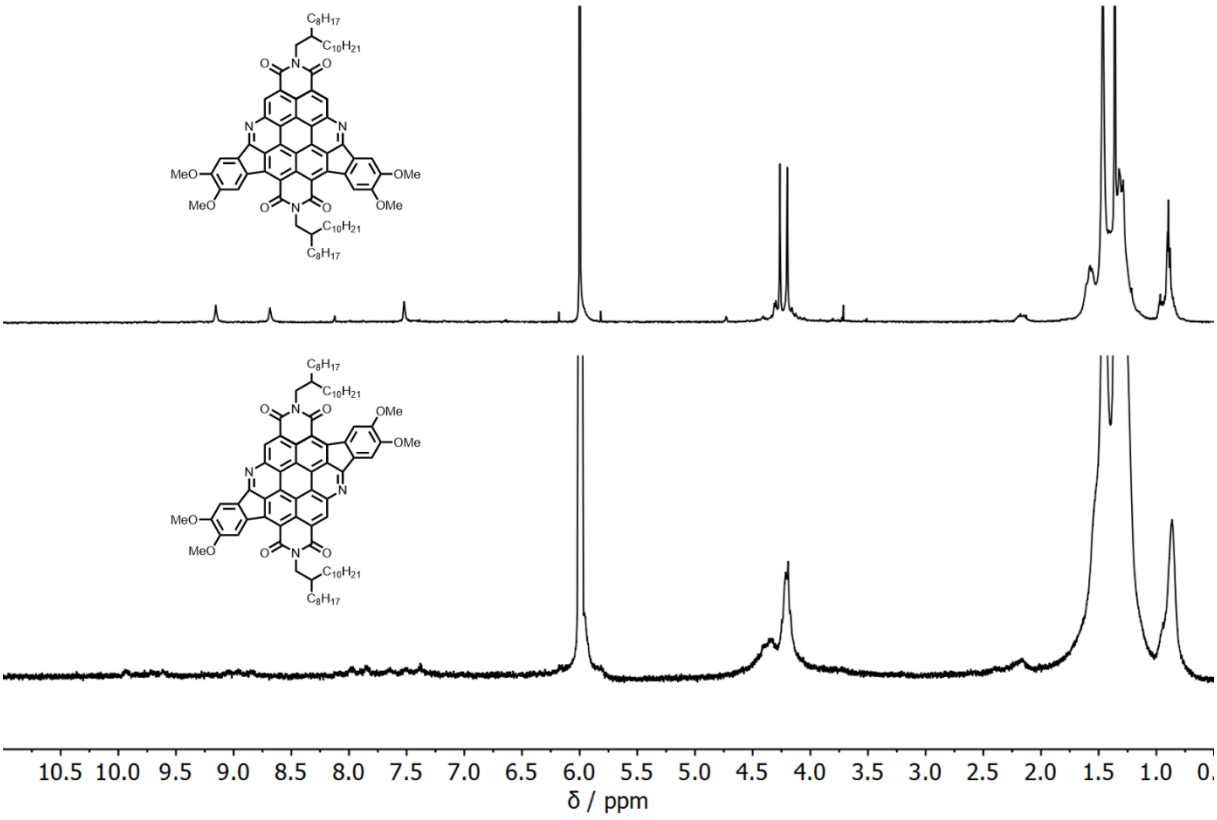

Figure S151. ^{1}H NMR (500 MHz, 393 K, $C_2D_2Cl_4$) spectrum of **1,6-OMe** (top) and **1,7-OMe** (bottom) showing the differences of their proton resonances

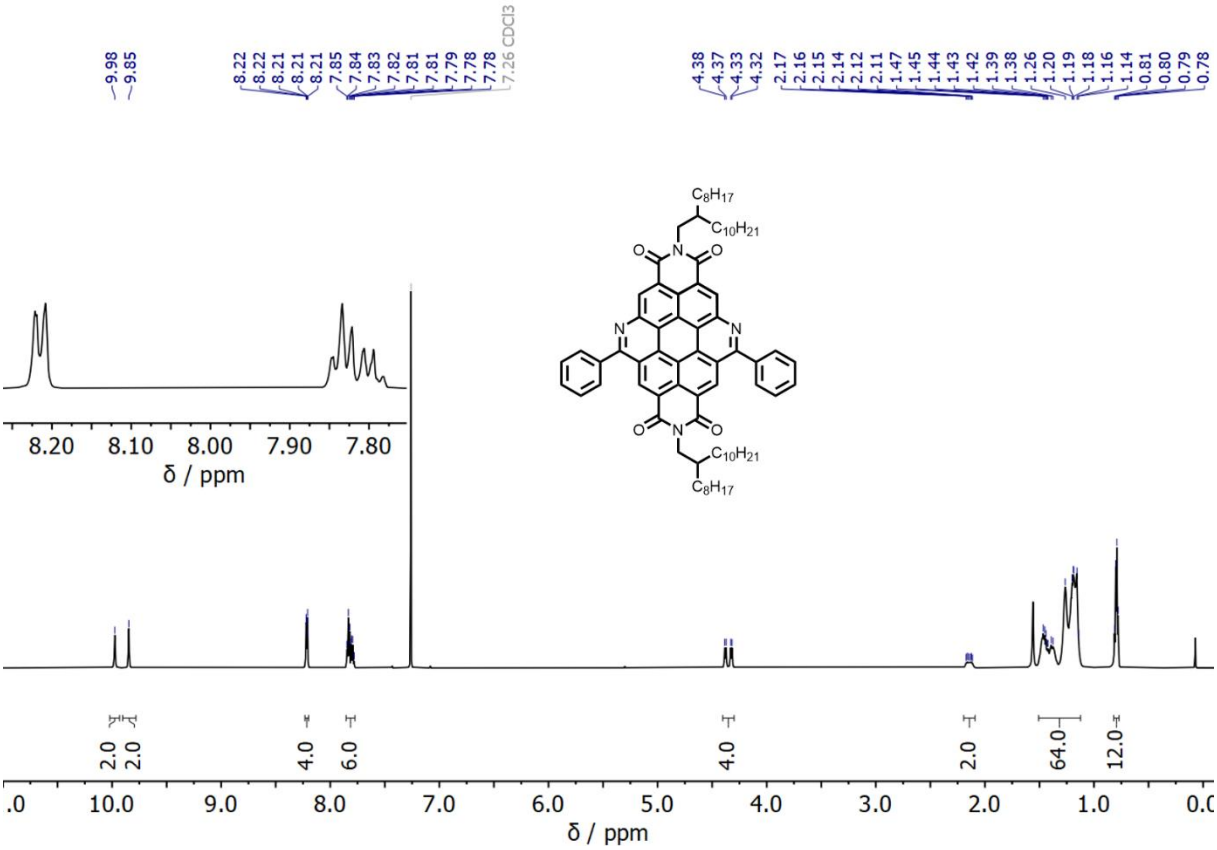

Figure S152. ^{1}H NMR (600 MHz, $CDCl_3$) spectrum of **C-1,6**

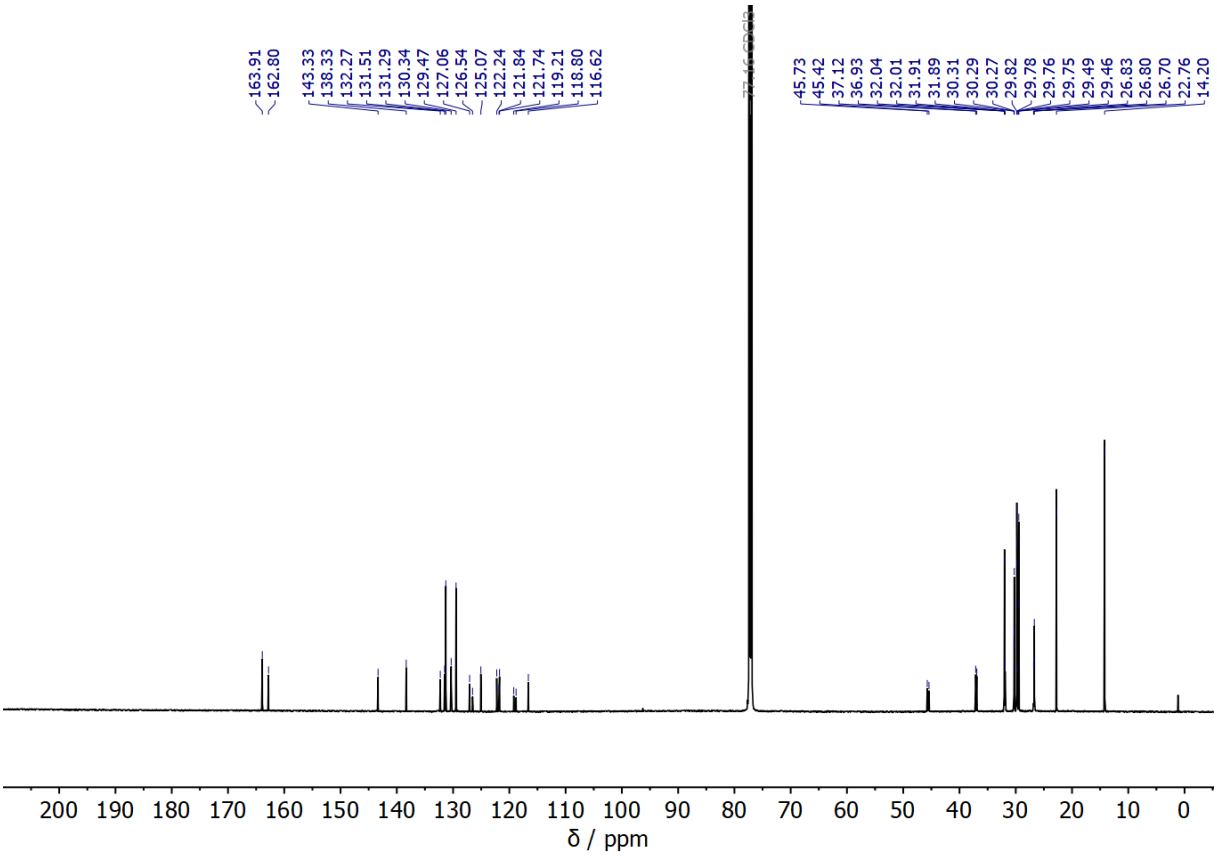

Figure S153. ^{13}C NMR (150 MHz, $CDCl_3$) spectrum of **C-1,6**

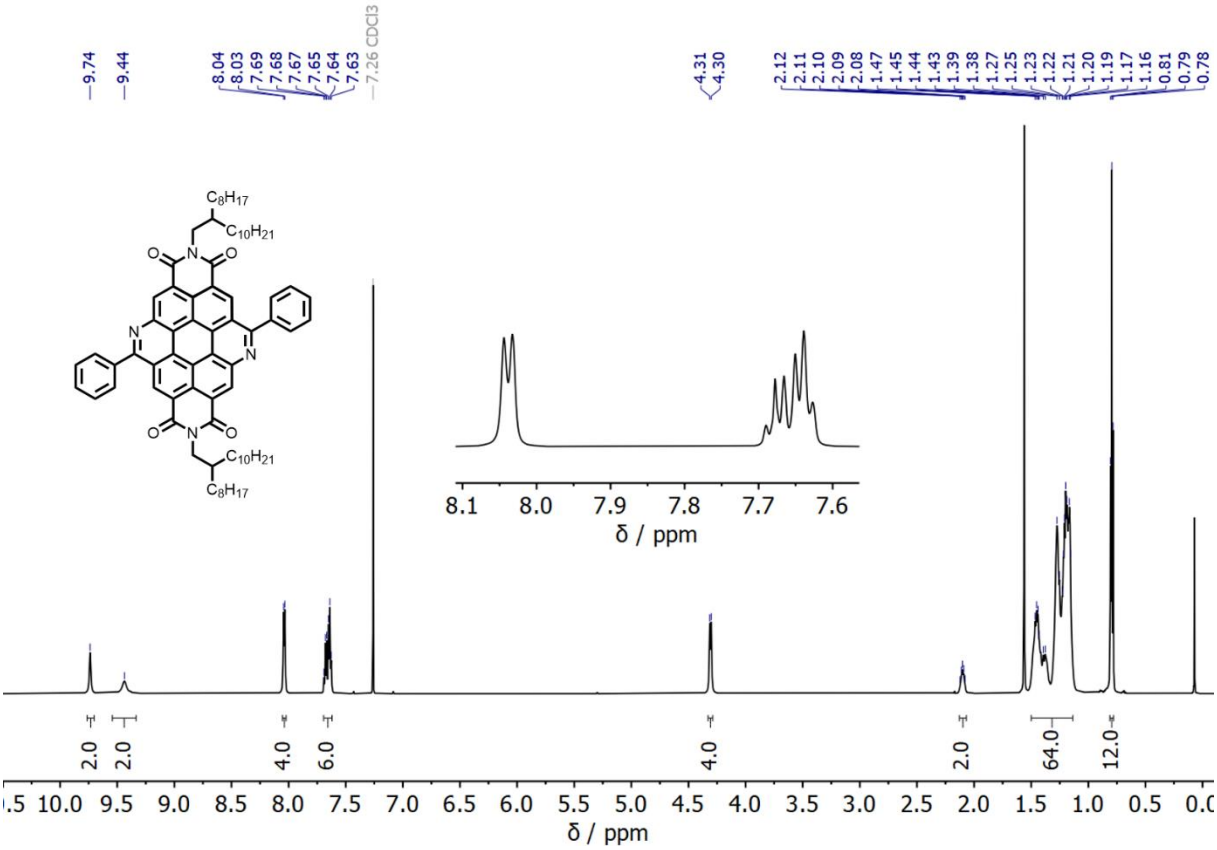

Figure S154. ^{1}H NMR (600 MHz, $CDCl_3$) spectrum of **C-1,7**

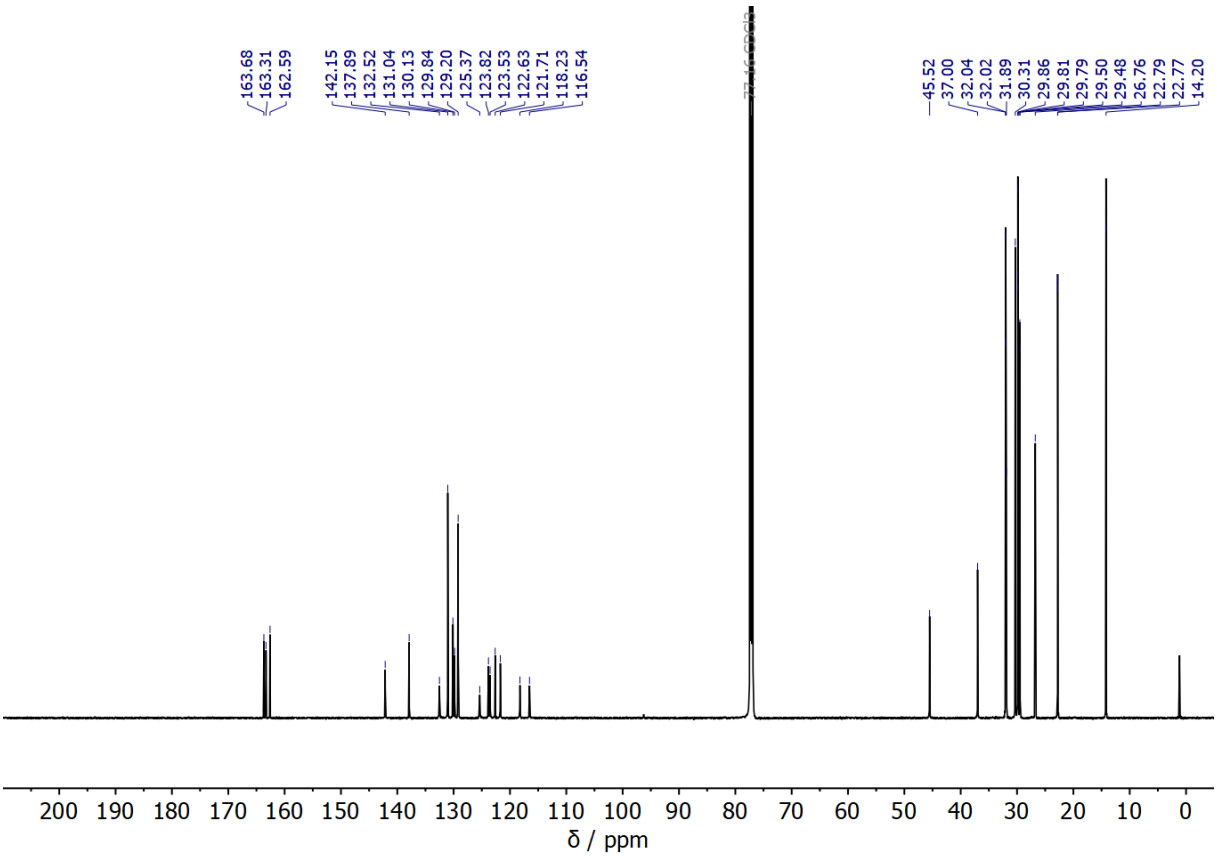

Figure S155. ^{13}C NMR (150 MHz, $CDCl_3$) spectrum of **C-1,7**

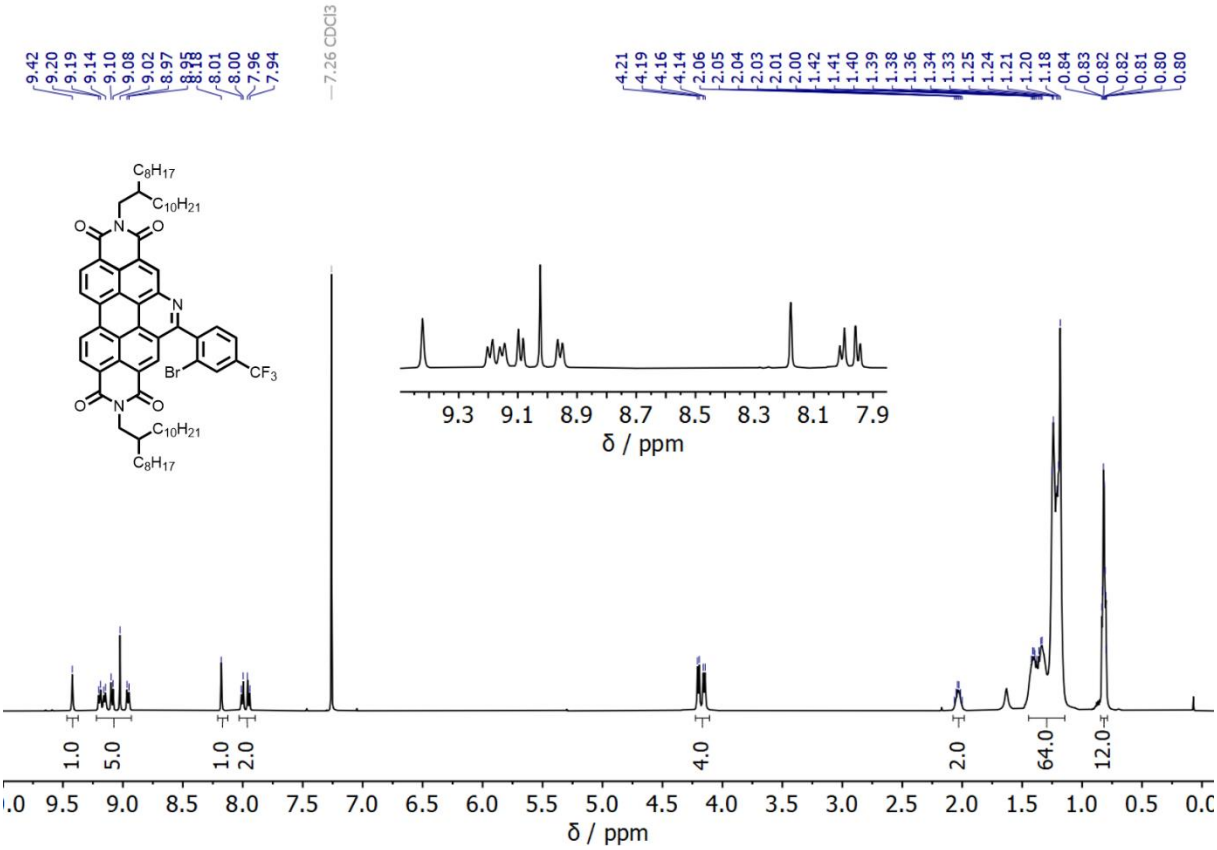

Figure S156. ^{1}H NMR (500 MHz, $CDCl_3$) spectrum of **S2**

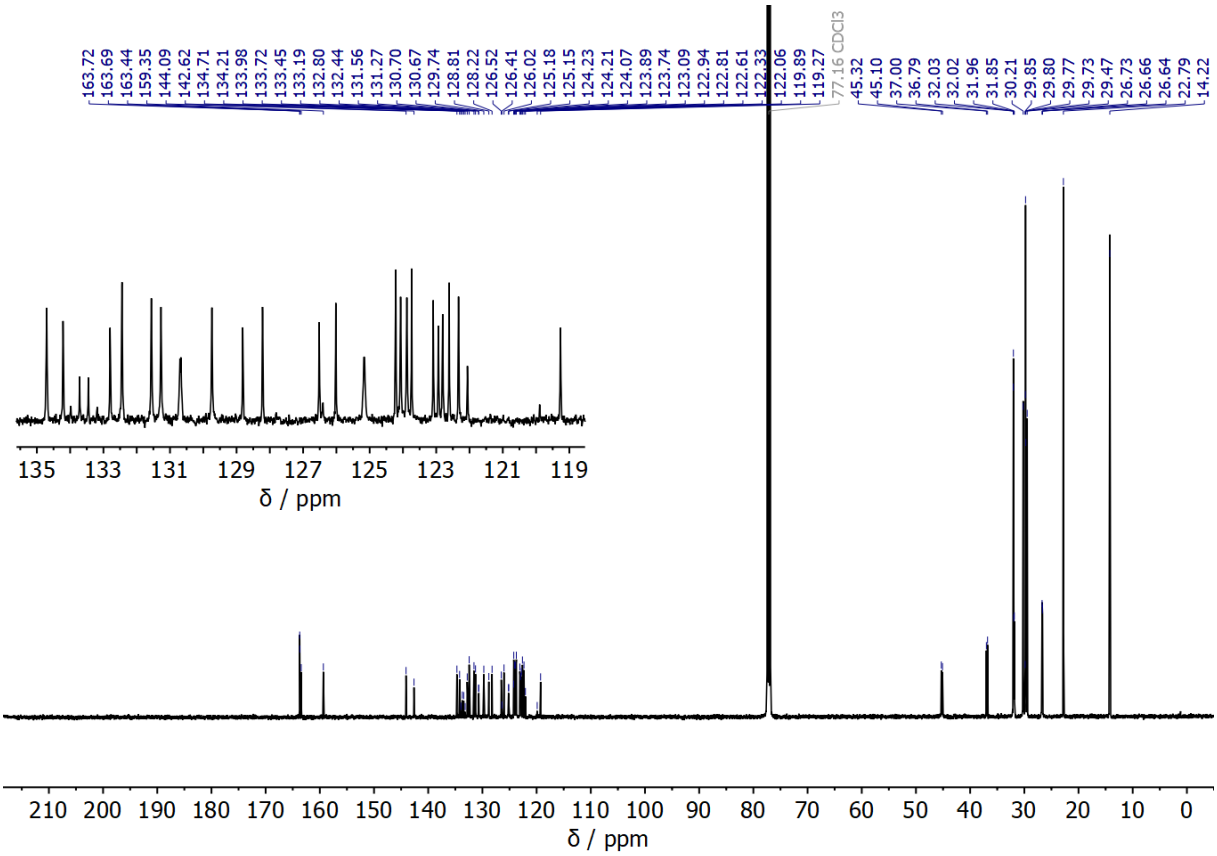

Figure S157. ^{13}C NMR (125 MHz, $CDCl_3$) spectrum of **S2**

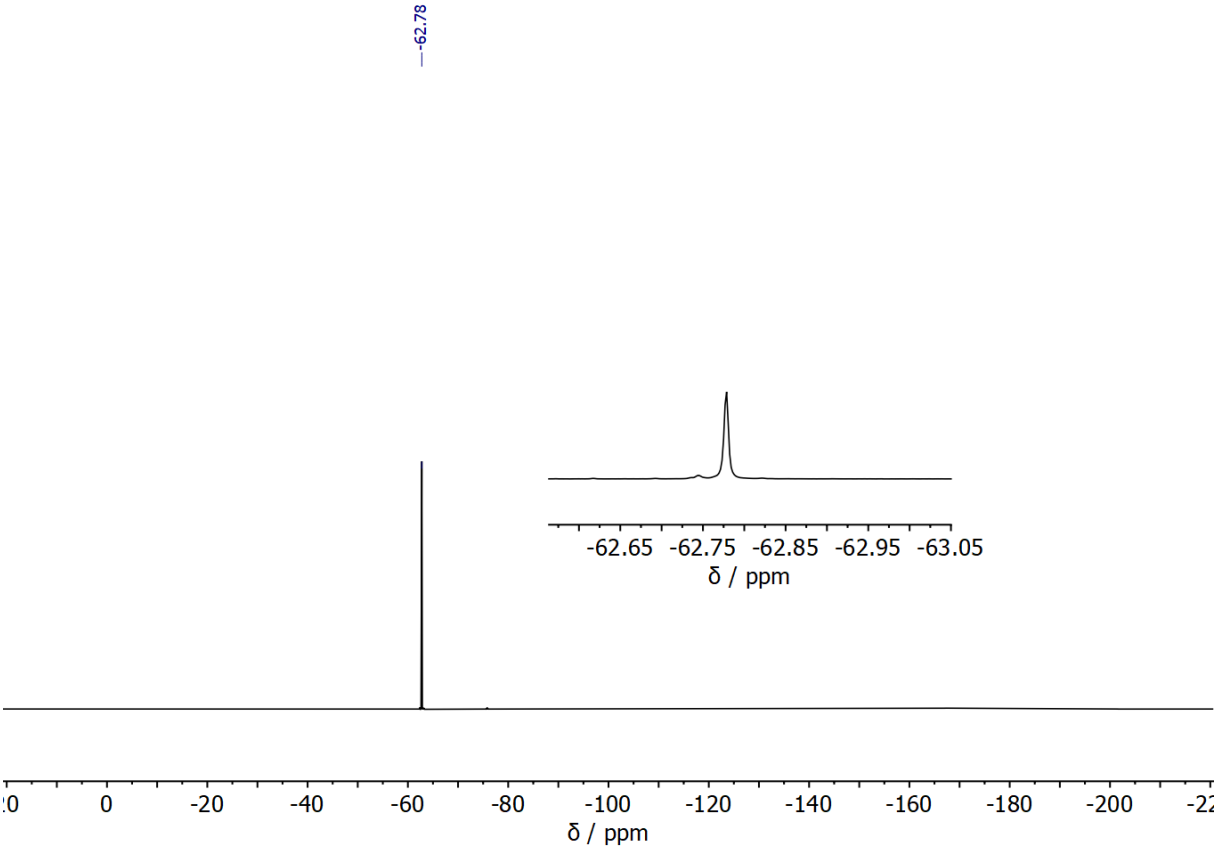

Figure S158. ^{19}F NMR (470 MHz, $CDCl_3$) spectrum of **S2**

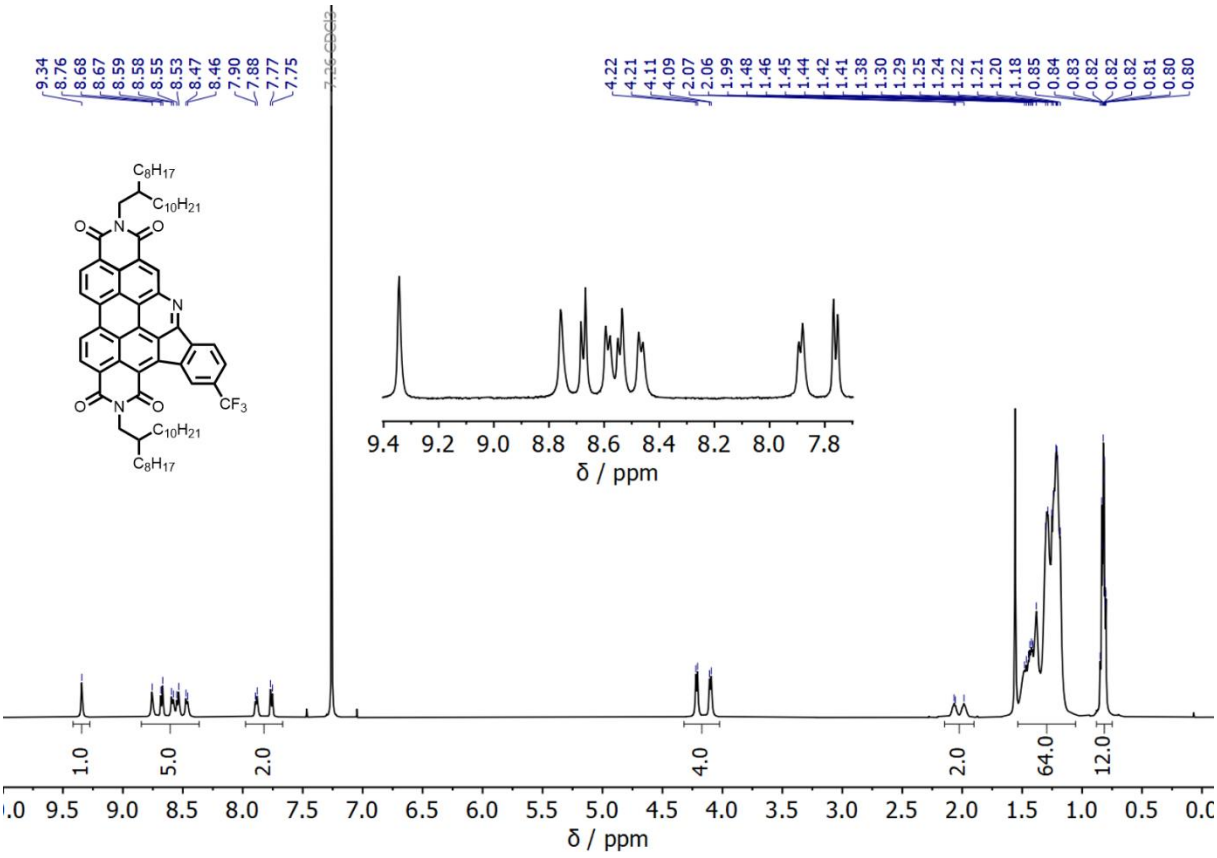

Figure S159. ^{1}H NMR (500 MHz, $CDCl_3$) spectrum of **C-CF_3**

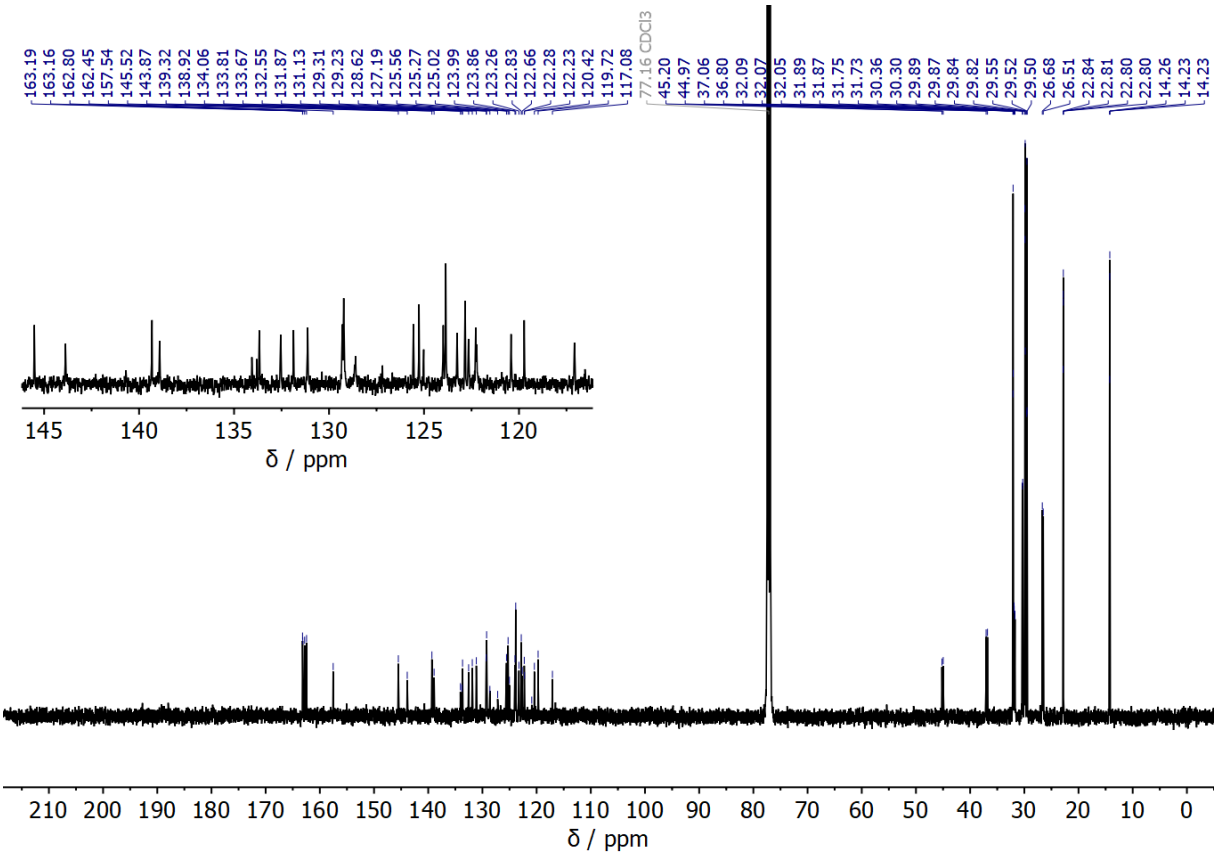

Figure S160. ^{13}C NMR (125 MHz, $CDCl_3$) spectrum of **C-CF₃**

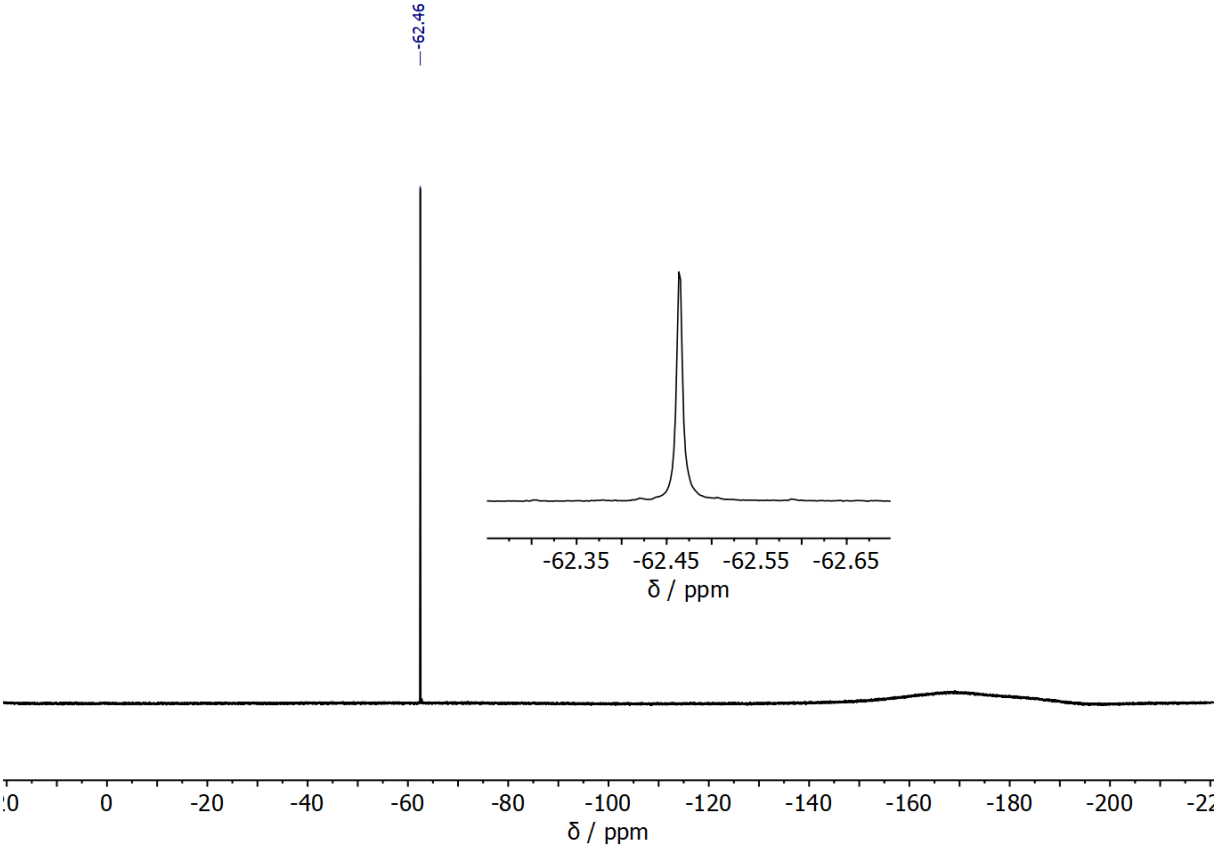

Figure S161. ^{19}F NMR (470 MHz, $CDCl_3$) spectrum of **C-CF₃**

8. Mass Spectrometry

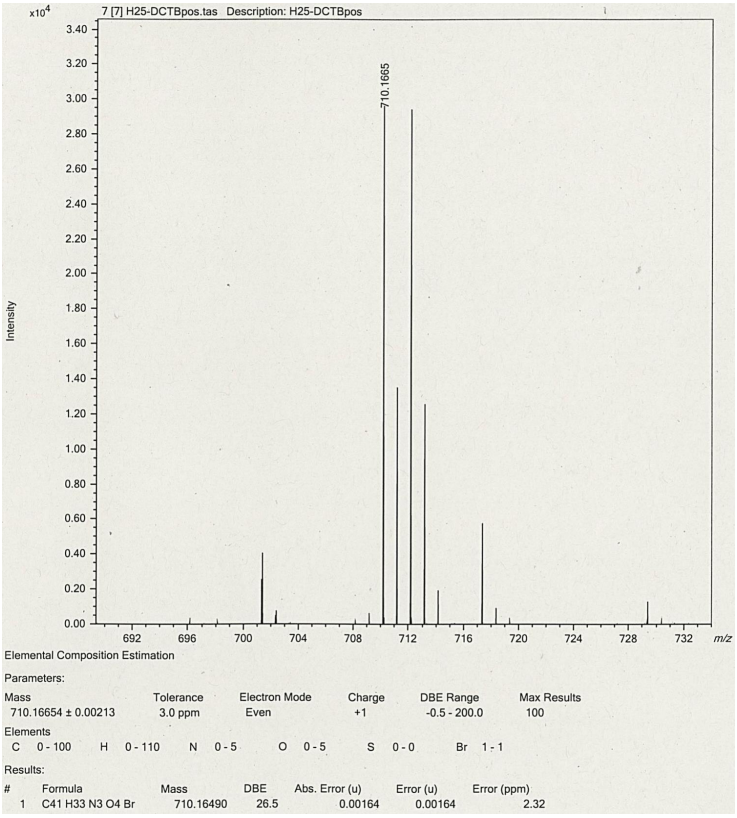

Figure S162. HRMS spectrum of compound **Br-aPDI-Ph**

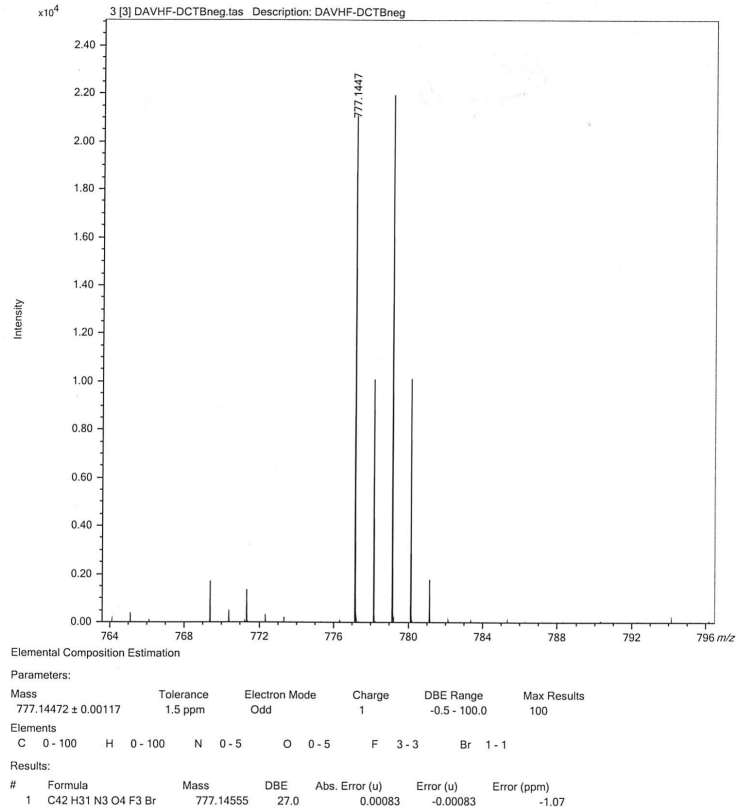

Figure S163. HRMS spectrum of compound **Br-aPDI-CF_3**

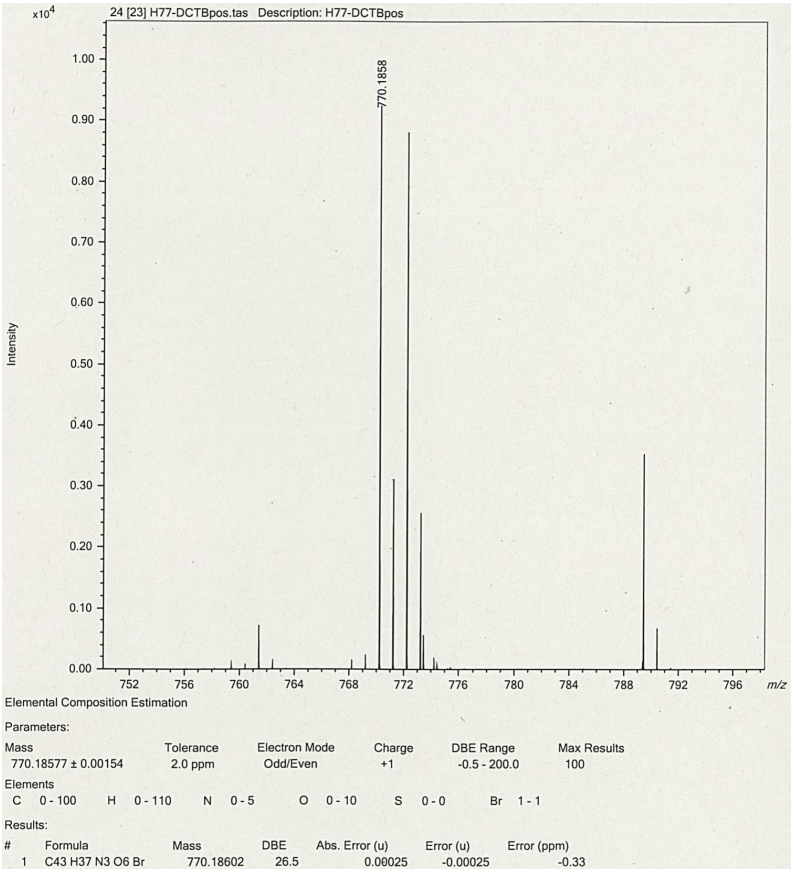

Figure S164. HRMS spectrum of compound **Br-aPDI-OMe**

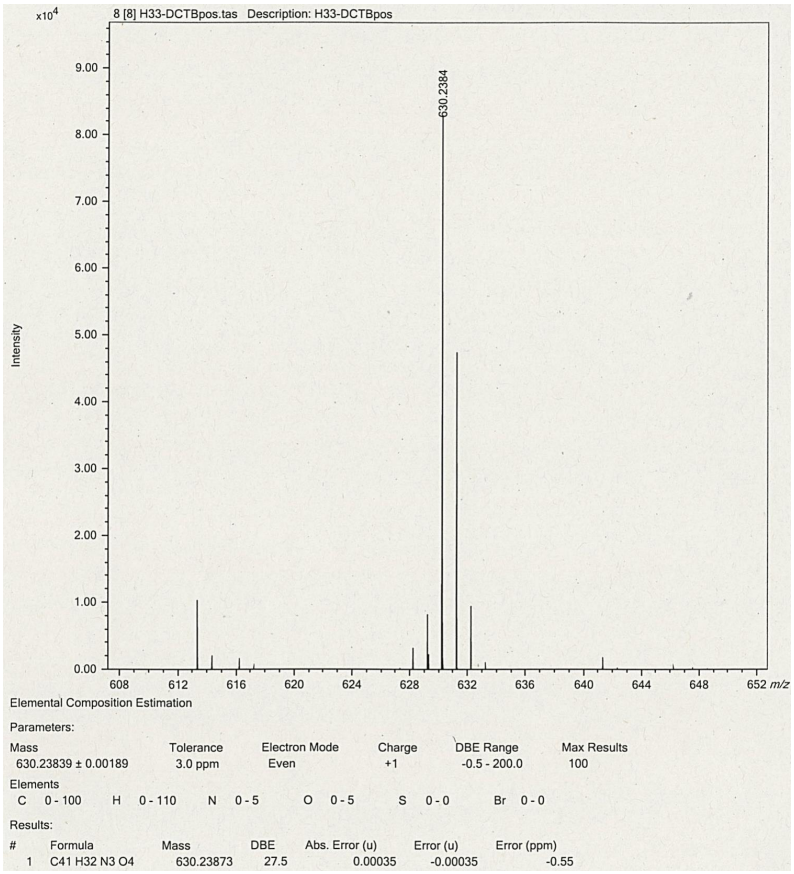

Figure S165. HRMS spectrum of compound **aPDI-Ph**

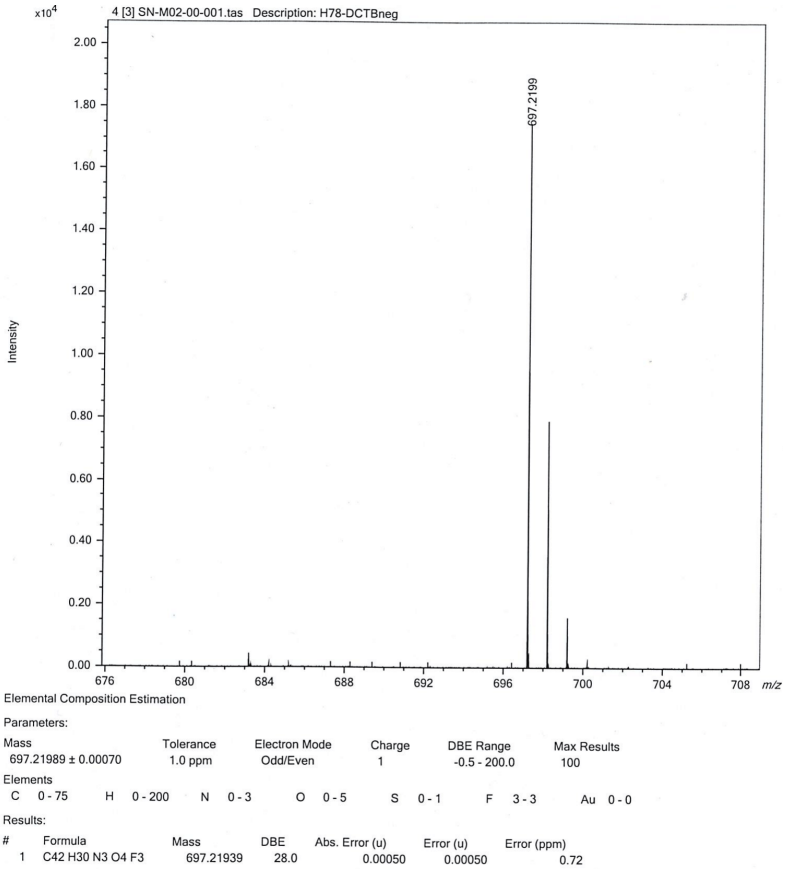

Figure S166. HRMS spectrum of compound **aPDI-CF$_3$**

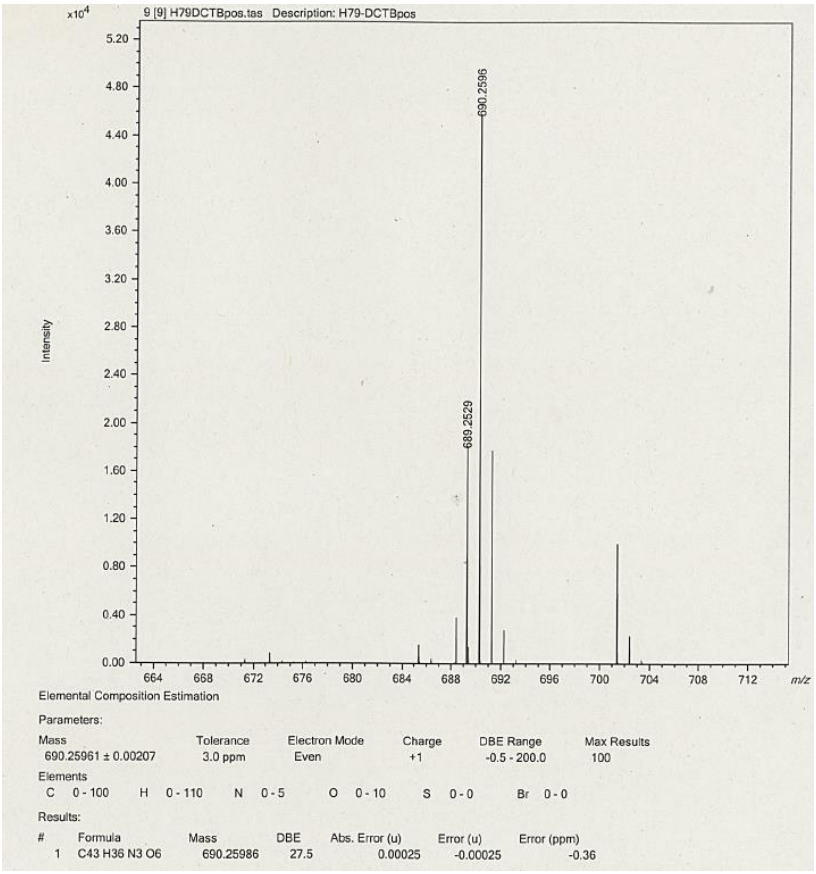

Figure S167. HRMS spectrum of compound **aPDI-OMe**

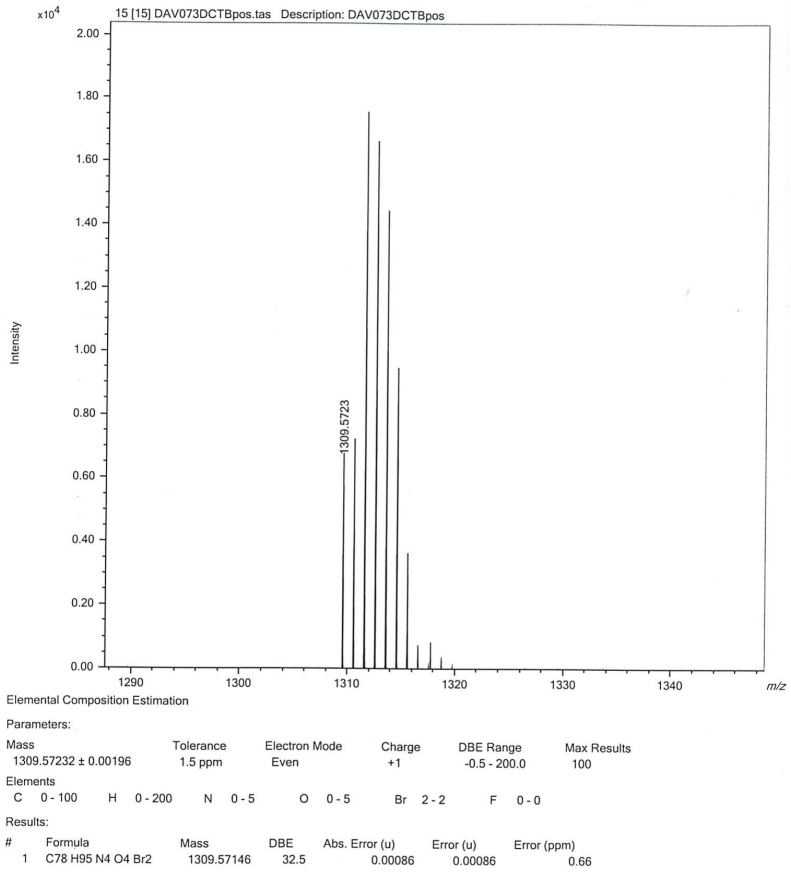

Figure S168. HRMS spectrum of compound **1,6-BACD-Ph**

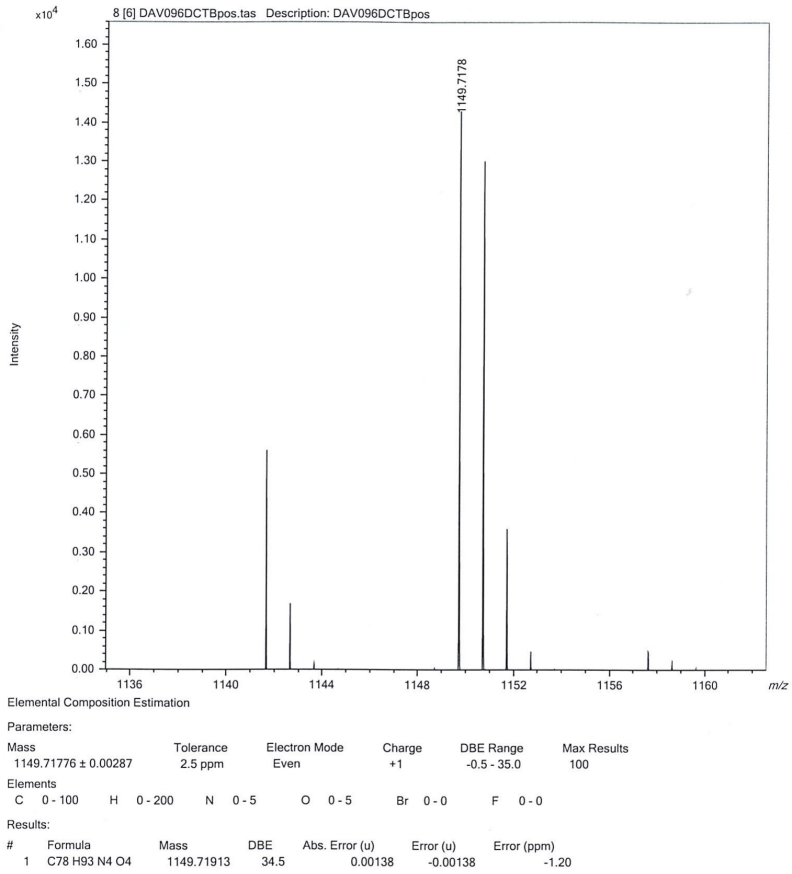

Figure S169. HRMS spectrum of compound **1,6-Ph**

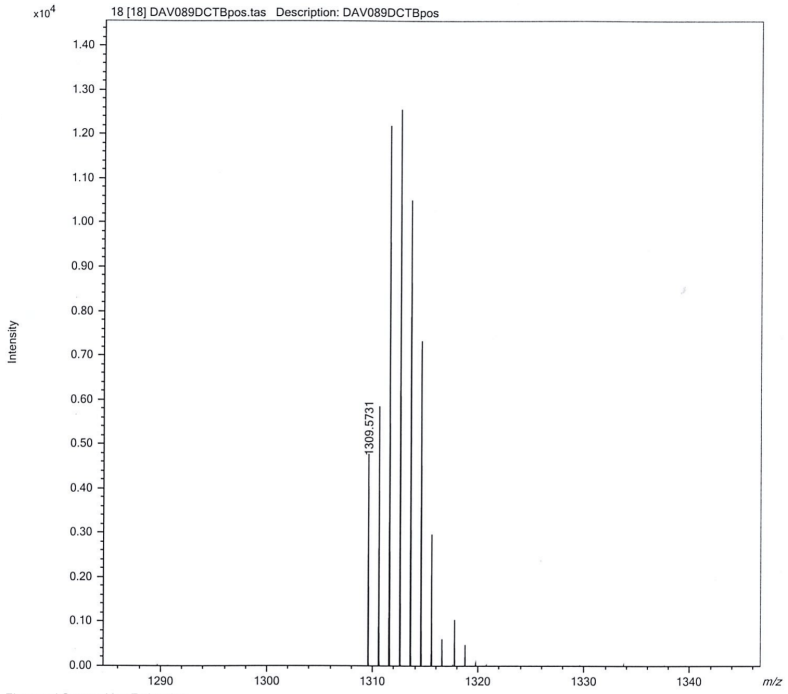

Elemental Composition Estimation

Parameters:

Mass	Tolerance	Electron Mode	Charge	DBE Range	Max Results
1309.57312 ± 0.00262	2.0 ppm	Even	+1	-0.5 - 35.0	100

Elements

C	H	N	O	Br	F
0 - 100	0 - 200	0 - 5	0 - 5	2 - 2	0 - 0

Results:

#	Formula	Mass	DBE	Abs. Error (u)	Error (u)	Error (ppm)
1	C78 H95 N4 O4 Br2	1309.57146	32.5	0.00166	0.00166	1.27

Figure S170. HRMS spectrum of compound **1,7-BACD-Ph**

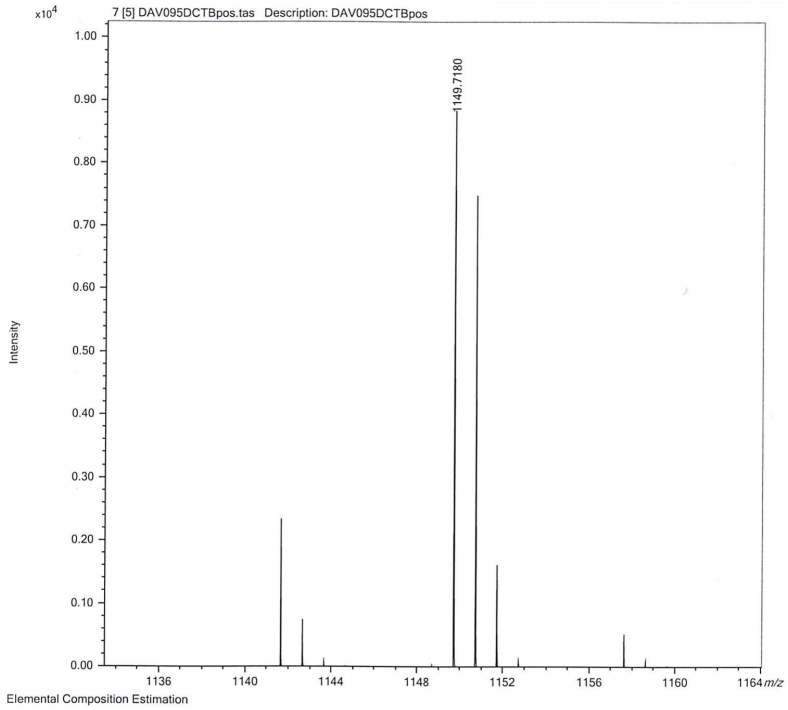

Elemental Composition Estimation

Parameters:

Mass	Tolerance	Electron Mode	Charge	DBE Range	Max Results
1149.71798 ± 0.00287	2.5 ppm	Even	+1	-0.5 - 35.0	100

Elements

C	H	N	O	Br	F
0 - 100	0 - 200	0 - 5	0 - 5	0 - 0	0 - 0

Results:

#	Formula	Mass	DBE	Abs. Error (u)	Error (u)	Error (ppm)
1	C78 H93 N4 O4	1149.71913	34.5	0.00116	-0.00116	-1.01

Figure S171. HRMS spectrum of compound **1,7-Ph**

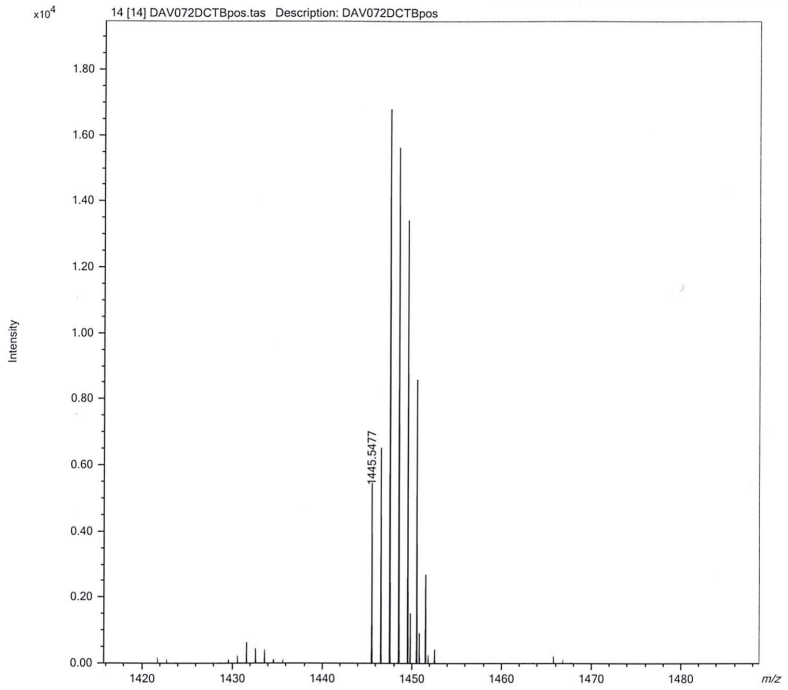

Elemental Composition Estimation

Parameters:

Mass	Tolerance	Electron Mode	Charge	DBE Range	Max Results
1445.54772 ± 0.00217	1.5 ppm	Even	+1	-0.5 - 200.0	100

Elements

C 0 - 100 H 0 - 200 N 0 - 5 O 0 - 5 Br 2 - 2 F 6 - 6

Results:

#	Formula	Mass	DBE	Abs. Error (u)	Error (u)	Error (ppm)
1	C80 H93 N4 O4 F6 Br2	1445.54623	32.5	0.00149	0.00149	1.03

Figure S172. HRMS spectrum of compound **1,6-BACD-CF_3**

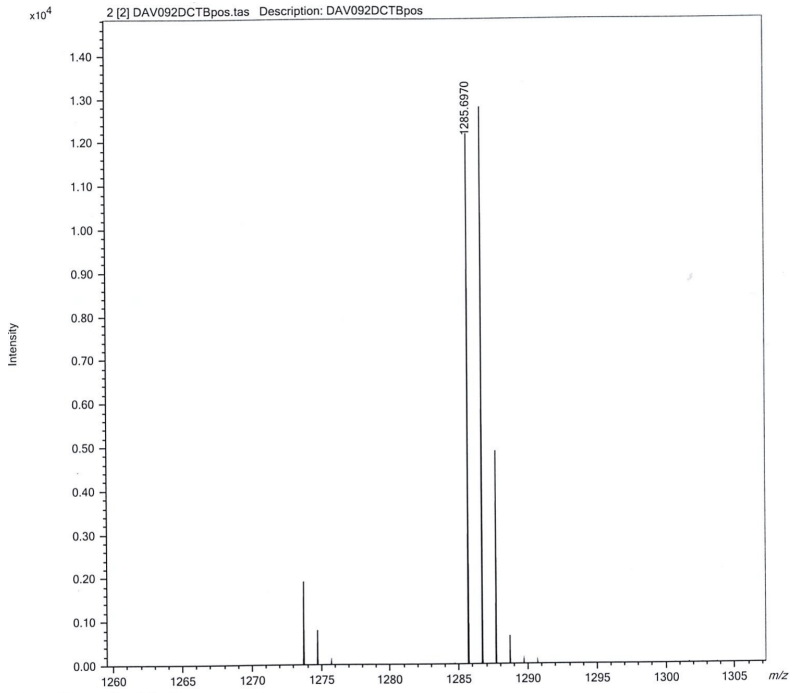

Elemental Composition Estimation

Parameters:

Mass	Tolerance	Electron Mode	Charge	DBE Range	Max Results
1285.69702 ± 0.00321	2.5 ppm	Even	+1	-0.5 - 35.0	100

Elements

C 0 - 100 H 0 - 200 N 0 - 5 O 0 - 5 Br 0 - 0 F 6 - 6

Results:

#	Formula	Mass	DBE	Abs. Error (u)	Error (u)	Error (ppm)
1	C80 H91 N4 O4 F6	1285.69390	34.5	0.00312	0.00312	2.43

Figure S173. HRMS spectrum of compound **1,6-CF_3**

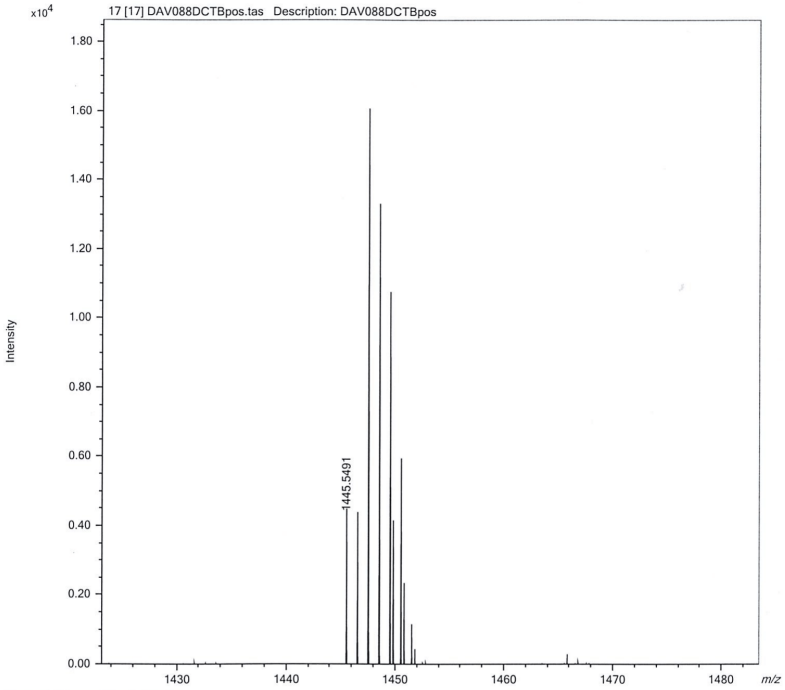

Elemental Composition Estimation

Parameters:

Mass	Tolerance	Electron Mode	Charge	DBE Range	Max Results
1445.54911 ± 0.00289	2.0 ppm	Even	+1	-0.5 - 35.0	100

Elements

C	H	N	O	Br	F
0 - 100	0 - 200	0 - 5	0 - 5	2 - 2	6 - 6

Results:

#	Formula	Mass	DBE	Abs. Error (u)	Error (u)	Error (ppm)
1	C80 H93 N4 O4 F6 Br2	1445.54623	32.5	0.00288	0.00288	1.99

Figure S174. HRMS spectrum of compound **1,7-BACD-CF$_3$**

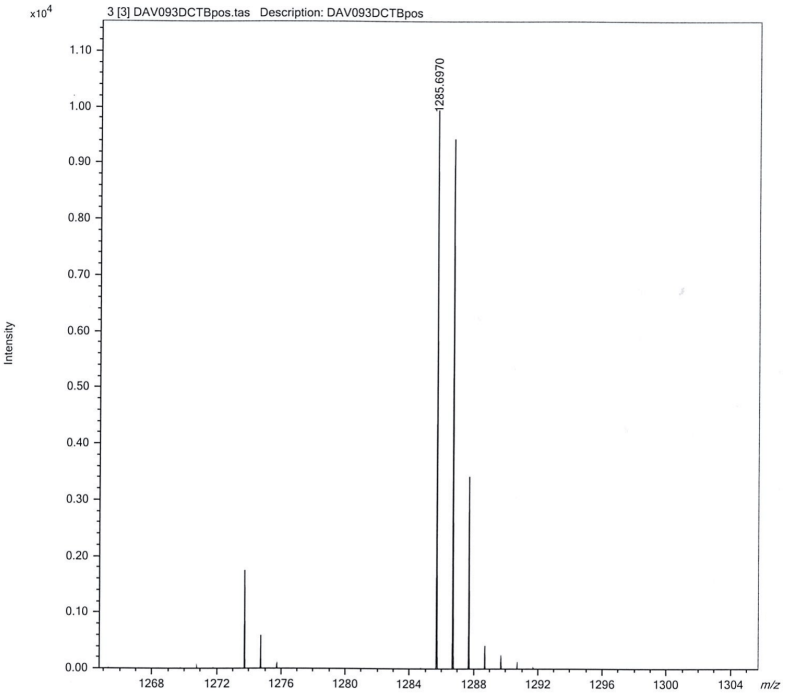

Elemental Composition Estimation

Parameters:

Mass	Tolerance	Electron Mode	Charge	DBE Range	Max Results
1285.69695 ± 0.00321	2.5 ppm	Even	+1	-0.5 - 35.0	100

Elements

C	H	N	O	Br	F
0 - 100	0 - 200	0 - 5	0 - 5	0 - 0	6 - 6

Results:

#	Formula	Mass	DBE	Abs. Error (u)	Error (u)	Error (ppm)
1	C80 H91 N4 O4 F6	1285.69390	34.5	0.00305	0.00305	2.37

Figure S175. HRMS spectrum of compound **1,7-CF$_3$**

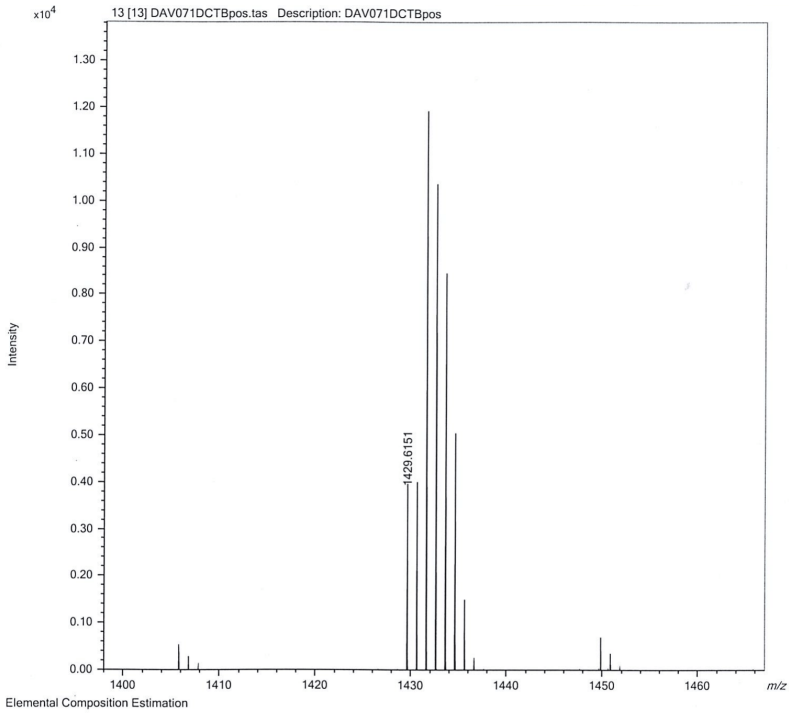

Figure S176. HRMS spectrum of compound **1,6-BACD-OMe**

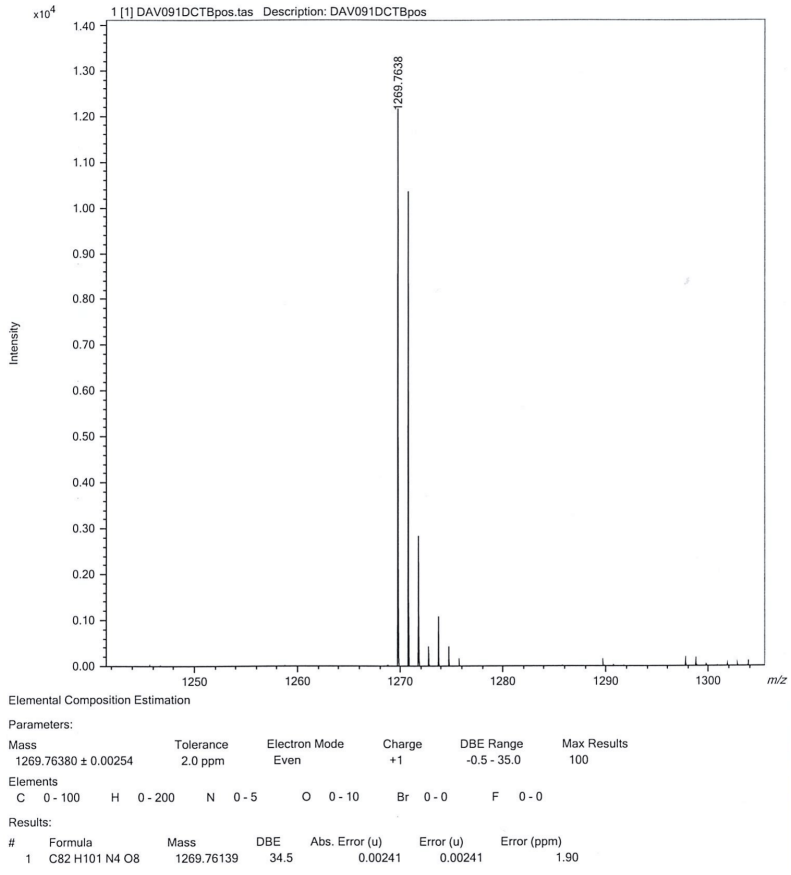

Figure S177. HRMS spectrum of compound **1,6-OMe**

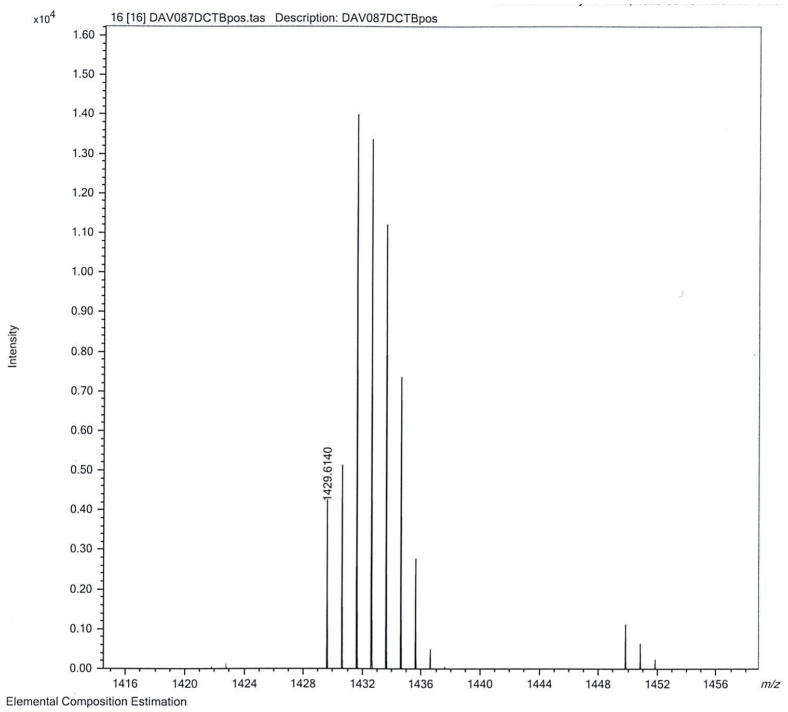

Figure S178. HRMS spectrum of compound **1,7-BACD-OMe**

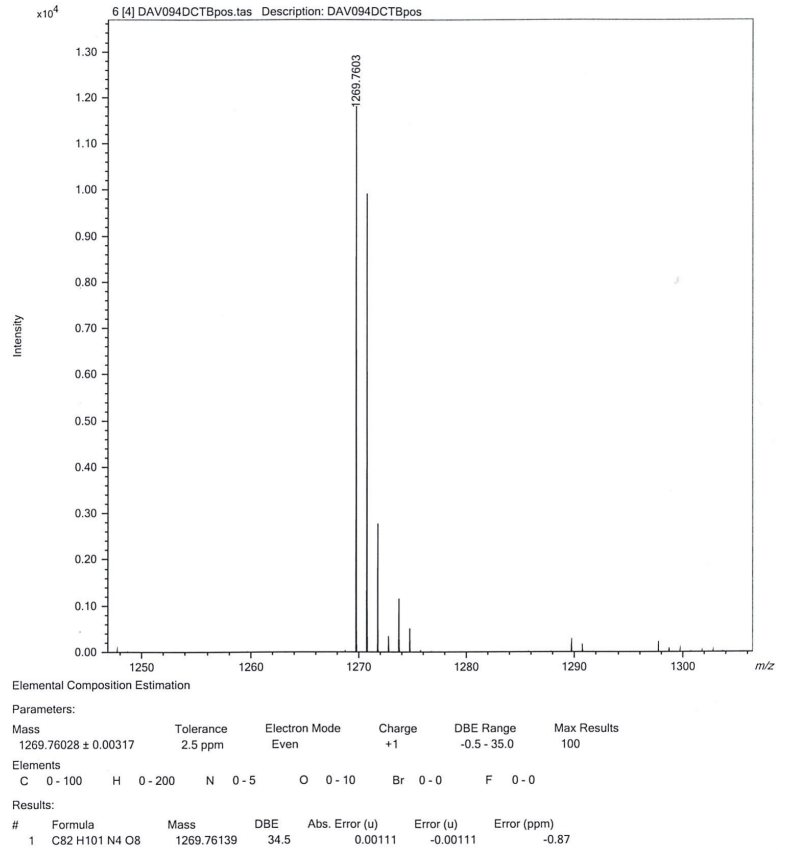

Figure S179. HRMS spectrum of compound **1,7-OMe**

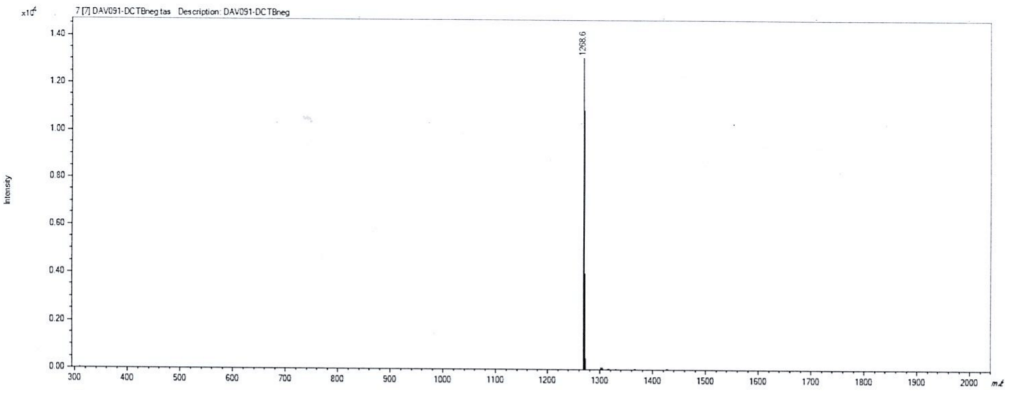

Figure S180. MS spectrum of compound **1,6-OMe**

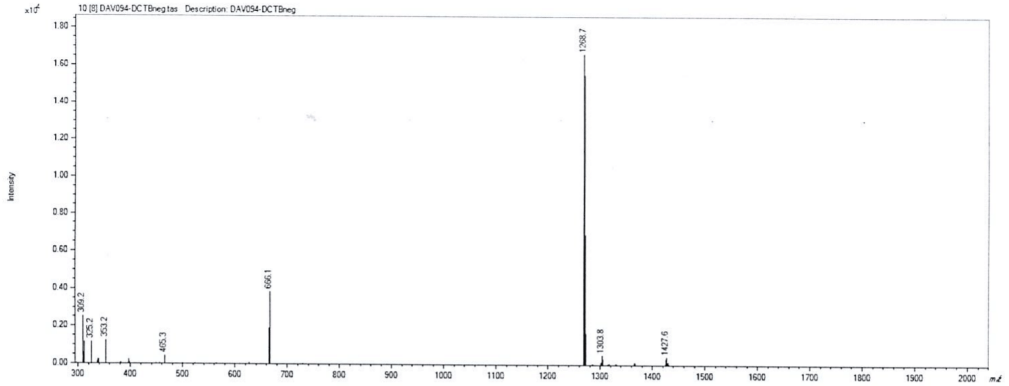

Figure S181. MS spectrum of compound **1,7-OMe**

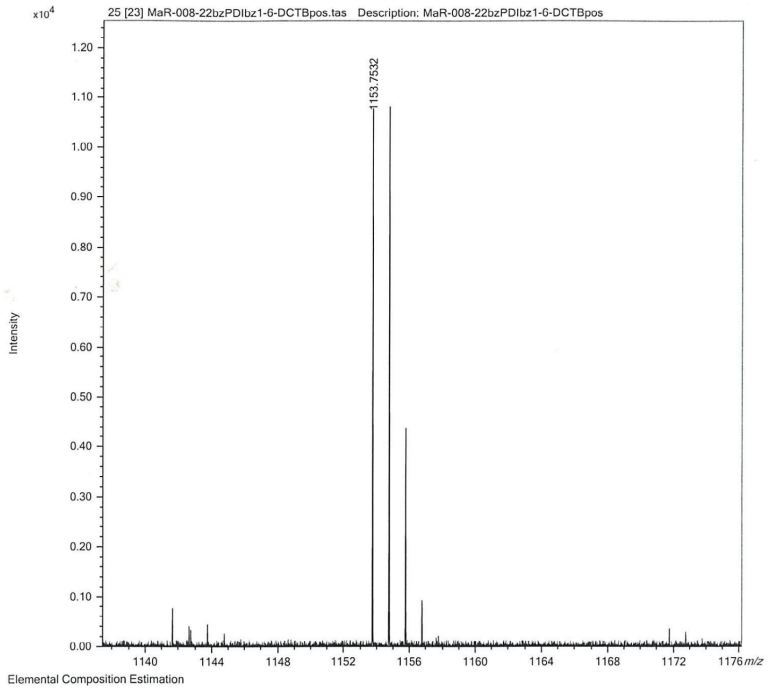

Elemental Composition Estimation

Parameters:

Mass	Tolerance	Electron Mode	Charge	DBE Range	Max Results
1153.75317 ± 0.00288	2.5 ppm	Odd/Even	+1	-0.5 - 200.0	100

Elements

C	H	N	O	Br	S	Na
0 - 80	0 - 100	2 - 5	2 - 5	0 - 0	0 - 0	0 - 0

Results:

#	Formula	Mass	DBE	Abs. Error (u)	Error (u)	Error (ppm)
1	C78 H97 N4 O4	1153.75043	32.5	0.00274	0.00274	2.37

Figure S182. HRMS spectrum of compound **C-1,6**

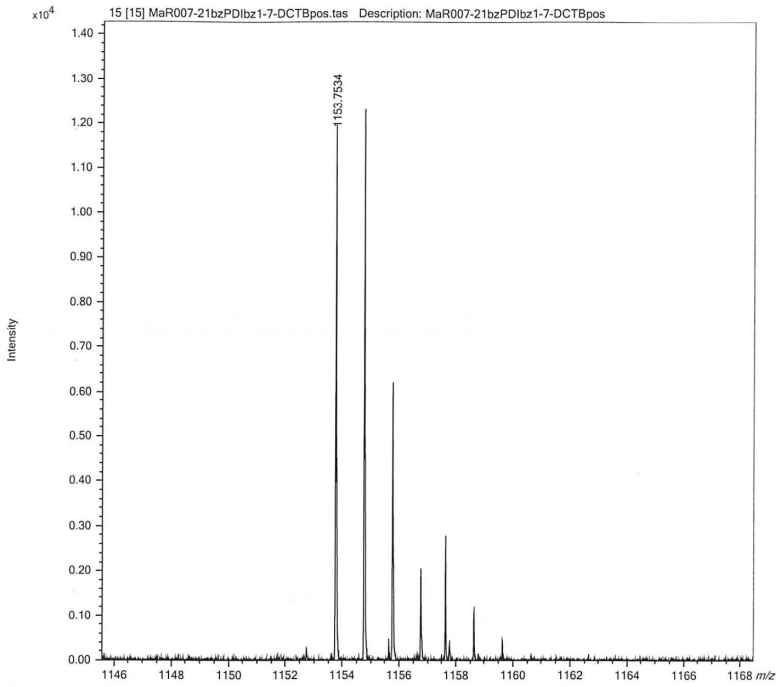

Figure S183. HRMS spectrum of compound **C-1,7**

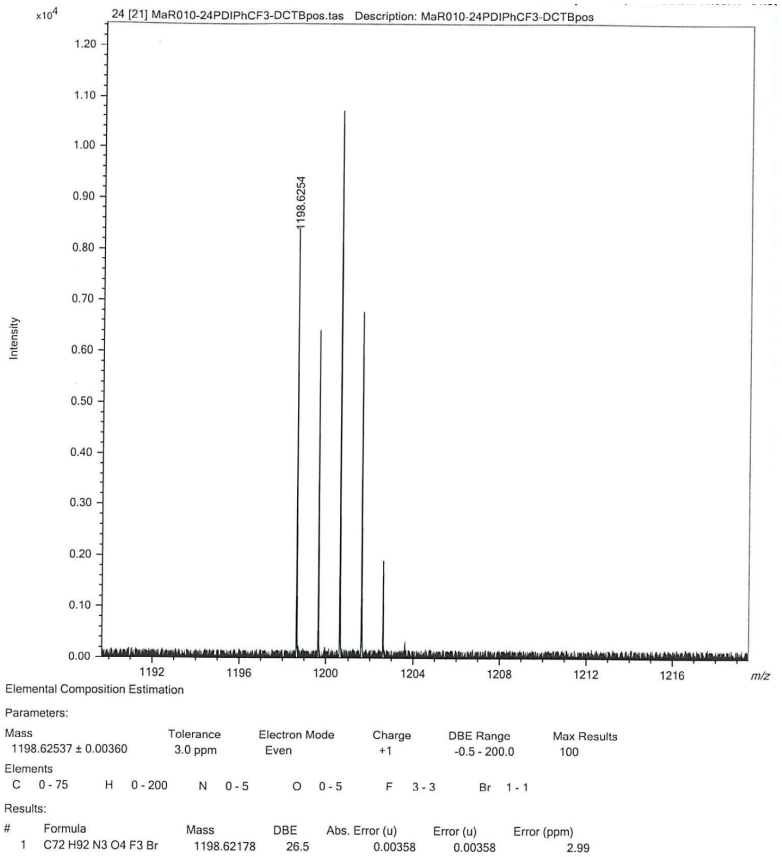

Figure S184. HRMS spectrum of compound **S2**

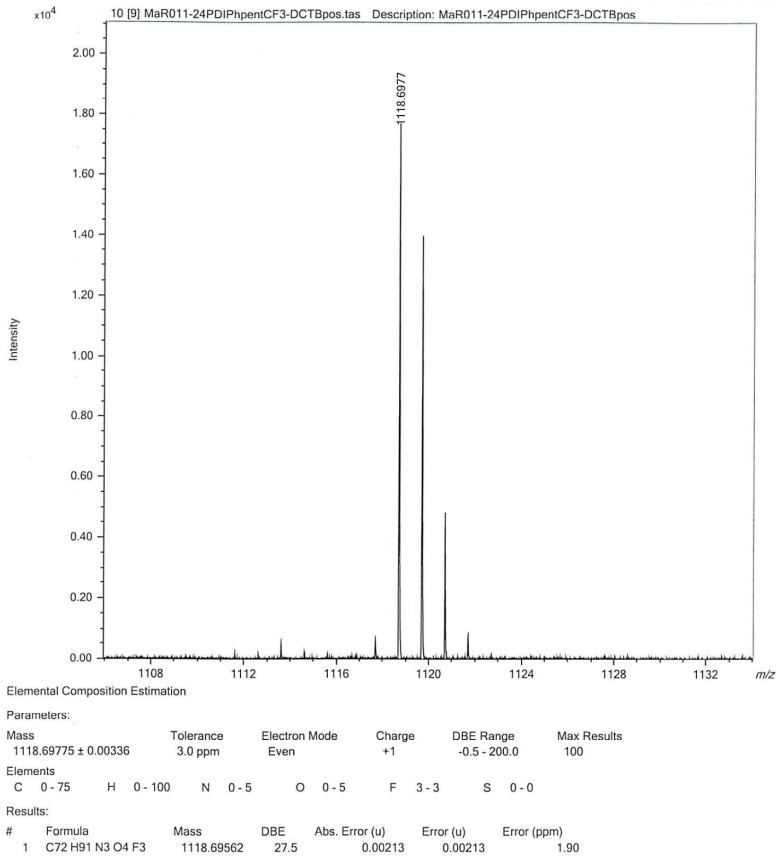

Figure S185. HRMS spectrum of compound **C-CF$_3$**

9. X-Ray Crystallography

Crystal data and structure refinement

Single crystals of AzaBPDIs, **Br-aPDI-Ph** and **aPDI-Ph**, were grown by slow evaporation of Et_2O in $CHCl_3$ solution of the compounds. Single crystals of AzaBPDI **aPDI-CF$_3$** were grown by slow evaporation of Et_2O in CH_2Cl_2 solution of **aPDI-CF$_3$**.

X-ray single-crystal diffraction data were collected at different temperature on a Rigaku Oxford Diffraction SuperNova diffractometer equipped with an Atlas CCD detector and micro-focus Cu-K_α radiation (λ = 1.54184 Å). The structures were solved by dual-space algorithm and refined on F^2 by full matrix least-squares techniques using SHELX programs (G. M. Sheldrick, SHELXT 2018/2 and SHELXL 2018/3). All non-H atoms were refined anisotropically and multiscan empirical absorption was corrected using CrysAlisPro program (CrysAlisPro 1.171.40.45a/41.118a, Rigaku Oxford Diffraction, 2019-2021). The H atoms were placed at

calculated positions and refined using a riding model. The structure refinements for **Br-aPDI-Ph** and **aPDI-CF$_3$** showed disordered electron density which could not be reliably modeled but the corresponding scattering contribution were taken into account using the program PLATON/SQUEEZE (A.L. Spek V90522 (1980-2022)). This electron density can be attributed to 8 water molecules for **Br-aPDI-Ph** and 5 dichloromethane molecules for **aPDI-CF$_3$** in the corresponding unit cell. The assumed solvent composition was used in the subsequent calculation of the empirical formula, formula weight, density, linear absorption coefficient and F(000). Deposition Number(s) 2360838 (for **aPDI-Ph**), 2360839 (for **Br-aPDI-Ph**) and 2360840 (for **aPDI-CF$_3$**) contain(s) the supplementary crystallographic data for this paper. These data are provided free of charge by the joint Cambridge Crystallographic Data Centre and Fachinformationszentrum Karlsruhe Access Structures service.

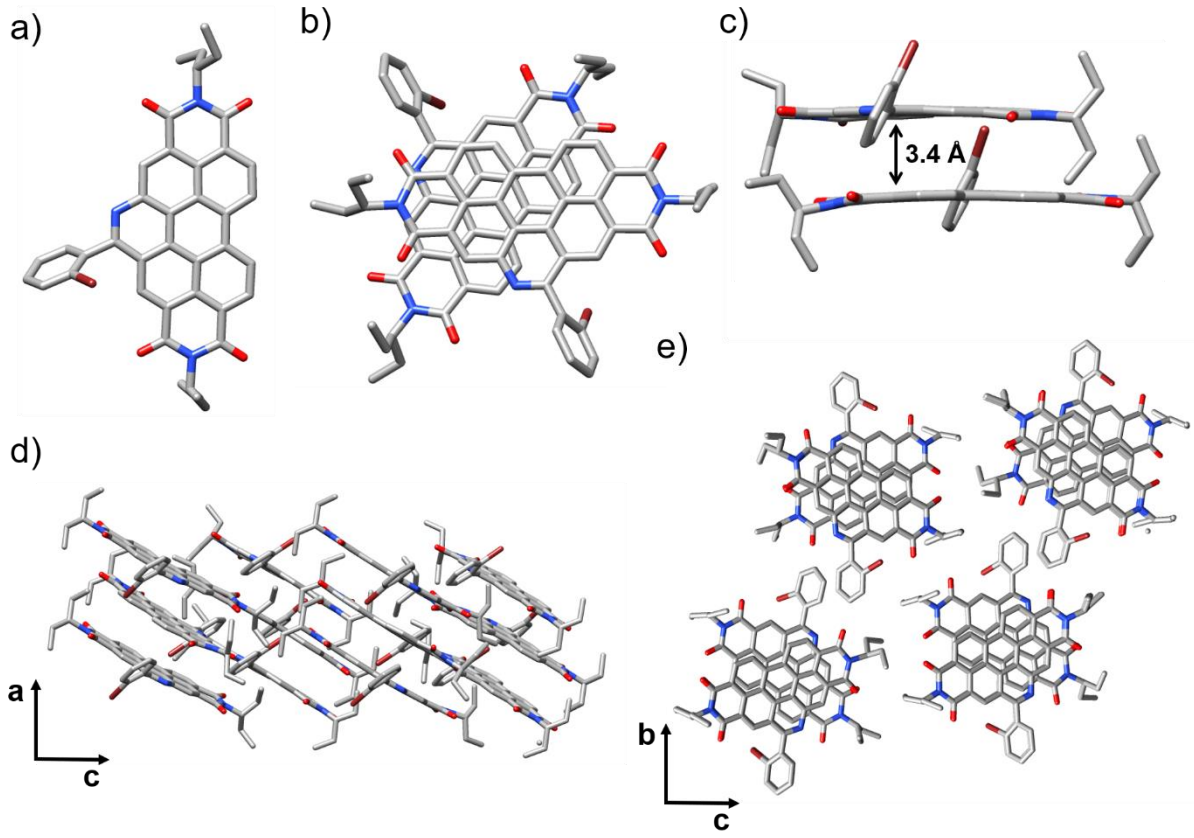

Figure S186. (a) Top-down view of the X-ray diffraction structure of AzaBPDI **Br-aPDI-Ph**. (b) Top-down and (c) side-on views of the π-stack dimers of AzaBPDI **Br-aPDI-Ph**. Illustration of the packing of along the (d) b-axis, and (e) a-axis. Hydrogen atoms were omitted for the sake of clarity. Color coding: C, grey; O, red; N, blue; Br, brown.

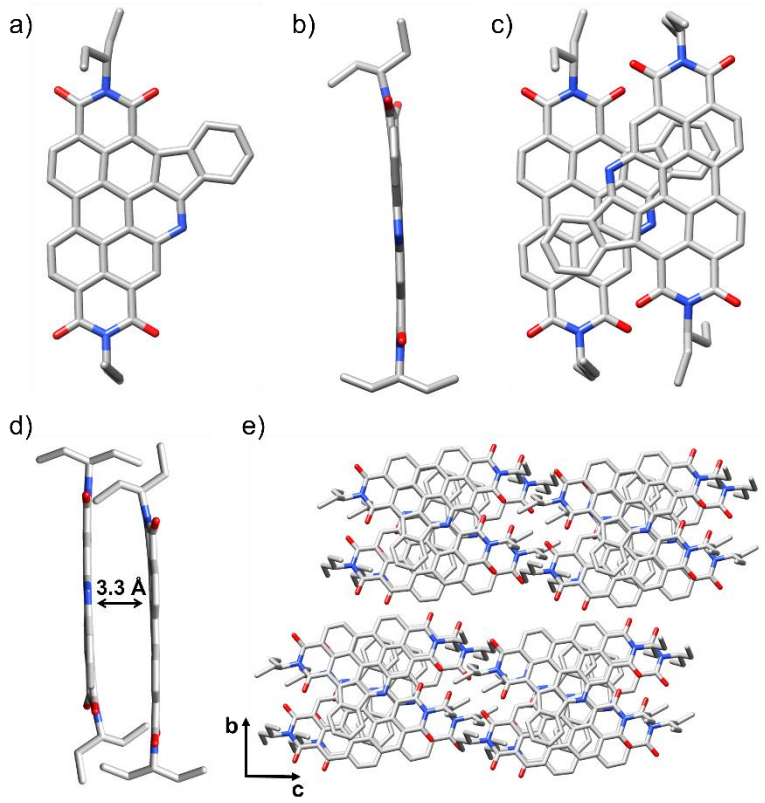

Figure S187. (a) Top-down and (b) side-on views of the X-ray diffraction structure of pentannulated AzaBPDI **aPDI-Ph**. (c) Top-down and (d) side-on views of the π-stack dimers of pentannulated AzaBPDI **aPDI-Ph**. Illustration of the packing of along the (e) a-axis. Hydrogen atoms were omitted for the sake of clarity. Color coding: C, grey; O, red; N, blue.

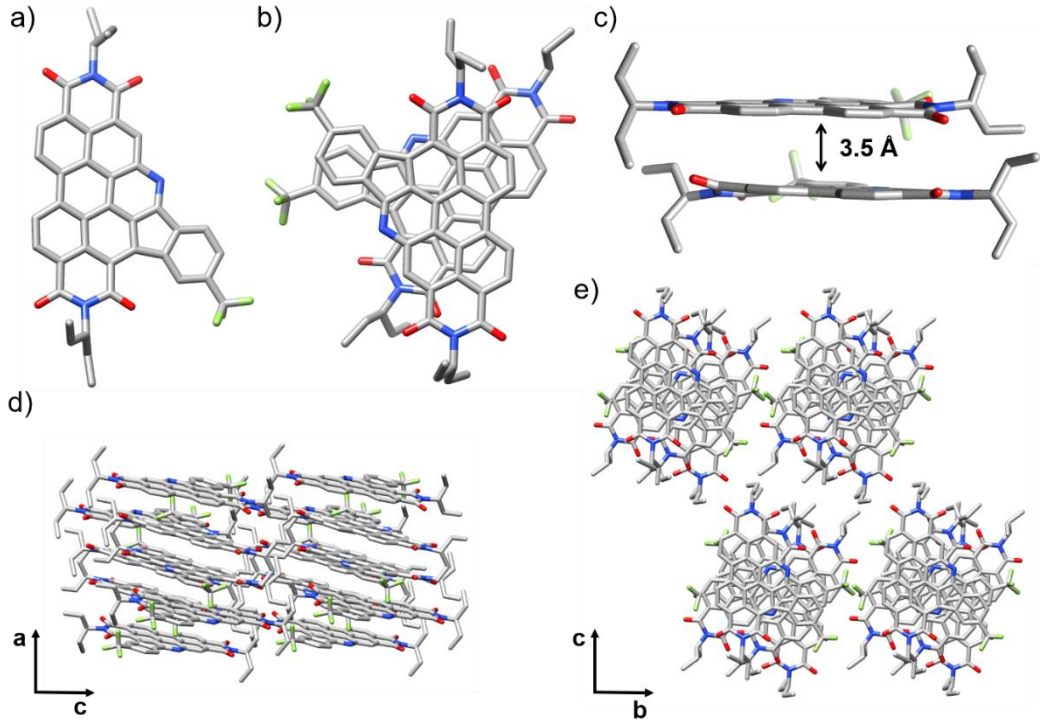

Figure S188. (a) Top-down view of the X-ray diffraction structure of pentannulated AzaBPDI **aPDI-CF_3**. (b) Top-down and (c) side-on views of the π-stack dimers of pentannulated AzaBPDI **aPDI-CF_3**. Illustration of the packing of along the (d) b-axis, and (e) a-axis. Hydrogen atoms were omitted for the sake of clarity. Color coding: C, grey; O, red; N, blue; F, green.

Table S7. X-ray crystallographic data of single crystals of **aPDI-Ph**, **Br-aPDI-Ph** and **aPDI-CF_3**.

Crystal	**aPDI-Ph·$CHCl_3$**	**Br-aPDI-Ph·H_2O**	**4(aPDI-CF_3)·5(CH_2Cl_2)**
Formula	$C_{42}H_{32}Cl_3N_3O_4$	$C_{41}H_{34}BrN_3O_5$	$C_{173}H_{130}Cl_{10}F_{12}N_{12}O_{16}$
Molecular Weight	749.05	728.62	3215.38
Temperature (K)	200	200	220
Crystal system	Triclinic	Monoclinic	Triclinic
Space group	*P*-1	*P* $2_1/n$	*P*-1
a (Å)	7.5989(6)	7.3754(2)	14.4986(9)
b (Å)	14.644(1)	28.5511(6)	15.431(1)
c (Å)	16.770(2)	31.9705(9)	18.862(1)
α (°)	69.068(8)	90	65.998(6)
β (°)	89.101(7)	95.878(3)	85.671(5)
γ (°)	81.248(6)	90	72.361(6)
V ($Å^3$)	1721.3(3)	6696.8(3)	3668.4(4)
Z	2	8	1
Crystal color	red	yellow	orange
Crystal size (mm^3)	0.374 x 0.030 x 0.023	0.178 x 0.117 x 0.113	0.248 x 0.039 x 0.034
D_c (g cm^{-3})	1.445	1.445	1.455
μ (mm^{-1})	2.818	2.096	2.479
F(000)	776	3008	1658
Transmission (min/max)	0.816 / 1.000	0.270 / 1.000	0.026 / 1.000
θ (min/max) (°)	2.824 / 76.507	2.779 / 72.804	2.568 / 72.711
Data collected	13108	55469	29959
Data unique	6870	13125	13917
Data observed	4841	9537	6805
R (int)	0.0315	0.0916	0.1018
Nb of parameters	473	903	963
R_1 [I > 2σ(I)]	0.0680	0.0682	0.0842
wR_2 [I > 2σ(I)]	0.1803	0.1819	0.2243
R_1 [all data]	0.0938	0.0874	0.1438
wR_2 [all data]	0.2072	0.2082	0.2872
GOF on F^2	1.024	1.036	1.024
Largest peak in final: difference (e A^{-3})	0.826 / -0.593	0.815 / -0.930	0.504 / -0.343

10. Atomic Force Microscopy

Atomic force microscopy (AFM) experiments were performed using the Nano-Observer device (CSInstrument, Les Ulis, France). The topographic images were obtained at room temperature in tapping mode using ACTA-50 SPM Probe (AppNano, USA). Images were processed with the Gwyddion free SPM data analysis software (v2.64, Czech Metrology Institute, Brno, Czech Republic).

The topographic images of the thin film of **1,7-Ph** (prepared following the method described in section 3. Absorption and Emission Spectroscopies) at 5 μm show a smooth homogeneous surface with an average roughness (RMS) of 2.47 nm. Examination of these films shows that these patterns consist of micrometric fibrils of *ca*. 125 nm diameter.

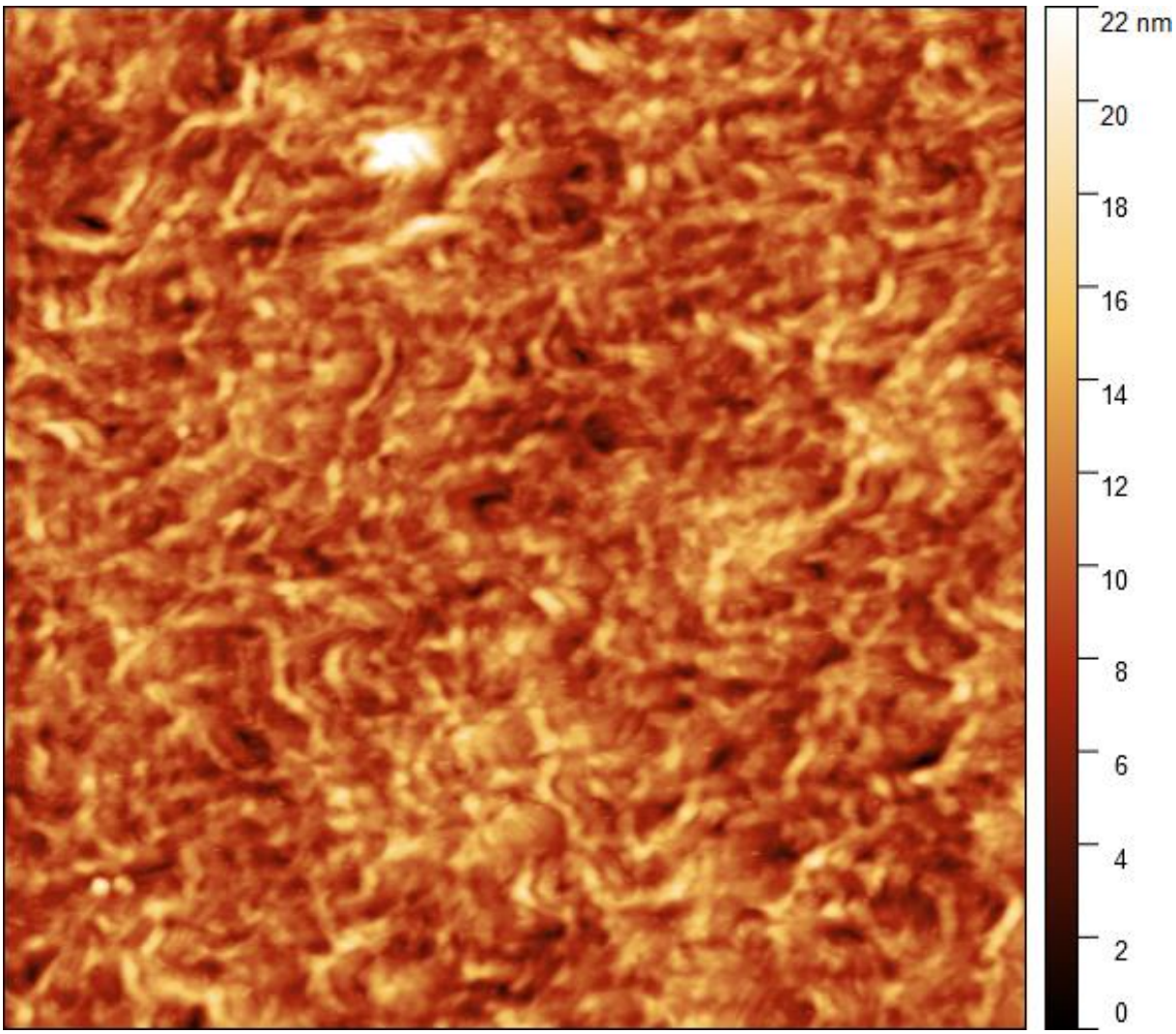

Figure S189. AFM image of the thin film of **1,7-Ph** in tapping mode

11. References

S1 A. H. G. David, D. Shymon, H. Melville, L.-A. Accou, A. Gapin, M. Allain, O. Alévêque, M. Force, A. Grosjean, P. Hudhomme, L. Le Bras, A. Goujon, *J. Mater. Chem. C* **2023**, *11*, 14631–14640.

S2 A. Gapin, A. H. G. David, M. Allain, D. Masson, O. Alévêque, T. Ave, L. Le Bras, P. Hudhomme, A. Goujon, *Chem. Eur. J.* **2023**, *29*, e202300652.

S3 Z. Chen, A. Lohr, C. R. Saha-Möller, F. Würthner, *Chem. Soc. Rev.* **2009**, *38*, 564–584.

S4 R. B. Martin, *Chem. Rev.* **1996**, *96*, 3043–3064.

S5 O. Alévêque, C. Gautier, E. Levillain, *Curr. Opin. Electrochem.* **2019**, *15*, 34–41.

S6 M. J. Abraham, T. Murtola, R. Schulz, S. Páll, J. C. Smith, B. Hess, E. Lindahl, *GROMACS: SoftwareX* **2015**, *1–2*, 19–25.

S7 J. Wang, R. M. Wolf, J. W. Caldwell, P. A. Kollman, D. A. Case, *J. Comput. Chem.* **2004**, *25*, 1157–1174.

S8 (a) J. Wang, W. Wang, P. A. Kollman, D. A. Case, *J. Mol. Graph.* **2006**, *25*, 247– 260. (b) P. R. Batista, A. Wilter, E. H. A. B. Durham, P. G. Pascutti, *Cell Biochem. Biophys.* **2006**, *44*, 395–404.

S9 (a) T. Darden, D. York, L. Pedersen, *J. Chem. Phys.* **1993**, *98*, 10089–10092. (b) U. Essmann, L. Perera, M. L. Berkowitz, T. Darden, H. Lee, L. G. Pedersen, *J. Chem. Phys.* **1995**, *103*, 8577–8593.

S10 H. J. C. Berendsen, J. P. M. Postma, W. F. van Gunsteren, A. DiNola, J. R. Haak, *J. Chem. Phys.* **1984**, *81*, 3684–3690.

S11 (a) S. Nosé, M. Klein, *Mol. Phys.* **1983**, *50*, 1055–1076. (b) S. Nosé, *J. Chem. Phys.* **1984**, *81*, 511–519. (c) W. G. Hoover, *Phys. Rev. A* **1985**, *31*, 1695–1697.

S12 M. Parrinello, A. Rahman, *J. Appl. Phys.* **1981**, *52*, 7182–7190.

S13 J. Tomasi, B. Mennucci, R. Cammi, *Chem. Rev.* **2005**, *105*, 2999–3094.

S14 M. J. Frisch, G. W. Trucks, H. B. Schlegel, G. E. Scuseria, M. A. Robb, J. R. Cheeseman, G. Scalmani, V. Barone, G. A. Petersson, H. Nakatsuji, X. Li, M. Caricato, A. Marenich, J. Bloino, B. G. Janesko, R. Gomperts, B. Mennucci, H. P. Hratchian, J. V. Ortiz, A. F. Izmaylov, J. L. Sonnenberg, D. Williams-Young, F. Ding, F. Lipparini, F. Egidi, J. Goings, B. Peng, A. Petrone, T. Henderson, D. Ranasinghe, V. G. Zakrzewski, J. Gao, N. Rega, G. Zheng, W. Liang, M. Hada, M. Ehara, K. Toyota, R. Fukuda, J. Hasegawa, M. Ishida, T. Nakajima, Y. Honda, O. Kitao, H. Nakai, T. Vreven, K. Throssell, J. A. Montgomery, Jr., J. E. Peralta, F. Ogliaro, M. Bearpark, J. J. Heyd, E. Brothers, K. N. Kudin, V. N. Staroverov, T. Keith, R. Kobayashi, J. Normand, K. Raghavachari, A. Rendell, J. C. Burant, S. S. Iyengar, J. Tomasi, M. Cossi, J. M. Millam, M. Klene, C. Adamo, R. Cammi, J. W. Ochterski, R. L. Martin, K. Morokuma, O. Farkas, J. B. Foresman, D. J. Fox, *Gaussian 09, Revision C.01*, Gaussian, Inc., Wallingford CT, 2016.